SOLID-LIQUID MIXING

IN MECHANICALLY AGITATED VESSELS

Thesis submitted for the degree of Doctor of Philosophy
in the University of London by:

Andrew Tsz-Chung Mak, MEng

Ramsay Memorial Laboratory
Department of Chemical and Biochemical Engineering
University College London
Torrington Place
London WC1E 7JE
England

June 1992

ABSTRACT

Experimental data are reported for solids suspension and distribution in four geometrically similar vessels with diameters equal to 0.31, 0.61, 1.83 and 2.67 m. Agitation was provided by a series of pitched blade turbines with impeller to vessel diameter ratios from 0.3 to 0.6 and pitched angles between 30° and 90°. The effect of impeller clearance on solids suspension was examined for a clearance range of T/4 to T/8. Dual impeller systems were also studied, covering two combinations (dual pitched and flat/pitched) and impeller spacing of half to two diameters apart. The majority of the experiments were carried out with 150-210 μm round-grained sand (density: 2630 kg m^{-3} and settling velocity: 0.015 m s^{-1}) and tap water. Solids concentration was varied between 0.1 to 40% by weight.

Four parameters were measured; impeller speed, using an optical tachometer, power input, calculated from the shaft torque given by strain gauges, just suspension speed, ascertained both visually and by use of an ultrasonic Doppler flowmetering (UDF) technique and the local solids concentration, measured by a in-house solids concentration probe. In addition extensive flow visualisations were made with the 0.61 m vessel in order to establish both liquid and particles flow patterns during the experiments.

Results from this study were compared with previous publications in order to examine the effects of some of the important geometrical variables on solids suspension and distribution. This work revealed that for the range of parameters covered, the smallest (D/T=0.3) and the largest (D/T=0.6) impellers are the most and least efficient ones for solids suspension. Distribution tests with the three geometrically similar impellers show that the results are neither correlated in terms of tip speed nor power input but are best described by the thrust force generated by the impellers. In general, dual impeller systems improve solids distribution but require more power to just suspend solids compared with a single impeller. The scaling effect proposed by Zwietering (1958) for solids suspension has been confirmed by this study for vessel up to 2.67 m in diameter. The constant tip speed rule for solids distribution, which is based on one-dimensional dispersion models was found to underestimate the power requirement in large scale applications. This study indicates that equal power per unit volume is required to achieve the same degree of homogeneity.

ACKNOWLEDGEMENTS

I am most grateful to my colleagues, Mr Robert Burnapp and Mr Kevin Lee, who proof read this thesis. They have been a constant source of help, support and inspiration during all these years in BHR Group Ltd, without them completion of this thesis would not have been possible.

Thanks are also due to:

My brothers and sister; Yan, King and Kin for sharing out my house duties and keeping my parents company while I was abroad.

My friends and colleagues; Lorna Brooker, I S Fan, Emily and Jack Ho, Steve and Marie-Ann Hobbs, Maha Soundra-Nayagam, Trevor Sparks, Mike Whitton and Ming Zhu for their encouragement and interest in this work.

Fred and Theresea Haines for providing me with a nice comfortable home.

My industrial supervisor, Andrew Green, for his moral support.

The author also wishes to thank the members of the Fluid Mixing Processes Consortium for their permission to publish part of the generic research results.

Finally, my deepest gratitude to my supervisor, Dr P Ayazi Shamlou, for his enthusiasm, guidance and friendship, from whom I have learnt so much.

Human kind cannot bear much reality T. S. Eliot

Dedicated to my parents to whom I owe so much that can never be repaid

All this I tested by wisdom and I said, "I am determined to be wise" - but this was beyond me. Whatever wisdom may be, it is far off and most profound - who can discover it? So I turned my mind to understand, to investigate and to search out wisdom and the scheme of things and to understand the stupidity of wickedness and the madness of folly.

Ecclesiastes 6: 23-25

子亮我兒勉之

遠涉重洋

成就一番事業

放眼宇宙

力求世界大同

父大江壬申年四月初八日

九二年五月一日

LIST OF CONTENTS

Appendices

NOMENCLATURE

Symbol	Meaning	Units
A	A Calibration Constant	-
a	A Parameter	-
A_i	A Constant	-
A_{min}	A Parameter Which Depends on Impeller Type	-
A_p	Projected Area of the Particle	m^2
B_{js}	A Critical Constant for Just Suspension Condition	-
C	Impeller Bottom Clearance	m
c	A Parameter	-
C_D	Drag Coefficient	-
C_{ij}	Local Solids Distribution at i^{th} Speed and j^{th} Position	-
C_L	Lift Coefficient	-
C_M	Mean Volume Fraction of Solids	-
C_t	Top Impeller Clearance in Dual Impeller Systems	m
C_v	Volume Fraction of Solids	-
C_z	Mean Volume Fraction of Solids across Height z	-
D	Impeller Diameter	m
$D_{e,l}$	Liquid Diffusion Coefficient	$m^2\ s^{-1}$
$D_{e,p}$	Particle Dispersion Coefficient	$m^2\ s^{-1}$
d_p	Particle Diameter	m
d_p^*	A Normalised Particle Diameter	-
F	Thrust Force Generated by an Impeller	N
F_B	Buoyancy Force Acting on the Particle	N
F_D	Drag Force Acting on the Particle	N
F_L	Lift Force Acting on the Particle	N
F_W	Effect Weight of Particle	N
g	Gravitational Acceleration	$m\ s^{-2}$
H	Height of Slurry	m
h	Height of Clear Liquid/Solid-liquid Interface	m
H_h	Impeller Hub Height	m
H_{od}	Impeller Hub Outside Diameter	m

k	A Constant	-
K	A Parameter	-
L_e	Length Scale of Large Energy Containing Eddies	m
L_o	Length Scale of Small Eddies	m
L^*	Characteristic Linear Dimension	m
M	Mass of Slurry	kg
M_L	Mass of Liquid in Vessel	kg
M_S	Mass of Solids in Vessel	kg
N	Impeller Speed	rev s^{-1} (or rpm)
n	Number of Blades	-
N_{js}	Just Suspension Speed	rev s^{-1} (or rpm)
$N_{js,o}$	Just Suspension Speed by Visual Observation	rev s^{-1} (or rpm)
$N_{js,u}$	Just Suspension Speed by Ultrasonic Doppler Flowmeter	rev s^{-1} (or rpm)
n_p	Number of Particles	-
P	Power	W
P_i	Power Index ($P_i = Po\ s^3\ D^{2.45}$)	$m^{2.45}$
P_{js}	Power Drawn by Impeller at N_{js}	W
Po	Power Number ($Po = P/\rho\ N^3\ D^5$)	-
Po_c	Combined Power Number in Multiple Impeller Systems	-
r	Correlation Coefficient	-
RSD	Relative Standard Deviation of Solids Concentration	-
s	Geometrical Constant in Zwietering Correlation	-
s_1	Modified Geometrical Constant	-
T	Vessel Diameter	m
u	Linear velocity	m s^{-1}
u_{al}	Axial Component of Local Velocity of Liquid at Point of Incipient Particle Motion	m s^{-1}
U_{fo}	Mean Upward Velocity Outside the Fictitious Tube	m s^{-1}
U_{fz}	Eulerian Velocity of Fluid at z Direction	m s^{-1}
U_m	Mean Liquid Velocity near the Base of Vessel	m s^{-1}
U_{pz}	Eulerian Velocity of Particles at z Direction	m s^{-1}
U_{rl}	Radial Component of Local Velocity of Liquid at Point of Incipient Particle Motion	m s^{-1}
U_s	Terminal Velocity of Particles in a Swarm	m s^{-1}

U_t	Terminal Velocity	m s^{-1}
U_{to}, U_{tt}	Terminal Velocity at Stagnant and Turbulent Medium	m s^{-1}
U_τ	Shear Stress Velocity	m s^{-1}
U_∞	Maximum Fluid Velocity Close to the Boundary Layer	m s^{-1}
V	Volume of the Slurry	m^3
v'	Fluctuating Velocity of the Critical Eddies	m s^{-1}
V_r	Mean Radial Velocity	m s^{-1}
V_z	Mean Axial Velocity	m s^{-1}
W	Blade Width	m
W_p	Projected Blade Width	m
X	Percentage Mass Ratio of Solids to Liquid in Suspension	-
Z	A Constant	-
z	Cartesian Coordinate in Axial Direction	m
α	Blade Angle to Horizontal	-
β	A Constant	-
γ	A Constant	-
γ_B	Characteristic Shear Rate at Vessel Base	s^{-1}
ΔP_i	Static Pressure Difference Inside Impeller Region	N m^{-2}
ΔP_o	Static Pressure Difference Outside Impeller Region	N m^{-2}
ΔP_{stat}	Static Pressure Difference	N m^{-2}
ε_m	Power per unit Mass	W kg^{-1}
ε_p	Power Dissipation for Entrainment of Single Particle	W m^{-3}
ε_t	Total Power Dissipation for Complete Suspension	W m^{-3}
ε_v	Average Power per unit Volume	W m^{-3}
ε_{vb}	Power per unit Volume near the Vessel Base	W m^{-3}
ζ	A Proportionality Constant	-
η_t	Characteristic Eddy Scale	m $s^{-1/4}$
κ_c	Corrected Conductivity	microsiemens
κ_m	Measured Conductivity	microsiemens
κ_{om}	Conductivity of Water at Measured Temperature	microsiemens
κ_{or}	Conductivity of Water at Reference Temperature	microsiemens
χ	Blade Thickness	m
ρ	Density	kg m^{-3}
ρ_{av}	Average Density of Vessel Contents	kg m^{-3}

ρ_L	Density of Liquid	kg m^{-3}
ρ_S	Density of Solids	kg m^{-3}
σ_{n-1}	Standard Deviation	-
τ	Torque	N m
τ_w	Wall Shear Stress	N m^{-2}
μ	Dynamic Viscosity	kg m^{-1} s^{-1}
ν	Kinematic Viscosity	m^2 s^{-1}
ϕ_{av}	Nondimensional Group for Pumping Characteristics	-
ϕ_o, ϕ_t	Particle Resistance Coefficient for Free Fall at Stagnant and in Turbulent Medium	-
ψ_{av}	Nondimensional Group for Pumping Characteristics	-

Dimensionless Groups

Ar	Archimedes Number	$\frac{g\,\Delta\rho\,d_p^3}{\nu^2\,\rho_L}$
Eu_{fl}	Euler Number for Particulate Fluidisation	$\frac{4\,\Delta\rho\,d_p\,g\,(1-C_v)^2}{3\,\rho_L\,U_{fo}^2}$
Fl	Flow Number	$\frac{Q}{N\,D^3}$
Fr	Froude Number	$\frac{N^2\,D}{g}$
Fr^*	Modified Froude Number	$\frac{N^2\,D^2\,\rho_L}{d_p\,\Delta\rho\,g}$
Ft	Thrust Number	$\frac{F}{\rho\,N^2\,D^4}$
Pe	Peclet Number	$\frac{U_s\,H}{D_{ep}}$
Pe^*	Modified Peclet Number	$\frac{U_{to}\,L^*}{D_{ep}}$
Po	Power Number	$\frac{P}{\rho\,N^3\,D^5}$
Re	Reynolds Number	$\frac{\rho\,u\,d}{\mu}$
Re_i	Impeller Reynolds Number	$\frac{\rho\,N\,D^2}{\mu}$
Re^*	Modified Reynolds Number	$\frac{N\,D^3}{\nu\,T}$
Re_τ	Reynolds Number for Shear Stress	$\frac{d_p\,U_\tau}{\nu}$

CHAPTER 1: INTRODUCTION

1.1 BACKGROUND

Mixing is one of the most widely used unit operations in the chemical and allied industries. There is a general acceptance of the importance of mixing processes for the commercial success of industrial operations. In 1989 during a workshop conducted by the Mixing 3A of AIChE (Mixing 3A 1989), it was found that in many case studies presented, the monetary values of the solutions to the particular problems represented a saving in the region of $0.5 to $5M. Increasing process yields, avoiding the need for expensive and prolonged pilot plant development together with improved exploitation times in bringing new products onto the market, might represent a monetary value in the region of 1 to 3% of turnover for the chemical process industries, which for the USA was around $10 bn per year in 1989.

A stirred tank unit typically consists of a rotating impeller in a vessel. Fluid motion is promoted by the transfer of energy from the impeller into the process fluid. The process fluid may be single phase (eg viscous, Newtonian and non-Newtonian) or multiple phases (eg solids, liquid and gas) and, in some cases, physical changes may take place during the operation (eg suspension polymerisation and dissolution of solids in liquid).

Mixing processes are usually classified according to the type of the process materials, eg viscous liquid, solid-liquid, gas-liquid, liquid-liquid, etc, and of these, solid-liquid is certainly one of the most important. This has been highlighted in the survey conducted by the Mixing 3A Workshop which found that 80% of the chemical products made involved solid-liquid processing.

The main objectives of agitation in solid-liquid systems can be divided into three categories;

a) to avoid solids accumulation in a stirred tank
b) to maximise the contacting area between the solids and liquid
c) to ensure the solids particles are uniformly distributed throughout the vessel

In many operations, it is essential to ensure that all the solids are kept in motion in order to prevent the building up of solids on the vessel base which may, in extreme cases, invoke system malfunction. Examples of such operations include settling tanks for filter cakes and absorber sump of a flue gas desulphurisation process. The stirred tank may also be used as a reactor, for example when catalysts are to be suspended for mass transfer operations. The mass transfer rate per unit energy input is at its maximum when the interfacial area between the solids and liquid is maximised. This happens when the fluid motion is vigorous enough to keep all particles in motion (i.e. at N_{js}, Fig 1.1.1). Even though the design objectives for (a) and (b) set out to achieve different goals, both require good knowledge of the just suspension speed (N_{js}) prediction, that is the impeller speed at which no solid particle rests on the vessel base.

However operating the stirred vessel at the just suspension condition may not be sufficient in certain processes. For example, the ratio between the mean solids concentration in the vessel and that in the withdrawal tube depends on the position of the tube thus, solids distribution information is required to ensure good mass balance between inward and outward flow in a continuous stirred tank reactor. Sometimes the product characteristics depend on the distribution quality, knowledge of which is then becomes vital for quality control.

In this work, flow pattern, power consumption, solids suspension and distribution for a wide range of geometries and scales were investigated.

1.2 RESEARCH NEEDS FOR SOLID-LIQUID MIXING

The Zwietering correlation (1958) is generally being accepted as the best correlation for just suspension prediction for low viscosity systems. This empirical correlation is based on more than a thousand experiments together with dimensionless analysis. However, there are a number of other correlations which are different and, in some ways, contradictory to Zwietering (eg effect of particle size and scale) and most of them have their own experimental data to back them up. Unfortunately, the discrepancies between many of these correlations are large.

Most of the contradictions are believed to be caused by a lack of understanding of the suspension mechanism and reliable large scale data which can be used to verify existing

models. Some of the assumptions adopted in establishing the theoretical models bear little resemblance to the actual suspension mechanisms. Therefore, more detailed observations of particle flow patterns would help to clarify this point. Scale-up data in literature is inadequate and extrapolation beyond the experimental range can be disastrous. For the just suspension conditions, published literature recommended $\varepsilon_v \propto T^n$ with n ranging from 0.5 (eg Kneule 1967) to -1 (eg Bourne 1974) (ε_v = power per unit volume, T = tank diameter). For 100-fold change in scale, the two extremes give 1000-fold difference in power requirement prediction. An incorrectly sized mixing vessel could cause shut down of the whole plant and millions of pounds in lost production. Large scale data is urgently needed to verify the scale-up rules and the data should shed light on the validity of various models.

Another important feature for the evaluation of solid-liquid mixing performance is the distribution of solids throughout the vessel. However, quantitative information in this area is limited and mostly are confined to low concentration in small vessels. The distribution of solids in an agitated vessel is a rather complex function of the velocity field, distribution of turbulence and solid-liquid interaction. Progress has been hampered by the difficulties in establishing a reliable measuring technique to be used in a wide range of geometrical set-ups which can provide useful information for modelling.

In the past agitation units were often greatly over-specified, in order to accommodate for the uncertainty in design. This may lower the yield (eg side reactions) and quality (eg particles breakage in crystallisation) of the desirable product. In additional, over-specification may lead to extra initial and operating costs. Apart from that, treatment of undesirable products means extra production cost.

1.3 AIMS, APPROACH AND THESIS LAYOUT

This thesis is an experimental study of solid-liquid mixing in mechanically agitated vessels. It is confined to the mixing of sinking particles with water in the turbulent regime. All impellers tested are downwards pumping unless otherwise stated. This is because over 95% of solid-liquid mixing processes use downwards pumping impellers. Upward pumping is employed only if other design constraints have to be imposed, such as gas dispersion in a 3-phase (solid-liquid-gas) reactor, and this is out of the scope of this thesis. This work has the following objectives:

To obtain an insight into the hydrodynamic conditions which govern the suspension and distribution of solid particles in mixing vessels.

To gain an understanding of the effects of some of the more important system parameters (eg geometric scale) on solid-liquid mixing.

To utilise the qualitative and quantitative information obtained, together with theoretical understanding to formulate and/or refine the existing models.

This work commences with a literature survey on solids suspension and distribution models (Chapter 2). Mathematical models developed in the literature to interpret the two phase flow mechanisms in stirred vessels are compared and contrasted. The survey highlights areas which demand more research effort and the type of measurements which ought to be made in order to verify/improve some of the existing models (eg particle flow pattern near the just suspension condition).

Chapter 3 describes the test facilities, methods and various physical and geometrical parameters that were encompassed in this programme. Three types of measurements were made in this work, namely just suspension speed (N_{js}), shaft torque for power calculation (τ) and local solids concentration at i^{th} speed and j^{th} position (C_{ij}). Extensive flow visualisations were made during the experiments to aid interpretation of the results. The selection and verification of reliable and consistent methods for solids suspension and distribution measurements across a wide range of scale and geometries constitute a very important part of this thesis. The development and calibration of ultrasonic and conductivity techniques are also presented in Chapter 3.

In Chapter 4, the effects of the experimental parameters on flow pattern, N_{js} and C_{ij} are investigated. Four major geometrical effects were included in this study namely, the scale of equipment, number of impellers, impeller to tank diameter ratio and pitch angle of the turbines. They were chosen because of their importance and the lack of conclusive information in the literature. The results are analysed and compared with data from previous studies. Information obtained from the experiments is also utilised to verify/refine the existing models. A common criticism of the literature is that too many papers have based their models on small scale work (eg $\leq$ 0.3 m vessel). The correlations so developed to a large extent

contradict each other. One of the major tasks of this work is to validate the correlations by conducting a series experiments in four geometrically similar vessels (T = 0.31 to 2.67 m).

The final chapter (Chapter 5) draws together the major conclusions and recommendations for future work are made. Most of the suspension data are presented within the text of the thesis but, due to spatial considerations, distribution data are included in the appendices.

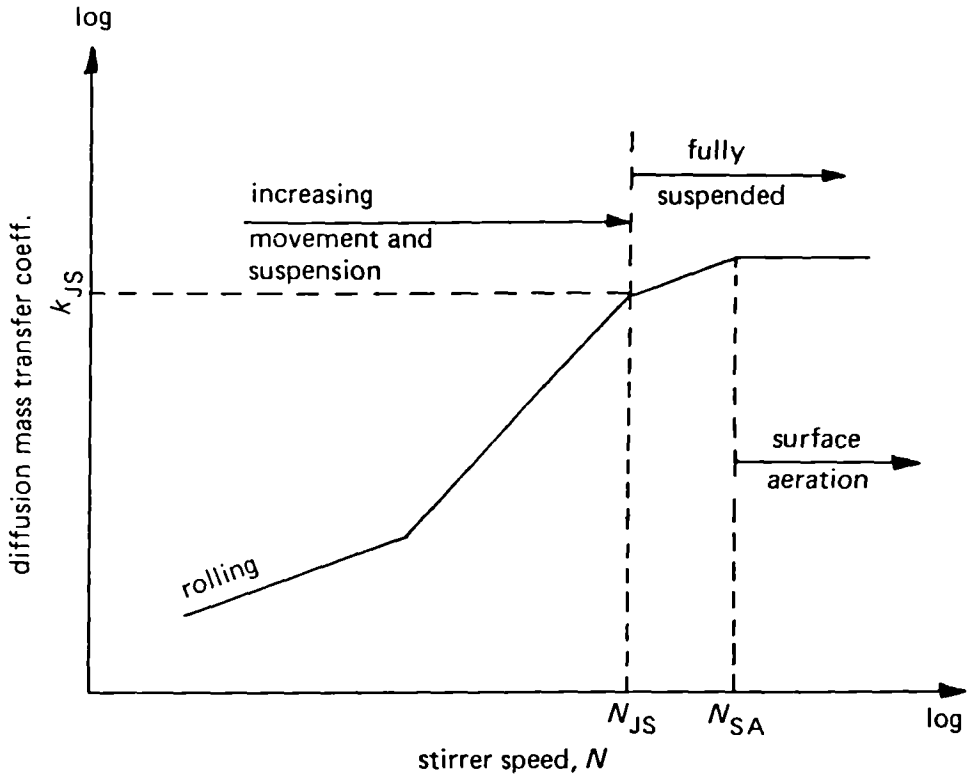

Fig 1.1.1 Mass Transfer Coefficient over Wide Range of Stirrer Speeds (Harnby et al 1985)

CHAPTER 2 : LITERATURE SURVEY

There are three objectives to this chapter. It generalises the present state of the art in understanding and designing a solid-liquid agitated vessel. It compares and contrasts the various mathematical models so developed to interpret the various phenomena taking place in the vessel. Furthermore, scaling up implications as well as particle-fluid mechanisms are commented upon in this section.

Solid-liquid mixing phenomenon in stirred vessels can be categorised into two regimes, namely solids suspension and distribution. Solids suspension is concerned with the last suspended particles on the vessel base and thus would be very geometry dependent, compared to solids distribution in which the bulk mixing of the vessel contents has to be taken into consideration. However, solids suspension and distribution are related, a solid particle has firstly be lifted by the fluid (suspension) before distributed into the bulk of the vessel contents (distribution).

2.1 SOLIDS SUSPENSION

2.1.1 Zwietering's Empirical Correlation (1958)

Zwietering published a classical paper on solids suspension in 1958 in which he adopted a rigid definition for the determination of just suspension speed (N_{js}). He defined this as being the minimum stirring speed at which no solid particle remains stationary on the vessel base for more than one to two seconds and claimed that this could be measured within an accuracy of 2 to 3%. This helped to bring many solid-liquid mixing research techniques together, as confusion had arisen in the past when researchers had not used a common N_{js} definition that would allow results to be compared.

He conducted more than a thousand experiments on vessels with diameters ranging between 0.15 and 0.60 m. A variety of impellers were used: 2-bladed paddles, 6-bladed disc turbine, vane disc and marine propeller. Sand and sodium chloride were used as the test solids and he covered concentrations between 0.5 and 20% by weight with particle sizes between 125 and 850 μm in three relatively narrow size distributions. By using different fluids, a liquid density range of 790 to 1600 kg m^{-3} and a viscosity range of 0.31×10^{-3} to

9.3×10^{-3} Pa s were covered.

Zwietering proposed a list of 10 factors to determine the suspension of solid particles in stirred vessels :

T	vessel diameter
C	distance between stirrer and vessel base
D	stirrer diameter
N	stirrer speed
d_p	particle size
ρ_S	density of solids
ρ_L	density of liquid
ν	kinematic viscosity
X	percentage mass ratio of solids to liquid in suspension
g	acceleration due to gravity

Following a dimensional analysis, a set of seven dimensionless groups were obtained:

T/D, T/C, D/d_p	geometrical ratios
$N D^2/\nu$	Reynolds number
$N^2 D/g$	Froude number
ρ_S/ρ_L	density ratio
X	solids concentration weight percentage ratio

The following relationship was obtained by analysis of the experimental data:

$$\left(\frac{N D^2}{\nu}\right)^{0.1} \left(\frac{\rho_L N^2 D}{g \Delta\rho}\right)^{0.45} \left(\frac{D}{d_p}\right)^{0.2} = K \left(\frac{T}{D}\right)^{\alpha} X^{0.13} \qquad \text{...eqn(2.1.1)}$$

The constant K and the exponent α depend on the type and position of the stirrer and the above equation can be rewritten as :

$$N_{js} = s\, \nu^{0.1} \left(\frac{g \Delta\rho}{\rho_L}\right)^{0.45} d_p^{0.2}\, X^{0.13}\, D^{-0.85} \qquad \text{...eqn(2.1.2)}$$

The parameter "s" in eqn 2.1.2 is the geometrical constant and it is a function of the vessel and impeller configuration.

The Zwietering correlation is widely used for estimation of the just suspension speed. Its advantage is that it was based on a very large number of experiments and is dimensionless but, because it is an empirical correlation, it should not be applied outside its test range. Even though it has been re-confirmed by a number of researchers (eg Chapman 1981, Nienow 1968), the range of test parameters are still limited. So, it would be useful to expand the experimental conditions to discover under what circumstances this correlation would become invalid.

Zwietering used a mass ratio, X, defined as the percentage mass of solids to liquid in the vessel, to quantify the solids concentration but one would expect volume fraction to be a better parameter to account for the fluid-particle effects.

2.1.2 Baldi et al Turbulence Model (1978)

Baldi et al (1978) postulated that the suspension of particles is mainly due to eddies of size similar to that of the particle diameter, and the energy transferred by these eddies to the particles is able to lift them to a height of the order of the particle diameter.

By performing an energy balance on the basis that kinetic energy imparted by the eddies is proportional to the potential energy gained by the particle, they showed:

$$\rho_L \, v'^2 \propto d_p \, \Delta\rho \, g \qquad \text{...eqn(2.1.3)}$$

where v' is the fluctuating velocity of the critical eddies

If the scale of the critical eddies is much higher than that of the eddies which dissipate their energy by viscous forces, and isotropic turbulence is assumed:

$$v' \propto \left(\frac{\varepsilon_{vb} \, d_p}{\rho_L} \right)^{1/3} \qquad \text{...eqn(2.1.4)}$$

Schwartzberg and Treybal (1968) showed that the mean turbulent velocity in a stirred vessel can be expressed by the above equation, even if the turbulence is anisotropic.

Baldi et al (1978) went on to assume that the local dissipated power per unit volume near the tank bottom (ε_{vb}) could be approximated to the average dissipated power per unit volume, ε_v :

$$\varepsilon_v = \frac{4\ Po\ \rho_L\ N^3\ D^5}{\pi\ T^3} \qquad \text{...eqn(2.1.5)}$$

Combining equations 2.1.3, 2.1.4 and 2.1.5 :

$$Z = \left(\frac{\Delta\rho\ g}{\rho_L}\right)^{1/2} \left(\frac{T\ d_p^{1/6}}{Po^{1/3}\ D^{5/3}\ N_{js}}\right) = constant$$

From an analogy of the decay of turbulence behind a grid the authors deduced that:

$$Z = \left(\frac{\Delta\rho\ g}{\rho_L}\right)^{1/2} \left(\frac{T\ d_p^{1/6}}{Po^{1/3}\ D^{5/3}\ N_{js}}\right) = f\left(\left(\frac{D^3\ N_{js}}{\nu\ T}\right), \left(\frac{T}{D}\right), \left(\frac{C}{D}\right)\right) \qquad \text{...eqn(2.1.6)}$$

From experimental data at C/D=1, eqn 2.1.6 becomes:

$$N_{js} \propto \frac{\mu^{0.17}\ (g\ \Delta\rho)^{0.42}\ d_p^{0.14}\ T}{\rho_L^{0.58}\ Po^{0.28}\ D^{1.89}}\ X^{0.125} \qquad \text{...eqn(2.1.7)}$$

Assuming D/T and Po are constant:

$$N_{js} \propto \nu^{0.17} \left(\frac{g\ \Delta\rho}{\rho_L}\right)^{0.42} X^{0.125}\ d_p^{0.14}\ D^{-0.89} \qquad \text{...eqn(2.1.8)}$$

It was found that Z, as defined in equation 2.1.6 is a function of ($\varepsilon_{vb}/\varepsilon_v$) and was independent of the modified Reynolds Number, Re^* (= $D^3N/\nu T$) when C/D was low. Under this condition, the bottom zone of the tank is swept by the discharge flow from the impeller. In other cases the value of ($\varepsilon_{vb}/\varepsilon_v$) decreases as C/D increases, and increases with Re^*.

The semi-theoretical model (eqn 2.1.8) was verified by Conti and Baldi (1978) in a variety of flat bottomed tanks equipped with baffles; tank diameter varied between 0.122 and 0.229 m. The impellers used were 8-bladed disc and axial turbines. Seven classes of sand (42-540 μm) and nine classes of ballotini (97-1200 μm) were tested. Both mono-modal and bi-modal particle size distributions were employed.

The conclusion was drawn that the effect of particle size on N_{js} is $N_{js} \propto d_p^a$, where the value of 'a' is between 0.14 and 0.16. However, they commented that particles with $d_p < 200$ μm generally do not follow their model and suggested that the smaller particles are subject to a different suspension mechanism as yet not fully understood. Their results also suggested a strong clearance effect, and the exponents on eqn 2.1.8 will change with C/D. It is very likely that the solids suspension mechanism involves more than one hydrodynamic regime and that these are a function of the geometrical configuration.

The authors justified their application of turbulent theory to solids suspension by arguing that the solid particles can be seen to be periodically picked up and re-deposited on the vessel base, a phenomenon difficult to explain using the alternative average velocity theory. Although this is a reasonable assumption, turbulence cannot be solely responsible for the suspension of solids. This has been demonstrated by filming of the suspension phenomenon in a viscous fluid (Shamlou 1991).

The reasoning that suspension of particles is mainly due to eddies of a certain critical scale is also somewhat arguable. It is quite correct to say that eddies of smaller size than the critical one do not possess enough energy to move particles from rest. However, despite the fact that large scale eddies have frequencies lower than those of critical size and have a lower probability to "hit" and suspend the particle, there is no reason why a large eddy (i.e. a vortex) could not generate enough pressure difference to entrain particles within the vortex itself. Remember, in autumn, it is not uncommon to see dead leaves being picked up from the ground by vortices. Rotating vortices beneath an impeller have been observed (Tatterson 1980). During a three phase mixing study in a 2.1 m diameter vessel with side entering mixers, Mak (1990) found that the vortices close to the vessel base are the primary vehicle responsible for the suspension of solids and they are related to the vortices on the water surface.

In the turbulence model, eddies are thought to be the primary means of getting the solids suspended and the intensity of turbulence within the reactor is a function of power dissipation per unit volume. Therefore, if turbulence is solely responsible for the lifting up of solid particles, one would expect a constant power per unit volume scale-up relationship as proposed in eqn 2.1.7 (i.e. $N_{js} \propto D^{-0.67}$). However, after incorporating the experimental data into eqn 2.1.7, the authors proposed a scale-up relationship of $N_{js} \propto D^{-0.89}$, which lies between the constant power per unit volume and constant tip speed criterion. This casts doubt on their assumption that particles are solely picked up by turbulence.

2.1.3 Mersmann et al Two Basic Laws of Solids Suspension (1985)

Mersmann et al (1985) suggested that the mean specific power input (P) is dissipated into the vessel by two superimposed processes :-

(i) The consumption of power to counteract the sinking of the particles in order to avoid settling.

(ii) The generation of the discharge flow rate in the vessel so as to generate off-bottom suspension.

The 'to avoid settling' law is valid for small particles in a large vessel where the impeller has only to produce a mean upstream velocity greater than the settling velocity of the particles. By equating the two velocities, the stirrer speed which is necessary to avoid settling can be given as a constant modified Froude Number (Fr^*);

$$Fr^* = \frac{N^2 D^2 \rho_L}{d_p \Delta\rho g} = constant \qquad \text{...eqn(2.1.9)}$$

$$\text{Hence} \quad N_{js} \propto \left(\frac{g \Delta\rho}{\rho_L}\right)^{0.5} d_p^{0.5} D^{-1} \qquad \text{...eqn(2.1.10)}$$

This suggests a constant tip speed rule for solids suspension scale-up. It is interesting to note that eqn 2.1.9 is exactly the same as Buurman's modified Froude number model for

solids distribution (eqn 2.2.26, Buurman 1985), even though the two authors were adopting different approaches and trying to describe different mixing phenomena (Sec 2.2.3).

When suspending large particles, the authors suggested that the stirrer has to provide sufficient kinetic energy in the liquid to compensate for the difference between potential energy of the deposited solids and for homogeneous suspension.

$$Fr^* = \frac{N^2 D^2 \rho_L}{d_p \Delta\rho g} = \frac{T}{d_p} \qquad \text{...eqn(2.1.11)}$$

$$\text{i.e. } N_{js} \propto \left(\frac{g \Delta\rho}{\rho_L}\right)^{0.5} D^{-0.5} \qquad \text{...eqn(2.1.12)}$$

Eqn 2.1.12 suggests power input per unit volume has to be increased with scale in order to maintain the solids in suspension.

To establish when the power input was being consumed to counteract the sinking of the particle in order to avoid settling, as opposed to the circumstances when it was generating discharge flow in the vessel to get off-bottom suspension, the authors used a characteristic diameter ratio $(d_p/T)^*$ to distinguish between these two basic suspension mechanisms. The ratio is a function of settling velocity, discharge coefficient, solids volume fraction, porosity and the liquid depth to tank diameter ratio. If the real diameter ratio (d_p/T) is smaller than its characteristic diameter ratio, it is relevant to assume avoidance of settling. On the other hand, the off-bottom suspension law should apply if $(d_p/T) > (d_p/T)^*$.

This hypothesis was verified with a T/3 diameter marine-type propeller with a particle diameter ratio $10^{-5} \leq (d_p/T) \leq 10^{-1}$ (Mersmann 1985). The transition point between the two basic suspension laws was found to be at $(d_p/T) \approx 10^{-3}$, which agreed well with Ditl's transition region of $4.05 \times 10^{-3} \leq d_p/T \leq 1.7 \times 10^{-2}$ (Ditl 1985).

In a subsequent paper Voit and Mersmann (1986) claimed that the Fr^*=constant relationship (eqn 2.1.9) for small particles was confirmed experimentally for an agitated vessel

with T = 14 m with a d_p/T ratio of 7×10^{-6}. By plotting the ratio of Froude number as a function of the diameter ratio, they showed that a number of other researchers' results could fit into their model very well (Fig 2.1.1). However, based on the plots in the paper, the validity of this could not be substantiated.

2.1.4 Shamlou and Zolfagharian's Average Velocity Model (1987)

Shamlou and Zolfagharian (1987) proposed a model for the estimation of the necessary conditions for the incipient motion of particles, which was based upon the average velocity of the fluid near the bottom of the tank and the hydrodynamic forces of lift, drag, buoyancy and gravity acting upon the particles resting at the tank base.

They suggested that at the point of dislodgement, assuming that all the forces are acting through the centre of mass of the particle, the moment of these forces about point 0 (Fig 2.1.3) must be zero, i.e.

$$xF_W - xF_B = yF_D + xF_L \qquad \text{...eqn(2.1.13)}$$

$$F_D = \frac{1}{2} C_D \rho_L U_m^2 A_p \quad \text{and} \quad F_L = \frac{1}{2} C_L \rho_L U_m^2 A_p \qquad \text{...eqn(2.1.14)}$$

$$\frac{\pi d_p^3}{6} (\rho_S - \rho_L) g = \frac{\pi \rho_L U_m^2 A_p}{2} (C_L + \zeta C_D) \qquad \text{...eqn(2.1.15)}$$

$$\text{i.e} \quad U_m \propto \left(\frac{g \Delta\rho d_p}{\rho_L (C_L + \zeta C_D)} \right)^{1/2} \qquad \text{...eqn(2.1.16)}$$

Shamlou (1990) refined the model by assuming that at the point of incipient suspension of a particle, the rate of dissipation of fluid energy for particle lift-off is due to and given by the total flow forces acting on the particle (Oroskar and Turian 1980).

$$\varepsilon_p = (F_L + F_D) U_{al}$$

$$\varepsilon_p = \frac{1}{2} \rho_L U_m^2 U_{al} A_p (C_L + \zeta C_D) \quad \text{...eqn(2.1.17)}$$

He further assumed that the total rate of energy dissipation, ε_t, required to entrain all the particles is proportional to the total number of particles, n_p, in the liquid. Since $U_{al} \propto U_m$, $A_p \propto d_p^2$ and $(C_L + \zeta C_D) \sim constant$, from 2.1.17 :

$$\varepsilon_t \propto \rho_L U_{al}^3 d_p^2 n_p \quad \text{...eqn(2.1.18)}$$

$$\varepsilon_t \propto \frac{\rho_L U_{al}^3 C_v T^3}{d_p} \quad \text{...eqn(2.1.19)}$$

From the power number relationship: $P = Po\ \rho_L N^3 D^5$

$$\varepsilon_{vb} = k P = k Po\ \rho_L N^3 D^5 \quad \text{...eqn(2.1.20)}$$

Since $U_{al} \propto U_{rl} \propto U_m$ and $\varepsilon_{vb} \propto \varepsilon_t$, combining eqn 2.1.16, 2.1.19 and 2.1.20:

$$N_{js} = A\ Po^{-1/3} \left(\frac{g\ \Delta\rho}{\rho_L} \right)^{1/2} d_p^{1/6} C_v^{1/3} T\ D^{-5/3} \quad \text{...eqn(2.2.21)}$$

This equation suggests a particle size effect of $d_p^{1/6}$ and a scale-up effect of $D^{-2/3}$ on N_{js} (assuming $D \propto T$), as compared to $d_p^{0.2}$ and $D^{-0.85}$ as proposed by the Zwietering correlation. The author confirmed his model by testing several 4-bladed pitched blade turbines in a 0.24 m diameter glass vessel. The particle diameters ranged between 175 and 3015 μm. Their results produced a value of N_{js} proportional to $d_p^{0.17} D^{-0.67}$ which is in good agreement with the theoretical model.

An important feature of Shamlou et al (1987, 1990)'s work is that their concise theoretical derivation is completely free from any experimental adjustment, therefore the validity of the model is not restricted by experimental conditions, as long as the underlying hypothesis is satisfied. To justify their average velocity model, Shamlou (1991) showed that solid particles can be lifted up by fluid velocity alone (in the absence of any turbulence).

Now the question is, could the solid particles be lifted up by turbulence or even a combination of both flow and turbulence? If so, should the exponent on D be different? It is interesting to note that the exponents on Shamlou and Zolfagharian's model are very similar to that of Baldi's, even though their initial assumptions differ. The exponent of -0.67 on D (constant power per unit volume) suggests that for whichever type of suspension mechanism is involved, its intensity is a function of power input.

2.1.5 Molerus and Latzel's Two Suspending Mechanisms (1987)

Molerus and Latzel (1987) suggested that the suspension of solid particles in a stirred vessel is governed by two different mechanisms, depending on the Archimedes number. The first one defines the complete suspension of fine grained particles ($Ar \leq 40$) being attained at sufficiently high shear stresses in the wall boundary layer of the vessel. The second criterion, generally applicable to coarse grained particles ($Ar > 40$), is based on an analysis of the pump characteristics of an agitated vessel.

(i) Fine Particles ($Ar \leq 40$)

The authors observed that the settling velocity of 66 μm glass ballotini suspended in water was almost two orders of magnitude lower than its circulation velocity in a 1.5 m diameter vessel. This leads to the conclusion that the region responsible for the complete suspension of the particle is the wall boundary layer of the vessel where the local fluid velocities are similar to the particle settling velocity.

They took the maximum fluid velocity U_∞ close to the boundary layer as a reference velocity. Measurements in three geometrically similar vessels (T = 0.19, 0.45 and 1.5 m) showed a linear dependence of U_∞ on the circumferential stirrer velocity (ie $U_\infty \propto N D$).

Close to the bottom of an agitated vessel, the streamlines are curved and flow is axisymmetric. The wall shear stress τ_w in the critical point is approximated by a plane turbulent boundary layer flow along a flat plate at a distance of T/2 from the leading edge of the plate.

This gives the shear stress velocity of:

$$U_\tau = \left(\frac{\tau_w}{\rho_L}\right)^{0.5} \qquad \text{...eqn(2.1.22)}$$

From the wall shear stress relationship described by Schlichting (1965)

$$U_\tau = 0.182\ \nu^{0.1}\ U_\infty^{0.9}\ T^{-0.1} \qquad \text{...eqn(2.1.23)}$$

In order to establish the flow forces exerted on particles settled in the boundary layer, the shear stress for a particle layer is assumed to cover the wall surface and hence;

$$\left(\frac{\pi\ d_p^2}{4}\right)\tau_w = \Delta\rho\ \left(\frac{\pi\ d_p^3}{6}\right) g \qquad \text{...eqn(2.1.24)}$$

$$\text{and } Re_\tau^2 = \left(\frac{d_p\ U_\tau}{\nu}\right)^2 \qquad \text{...eqn(2.1.25)}$$

Combining eqn 2.1.22, 2.1.24 and 2.1.25

$$Re_\tau^2 = \frac{2}{3}\left(\frac{d_p^3\ g}{\nu^2}\right)\left(\frac{\Delta\rho}{\rho_L}\right) = \frac{2}{3}\ Ar \qquad \text{...eqn(2.1.26)}$$

The above equation was confirmed with tests on various sizes of glass and steel beads ($34 \le d_p \le 1937$ μm), with a concentration range of 0.5 to 30% by volume, in geometrically similar vessels (T = 0.19, 0.45 and 1.5 m). Tap water and water/ethylene glycol mixtures were used as the test fluid. The experimental results agreed with the model in the regime $Ar \le 40$.

From equation 2.1.26;

$$U_\tau \propto \left(\frac{d_p\ g\ \Delta\rho}{\rho_L}\right)^{0.5} \qquad \text{...eqn(2.1.27)}$$

Substituting into equation 2.1.23;

$$U_{ss} \propto \left(\frac{d_p \, g \, \Delta\rho}{\rho_L} \right)^{0.56} \nu^{-0.11} \, T^{0.11} \qquad \text{...eqn(2.1.28)}$$

Since $U_{ss} \propto N \, D$, thus;

$$N_{js} \propto \left(\frac{d_p \, g \, \Delta\rho}{\rho_L} \right)^{0.56} \nu^{-0.11} \, D^{-1} \, T^{0.11} \qquad \text{...eqn(2.1.29)}$$

The above equation suggests a particle size effect of $N_{js} \propto d_p^{0.56}$ and a scale effect of $N_{js} \propto D^{-0.89}$ for geometrically similar vessels, but that just suspension speed is independent of solids concentration.

(ii) Coarse Particles (Ar > 40)

Molerus and Latzel (1987) also developed a criterion for predicting minimum speed for solids suspension for coarse particles, which was based on :

(i) An appropriate representation of the dependence of the drag on fluidised particles on the concentration and

(ii) An analysis of the pump characteristics of an agitated vessel, analogous to the theory of similarity of fluid-kinetic machines.

They started by assuming a fictitious tube of a diameter D around the impeller. Assuming complete fluidisation outside the impeller region, the static pressure difference required by the stirrer, ΔP_{stat} can be given by :

$$\Delta P_{stat} = \Delta P_o - \Delta P_i \qquad \text{...eqn(2.1.30)}$$

$$= [\, C_v \, \rho_S + (1-C_v) \, \rho_L \,] \, g \, H - \rho_L \, g \, H$$

$$\Rightarrow \Delta P_{stat} = C_v \, (\rho_S - \rho_L) \, g \, H \qquad \text{...eqn(2.1.31)}$$

Where ΔP_i and ΔP_o are the static pressure difference between the top and bottom, inside and outside the impeller region respectively.

From the Euler Number for particulate fluidisation :

$$Eu_{fl} = \frac{4}{3} \frac{\Delta\rho}{\rho_L} \frac{d_p\, g}{U_{fo}^2} (1-C_v)^2 \qquad \text{...eqn(2.1.32)}$$

$$Eu_{fl} = \frac{4}{3} \frac{\Delta P_{stat}}{\rho_L\, U_{fo}^2} \frac{d_p}{H} \frac{(1-C_v)^2}{C_v} \qquad \text{...eqn(2.1.33)}$$

and for constant Eu_{fl}, from eqn 2.1.32 :

$$U_{fo}^2 \propto \frac{\Delta\rho\; d_p\, g}{\rho_L} (1-C_v)^2 \qquad \text{...eqn(2.1.34)}$$

By comparing the flow in an agitated vessel with a pumping system, the authors generated two nondimensional groups to describe the pumping characteristics of two-phase flows in agitated vessels :

$$\phi_{av} = \frac{U_{fo}}{(1-C_v)\, D\, N} \qquad \text{...eqn(2.1.35)}$$

$$\psi_{av} = \frac{(1-C_v)^2\, \Delta P_{stat}}{[\,(1-C_v)\,\rho_L + C_v\,\rho_S\,]\, U_{fo}^2} \qquad \text{...eqn(2.1.36)}$$

Experiments were performed in two geometrically similar vessels (T=0.19 and 1.5 m) with marine propellers. Glass ballotini and iron particles of dimensional range 220 to 1900 μm were used. The solids concentration covered a range of 0.5 to 30% Vol.

It was found that $\phi_{av} \propto (\psi_{av})^{-2.77}$ for Ar > 40, hence :

$$\frac{(1-C_v)^2\ \Delta P_{stat}}{[\ (1-C_v)\rho_L + C_v\ \rho_S\ ]\ U_{fo}^2} \propto \left(\frac{U_{fo}}{(1-C_v)\ D\ N}\right)^{-2.77} \qquad \text{...eqn(2.1.37)}$$

Substituting ΔP_{stat} and U_{fo} and for a given scale, $(1-C_v)\ \rho_L + C_v\ \rho_S = constant$

$$N_{js} \propto \left(\frac{\Delta\rho\ d_p\ g}{\rho_L\ D^2}\right)^{0.5} \left(\frac{C_v\ H\ \rho_L}{d_p}\right)^{0.36}$$

$$\text{i.e. } N_{js} \propto (g\ \Delta\rho)^{0.5} \left(\frac{d_p}{\rho_L}\right)^{0.14} (C_v\ H)^{0.36}\ D^{-1} \qquad \text{...eqn(2.1.38)}$$

The above equation suggested the influence of particle size and scale on N_{js} were $d_p^{0.14}$ and $D^{-0.64}$. It is interesting to note that their effect of liquid density on N_{js} (i.e. $N_{js} \propto \rho_L^{-0.14}$) is much smaller than that are proposed by the other researchers. Moreover, the dividing criterion of Molerus's model (Archimedes Number) depends on densities, particle size and viscosity but not tank diameter as proposed by Mersmann nor power input as in Ditl's model. Influence of solids concentration is included in Molerus's model only when Ar > 40, for Ar ≤ 40, the authors observed no dependence of N_{js} on solids concentration.

2.1.6 Wichterle's Characteristic Velocity Model (1988)

Wichterle (1988) developed a theoretical model for solids suspension based on the comparison of the terminal settling velocity of a particle and the characteristic velocity of the agitated liquid around the particle at the vessel base. He suggested that the flow acting on a particle of diameter d_p lying on the bottom can be characterized by a velocity V_B (Fig 2.1.4) and $V_B = \gamma_B\ d_p$. If V_B is higher than the settling velocity of the particle (U_t), the particle will be suspended and thus, the suspension condition can be related by a critical value B_{js}, which is a function of particle shape;

$$B_{js} = \frac{\gamma_B\ d_p}{U_t} \qquad \text{...eqn(2.1.39)}$$

The relationship between the particle diameter and settling velocity was related by a semi-empirical correlation :

$$\frac{U_t\, d_p\, \rho_L}{\mu} = \frac{Ar}{(18 + 0.6\, Ar^{0.5})} \qquad \text{...eqn(2.1.40)}$$

He defined a normalised particle diameter, d_p^*

$$Ar = d_p^{*3} = \frac{d_p^3\, \rho_L\, g\, \Delta\rho}{\mu^2} \qquad \text{...eqn(2.1.41)}$$

From a laminar boundary layer of an impinging jet :

$$\gamma_B = N\, A_{min}\, Re_i^{0.5} \left(\frac{D}{T}\right)^2 \qquad \text{...eqn(2.1.42)}$$

Where A_{min} is a minimum value of a constant A, which is dependent on the geometrical configuration of the mixing vessel according to the author's electrodiffusion experiments. A_{min} is equal to 2.5 for disc turbines at T/3 clearance and 3.5 for 6-bladed pitched bladed turbines at T/2.5 to T/5 clearance.

Wichterle then introduced a dimensionless critical impeller speed for just suspension, N_{js}^*, where :

$$N_{js}^* = N_{js}\, \nu^{-1/9} \left(\frac{\rho_L}{g\, \Delta\rho}\right)^{4/9} D^2\, T^{-4/3} \qquad \text{...eqn(2.1.43)}$$

From equations 2.1.40, 2.1.42 and 2.1.43

$$N_{js}^* = \left(\frac{B_{js}}{A_{min}}\right)^{2/3} N_o^*\, d_p^* \qquad \text{...eqn(2.1.44)}$$

$$N_o^* = \left(\frac{d_p^*}{18 + 0.6\, d_p^{*3/2}}\right)^{2/3} \qquad \text{...eqn(2.1.45)}$$

The proposed correlation was verified by plotting other researchers' results in the format of N_{js}^* against d_p^* (Fig 2.1.2). From open publications (Einenkel 1980, Pavlushenko 1967, Rieger 1982, Staudinger, Tay 1984 and Zwietering 1958), a value of 10 ± 2 was estimated for B_{js}.

The author's model predicts that in the whole range of variables, a single-power function $N_{js} \propto D^{-2/3} (D/T)^{-4/3}$ applies (eqn 2.1.43), which suggests a constant power per unit volume scale up rule. However, influences of other parameters (d_p, μ, ρ_L and $\Delta\rho$) on N_{js} are a function of the normalised d_p, i.e. $Ar^{1/3}$ (eqn 2.1.41). A single power law relationship will be given for a constant Ar. Work conducted by other researchers had already suggested that the effect of particle size on just suspension speed is not a simple single power law relationship, but divided by critical values, which could be a function of Ar (Molerus 1987, Rieger 1982). Wichterle further proposed that there were not just two different exponents on d_p, but a continual variation of exponents both on d_p and other parameters.

The scale-up rule of $D^{-2/3}$ on just suspension speed is somewhat questionable. The reasons are two fold; firstly, the author did not deduce the scale-up relationship theoretically but instead, assumed a dimensionless critical speed (eqn 2.1.43) for solids suspension without proof. Secondly, the other researchers' data with which the author tested his model were all obtained from a rather limited range of vessel sizes. If the particle is being picked up by flow rather than turbulence as the author suggested, one would expect scale-up to be more likely to be governed by constant tip speed criterion.

2.1.7 Other Models

Narayanan et al (1969) derived an expression for N_{js} based on a balance of the vertical forces acting on a particle. It was assumed there was no slip between the particle and the fluid, the fraction of solids inside the agitated vessel was very low compared to the bulk volume of the liquid and that the solids were uniformly dispersed throughout the liquid. The necessary knowledge of fluid velocities was obtained from the mean circulation time data produced by Holmes et al (1964) without taking account of the local conditions on the vessel base where suspension occurred. By equating the circulation time constant with the flow pattern and correlating for the discrepancy between the experimental and theoretical results;

$$N_{js} = 1.782\ X^{-0.22}\ (\frac{T}{D})^2\ (\frac{1}{2T-D})\left((2\ g\ \Delta\rho)\ [\frac{2d_p}{3\rho_L} + \frac{H\ X}{100\ (\rho_S + X\ \rho_L)}] \right)^{0.5}$$

...eqn(2.1.46)

Although the above equation showed very good agreement with the experimental results, its fundamental assumptions were somewhat questionable and its range of application should thus be restricted to that within which the empirical constants were established. However, the approach adopted by the author does look somewhat more appropriate to describe the distribution of solids in a stirred vessel.

Subbarao and Taneja (1979) proposed a simplistic model based on a balance of the fluid velocity and particle settling velocity for a propeller agitated system. The particle settling velocity was estimated from a correlation for the porosity of a liquid fluidised bed as a function of liquid velocity. Their model indicated a negative exponent on d_p in all circumstances which is questionable.

Kolar (1961) proposed that the mixing energy at the critical condition can be related to the potential energy of the particles (i.e. power input equal to the effective weight of solids times the particle free falling velocity) and that the particle settling velocity is proportional to the impeller tip speed. The author tried to account for the effect of turbulent dissipation on the settling velocity by the relation;

$$\phi_i\ U_u^2 = \phi_o\ U_o^2 \qquad \text{...eqn(2.1.47)}$$

However, his assumption is too simplistic to describe the actual suspension phenomenon.

Ditl and Rieger (1985) utilised a similar turbulence concept to that of Baldi et al (1978), to model the suspension of solid particles. They suggested that particles were picked up by different sizes of eddies (primary, small and medium). If the particle size is comparable with the size of the eddies, the suspension mechanism is therefore governed by them. In other words, the suspension of larger particles is governed by the motion of primary eddies whereas the suspension mechanism for the smaller ones is determined by the small and medium eddies.

They postulated that the dividing criterion between different mechanisms can be defined by the relative size of particles to characteristic eddies. For the smaller particles the characteristic scale can be given as:

$$\eta_t = \left(\frac{\nu^3}{\varepsilon_m}\right)^{1/4} \qquad \text{...eqn(2.1.48)}$$

Thus $$\frac{d_p}{\eta_t} = \left(\frac{4\,Po}{\pi}\right)^{1/4}\left(\frac{d_p}{D}\right)\left(\frac{N\,D^2\,\rho_L}{\mu}\right)^{3/4}\left(\frac{T}{D}\right)^{-3/4} \qquad \text{...eqn(2.1.49)}$$

Results from thirty eight set of experiments were correlated, to evaluate the critical particle diameter. Based on statistical analysis :

$$Re_i \propto Ar^{0.45}\left(\frac{d_p}{T}\right)^{\beta}\left(\frac{T}{D}\right)^{-0.56} \qquad \text{...eqn(2.1.50)}$$

For large particles; $(d_p / \eta_t) \geq 32$, $\beta = -1.42$

$\Rightarrow N_{js} \propto d_p^{-0.07}$ and $D^{-0.58}$

For small particles; $(d_p / \eta_t) < 32$, $\beta = -1.25$

$\Rightarrow N_{js} \propto d_p^{0.1}$ and $D^{-0.75}$

The authors conducted their tests in 0.15-0.4 m vessels and covered a much wider range of particle sizes (85-4000 μm) than Zwietering and Baldi. The exponents of d_p for small particles were lower than those of Baldi et al's. Even though the two models seem to be based on similar theories, Baldi also introduces empirical reasoning to adjust the exponents on d_p and X. Ditl et al do not use their experimental data to correct their model and therefore their model is in a way more absolute than Baldi's. Once again, the negative exponent of d_p for large particles looks very doubtful. The scale-up factor of -0.58 for large particles implying the power per unit mass has to be increased with scale is very suspicious. It is also interesting to note that the authors' model does not account for the effect of solids concentration.

Musil and Vlk (1978) based their theory on the balance of the liquid and particle kinetic energies, which was very similar to Kolar's initial assumption. Their results were expressed in the form of a critical Reynolds Number, which is a function of Archimedes and Particle Reynolds Number. However, their mathematical reasoning for the derivation is impossible to follow. It has been pointed out that there are a number of mistakes in Musil's physical assumptions and mathematical treatment (Ditl 1980).

Buurman et al (1985) employed a similar hypothesis to that of Baldi et al, relating the kinetic energy of the eddies to the potential energy of the particles;

$$\rho\, v'^2\, d_p^3 \propto g\, \Delta\rho\, d_p^4 \qquad \text{...eqn(2.1.51)}$$

The equation led to the form of a modified Froude Number, which suggests a constant power per unit volume scale-up relationship;

$$\frac{\rho_L\, N_{js}^2\, D^{4/3}}{g\, \Delta\rho\, d_p^{1/3}} = constant \qquad \text{...eqn(2.1.52)}$$

2.1.8 Summary of the Suspension Models

According to the suspension mechanisms, the theoretical models which have been reviewed so far can generally be classified into two categories; namely those in which particles are believed to be picked up by turbulent eddies (eg Baldi 1978, Ditl 1985) and those in which particles are believed to be picked up by fluid flow (eg Shamlou 1987, Wichterle 1988). There is a third category in which the suspension model is not based on an independent mechanism but is simulated by another phenomenon of which the researchers had more modelling experience, such as pump flow or fluidisation (Molerus 1987). This section will compare and contrast models derived from the first two categories, as they gave a better fundamental understanding of the suspension mechanism as compared to the simulation models.

The proposed turbulence models argue that the solid particles are being periodically picked up and re-deposited on the vessel base, an observation difficult to explain by the

average velocity concept. However, the turbulence models on their own cannot explain why axial flow impellers, which have a lower power number than their radial flow counterparts and hence, a lower level of turbulence, are nevertheless able to suspend solids at a lower energy input, bearing in mind that an axial flow impeller is generally flow dominated. Moreover, Al-Dhahir (1990) has shown that solids suspension is possible with viscous liquid operating in the laminar regimes well before turbulence sets in.

Although both of these theories display considerable merit, there remain a few questions to be answered. In the turbulent model, mean energy dissipation is assumed and the related kinematic quantities are usually derived according to the concepts of Kolomogoroff's theory of homogeneous turbulence. However, it is obvious that the energy input does not dissipate uniformly throughout the vessel and there is as yet insufficient knowledge of the dissipation intensity in the vicinity of the bottom where the solid particles are to be suspended. Moreover, the damping effect due to the presence of solids is extremely difficult to quantify. It has also been reported (Squires 1990) that the turbulence field was modified differently by light particles than by heavy particles. Moreover, the validity of Kolomogoroff's theory in a mechanically agitated vessel has yet to be verified.

On the other hand, the velocity model approach also presents problems. The flow model assumes that regardless of the flow condition in the core (turbulent or laminar), flow near the base is not turbulent during suspension. Most of the models that have been reviewed were too simplistic to quantify the complex interaction between fluid flow and geometry. For example, flow within the core of the vessel could be very different from flow near the vessel base. The location of the last suspension region depends on a combined effect between vessel base and impeller discharge flow. The influence of geometrical configuration on N_{js} may vary from one location to another due to differences in flow nature. If one wishes to explain the periodically picked up and re-deposited motion of the particles on the vessel base by means of the velocity model approach, one has to accept that the fluid velocity must be unsteady, varying considerably across the vessel base. Therefore, a more accurate way of relating the impeller rotational speed to the fluid flow adjacent to the solid particle to be suspended is necessary.

The suspension models reviewed are summarised in Table 2.1. According to the various theoretical models compared, the prediction of the viscosity and density effects agree

reasonably well. They suggest ν and $\Delta\rho$ exponents ranging from 0.11 to 0.17 and 0.42 to 0.56 respectively. However, almost all the turbulence models suggest an exponent of 0.17 (eg Baldi 1978) and -0.67 (eg Buurman 1985) for the particle size and scale-up effect and the flow model recommended an exponent of 0.5 (eg Mersmann 1985) and -1 (eg Molerus 1987) for the corresponding effect. Incidently, most of the exponents reported in open literature lie between 0.14 and 0.5 for particle size effect and -0.67 and -1 for scale-up effect. This makes one wonder if the solid particles are being picked up by a combination of these two effects and that the magnitude of the exponent is dependent upon the proportion of particles being picked up by each of the two mechanisms.

Most of the models formulated have not allowed for the effect of liquid viscosity and solids concentration. These are extremely important, for both the liquid velocity and turbulence intensity will be modified by these parameters. Shamlou (1990) considers the concentration effect by relating the number of particles in the vessel to the power input and he found that $N_{js} \propto C_v^{1/3}$. Buurman (1990) suggests that the effect of solids concentration is a function of liquid and solid density, particle size and scale of equipment. Until models have been developed which account for all these complex interactions, it is unlikely that any pure theoretical model will be able to bring all the available experimental data together.

To summarise, there has been much effort devoted to the modelling of the suspension mechanism but these models still require refinement. There remains a need for confirmation of the models by conducting flow visualisation tests and validation by conducting experiments in more critical conditions, such as high solids concentration and large scale tests. This is because many models developed have only been verified in limited test range (eg in relatively small scales).

Table 2.1.1 Summary of the Suspension Models

Reference	Approach	Status	Exponent on						Remarks
			ν	$\Delta\rho$	ρ_L	d_p	X	D	
Zwietering 1958	Empirical	-	0.1	0.45	-0.45	0.2	0.13	-0.85	with dimensional analysis
Baldi 1978	Turbulent	without adjustment	-	0.5	-0.5	0.17	-	-0.67	$N_{js} \propto Po^{-0.33}$
"	"	adjusted with expt data	0.17	0.42	-0.41	0.14	0.125*	-0.89	1. When C/D=1, constant Po & D/T, 2. exponents varies with geometry
Mersmann 1985	Velocity	$d_p/T < 10^{-3}$	-	0.5	-0.5	0.5	-	-1	
"	Not clear	$d_p/T > 10^{-3}$	-	0.5	-0.5	Nil	-	-0.5	
Shamlou 1987	Velocity	Theoretical	-	0.5	-0.5	0.17	-	-0.67	Also $N_{js} \propto Po^{-1/3} C_v^{1/3} T$, model confirmed by experiments
Molerus 1987	Fluidised bed	Ar < 40	-0.11	0.56	-0.56	0.56	-	-0.89	no concentration effect, model supplement with expts
"	Pump flow	Ar > 40	-	0.5	-0.14	0.14	-	-0.64	$N_{js} \propto C_v^{0.36}$
Wichterle 1988	Velocity		function of Archimedes No.					-0.67	

'-' parameter not included in the modelling

* experimental result

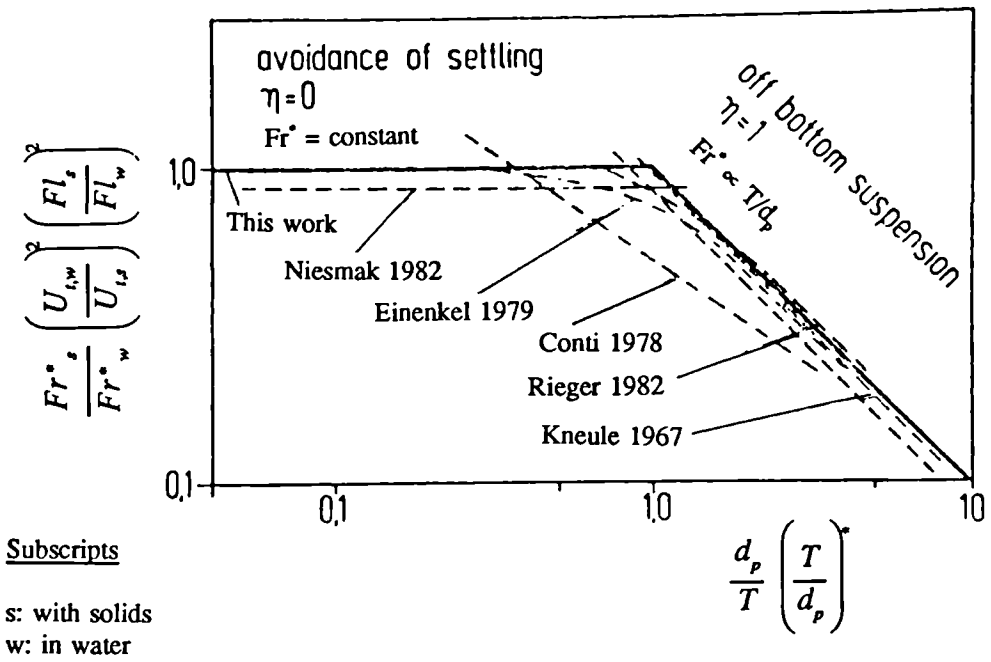

Fig 2.1.1 Ratio of Froude Numbers as a Function of Diameter Ratio according to Void & Mersmann's Model (1986)

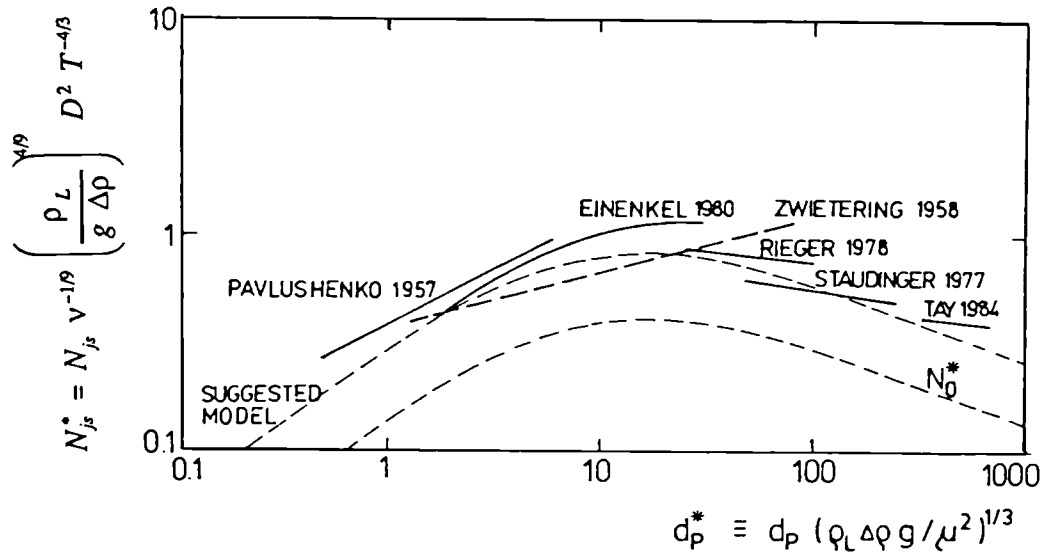

Fig 2.1.2 Comparison between Wichterle's Theoretical Model (1988) and Literature Data – Axial Impellers

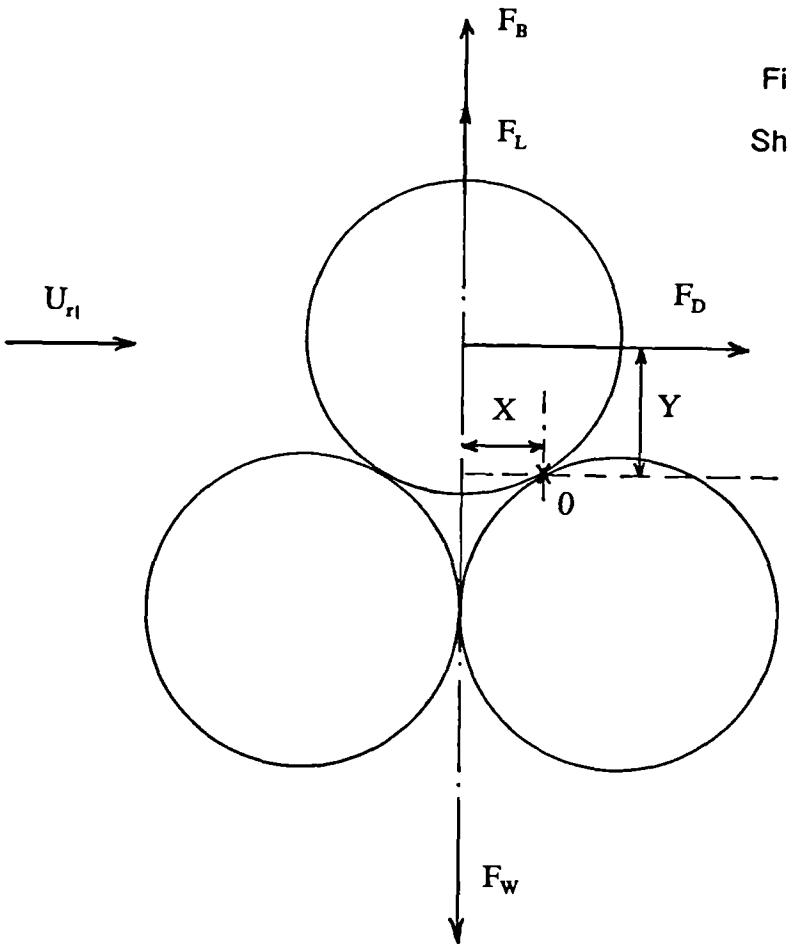

Fig 2.1.3 Force Balance for Shamlou's Average Velocity Model

$\zeta = Y/X$

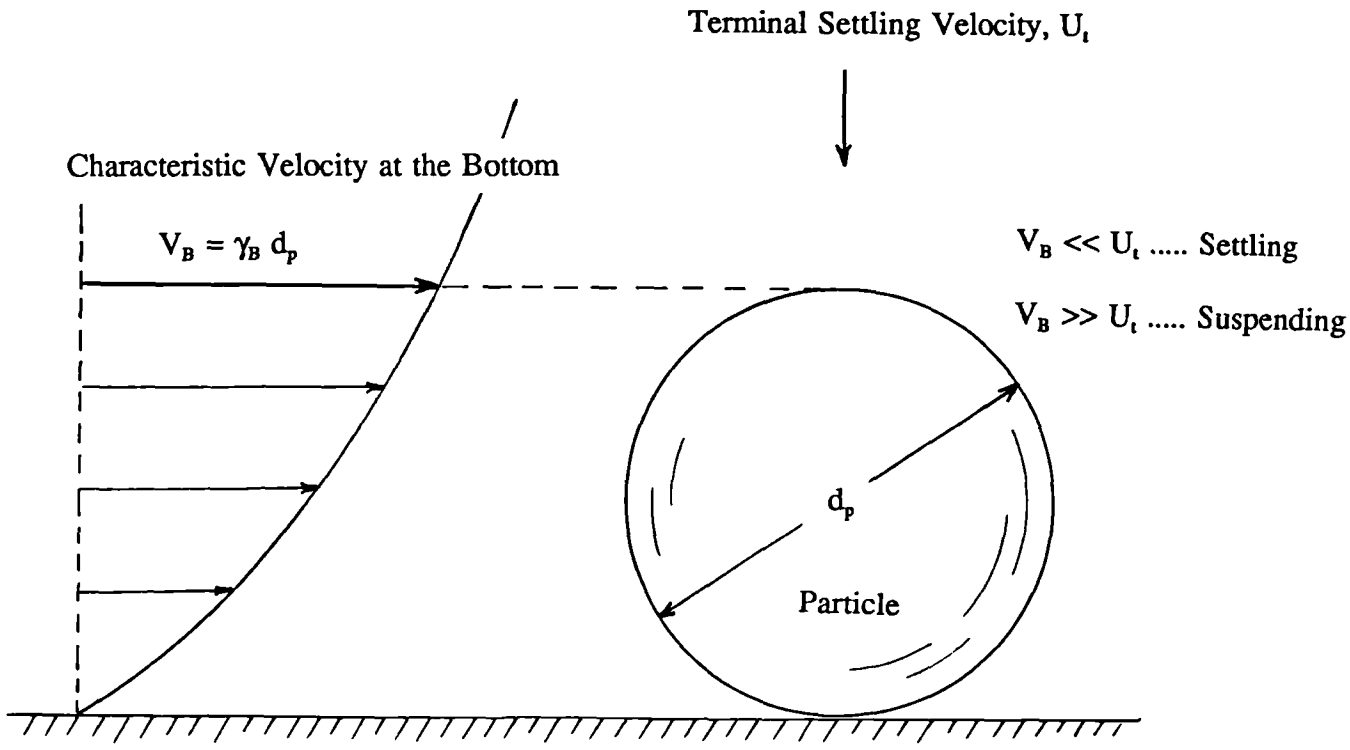

Fig 2.1.4 Model of Flow around a Particle at Vessel Base

2.2 SOLIDS DISTRIBUTION

The distribution of solid particles in a stirred vessel can be described by means of the degree of homogeneity within the vessel contents. Very often, a uniform dispersion of solids throughout the mixing vessel is necessary to ensure adequate exposure to the process conditions. However, the amount of research in this area is limited when compared to the study of solids suspension, attributable mainly to the difficulties in the development of a reliable experimental technique (Sec 3.10). This part of the survey will focus on major experimental and theoretical findings in solids distribution literature.

2.2.1 Relative Standard Derivation and Variance

Relative standard derivation (RSD) is very often quoted to quantify the distribution quality of solids in multiphase stirred vessels. It is a measure of the deviation of the local solids concentration from the mean holding solids concentration. The magnitude of RSD decreases as the distribution becomes more homogeneous and perfect homogeneity will give a zero value.

Definition of RSD in open literature can differ slightly, depending on which statistical mean is taken {number of samples equal to n for sample mean and (n-1) for population mean}. Throughout this study, the following definition is adopted:

$$RSD = \frac{1}{C_M}\left(\frac{1}{(n-1)} \sum_{i=1}^{n} (C_{ij} - C_M)^2 \right)^{1/2} \qquad \text{...eqn(2.2.1)}$$

C_{ij} is the local solids concentration at i^{th} position and j^{th} speed

C_M is the mean bulk solids concentration from calculation

n is the number of sampling positions and n is equal to 5 in this investigation

In some literature, variance (σ) is used to define the distribution quality and the relationship between variance and relative standard deviation is :

$$RSD = \sigma^{1/2} / C_M$$

2.2.2 The One Dimensional Dispersion Models

In modelling the distribution phenomenon, most researchers based their analysis on a one-dimensional sedimentation-dispersion model. This can be derived from a general diffusion equation (Appendix G). To model the distribution processes, both the solid and liquid phases are taken as an upward moving continuum and a particle diffusion (dispersion) coefficient is employed to account for the relative movement between the two phases. This coefficient is a function of power input, physical properties and geometrical configurations.

Barresi and Baldi (1987) used the monodimensional model and assumed the solids phase to be a continuum. Neglecting the inertia forces, the local mean-time solids velocity in the axial direction is a vectorial sum of the liquid velocity and the terminal velocity:

$$U_{pz} = U_{fz} - U_{tt} \qquad \text{...eqn(2.2.2)}$$

Since the net flow rate of the liquid through a section is zero, an integration of equation 2.2.2 over a generic section leads to:

$$U_{pz} = -U_{tt} \qquad \text{...eqn(2.2.3)}$$

From the general diffusion equation, assuming $U_{tt} \propto U_{to}$:

$$U_{to}\, C_z + D_{e,p} \frac{dC_z}{dz} = 0 \qquad \text{...eqn(2.2.4)}$$

Therefore, the local concentration depends on $D_{e,p}/U_{to}$. They introduced a modified Peclet Number (Pe^*) to describe the local concentration. With L^* being a characteristic linear dimension of the system, Pe^* is defined as:

$$Pe^* = \frac{U_{to}\, L^*}{D_{e,p}} \qquad \text{...eqn(2.2.5)}$$

By relating the power input to the turbulent scale:

$$Pe^{*} \propto \frac{U_{to}}{Po^{1/3}\ N\ D} \qquad \text{...eqn(2.2.6)}$$

They went on to define a K parameter, which is the inverse of the modified Peclet Number, i.e. $K = Po^{1/3}\ N\ D\ /\ U_{to}$. This is so defined in order to stress the fact that the dispersing phenomenon is not due solely to the turbulent diffusion, but also to the anisotropic turbulent motion. By plotting relative standard derivation against $K/X^{0.13}$ to account for the concentration effect, they showed that the suspension quality can be correlated as a function of the stirrer speed (Fig 2.2.1). This is implying a constant tip speed scale up relationship for equal quality of solids distribution. It is important to point out that their plots of RSD versus $K/X^{0.13}$ for different impeller types can be somewhat misleading. Firstly, their impellers were confined to T/3 diameter only and therefore, their proposed effect of D on RSD is yet to be validated. Moreover, by overlaying their plots it can be shown that their results did not confirm $RSD \propto Po^{-1/3}$ (Fig 4.4.8).

Magelli et al (1987, 1989, 1990 and 1991) adopted the simplified diffusion equation;

$$-D_{ep}\ \frac{d^2C_z}{dz^2} + U_t\ \frac{dC_z}{dz} = 0 \qquad \text{...eqn(2.2.7)}$$

With the boundary conditions:

$$U_t\ C_{z\ (z=0^+)} - D_{ep}\ \frac{dC_z}{dz}_{(z=0^+)} = 0 \qquad \text{...eqn(2.2.8)}$$

$$C_M = \frac{1}{H} \int_{H}^{0} C_{ij}(z)\ dz \qquad \text{...eqn(2.2.9)}$$

The solution of the equation is:

$$\frac{C_{ij}}{C_M} = \frac{Pe}{1 - e^{-Pe}}\ e^{\frac{-Pe\ z}{H}} \qquad \text{...eqn(2.2.10)}$$

The authors suggested that suspension inhomogeneity can be characterized by the relative standard deviation (RSD) of the solids concentration with respect to the mean value and RSD can be expressed as a function of Peclet number (Pe). Note that their definition of RSD differs slightly from that presented in this investigation.

$$RSD = \frac{1}{C_M}\left(\frac{1}{n}\sum_{1}^{n} (C_{ij} - C_M)^2 \right)^{1/2} \qquad \text{...eqn(2.2.11)}$$

$$RSD = \left(\frac{Pe}{2}\,\frac{e^{2Pe} - 1}{(e^{Pe} - 1)^2} - 1 \right)^{1/2} \qquad \text{...eqn(2.2.12)}$$

and $$Pe = \frac{- U_{ti} H}{D_{ep}} \qquad \text{...eqn(2.2.13)}$$

They conducted a series of experiments in a 0.236 m diameter stirred vessel, with various liquid depth ($2.3 \leq H/T \leq 4$) and impeller combinations. A variety of solids and fluids were also tested. They established that a single interpolating line can be obtained for all the geometries studied, for each particle size and liquid viscosity. Therefore, they proposed the following relationship in order to account for the physical and geometrical parameters;

$$Pe = A_i \left(\frac{U_{to}}{N D} \right)^{\alpha} \left(\frac{\nu^3}{\varepsilon_m d_p^4} \right)^{\beta} \qquad \text{...eqn(2.2.14)}$$

Based on test results from Rushton turbines, the exponents on (H/T) ratio and ($\nu^3/\varepsilon_m d_p^4$) were found to equal 2 and 0.095 respectively. They observed a lower distribution efficiency of radial impellers in comparison to axial impellers. Incorporating results from axial impellers (with the above two exponents kept constant), further analysis yielded the following correlation (Fig 2.2.4):

$$Pe = 330 \left(\frac{H}{T} \right)^2 \left(\frac{U_{to}}{N D} \right)^{1.17} \left(\frac{\nu^3}{\varepsilon_m d_p^4} \right)^{0.095} \qquad \text{...eqn(2.2.15)}$$

By assuming a power law dependence of RSD on Pe, equation 2.2.12 can be simplified as:

$$RSD = 0.29\ Pe^{0.92} \qquad \text{for } 0 \leq Pe \leq 6 \qquad \text{...eqn(2.2.16)}$$

An important contribution of Magelli et al's work is the successful demonstration that all physical and geometrical parameters they have tested so far can be presented in terms of a single adjustable parameter (Pe - Peclet No, eqn 2.2.14). The relative standard derivation of solids concentration can be related to the Peclet number by a power law approximation. Thus, the homogeneity of a solids distribution system can be predicted from equation eqns 2.2.15 and 2.2.16. Since $\varepsilon_m \propto N^3$ and therefore $Pe \propto N^{1.46}$ and $RSD \propto N^{1.34}$. A scale up implication of $N \propto D^{-0.93}$ can be deduced from these two equations.

Shamlou and Koutsakos (1989, 1991) conducted a mass balance on the particles over a thin horizontal section of the liquid in the vessel, and assuming that there is no accumulation or depletion of the particles;

$$U_{tt}\, C_z + D_{e,p} \frac{dC_z}{dh} = 0 \qquad \text{...eqn(2.2.17)}$$

Where $D_{e,p}$ and U_{tt} are the dispersion coefficient and settling velocity of the particles in suspension. Eqn 2.2.17 can be rearranged into the format;

$$\frac{d\,(\ln C_z)}{dh} = -\frac{U_{tt}}{D_{e,p}} \qquad \text{...eqn(2.2.18)}$$

Thus, a plot of (ln C_z) against height, h, is expected to be a straight line with a slope of $-U_t / D_{e,p}$. To simplify eqn 2.2.17 further, the authors proposed the following assumptions;

- The particles in suspension were small and thus behaved in the same manner as the agitated liquid. So the particle diffusion coefficient, $D_{e,p}$, may be expected to coincide closely with the liquid diffusion coefficient, $D_{e,l}$.

i.e. $D_{e,p} \propto D_{e,l}$ ...eqn(2.2.19)

- Homogeneous and isotropic turbulence exists in the core of the agitated vessel.

$$\text{i.e. } \varepsilon_t \propto \frac{N^3 D^5}{T^2 H} \qquad \text{...eqn(2.2.20)}$$

- Away from the discharge zone of the impeller, the mean rate of energy dissipation in the core of the vessel is directly proportional to the total energy input per unit mass.

- The relationship for small eddies of scale L_o in the Kolmogoroff range applies to the larger energy containing eddies of scale L_e.

$$\text{i.e. } v' \propto (\varepsilon_m L_o)^{1/3} \propto (\varepsilon_m L_e)^{1/3} \qquad \text{...eqn(2.2.21)}$$

Assuming $U_{it} \propto U_{io}$, and for a fixed tank/impeller geometry :

$$\frac{U_{it}}{D_{ep}} \propto \frac{U_{io}}{N} \qquad \text{...eqn(2.2.22)}$$

By introducing the ratio d_p/D, the above equation can be expressed in dimensionless form by using a Peclet number defined as $U_{it}\, d_p/D_{ep}$

$$\frac{U_{it}\, d_p}{D_{ep}} \propto \frac{U_{io}}{N D} \qquad \text{...eqn(2.2.23)}$$

The authors therefore concluded that the distribution of particles in the agitated liquid can be characterized by a single parameter, namely the ratio of the turbulent diffusion coefficient of the particles to their terminal settling velocity (Fig 2.2.2). All other properties of the system, such as particle size and density, impeller diameter and speed and fluid properties exert their effects only through the value of this ratio. According to eqn 2.2.23, if the distribution quality is to be maintained, the tip speed of the impeller across scales has to be a constant.

These was demonstrated by plotting the experimental results in terms of $U_{it}\, d_p/D_{ep}$ against $U_{io}/N\, D$. However, it is worth pointing out that the relationship presented in the plot is valid only if $H \propto T \propto D$.

All three models used the settling velocity (single particle in still fluid) to account for the solids and liquid properties. Baldi et al (1987) used $RSD \propto X^{0.13}$ to account for the effect of solids concentration in homogeneity, an arbitrary correction taken from Zwietering's correlation for solids suspension which seemed to work well for low solids concentration. Apart from that, no analysis has been conducted to include this important parameter in their models. The models all point roughly to a constant tip speed scale-up implication. This was deduced by testing impellers of different diameter in the same vessel (ie varying D/T ratio). If turbulent eddies were responsible for the distribution of the solids as was assumed, one would expect power per unit volume must be kept constant between scales in order to produce the same degree of turbulence. Moreover, Buurman (Sec 2.2.3) correlated the solids distribution data taken from various sized vessels ($0.24 \leq T \leq 4.26$ m) and he concluded a $N \propto D^{-0.78}$ scale-up relationship. It may be the case that constant tip speed criteria work for different D/T ratios but not necessarily so if the different tank sizes were used with D/T maintained constant. This is a subject of further investigation in this thesis.

2.2.3 Buurman's Modified Froude No. Model (1985)

In order to achieve a certain degree of homogeneity in a stirred vessel, the solid particles have to be lifted up from the vessel base and then transported throughout the whole vessel. Buurman et al suggested that it is not only the eddies of the inertial sub-range that are responsible for the mechanism but that the largest eddies (i.e. circulation) also play a role.

They assume the fluctuating velocity, which is responsible for entrainment of the particles, to be proportional to the circulation velocity, i.e to the impeller tip speed.

$$v' \propto N D \qquad \text{...eqn(2.2.24)}$$

From an energy balance between the kinetic energy of eddies and the potential energy of the particles:

$$\rho_L d_p^3 v'^2 \propto g \Delta\rho d_p^3 d_p \qquad \text{...eqn(2.2.25)}$$

Combining equations 2.2.24 and 2.2.25

$$\frac{\rho_L N^2 D^2}{g \Delta\rho d_p} = constant \qquad \text{...eqn(2.2.26)}$$

The authors conducted a series of experiments in T=0.24, 0.48 and 4.26 vessels, with a T/2.5 diameter downward pumping pitched bladed turbine mounted at T/3 clearance. Particle sizes in the range of 157 to 2200 μm were used. The data were correlated in terms of height of homogeneous zone with a modified Froude No (Fig 2.2.3):

$$\frac{h}{T} = f\left(\frac{\rho_L N^2 D^2}{g \Delta\rho d_p} \cdot \left(\frac{d_p}{D}\right)^{0.45}\right) \qquad \text{...eqn(2.2.27)}$$

For h ~ 0.9T (H/T = 1), the necessary condition to maintain homogeneity across scales is:

$$\frac{\rho_L N^2 D^2}{g \Delta\rho d_p} \cdot \left(\frac{d_p}{D}\right)^{0.45} \geq 20 \qquad \text{...eqn(2.2.28)}$$

$$N_{RSD} \geq 4.47 \left(\frac{g \Delta\rho}{\rho_L}\right)^{0.5} \left(\frac{d_p}{D}\right)^{0.275} D^{-0.50} \qquad \text{...eqn(2.2.29)}$$

This indicates a scale up relationship of $N \propto D^{-0.78}$ for constant particle diameter.

2.2.4 Other Models

Penaz et al (1978) developed a solids concentration distribution model, again based on an equation of continuity and assuming molecular diffusion for particle flux due to turbulence. The model is very similar to those described in Section 2.2.2 except in this case, cylindrical coordinates were used and the radial solids distribution has also been accounted for. The model has been tested by measuring concentration distribution in a 0.447 m vessel equipped with 4 baffles and 45° pitched bladed turbines. They also demonstrated that the tangential liquid velocity component close to the impeller region is not negligible.

Einenkel (1980) measured the suspension and distribution behaviour of glass beads in 0.365 and 0.790 m stirred vessels. His results show that the behaviour of the particles in the swarm is very important and the influence of particle diameter, density difference and viscosity can be deduced from the settling behaviour of corresponding solid particles in non-stirred media. He suggested the ratio of settling velocity of a single particle to that of a swarm should be used instead of d_p/D. Likewise, volume fraction is more appropriate that mass fraction. Based on the results, a relationship of $P/V \propto T^{0.33}$ is recommended by the author for solids distribution scale-up. A criticism of Einenkel's work is that the concepts of solids suspension and distribution were mixed together when the results were discussed.

Bohnet and Niesmak (1980) measured solids distribution for a range of process and geometric parameters in a 0.29 m flat based vessel using a helium-neon laser. They suggested that the attainment of the lift-off impeller speed is not in itself sufficient to ensure homogeneity of the suspension. Nor does the determination of height reached by the slurry liquid interface, which is a function of impeller speed, help with the assessment of solids distribution. Their results were presented in graphical form, mostly by plotting solids concentration or relative quality of distribution against impeller speed. They found that among the impellers tested, the best results with respect to energy consumption were achieved for propellers with D=T/3 at C=D/2. Moreover, they showed that increase in the impeller speed does not automatically produce better results and this could due to the influence of centrifugal forces in the vicinity of the impeller which may have caused the segregation of the solids particles.

Table 2.2.1 Summary of the Distribution Models

Reference	T (m)	Impeller	C	Conc	d_p (μm)	ρ_S (kg m^{-3})	ρ_L (kg m^{-3})	Technique	Scale-up
Barresi 1987	0.39	A310, 45°PBT4, 45°DT6, all T/3	T/3	0.5-5.1 %Wt	100-500	2600-2670	1000	sampling	$N \propto D^{-1}$
	$RSD \propto \frac{U_t}{Po^{1/3}\, N\, D}\, X^{0.13}$								
Buurman 1985	0.24-4.26	45°PBT4(T/2.5)	T/3	3-40 %Vol	157-2200	~1200-2650	~800-1000	sampling	$N \propto D^{-0.78}$
	$\frac{\rho_L N^2 D^2}{g\, \Delta\rho\, d_p} \cdot (\frac{d_p}{D})^{0.45} \geq 20$, i.e. $N_{RSD} \geq 4.47\, (\frac{g\, \Delta\rho}{\rho_L})^{0.50}\, (\frac{d_p}{D})^{0.28}\, D^{-0.50}$								
Shamlou 1989	0.225	45° PBT6(T/3.5 -T/2.3)	vary	1-6 %Wt	175-1100	2900-3800	1000	optical	$N \propto D^{-1}$
	Distribution Quality, $\frac{U_{tt}\, d_p}{D_{e,p}} \propto \frac{U_t}{N\, D}$, H≠T								
Magelli 1991	0.236	multiple A310, PBT2,4, variable pitch	-	0.1-0.3 %Wt	140-980	2450	H_2O, PVP	optical	$N \propto D^{-0.93}$
	$Pe = 330\, (\frac{H}{T})^2\, (\frac{U_t}{N\, D})^{1.17}\, (\frac{\nu^3}{\varepsilon_m\, d_p^4})^{0.095}$, $RSD = 0.29\, Pe^{0.92}$, for $0 \leq Pe \leq 6$								

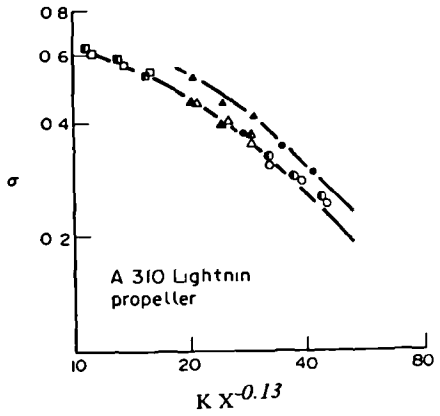

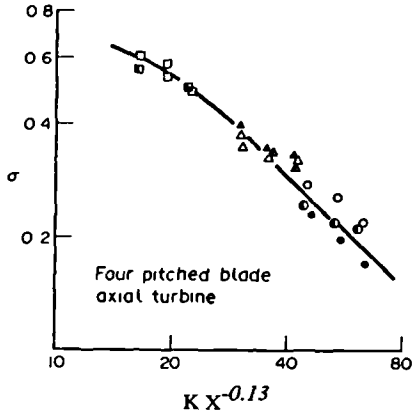

d_p \ X	0.50	1.51	5 10
100-177 μm	○	◐	●
208-250 μm	△	▲	▲
417-500 μm	□	■	

Barresi and Baldi's (1987) data

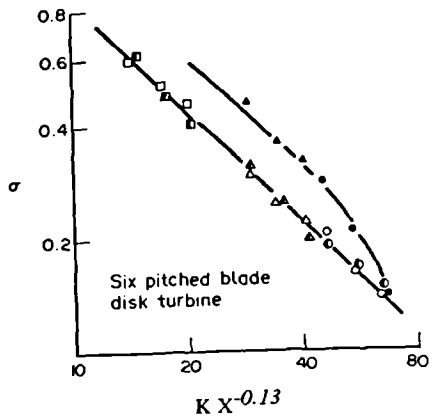

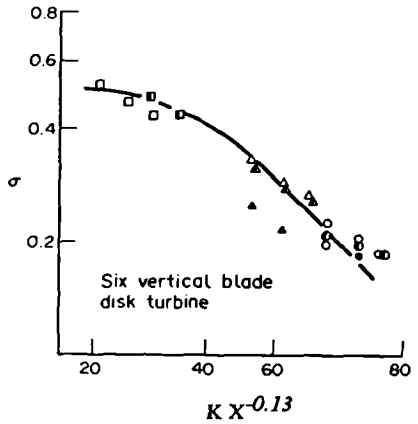

Fig 2.2.1 Distribution Quality against K Number ($K=Po^{1/3}ND/U_{to}$) (Barresi and Baldi 1987)

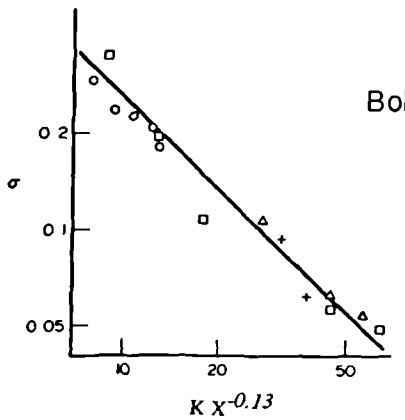

Bohnet and Niesmak's (1980) data

Key	Solid	d_p (mm)	ρ_s (kg/m³)	$u_t \times 10^2$ (m/s)	X (kg/kg %)
□	Styropor	1 125	1050	164	0 21
△	Glass	0 225	2480	2 24	0 744
+	Bronze	0 125	8850	3 49	1 77
○	Glass	0.715	2480	10 84	0 62

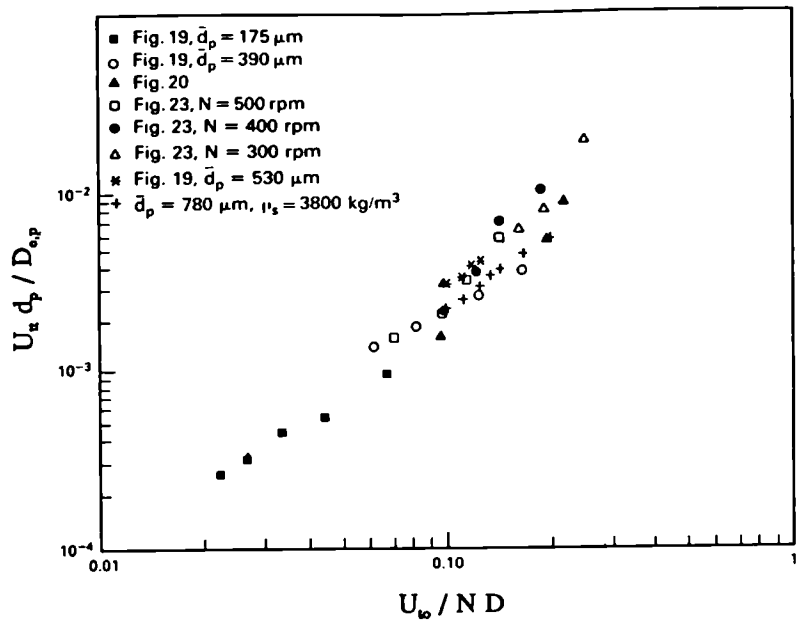

For figures cited in Fig 2.2.2, please refer to the original reference.

Fig 2.2.2 Dimensionless Ratio ($U_{tt}d_p/D_{e,p}$) as a Function of System Parameters (Shamlou and Koutsakos 1989)

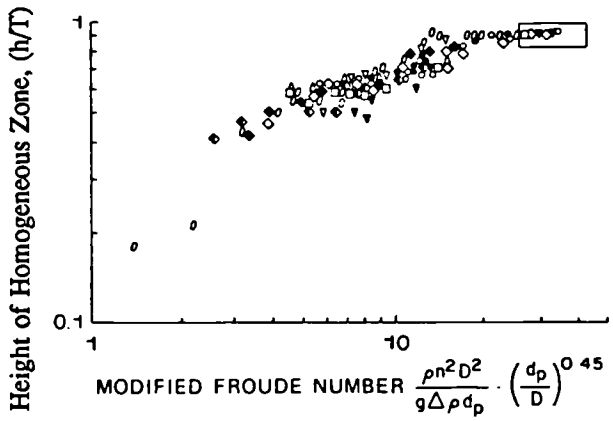

	SUSPENSION	d_p, μm	T, m
0	GLASS/WATER	200	0.24
◆	GLASS/WATER	800	0.24
▼	SAND/WATER	157	0.48
□	SAND/WATER	157	4.26
○	SAND/WATER	200	0.24
●	SAND/WATER	200	0.48
□	SAND/WATER	800	0.24
△	SAND/WATER	2200	0.24
▽	COAL/WATER	800	0.24
◇	POLYSTYRENE/ OCTANE	800	0.24
◆	POLYSTYRENE/ BUTANOL	800	0.24

Fig 2.2.3 Effect of Stirring Conditions on Homogeneity (Buurman 1985)

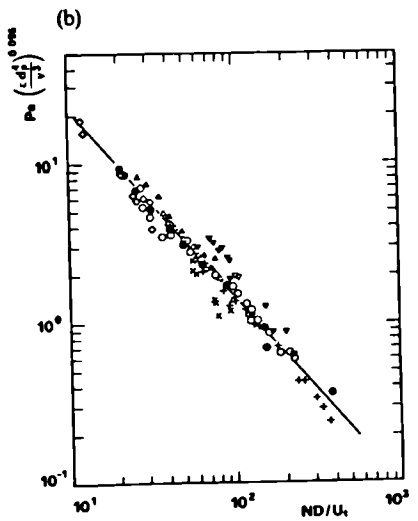

(a)

ρ_s (g/L)	1 15	2 45	2 45	8 41
D (cm)	7 87	4 35	7 87	7 87
d_p=0 14 mm		▼	▽	
0 23		△	△	
0.30		●		
0.33	+		○	×
0 98			◇	

Fig 2.2.4 Correlation of Solids Distribution Data according to Magelli et al (1990)

CHAPTER 3 : TEST FACILITIES AND METHODS

This section consists of two parts, the first outlines the test facilities which are common to the experiments discussed in subsequent chapters, while the second describes the experimental techniques employed to measure the test parameters. Calibration of instruments, accuracy and reproducibility of the measurements are also discussed. Comparisons with other measuring techniques currently being used are made.

Summaries of the experimental and geometrical variations covered in this work are included in Table 3.0.1 and 3.0.2.

Table 3.0.1 Experimentation

Vessel, T (m)	**0.305**	**0.61**	**1.83**	**2.67**
Flow Visualisation	Yes	Yes	No	No
Power Measurement	No	Yes	Yes	Yes
Solids Suspension	Visual	Visual & UDF	UDF	UDF
Solids Distribution	No	Yes	Yes	Yes

Five measurements were made during the tests :

a) Impeller Rotational Speed (N)
b) Shaft Torque (τ)
c) Just Suspension Speed by Visual Observation ($N_{js,o}$)
d) Just Suspension Speed by Ultrasonic Doppler Flowmeter ($N_{js,u}$)
e) Local Solids Distribution at i^{th} Speed and j^{th} Position (C_{ij})

3.1 BASE CONFIGURATIONS

Most experiments were carried out in a 0.61 m diameter baffled perspex vessel fitted with a torispherical base. A 45° PBT4 (T/2, D/3.6) downward pumping impeller was mounted at T/4 clearance and the liquid depth, H, is equal to the vessel diameter. This provided a base configuration and enabled test work with a wide range of set-ups and test conditions to be compared. This is the configuration adopted to compare scale-up rules from 0.31 to 2.67 m vessels.

3.2 THE VESSELS

Tests were performed in a series of four geometrically similar cylindrical vessels with a tank diameter of 0.305, 0.61, 1.83 and 2.67 m to examine the effect of scale-up.

The 0.305 m (T_{31}, Fig 3.2.1) and 0.61 m (T_{61}, Fig 3.2.2) vessels were constructed from perspex to enable visual observation of the solid particles. Different vessel bases could be fitted to the main body to investigate the effect of vessel base configuration.

The 1.83 m (T_{183}, Fig 3.2.3) vessel was constructed from mild steel with "PHEN-O-LINE 302" (Trademark of Tretol Protective Coatings Limited, London) internal coating. Four perspex windows were equipped to allow flow visualisation. The 2.67 m vessel (T_{267}, Fig 3.2.4) was a concrete structure below ground level and thus, visual observation was not possible. This vessel was also coated with "PHEN-O-LINE 302".

In all cases the impeller shaft was mounted centrally in the vessel. The slurry height, H, was equal to the vessel diameter, T, for all experiments unless otherwise stated. This gave a total slurry volume of 0.021, 0.165, 4.46 and 13.5 m^3 in T_{31}, T_{61}, T_{183} and T_{267} respectively. The vessel geometries are summarised in Fig 3.2.5.

3.3 THE VESSEL BASES

Torispherical vessel bases (Fig 3.2.5-b) were used throughout, the geometry of which are very similar to that of dished bases (Fig 3.2.5-a). The torispherical vessel base was manufactured according to Deutsche Norm 28011. It has a bottom and knuckle radius of T

and T/10 respectively, which gave a depth from the lower tangent line to the bottom of the vessel of T/5.1. A torispherical vessel base was used for its effectiveness in removing corner fillets in solids suspension (Mak 1988a).

Table 3.0.2 Geometrical Variations

Vessel	T_{31}	T_{61}	T_{183}	T_{267}
Liquid Depth	H = T	H = T	H = T	H = T
No. of Impeller	Single	Single & Dual	Single	Single
Impeller Type	45° PBT	30°-90° PBT & others	45° PBT	45° PBT
Impeller Diameter	0.5T	0.3 - 0.6T	0.5T	0.5T
Impeller Clearance	T/4	T/4 - T/8	T/4	T/4
Baffle	Standard	Standard	Standard	Standard
Vessel Base	Torispherical	Torispherical	Torispherical	Torispherical

3.4 BAFFLES

Four vertical strip baffles were spaced equally around the circumference of the vessel. Each baffle was T/12 wide and spaced T/60 from the vessel wall, giving a total distance of T/10 from inner baffle edge to the vessel wall.

3.5 IMPELLERS AND CLEARANCES

Most of the experiments were carried out with pitched blade turbines, however other impeller types such as hydrofoils and flat blade turbines were also used. Details of impeller geometries and dimensions can be found in Fig 3.5.1 and Table 3.5.1. An impeller series number is assigned to each impeller. The last three digits of the series number refers to the vessel in which the impeller is fitted. However, in the text of this thesis the impellers are distinguished using a short description. For example, 45° PBT4(T/2,D/3.6) is referring to a 45° 4-bladed pitched blade turbine of T/2 diameter with a blade width of D/3.6. The

experimental programme covered a clearance range from T/4 to T/8, the clearance was measured from the impeller centreline to the centre of the vessel base.

3.6 TEST MEDIA

Sand and water were the main media used in the test programme. Other solids types used will be described in the text. All the sands used had round grains (sphericity ≈ 0.8, Hepworth 1992). Measurements were made at solids concentrations of up to 45 %Wt. Four sizes of sand were tested :

Solids Type	Descriptions	Median Size
A	BIS Chelford 30 sieved to 500-710 μm	605 μm
B	BIS Chelford 50 sieved to 300-355 μm	328 μm
C	BIS Chelford 95 sieved to 150-210 μm	180 μm
D	BIS Chelford 95 sieved to 90-150 μm	120 μm

BIS is short for British Industrial Sand Limited (now known as Hepworth Minerals and Chemicals Limited) in Moneystone Quarry, Oakamoor, Stoke-on-Trent, Staffordshire. The densities of dry sand were between 2600 and 2650 kg m^{-3} and a value of 2630 kg m^{-3} was used in calculation.

The majority of experiments were conducted with solids type C (150-210 μm sand), which has a settling velocity of 0.015 m s^{-1}. This is the settling velocity for a single grain and was determined experimentally in a water column. Therefore, correction has to made for the corresponding velocity for a swarm of particles.

Table 3.5.1 Summary of Impeller Dimensions

Impeller Notation	T (m)	α (°)	n	D (mm)	W (mm)	χ (mm)	H_b (mm)	H_{od} (mm)	Series No.
45° PBT4 (T/2,D/3.6)	0.31	45	4	153	43	1.7	31	29	022-45-031
30° PBT4 (T/3,D/2.5)	0.61	30		202	82	3.4	43	56	023-46-061
41° PBT4 (T/3,D/3.5)		41		203	58	3.1	42	57	002-31-061
45° PBT4 (T/3.3,D/2.1)		45		183	86	3.3	61	57	001-52-061
45° PBT4 (T/3,D/3.5)				203	58	3.4	56	57	001-31-061
45° PBT4 (T/2.5,D/2.8)				244	86	3.3	62	57	001-51-061
45° PBT4 (T/2,D/3.5)				298	86	3.3	61	57	021-45-061
45° PBT4 (T/2,D/5.2)*				300	58	3.8	57	57	003-33-061
45° PBT4 (T/2,D/3.6)				310	86	3.4	61	57	022-45-061
45° PBT4 (T/1.7,D/4.3)				366	86	3.3	61	57	001-54-061
45° PBT4 (T/1.7,D/3.5)				368	105	3.4	74	57	001-55-061
45° PBT4 (T/1.4,D/5)				427	86	3.3	61	57	001-53-061
45° PBT6 (T/2,D/4.2)			6	305	70	1.6	60	60	058-00-061
60° PBT4 (T/3,D/4)		60	4	198	48	3.9	47	57	002-32-061
90° FBT4 (T/3,D/5)		90		203	41	3.3	41	56	008-37-061
90° FBT4 (T/2,D/6)		90	6	305	51	3.4	52	60	-
45° PBT4 (T/2,D/3.6)	1.83	45	4	930	258	9.5	183	172	022-45-183
45° PBT4 (T/2,D/3.6)[1]	2.67	45	4	1331	378	17	267	245	022-45-267
45° PBT4 (T/2,D/5.2)[2]				1333	250	13	267	245	003-33-267

* Average pitched angle is 44° [1] Actual blade width is D/3.5 [2] Actual blade width is D/5.3

Impeller Notation: α° (P/F)BT(n) (T/a,D/b)

α - Pitched angle to the horizontal

(P/F)BT(n) - n-bladed pitched/flat blade turbine

T/a - Overall impeller diameter expressed in terms of "T"

D/b - Actual blade width expressed in terms of "D"

Fig 3.2.1 0.305 m Vessel (T_{31})

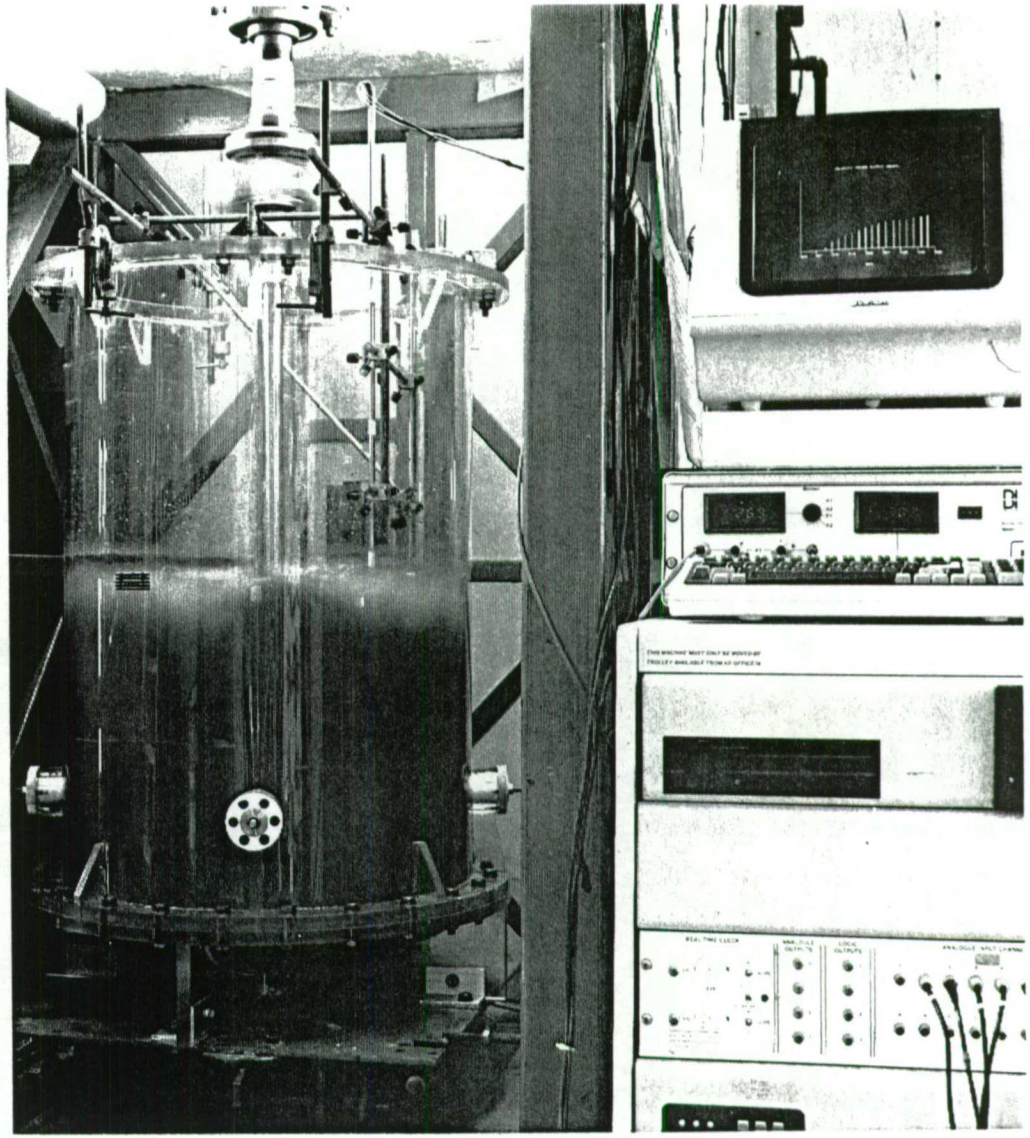

Fig 3.2.2 0.61 m Vessel (T_{61})

Fig 3.2.3 1.83 m Vessel (T_{183})

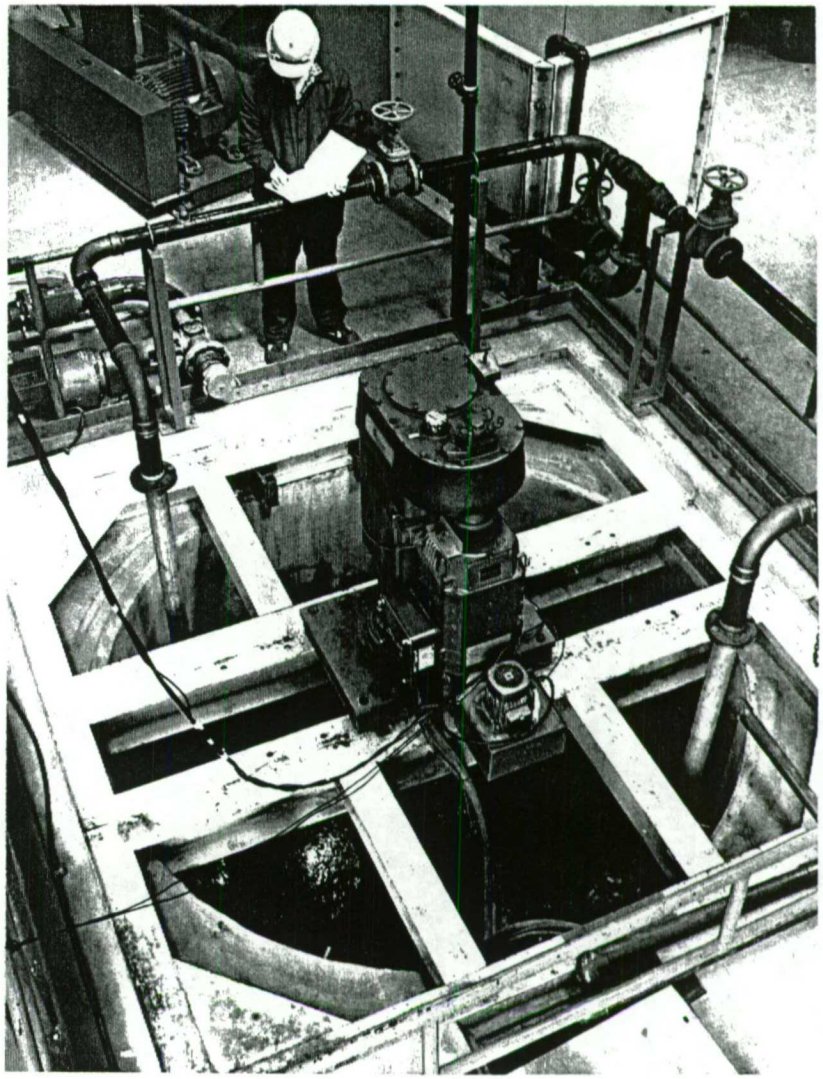

Fig 3.2.4 2.67 m Vessel (T_{267})

Fig 3.2.5 Vessel Configuration

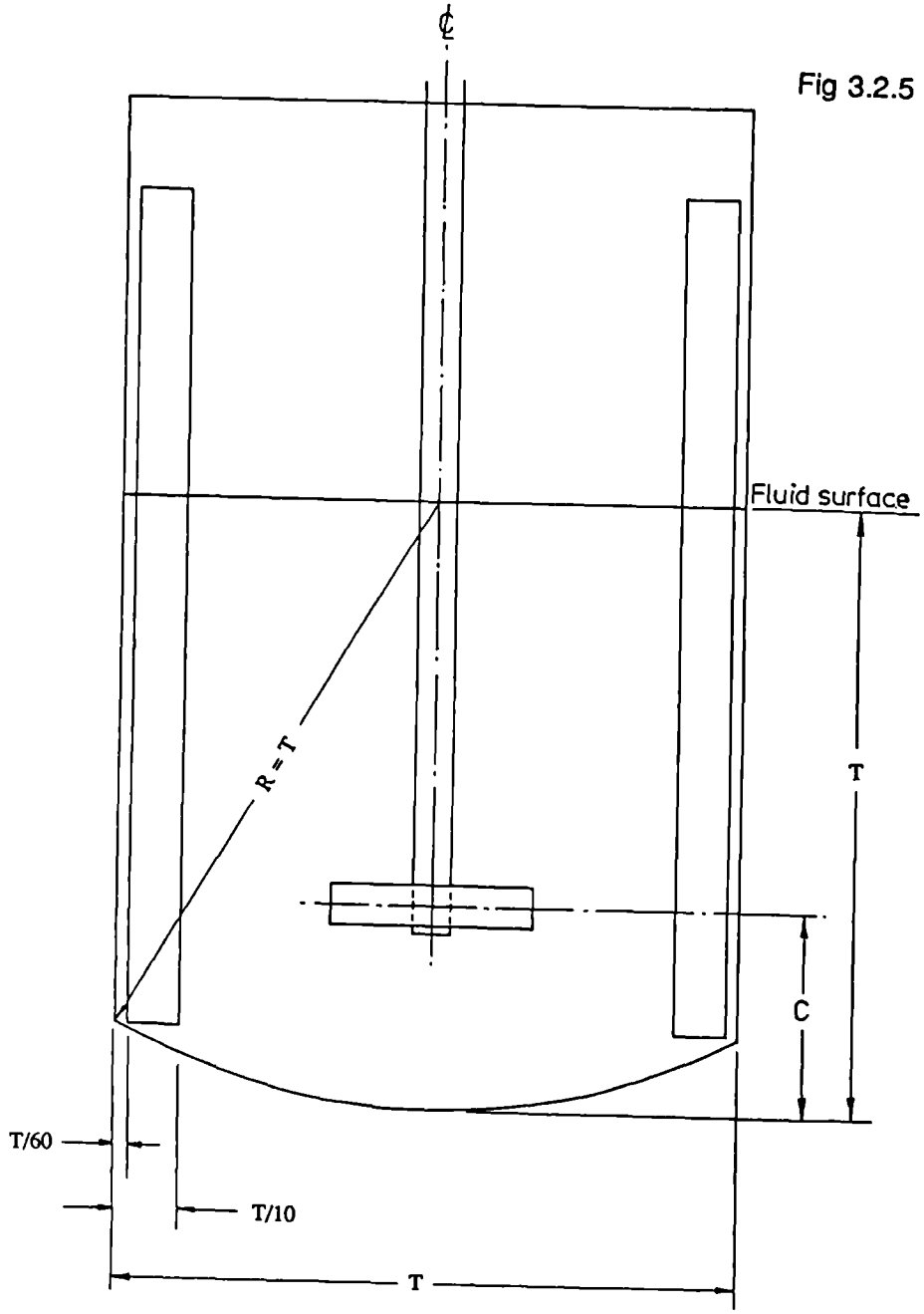

(a) Dished Base

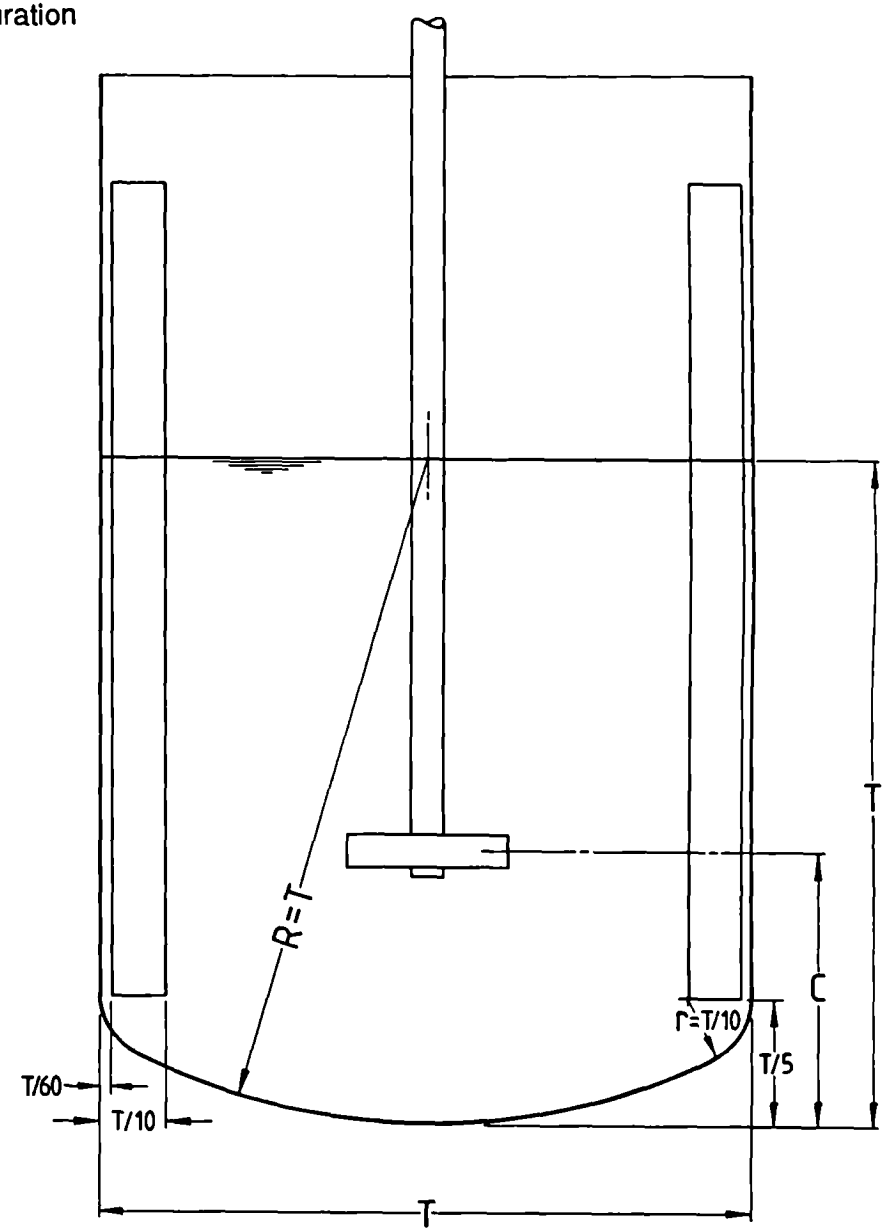

(b) Torispherical Base

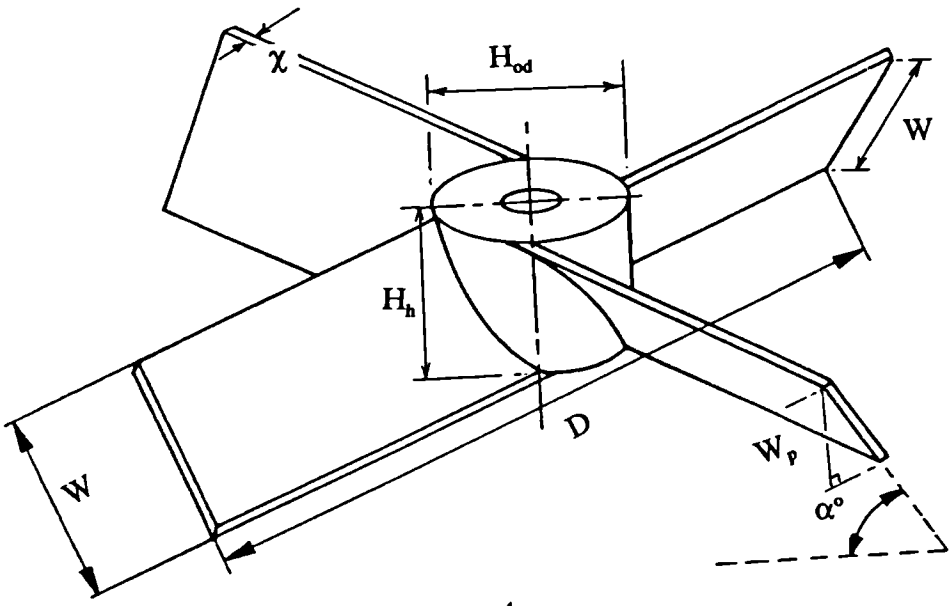

D	-	Impeller Diameter
H_h	-	Hub Height
H_{od}	-	Hub Outside Diameter
n	-	Number of Blades
W	-	Blade Width
W_p	-	Projected Blade Width
α	-	Pitched Angle to Horizontal
χ	-	Blade Thickness

Fig 3.5.1 Impeller Nomenclature

3.7 IMPELLER ROTATIONAL SPEED

The impeller rotational speed was measured using an optical device in which a toothed wheel is fixed to the shaft, interrupted by a light beam to generate on-off pulses from a photocell operated the tachometer. The tachometer meter had a visual display and analogue output to the computer for real time sampling. An accuracy of ± 0.5 rpm was obtained in the visual display. The instruments are all made in-house. Regular calibration of the system was carried out to ensure accuracy of shaft speed was maintained.

3.8 SHAFT TORQUE

3.8.1 General Outline

Torque was measured by strain gauges mounted on the shaft. The signal was transmitted from the rotating shaft via a pre-amplifier and a low noise slip ring unit to the major instrumentation chain (Fig 3.8.1). A full bridge of four gauges were cemented along the principal axes of torsion. Effects of temperature change were compensated for in this system.

From the torque data, the power dissipated into the fluid (P) and the power number (Po) were calculated :

$$P = 2 \pi \tau N \qquad \text{...eqn(3.8.1)}$$

$$Po = \frac{P}{\rho N^3 D^5} \qquad \text{...eqn(3.8.2)}$$

Power number is a vital parameter to be measured in the test programme for two reasons; it allows comparison of solid-liquid performance of various systems at the same power input and also provides information on the likely forms of flow mechanism that are present in the vessel.

3.8.2 Calibration and Accuracy

The system was calibrated by applying a series of known static torques to the shaft.

By correlating the applied torques to the change in output signal in the system, a linear relationship was established from which a calibration factor was worked out to be used for future analysis.

This direct measuring technique is one of the most accurate ways of ascertaining shaft torque in agitated systems. Since the only check of accuracy available is the reproducibility of test, the calibration is conducted on a very regular basis. Impellers with standard power number (eg Rushton Turbine and Lightnin A310) were often used to re-confirm the calibration prior to the start of experimentation. The reproducibility is good. For example, some torque measurements in T_{61} were conducted twice, with a two year interval between, during which the shaft was completely re-strain-gauged and re-calibrated. The results were proved to be highly repeatable. The accuracy of the torque data is estimated to be in the region of ± 2%.

3.9 MINIMUM SPEED FOR SOLIDS SUSPENSION

The minimum speed for solids suspension was measured by two methods, visual observation and using an ultrasonic Doppler flowmeter (UDF). The visual technique is widely adopted in solid-liquid mixing research to determine N_{js}. However, this technique is very subjective and can only be applied when using a vessel with a transparent vessel base. The ultrasonic device offers a convenient means of measuring N_{js} in large vessels or when visual observations are not possible. The technique has been fully tested over a range of test conditions during this research which will be discussed in more details in section 3.9.3.

Many other measuring techniques have been developed in recent years. Many researchers have suggested that N_{js} can be extrapolated from the solids concentration profiles (eg Koutsakos 1989). This technique must be interpreted with great care because some impellers are better for off-bottom suspension than homogeneity and vice versa as has already been proved in this research programme (Sec 4.3.2). Some (Bourne and Sharma 1974) deduce N_{js} from slurry samples removed just above the vessel base. This method has the potential of being less dependent on human observation and judgement than the normal visual technique, but there are severe experimental difficulties in withdrawing a representative sample.

3.9.1 Visual Observation Method

This method of estimating N_{js} visually through a perspex vessel base was first described by Zwietering (1958). The criterion used in this work is the minimum speed at which no solid particles remained stationary on the vessel base for more than one to two seconds. This technique is simple, direct and rigorous but often restricted to research environments.

A layer of solid particles rested on the vessel base at low impeller speeds. As the speed was increased, solids were partly entrained by the liquid. At the point at which no solid particles rested on the base for more than 1 to 2 seconds, observations were continued for a period of one minute to confirm the judgement. If some particles re-deposited on the base and remained stationary for more than 1 to 2 seconds during the observation, the impeller speed was increased further until the underlying criterion was satisfied.

The N_{js} measurement was repeated at least twice to ensure repeatability. The reproducibility of results was generally very good, especially at low solids concentration. The N_{js} judgement became more difficult at high concentration (i.e. > 30% Wt). In general, the visual results are repeatable to approximately ± 3 % on average, though occasionally only to ± 5 % in high solids concentrations.

3.9.2 Measurement of N_{js} with an Ultrasonic Doppler Flowmeter

An ultrasonic device was adopted to monitor the bottom motion of the solids, so that just suspension speed could be determined in metal bottomed vessels enabling scale-up relationship to be established. Moreover, possible error due to subjectivity in measuring N_{js} visually can be greatly reduced. This section describes the underlying principle of this technique and the experimental procedures developed.

(i) Principle

Buurman et al (1985) have described the use of an ultrasonic Doppler flowmeter (UDF) for the measurement of just suspension speed. This instrument offers a convenient means of measuring N_{js} in large vessels or where visual observations are not possible. An

extensive evaluation has been carried out in Fluid Mixing Processes (FMP) of BHR Group Ltd to determine the most suitable technique for scale-up investigations. The UDF technique appeared to be the most convenient and reliable one. The benefits of this technique is that the measurement is non-intrusive, independent of scale and unaffected by the material of the vessel wall.

The UDF measures the Doppler frequency shift of an ultrasonic signal reflected from discontinuities in flowing liquid. The discontinuities can be suspended solids (eg dust particles), bubbles or interfaces caused by turbulent eddies in the flow. It is normally used for measuring flow in pipes. The sensor is mounted on the outside of the pipe wall and an ultrasonic beam, generated by electrical excitation of a ceramic piezo crystal, is transmitted through the pipe into the fluid at an angle to the flow. Reflected signals are received by a second piezo-electric crystal in the same sensor. The Doppler shift can be converted to a velocity if the instrument is suitably calibrated.

The UDF can be used to measure the just suspension speed of solid particles if mounted on the vessel base. Knowledge of the last suspended position is required to mount the probe at the right position (eg centre bottom for torispherical vessel base with T/2 diameter impellers). This is normally determined from test results from 0.305 and 0.61 m perspex vessels. Without this information, experiments have to be conducted with various probe mounting locations to establish N_{js}. At low impeller speeds, the ultrasonic signal is reflected from the static layer of solids on the vessel base and there is no response from the meter. As the impeller speed is increased, solid particles are entrained by the fluid and become fully mobile and there is a large increase in the indicated velocity. As the impeller speed increases beyond N_{js}, the indicated velocity continues to increase, but at a slower rate (Fig 3.9.1 & 3.9.2).

(ii) Experimental Methods

With all impellers tested to date, visual observation indicated that the position where suspension finally occurs was directly beneath the impeller and this is where the UDF sensor was mounted. However, for some $D \leq T/3$ impellers, it is possible to have the last suspension position on the periphery of the vessel base. This is expected to be more likely to occur with a flat vessel base.

Prior to the start of the experiment, exploratory tests were conducted to optimise the incoming signals without picking up interference from the surroundings. This can easily be done by adjusting the signal and noise levels in the meter. The average penetration depth or focal point of the transmit and receive polar diagrams, known as the flow information window, is 10-20 mm into the fluid when the particle concentration is less than approximately 10% Vol. With high particle concentration applications the signal penetration may only be 2-3 mm into the fluid. PVC shims were used to space the UDF sensor away from the base of the vessel to ensure focus of the detection point right on the inner surface of the vessel base.

The output from the meter is connected to a computer (Fig 3.8.1). A program was written to allow a real time graphical display of the Doppler velocity. The Doppler velocity was then sampled for a range of stirrer speeds. Tangents to the curve were drawn at the point of maximum slope, and also the line of higher stirrer speed. N_{js} was the point at which the two tangents crossed (Fig 3.9.1).

The repeatability of results is good ($< \pm 3\%$ in small scales), especially in large vessels, and their transition points were very sharp. However, a less distinct transition was found in T_{61}. This is probably because the sand beds are proportionally thinner in the small vessel. A similar finding was also reported by Buurman (1985).

3.9.3 Calibration of the UDF Technique

An extensive comparison was made between the two experimental techniques, using the same configuration. This was done to gain confidence in the newly developed UDF arrangement and to establish the relationship between the two data sets so that they could all be used for future scale-up analysis. This included measurements from other researchers, with tests on four impellers, three solids types and two vessel bases.

Comparisons of 38 independent sets of data was made. It was found that the measurements made using the UDF technique followed the same trends as measurements of N_{js} made visually. The dependence of N_{js} on d_p and X was nearly identical using the two measuring techniques (Mak 1988a). It was discovered that the visual N_{js} results were consistently slightly higher than the corresponding UDF values, with one or two exceptions

at high solids concentrations. The results are presented as plots of UDF N_{js} against visual N_{js} in Fig 3.9.3.

The data can be correlated in the form of :

$$Visual\ N_{js} = k\ UDF\ N_{js} \qquad \text{...eqn(3.9.1)}$$

k was found to be equal to 1.07 with a standard deviation $\sigma_{n-1} = 0.04$, and 95 % confidence limits of ± 0.01 :

ie k = 1.07 ± 0.01

It is sufficient to assume k=1 for design purposes. However, the constant k (= 1.07) is to be retained in this work to correct the visual results for scale-up comparison. This investigation has given enough confidence to apply the UDF technique to large vessels, from which scale-up data is urgently needed.

3.10 LOCAL SOLIDS DISTRIBUTION

Good distribution of solid particles in a stirred vessel is very often required in solid-liquid processing. For example, a uniform dispersion of solid particles throughout the mixing vessel is necessary to ensure uniform exposure to the process conditions.

There are many different techniques adopted by researchers in the measurement of local solids concentration. Visual observation was employed in the early days, tracer and streak photography were used to complement the technique. This has provided a useful understanding of the flow patterns produced by different types of impellers and configurations but is limited to qualitative observations at low solids concentrations.

Predicting just suspension speed or solids homogeneity from the slurry interface in the vessel could be misleading. A high liquid/solid-liquid interface does not necessarily guarantee a good distribution within the bulk (Sec 4.3.4). Distinct differences in solids concentration at different heights has been reported in literature (Einenkel 1977). In fact, experience within BHR Group Ltd suggests that a hydrofoil impeller can produce a far better solids distribution

with a low level of slurry interface, compared to a T/2 diameter pitched blade turbine (Mak 1987).

Due to their non-intrusive nature and the capability of measuring solids concentration in localised regions, optical methods are very popular and much useful work has been produced (eg Magelli 1991, Shamlou 1989). However, this technique is usually limited to a low solids concentration, depending on the transparency of the test media, and to small scale vessels. Re-calibration is very often required for different test media.

Sample removal is another widely used technique (eg Barresi 1987). It is simple and convenient and has much potential. For example, it is the only existing method by which local particle size distribution can be determined. However, it is labour intensive and there is still uncertainty over how well it can measure the true local concentration. Further research on the understanding of isokinetic sampling is required.

The conductivity method does offer many advantages in measuring solids distribution. The equipment is relatively cheap and easy to construct. It can measure a solids concentration range from under 5 % up to 50 % by volume and can reliably detect a 1 % change in concentration. Of course, like all the other techniques, the conductivity method has its shortfalls; it is intrusive and therefore a certain degree of flow disturbance must be expected. Any solids likely to cause a rapid change in base conductivity (conductivity of the fluid) are undesirable. The conductivity technique is the one which has been adopted by this research in measuring solids distribution.

3.10.1 The Solids Concentration Probe

The solids distribution results in this work were acquired by means of a solids concentration probe. The probe was developed in Fluid Mixing Processes Group (FMP) in conjunction with the Instrumentation Department in BHR Group Ltd, based on a design used at the Warren Spring Laboratory. It consists of a "Y" shaped epoxy resin body and a stainless steel tube handle (Fig 3.10.1). This is so designed to be robust yet causes a minimum of flow disturbance. Two 10 × 10 mm platinum electrodes are mounted 10 mm apart, at both ends of the epoxy body, to give a measuring volume of 1 cm^3. The conductivity between the two electrodes is measured and transmitted to a computer via a solids concentration meter (Fig

concentration meter (Fig 3.8.1). The local temperature is measured simultaneously by using a platinum resistance thermometer, enabling correction for the effect of temperature upon conductivity measurement.

This technique is based on the principle that the conductivity of a liquid will be modified by the presence of foreign bodies. Thus, when solids particles pass between the two electrodes of the probe, a change of conductivity will be registered, from which the local concentration can be calculated, given that the relationship between change in conductivity and volume fraction of solids is known.

2.10.2 Probe Calibration

The probe was calibrated in a 200 mm diameter liquid fluidised bed (Ruszkowski 1985, Fig 3.10.2). Round grained silica sand up to 55 % volume was used. The sand was sieved to 500-700 μm and acid washed to remove impurities. The conductivity measured by the probe, after correcting for temperature, was found to be inversely proportional to the volume fraction of solids. There is some scatter in the results of these calibrations, due to the difficulty of maintaining perfectly homogeneous and steady conditions in the fluidised bed. A typical output is presented in Fig 3.10.3.

Further tests were conducted in a small stirred vessel in order to confirm the calibration. The vessel had a diameter of 150 mm and 90-150 μm round grained sands (Type D) were used as the test solids. The solution was agitated intensely to maintain a homogeneous distribution of solids in the vessel. The homogeneity of the distribution was verified by making measurements at several points and heights in the vessel. The results of this stirred vessel verification were limited to 10% solids concentration by volume, since at higher concentration a homogenous solids distribution could not be maintained without drawing air down into the suspension. A typical result for a stirred vessel calibration is shown in Fig 3.10.5. There is much less scatter, and this is the case for all stirred vessel calibrations carried out with a number of different solid types.

All the solids tested, with particle diameters ranging from 20 μm up to 700 μm, gave the same relationship :

$$\kappa_c = \kappa_{or} (1 - A C_v) \qquad \text{...eqn(3.10.1)}$$

where κ_c and κ_{or} are the corrected conductivity and the conductivity of water at reference temperature respectively. The calibration constant, A, was 1.4 in all cases.

Machon et al (1982) obtained the same functional relationship between conductivity and solids concentration, working with a radically different probe geometry. Unfortunately, the value of the calibration constant was not reported.

The measured conductivity, κ_m, and the reference conductivity, κ_{or}, were corrected for variations in temperature with the following equation :

$$\kappa_c = \kappa_m (\kappa_{or} / \kappa_{om}) \qquad \text{...eqn(3.10.2)}$$

3.10.3 Probe Location and Orientation

Most of the solids distribution measurements have been concentrated on a single radial location, the probe being placed midway between two baffles and at T/6 clearance from vessel wall. The radial solids concentration profiles with 30% Wt 150-210 μm sand in T_{183} were also studied (Fig 3.10.4). The radial concentration profiles were flat, except when the probe was at the clear liquid/solid-liquid interface (eg Fig 4.6.6). This normally happened when the probe was mounted towards the top of the vessel, with the impeller running at relatively low speed. The flatness of the radial profiles has already been reported by other authors (eg Barresi 1987, Shamlou 1989) but their results were established from vessels of limited sizes (T = 0.39 and 0.225 m). It is encouraging to have the results confirmed at a larger scale. The use of one-dimensional steady state model by a number of researchers (eg Magelli 1990) is justified. Thus, to focus on a single radial position (ie T/6 from the vessel wall) for system comparison is acceptable.

Prior to the start of experiments, tests were carried out to check the effect of probe orientation, and the reproducibility of results. For tests with standard baffled vessels, the

effect of probe orientation was not unduly significant. In the worst case there was a difference of 10% between the highest and lowest value recorded (Mak 1988a). The maximum response was observed when the open side of the probe faced the impeller leading edge (Fig 3.10.1). This orientation was subsequently adopted for all the tests. Thus, in all cases, the probe was placed midway between two baffles and kept parallel to the first baffle in an anti-clockwise direction, viewing from the top of the vessel. The solids distribution results measured in stirred vessels show excellent reproducibility (± 1%), especially those with a concentration greater than 5% Wt.

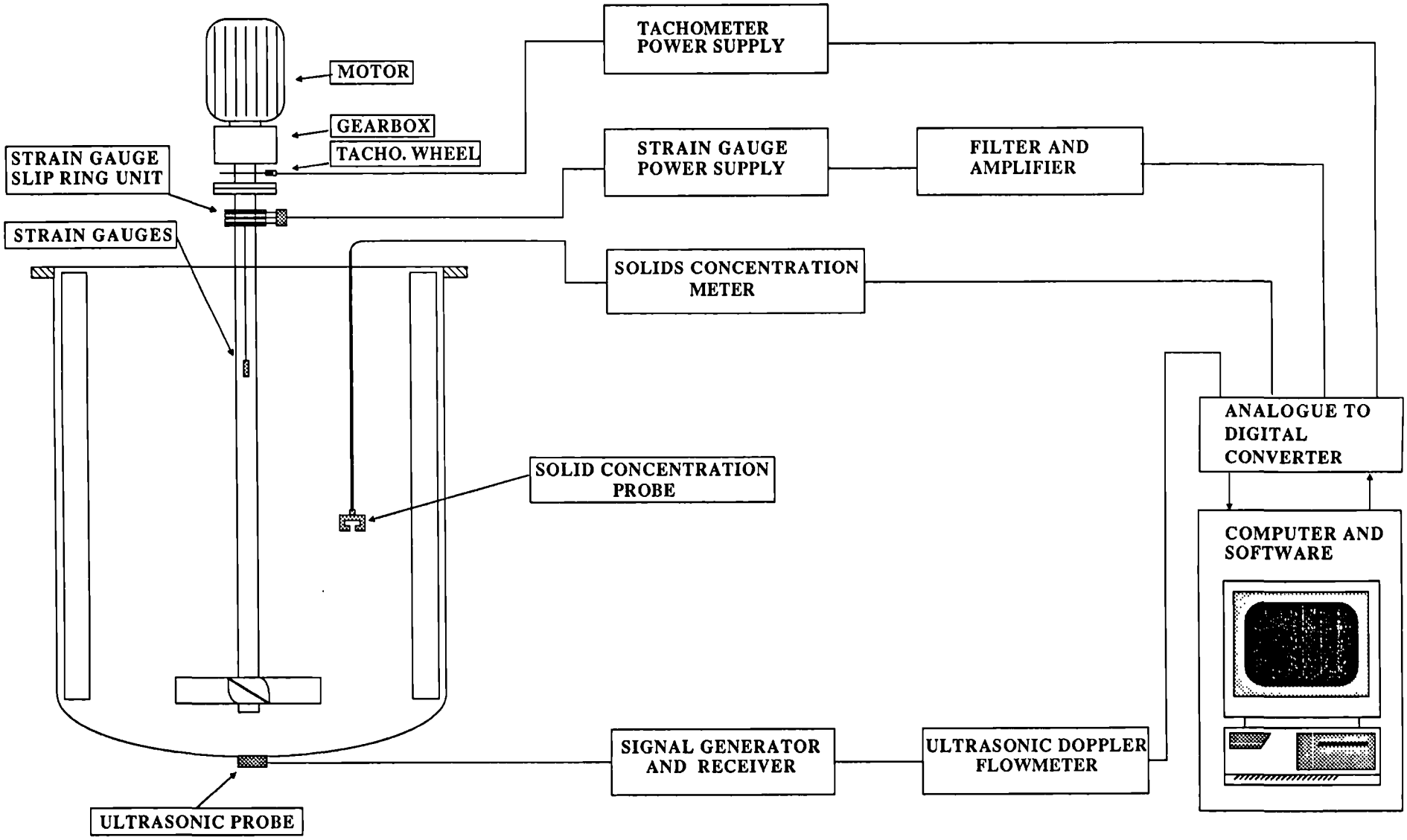

Fig 3.8.1 The Instrumentation Chain

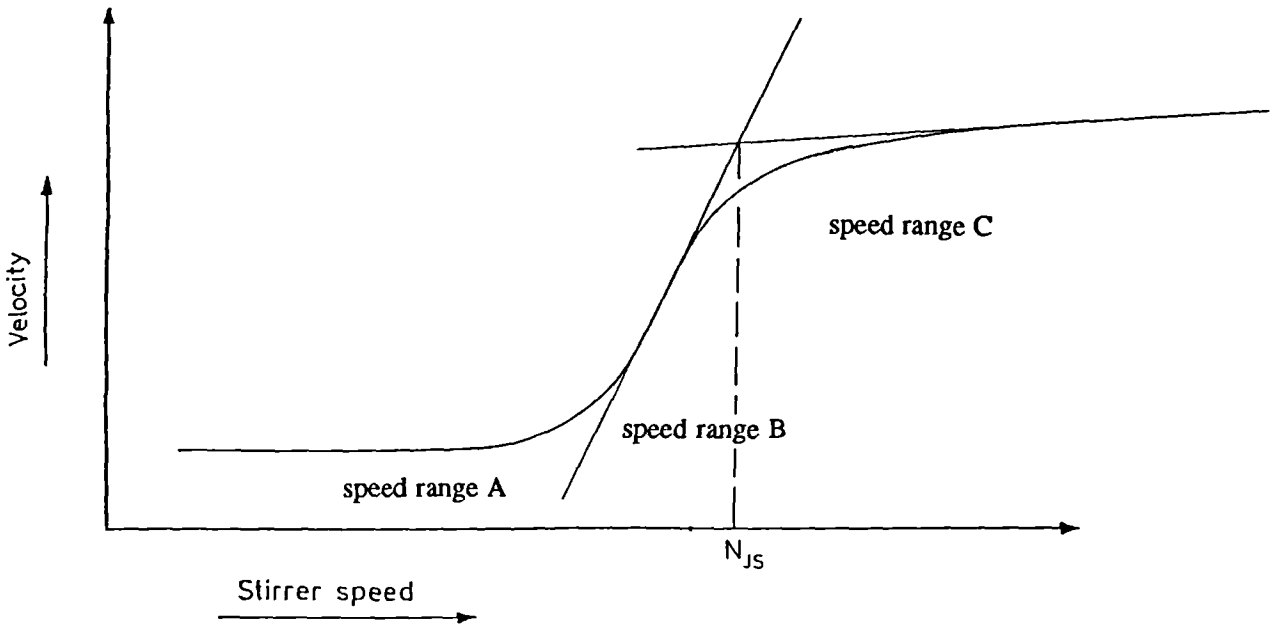

Fig 3.9.1 A Typical UDF Output

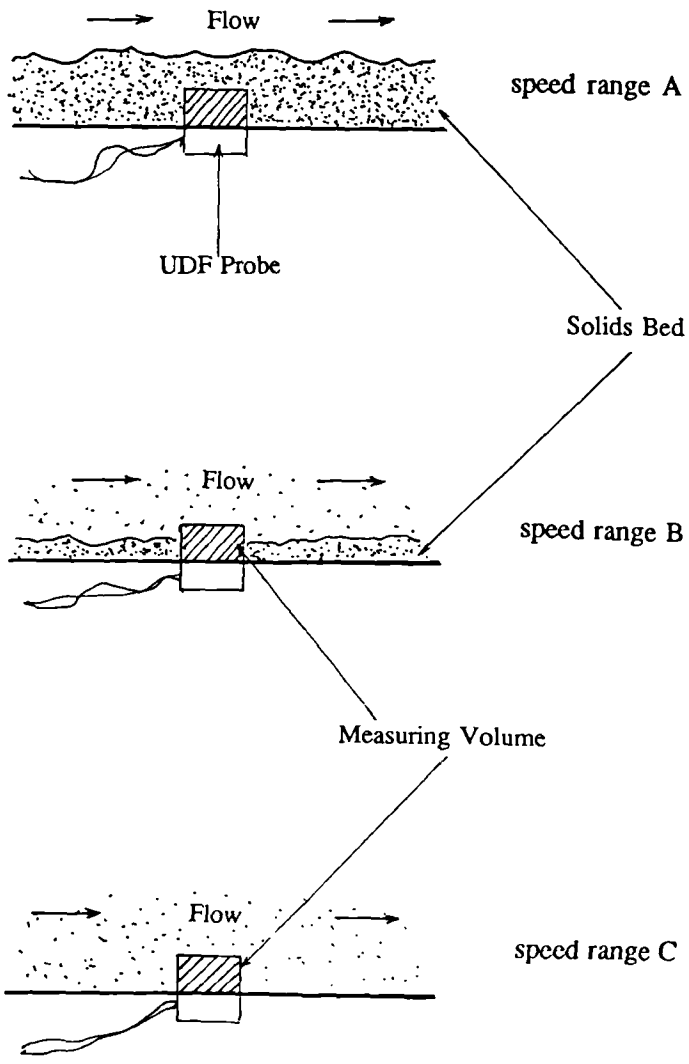

Fig 3.9.2

The Principle of the UDF Technique

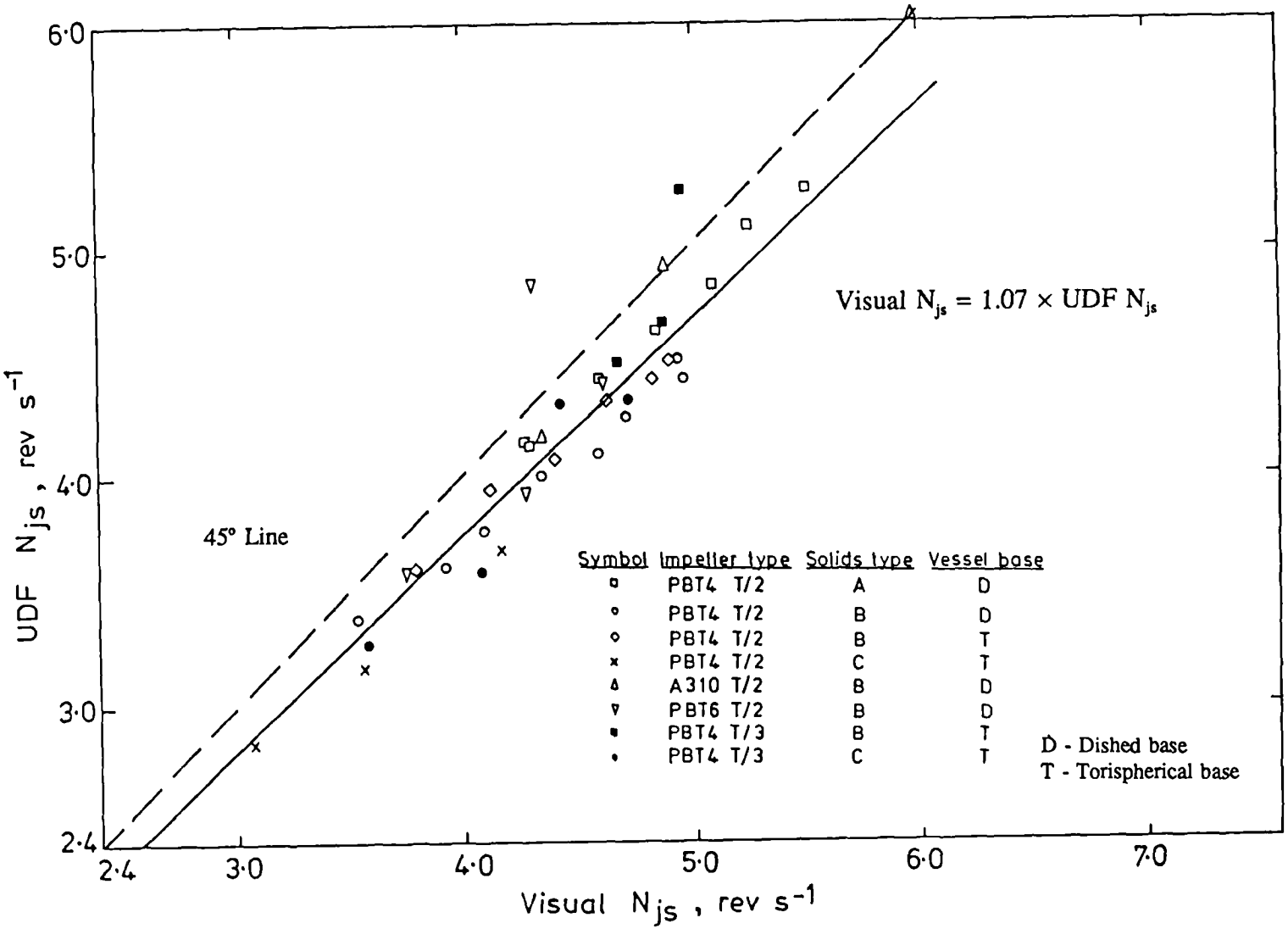

Fig 3.9.3 Relationship between UDF and Visual N_{js}

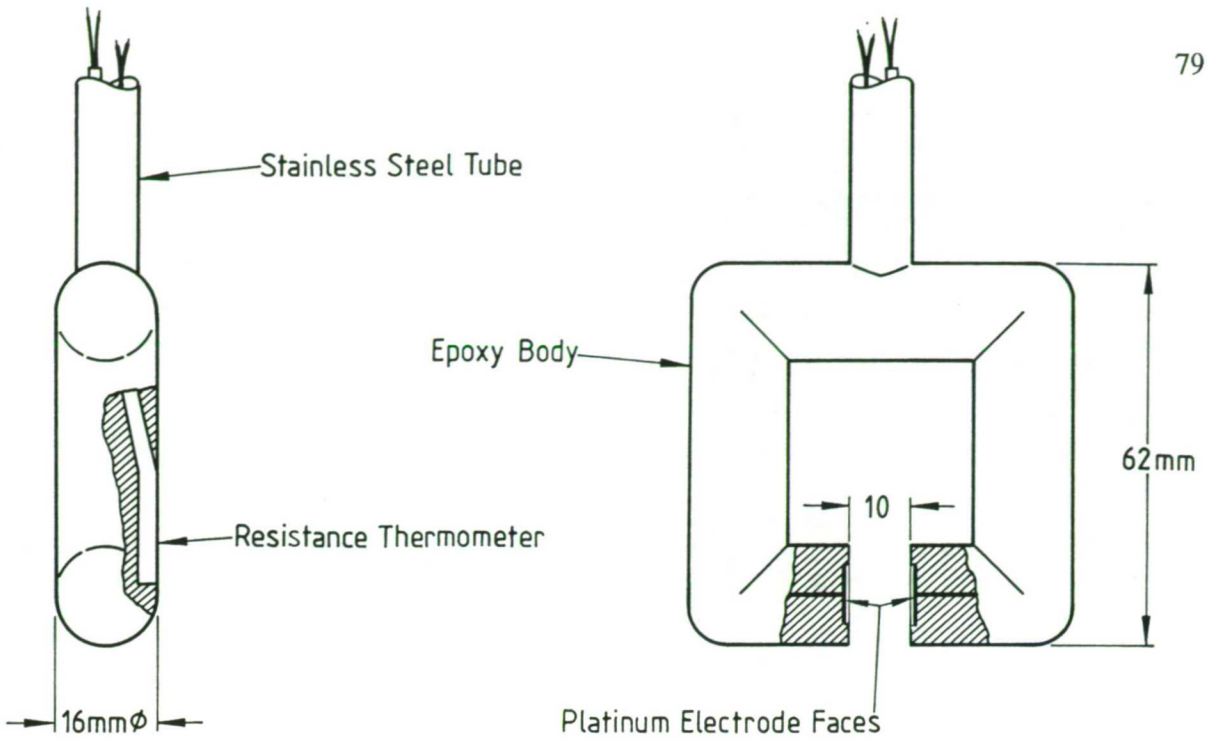

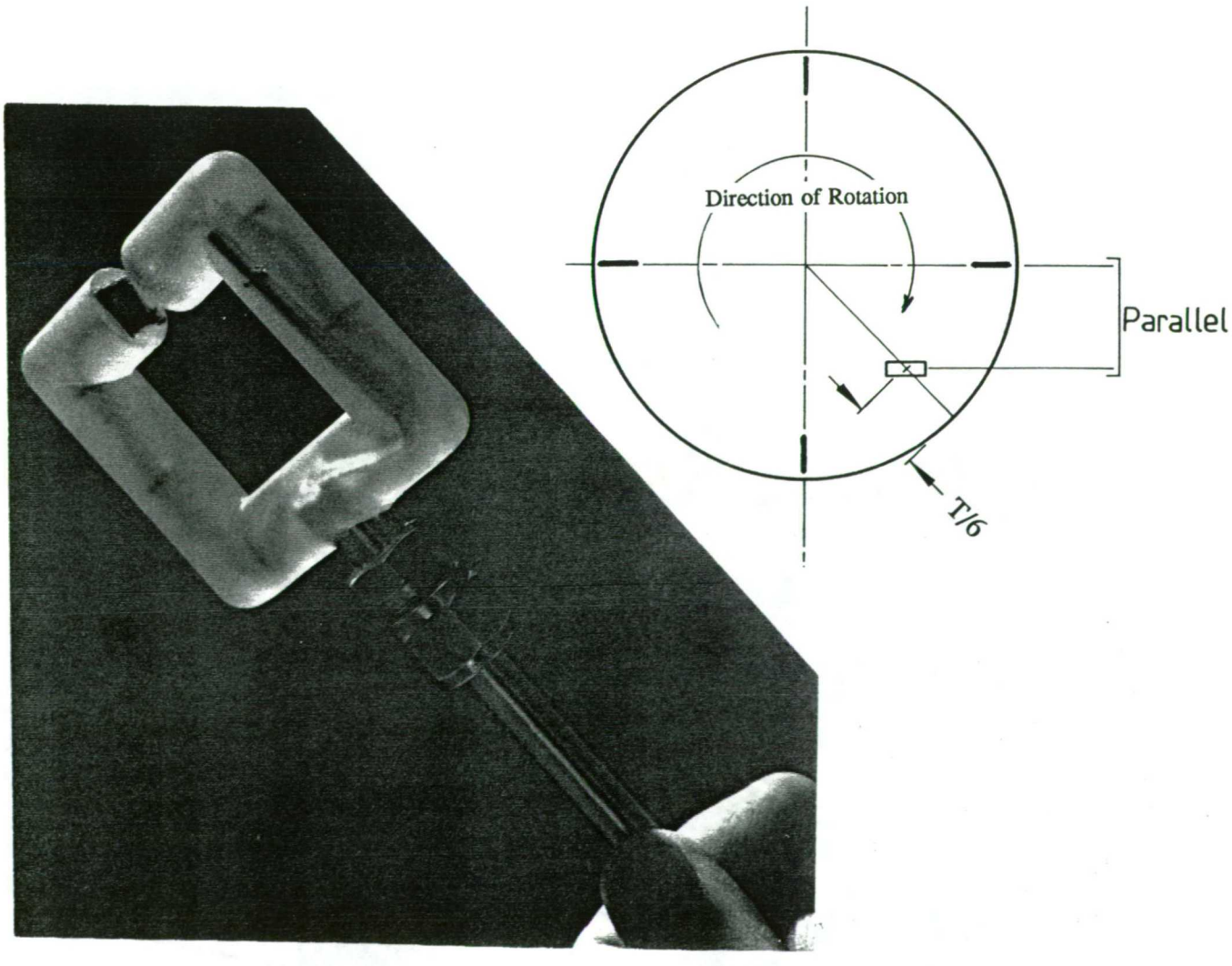

Fig 3.10.1 The Conductivity Probe: Construction and Orientation

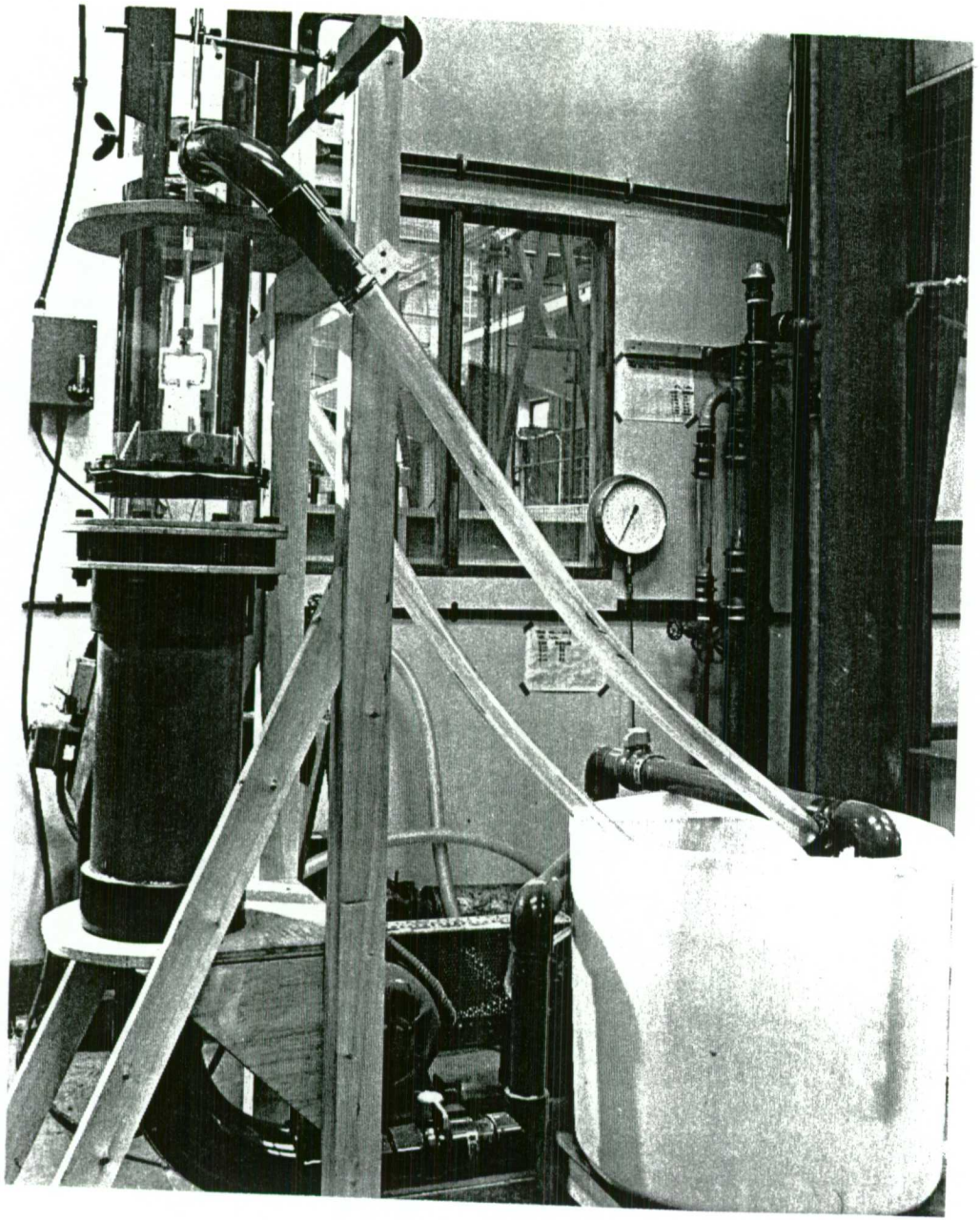

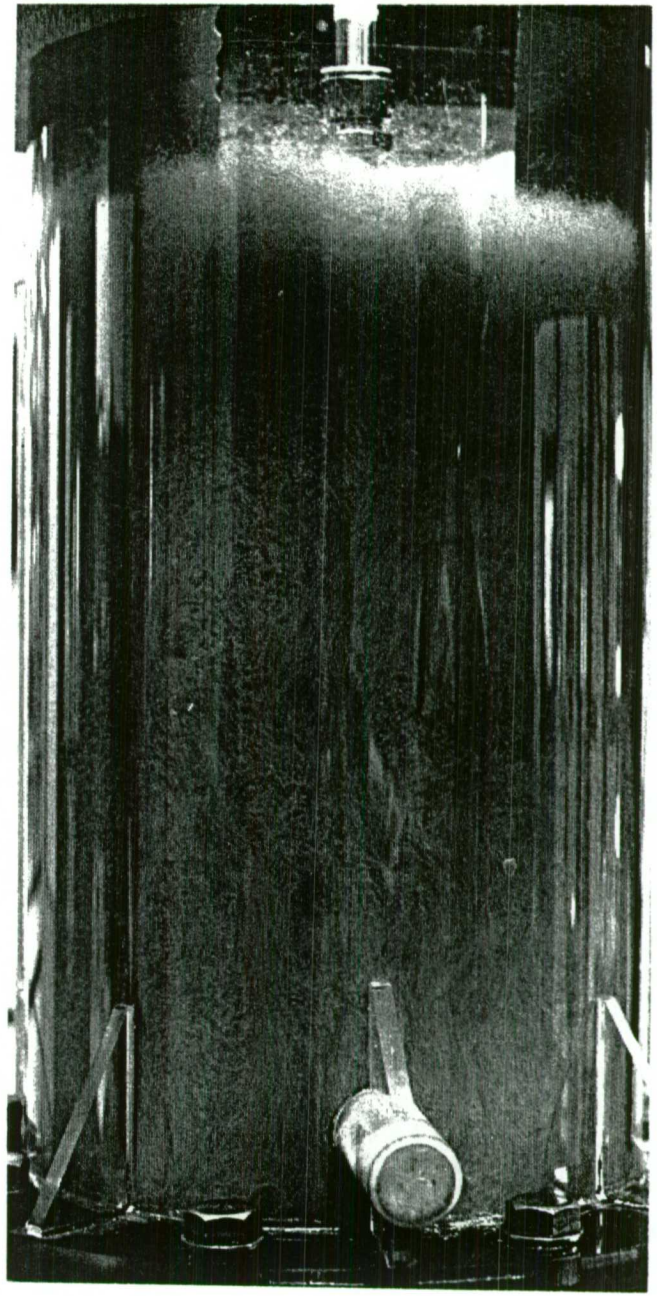

Fig 3.10.2 Fluidised Bed for Probe Calibration

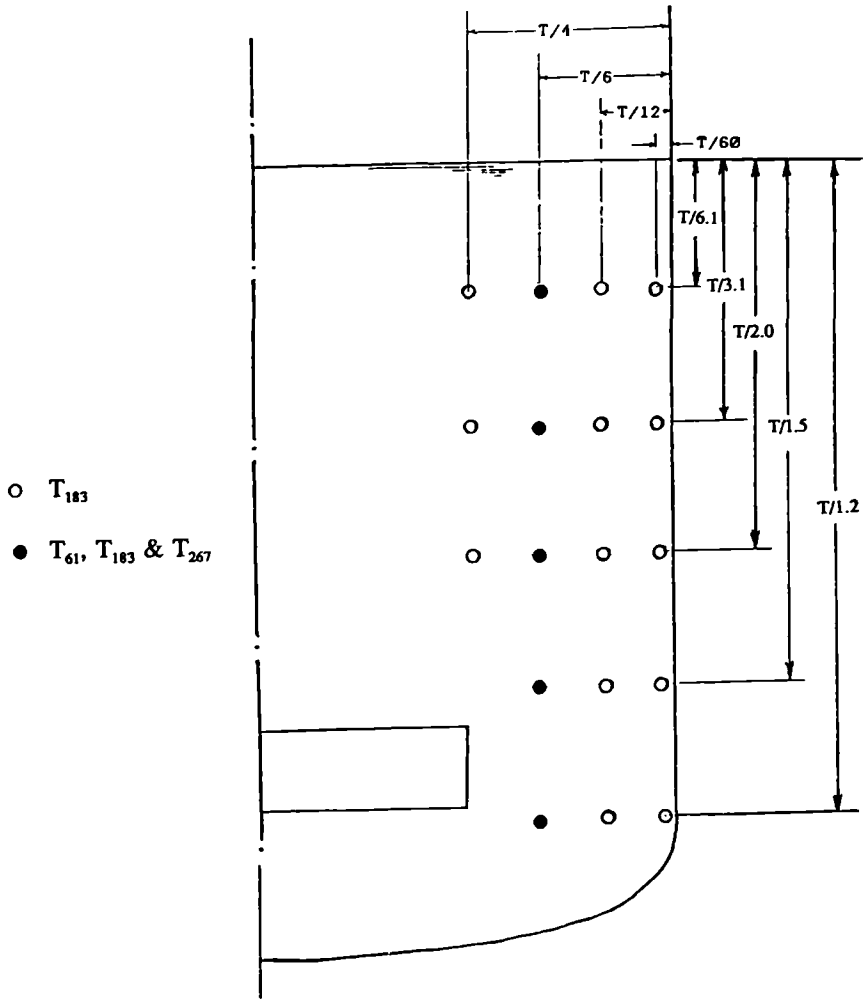

Fig 3.10.4 Sampling Positions

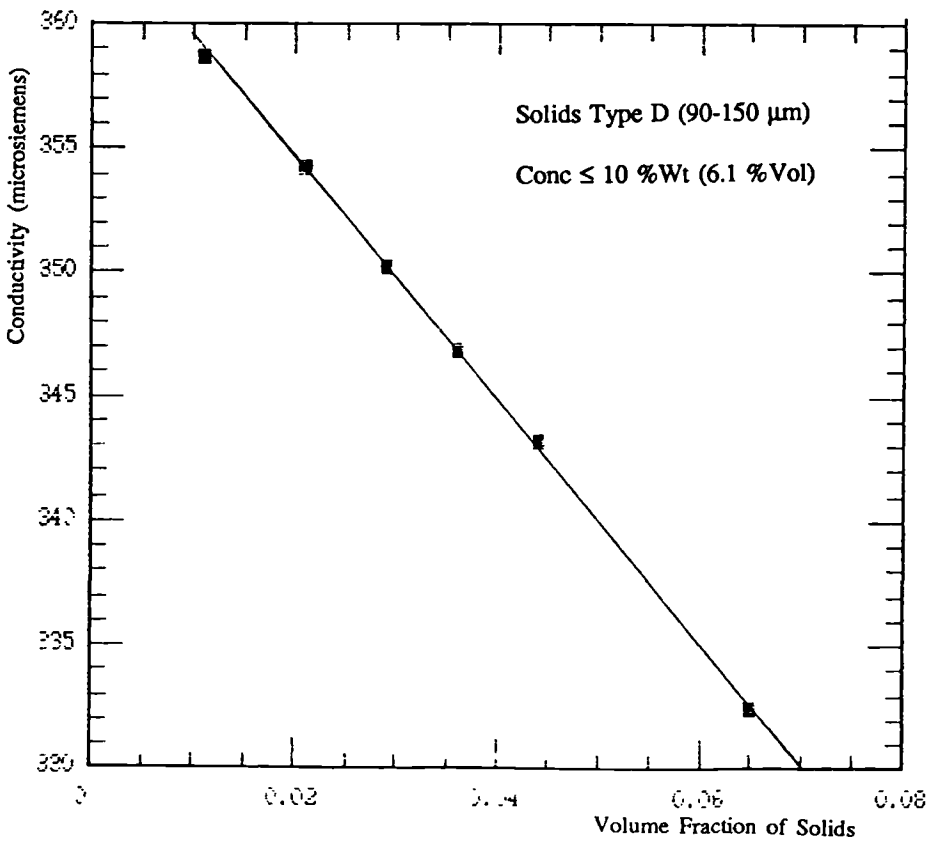

Fig 3.10.5 Calibration confirmation: Conductivity Test in a 150 mm Diameter Well-agitated Beaker

CHAPTER 4: RESULTS AND DISCUSSION

4.1 PARTICLE FLOW PATTERN

Flow pattern depends critically upon the impeller and vessel configuration. It is always useful to check the particles flow pattern in conjunction with any measurement in order to reveal the mixing mechanisms and to facilitate interpretation of the results. Flow visualisation of the experiments were made whenever possible during this study. Although solid-liquid mixing flow patterns have been investigated by a number of researchers, their results were confined to limited geometries and little effort has been made to relate their results to the observed flow pattern.

Most of the flow visualisation tests were made in the two transparent vessels (T_{31} and T_{61}). At high solids concentrations (eg > 15% vol), visualisations were inevitably confined to flow patterns near the vessel wall and on the vessel base. For tests in which an understanding of the internal flow loops were important, such as flow interactions in dual impeller systems, black PVC cylinders (cylindrical in shape, diameter = 1.5 mm, length = 4.5 mm, SG = 1.31 and U_t = 0.088 m s^{-1}) were used as flow followers to trace circulation within the vessel. Laser Doppler Anemometry measurements were also made available to facilitate the interpretation of the results. However, it must be realised that the presence of solid particles will have some modifying effect on the flow regime and the flow pattern at high solids concentration is not going to match exactly as that of low solids concentration.

This section describes an overall view on solid-liquid mixing flow pattern and the particles movements on the vessel base are generalised. The concepts and analogies introduced in this section will be used in later stages to explain some more specific investigations.

4.1.1 An Overall View

At low impeller speeds, the impeller pushes the solids sideways and digs a pit in the solids bed. As the speed increases, the solids bed is partially fluidised and this produces three distinct zones; a clear liquid layer at the top of the vessel, an unsuspended solids layer on the base and a region of fluidised mixture in between (Fig 4.1.1). The relative proportion of the

three zones depends on how easily the particles are picked by the fluid and how efficient the mixer is in producing bulk mixing. For example, impellers with a high pumping capacity tend to generate good overall mixing and hence, a relatively small clear liquid layer. On the other hand, mixing of heavy particles will result in a larger clear top region at the same power input.

Referring to Fig 4.1.1. As the impeller speed continues to increase, the fluidised region expands, while the amount of unsuspended solids decreases and eventually disappears (N_{js} attained). With a further increase in impeller speed, the clear liquid layer in the upper region also gradually disappears and the solid-liquid mixture reaches the point of maximum homogeneity before the solids redistribute themselves axially and radially. In the case of axial redistribution, this is believed to be caused by the circulation pattern produced by the impeller, which confines the particles to certain trajectories (eg Fig 4.1.4). The strong centrifugal force generated by the impeller at high speed tends to move the solid particles towards the circumference and thus radial redistribution occurs.

Referring to the same figures, if a sampling point is established close to the liquid surface (Position A) it will measure a gradual increase in solids concentration until the contents reach maximum homogeneity. Conversely, if the sampling point is positioned near the vessel base (Position C), it will experience a gradual decrease in solids concentration until the contents reach maximum homogeneity. However, if the sampling point is positioned midway in the vessel (Position B), it will first show a gradual increase in solids concentration with speed until the fluidised bed expands to reach the conductivity probe whereupon it will then measure a solids concentration greater than homogeneity. Subsequently, as the fluidised region expands still further the concentration at position B will decrease until it attains the value corresponding to the best homogeneity. A plot of relative solids concentration against impeller speed for positions A, B and C is presented in Fig 4.1.2.

When $N \approx N_{js}$, three distinct flow regimes were seen visually through the vessel wall (Fig 4.1.3). At the lower part of the vessel, the solids adjacent to the wall all move vertically upward indicating that the fluid velocity was strong and the solid particles were following a well defined trajectory. Eddies were found in a second region, immediately above the first. Here, the solid particles were swirling in all directions and there were seen to be frequent interactions between the particles within an eddy and its neighbourhood. Similar observations

were recorded by Hockey et al (1989) in their flow visualisation tests with Newtonian and Non-Newtonian fluids in stirred vessels (Fig 4.1.4). In the upper part of the vessel, the third region, there was a layer of clear liquid with very low solids concentration. This last phenomenon was more distinct with the hydrofoils and T/3 diameter pitched bladed turbines in which axial flow was dominated. The flow pattern directly beneath the impeller is rather complex, being a function of impeller type, clearance, diameter and vessel geometry and this will be discussed in more detail in the forthcoming sections.

4.1.2 Flow Pattern at Vessel Base

The flow pattern of particles on the vessel base was observed by means of a mirror placed beneath it. It was found possible to interpret the results according to the impeller discharge flow (Fig 4.1.6). Three types of flow were observed, swirl flow was found directly underneath the impeller and was primarily responsible for the suspension of the central piles of solids. Axial and radial flow were present outside the swirl flow region. The results are summarised in Fig 4.1.5 and 4.1.7.

(i) <u>Vortexing</u>

This is normally found at the centre of the base, rotating slightly off-centre in the same direction as the impellers (Fig 4.1.6 and 4.1.7). This is believed to be generated by the trailing vortices at the impeller tip and driven by high speed jets to the vessel base (Tatterson et al 1980, Fig 4.1.8). In certain impeller/clearance combinations, planetary motion is observed (Fig 4.1.5-a). The suspension of the central pile of particles with a dished base relies primarily on this vortexing effect.

(ii) <u>Radial Flow</u>

Radial flow is generated by the axial component of the impeller discharge. The flow turns radially outwards towards the vessel wall as it impinges on the vessel base (Fig 4.1.5 & 4.1.8). Radial flow starts outside the vortexing region and extends as far as the circumferential flow region of the base (Fig 4.1.7). This flow regime is very distinct with strong axial flow impellers such as Lightnin A310 and 30° PBT4 (T/3).

(iii) Circumferential Flow

This normally takes place towards the outermost regions of the base (Fig 4.1.7) and is usually associated with radial flow impellers such as the flat blade turbines. Circumferential flow is caused by the radial component of the impeller discharge on reaching the vessel base.

In general, as the impeller diameter increases, the radial flow region is reduced and the amount of circumferential flow increased. The effect of decreasing impeller clearance is very similar and will increase both the vortexing and circumferential flow regions. Since the flow pattern changes with configuration, it is likely that there is more than one mechanism responsible for the suspension of solid particles. The type of mechanisms causing solids suspension shall then be a function of vessel geometries (i.e. how easily certain mechanisms are being generated) and physical properties (i.e. how readily the solid particles are being picked up by the mechanisms).

Table 4.1.1 Just Suspension Speeds for 3 Solids Types at Periphery

Clearance	Just Suspension Speed (N_{js}) at Periphery, rpm			Regression Analysis
	Stainless Steel	Sand	Acrylic	
T/4	170	182	92	$N_{js} \propto \Delta\rho^{0.18}$
T/6	170	162	81	$N_{js} \propto \Delta\rho^{0.21}$
T/8	200	160	73	$N_{js} \propto \Delta\rho^{0.28}$

To demonstrate this, experiments were conducted with a 45° PBT4(T/3) in T_{31}. The solid particles used were acrylic (SG=1.18), sand (SG=2.63) and stainless steel powder (SG=8.0). They all have similar shape and they were sieved within a narrow range of particle sizes (150-200 μm). At low impeller speeds, a band of solids remained near the circumference, as well as the pile at the centre. The band near the circumference disappeared gradually as the impeller speed increased and the solids at the centre were the last to be suspended. The just suspension speeds of the peripheral ring and central pile for 1% Wt of solids are presented in Table 4.1.1 and 4.1.2.

Table 4.1.2 Just Suspension Speeds for 3 Solids Types at Centre

Clearance	Just Suspension Speed (N_{js}) at Centre, rpm			Regression Analysis
	Stainless Steel	Sand	Acrylic	
T/4	645	317	125	$N_{js} \propto \Delta\rho^{0.45}$
T/6	592	290	84	$N_{js} \propto \Delta\rho^{0.54}$
T/8	457	215	72	$N_{js} \propto \Delta\rho^{0.51}$

Note that the exponents on $\Delta\rho$ for N_{js} at the periphery (Table 4.1.1) are very different from those of N_{js} at the centre (close to Zwietering's conclusion, Table 4.1.2 and Eqn 2.1.2) and this confirms the visual observation that the suspension mechanism at these two locations are different. Another interesting phenomenon observed during the experiments was that the suspension mechanisms varied with types of solids. Acrylic powders were picked up by bursting eddies whilst rolling and sliding motion was found with the stainless steel powder at N_{js} (Fig 4.1.9). Thus the suspension mechanism seems to be both location and physical property dependent.

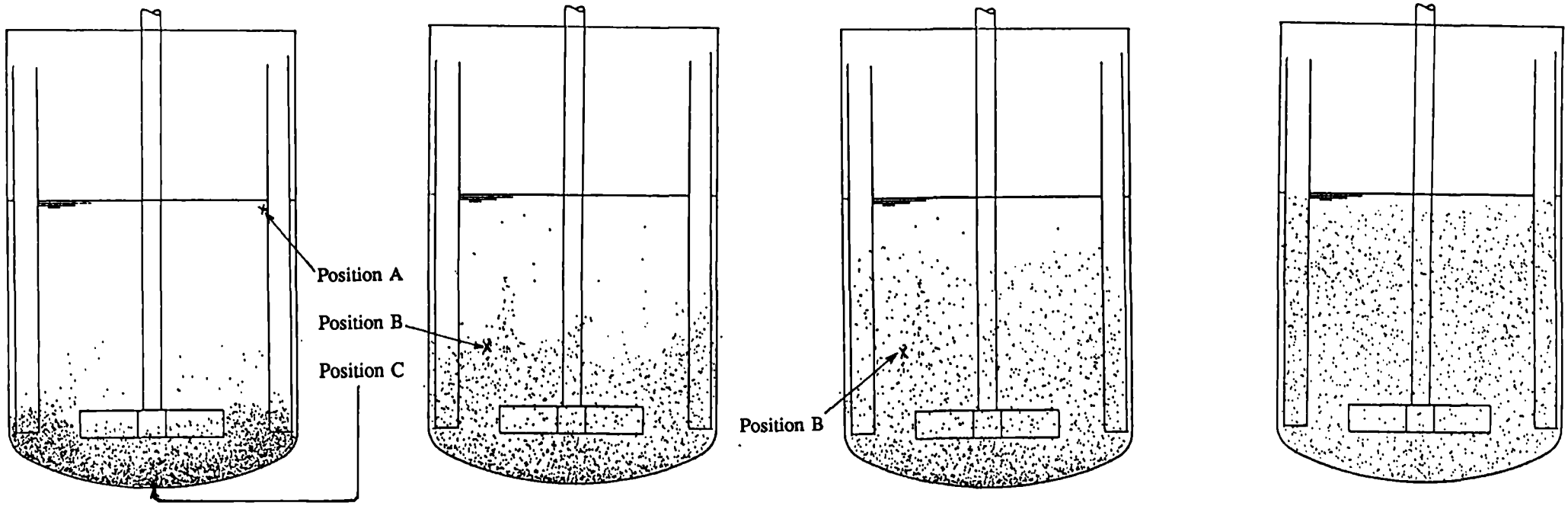

Fig 4.1.1

Particles Flow Pattern - An Overall View

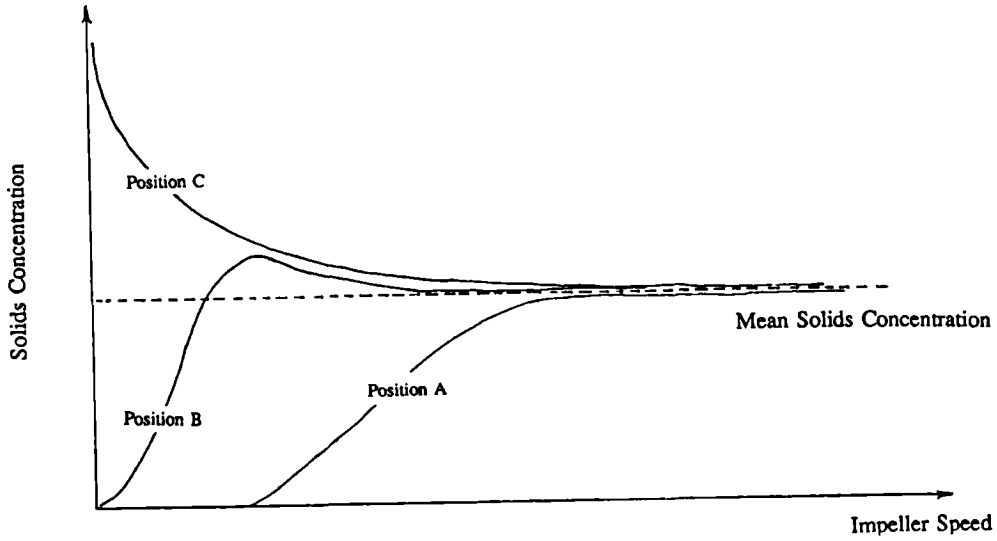

Fig 4.1.2

Relative Solids Concentration against Impeller Speeds at Various Positions

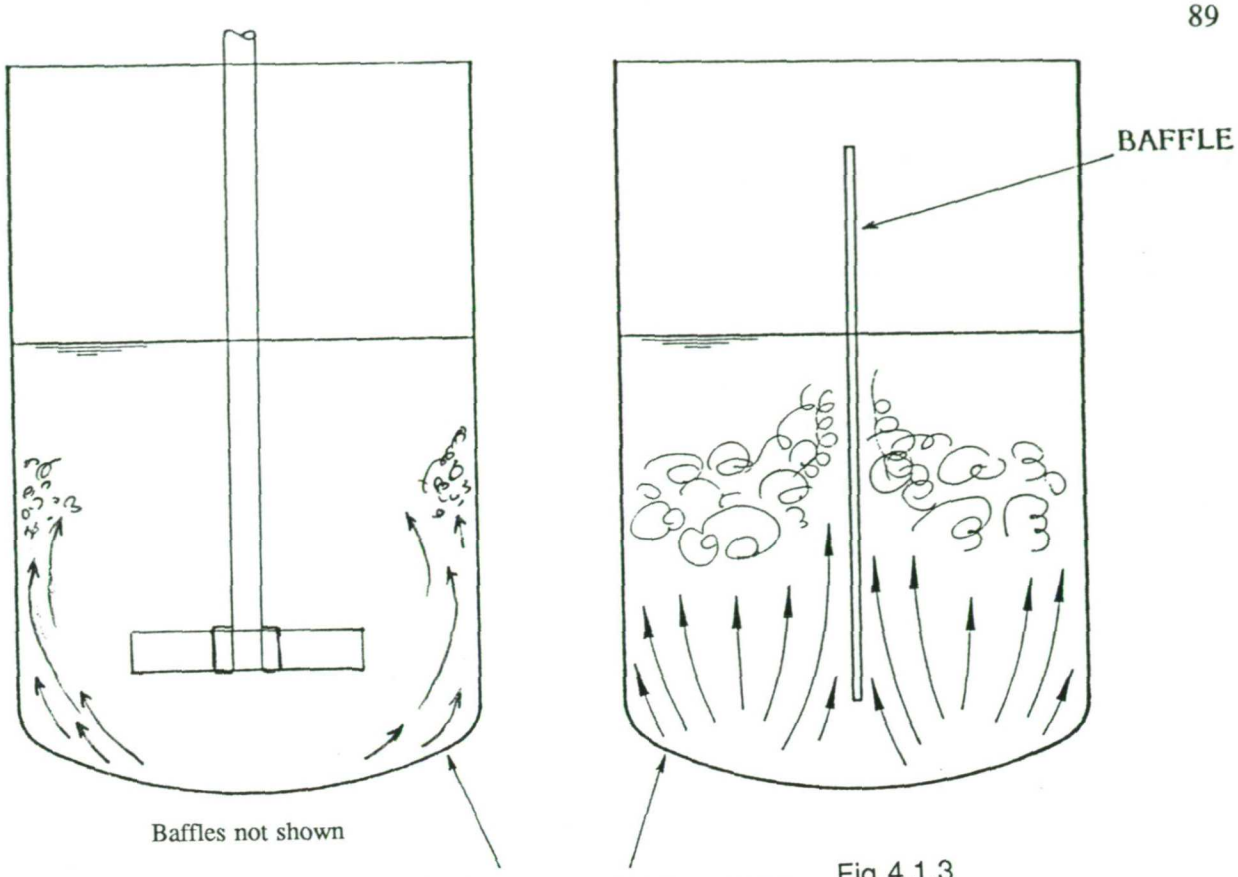

Fig 4.1.3

Flow Regimes - A Side View

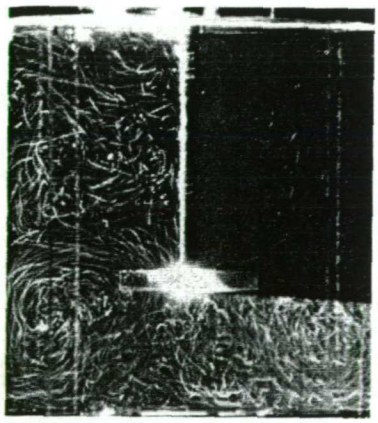

45° impeller, $Re = 3250$

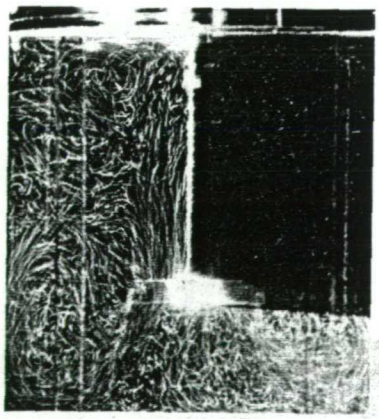

60° impeller, $Re = 3250$

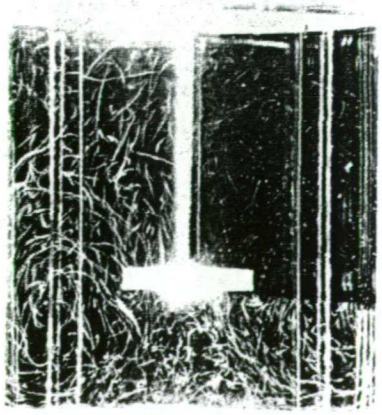

45° impeller, $Re = 24000$

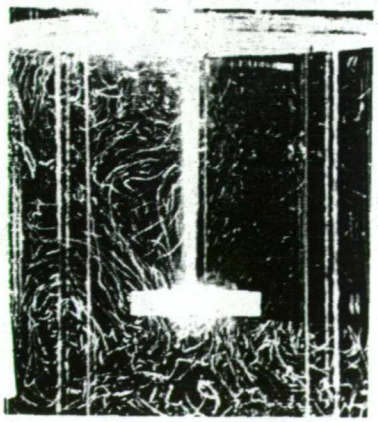

60° impeller, $Re = 24000$

Fig 4.1.4

Flow Visualisation at Impeller Region: Revealing the Particles Trajectory (Hockey et al 1989)

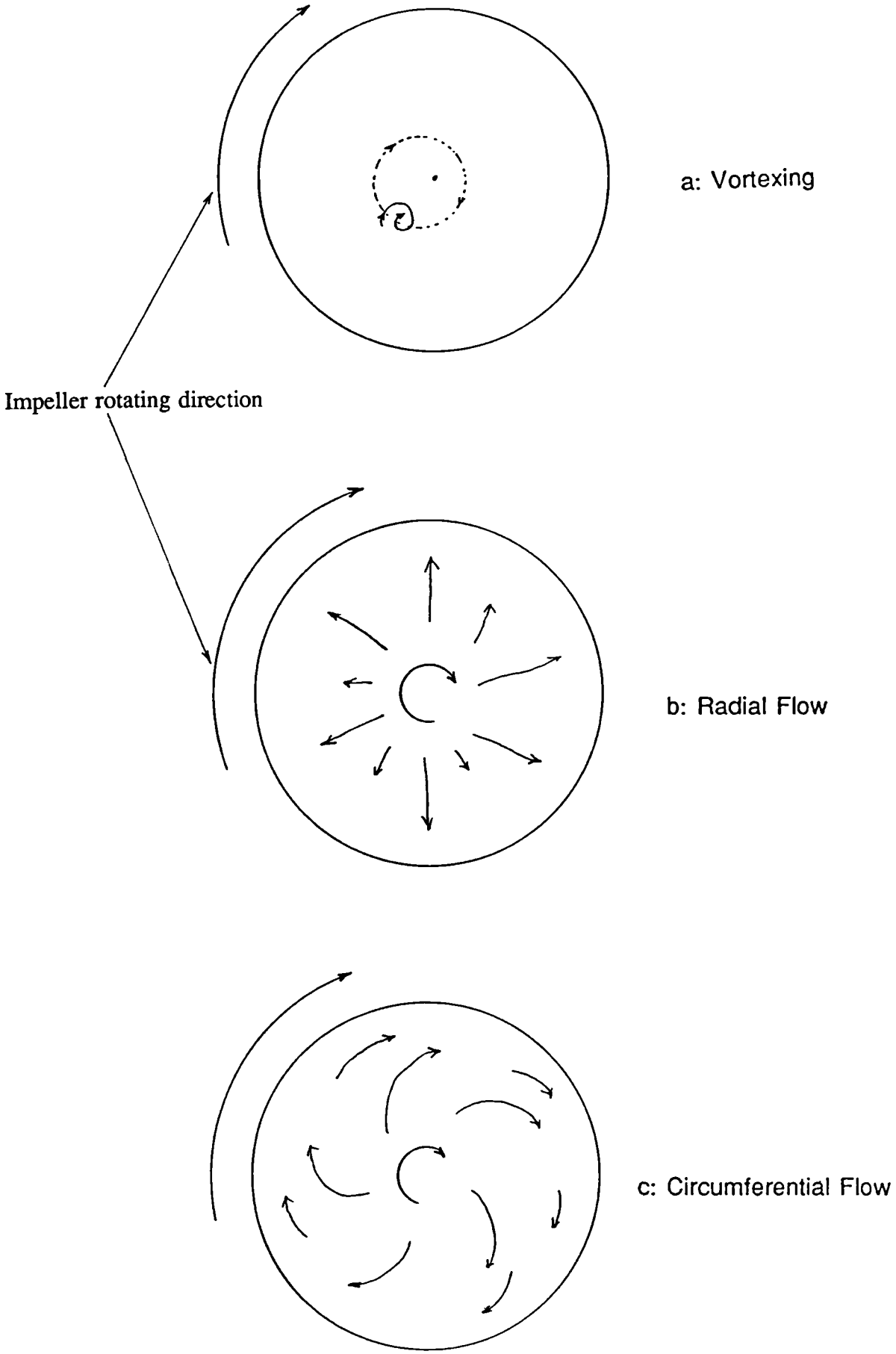

Fig 4.1.5 Particle Flow Pattern on Vessel Base near N_{js}

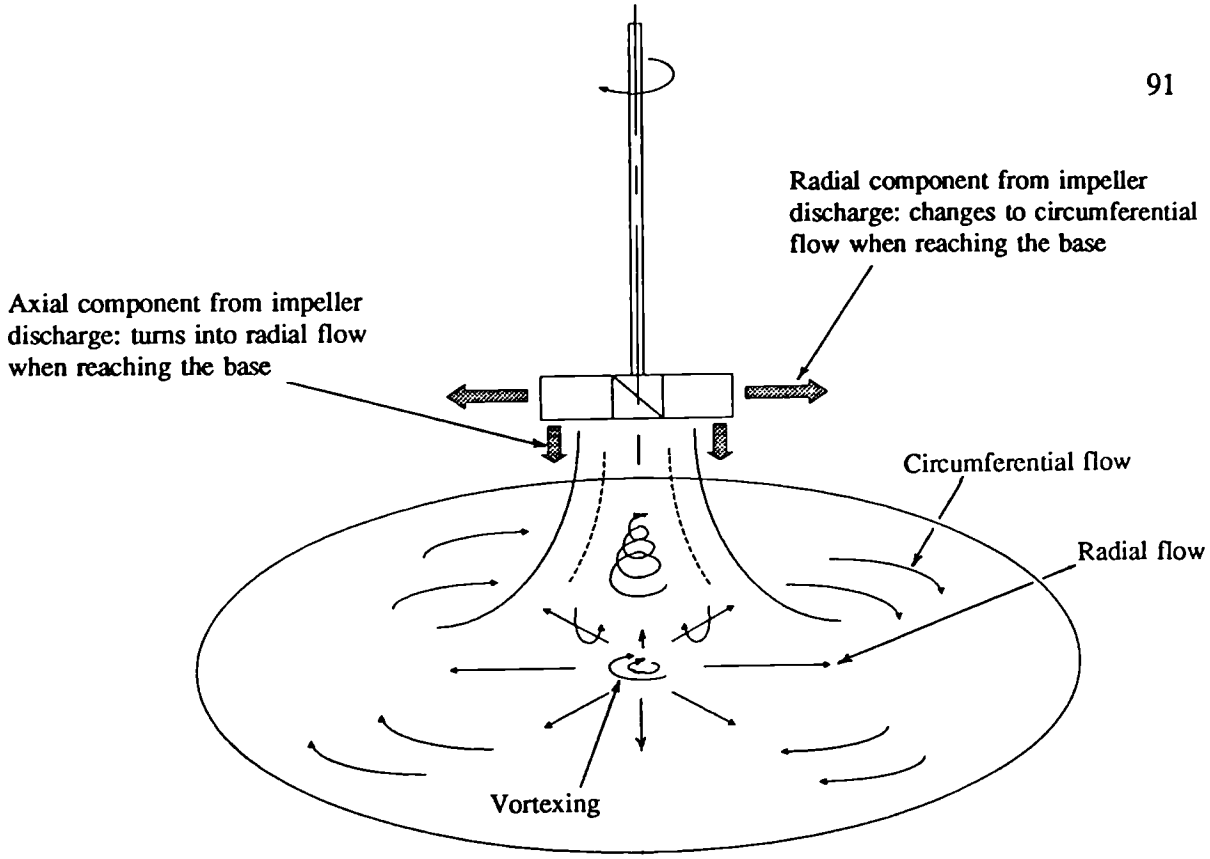

Fig 4.1.6 Relationship between Flow Components at Impeller Discharge and Particle flow Pattern on Vessel Base

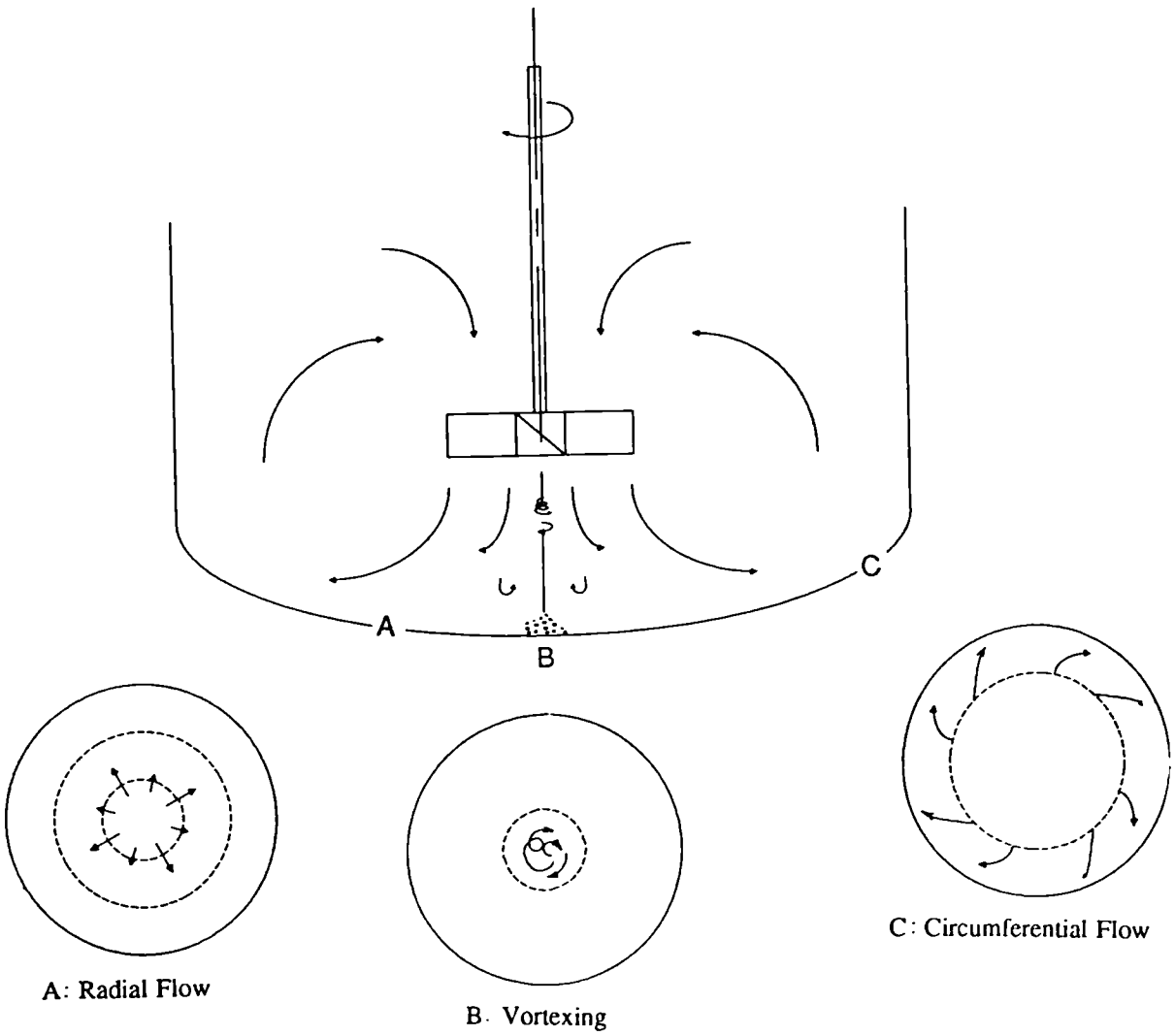

Fig 4.1.7 Relative Location of Particle Flow Regimes

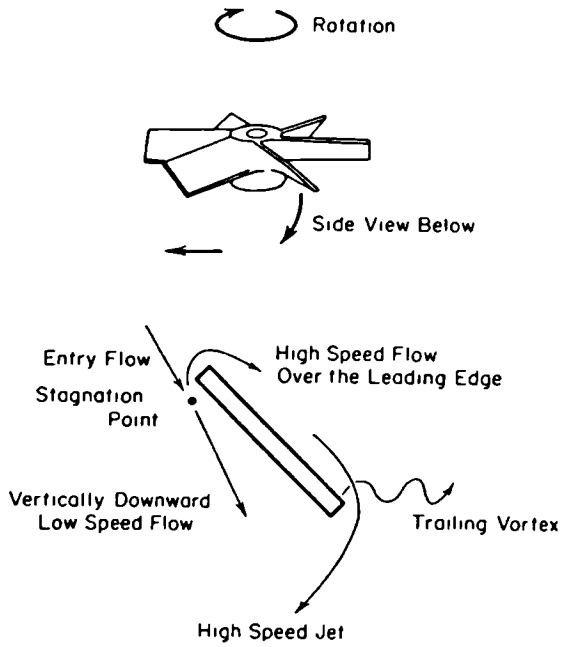

Fig 4.1.8 General Flows of a Pitched Blade Turbine (Tatterson 1980)

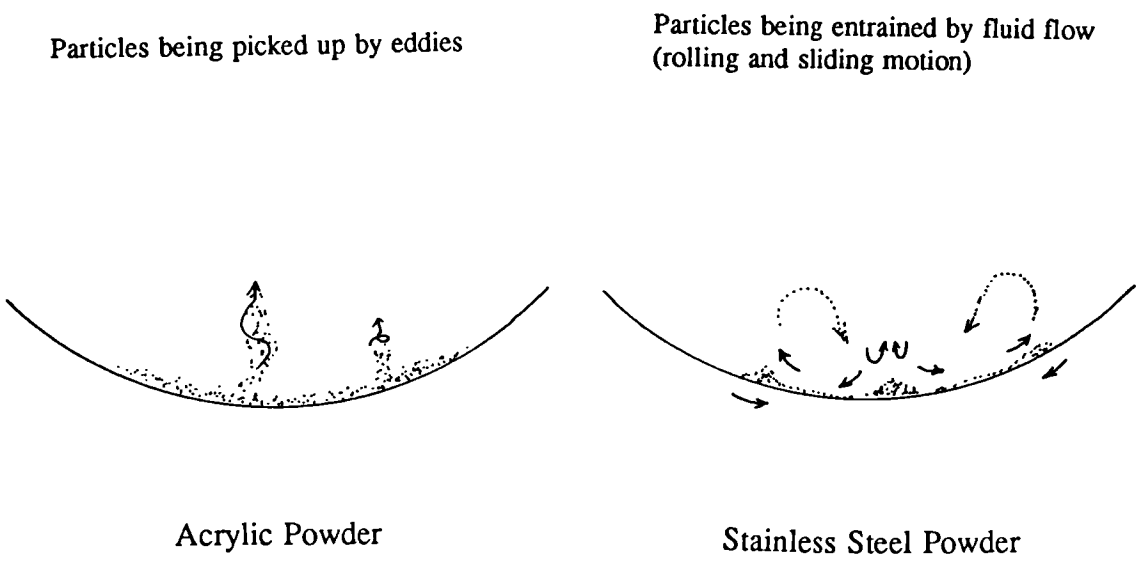

Fig 4.1.9 Suspension Mechanisms of Acrylic and Stainless Steel Powder

4.2 POWER REQUIREMENT FOR SOLID-LIQUID MIXING

The knowledge of impeller power consumption is a very important design consideration for several reasons.

An accurate prediction of power will enable the correct choice of drive system to be made, and the process itself can often be affected by the amount of energy dissipated within the fluid. For example, too high an input can cause particle degradation during crystallization or inhibition of mammalian cell activity during drug manufacture, while too low a value may lower the mass transfer rate to an unacceptable level.

Impeller power consumption is a function of the following parameters:

- Impeller size, geometry and its rotating speed
- Vessel geometry and internals
- Interactions between impeller and vessel
- Fluid Properties

This section serves two purposes. Firstly, it introduces and verifies the concept of using average slurry density to correlate solid-liquid mixing power. Secondly, it produces the mathematical derivations and physical arguments to use just suspension power and power index to compare impeller suspension efficiency, which will be referred to in the forthcoming sections.

4.2.1 Solid-liquid Mixing Power

Available power data on multiphase mixing is very limited when compared to single fluid phase systems. One of the objectives of this research is to identify a convenient way to evaluate the solid-liquid mixing power requirement. To do this, solid-liquid power numbers for a variety of impellers and vessel geometries were measured and compared. In most systems that had been tested, solid particles were well suspended and the power numbers, Po, were correlated satisfactorily by using the average slurry density ρ_{av} (eqn 4.2.1 & 4.2.2). The only exception occurred in those systems where the impellers were unable to satisfy the just suspension duty. This normally happened with small diameter impellers (eg D < T/3),

undertaking a very demanding mixing duty (eg dense particles).

$$P = Po\ \rho_{av}\ N^3\ D^5 \qquad \text{...eqn(4.2.1)}$$

$$\rho_{av} = \frac{M_S + M_L}{V} \qquad \text{...eqn(4.2.2)}$$

This approach is by far the most convenient way to correlate the solid-liquid mixing power data; it makes use of the readily existing single phase power data and with the average slurry density, the power requirement can be computed without further experimentation. It was found that for all systems tested so far, as long as the operating impeller speed is above the just suspension condition, the apparent Power number in equation 4.2.1 can be taken as the Power number of the same system measured in water.

Figures 4.2.3 to 4.2.7 present typical plots of Power numbers against impeller speeds, with and without the average density correction. Examples of three impeller types {RCI3 (T/1.7) - radial flow, 45° PBT4 (T/2) - mixed flow and A310 (T/2) - axial flow} and three scales (T = 0.61, 1.83 and 2.67 m) were chosen. The retreat curve impeller (RCI) together with two beavertail baffles (Fig 4.2.3) produced very good radial flow but tended to push the solids around on the vessel base rather than suspending them. The hydrofoil impeller {A310 (T/2), Fig 4.2.4} produced very good axial flow, it promoted good solids suspension near the vessel base but poor overall mixing in the bulk content. Examples of the mixed flow impeller power across the T_{61} to T_{267} scale was chosen because it is one of the most widely used impellers and it is also the impeller which was employed for the scale-up investigations in this work {45° PBT4(T/2), Fig 4.2.5 to 4.2.7}. Despite the scale of operation and the diversity in flow pattern between the three impeller types, they all confirmed the applicability of the average density correction concept for solid-liquid power estimation.

Nevertheless, the average density correction approach is only an engineering approximation for design purposes. The actual power consumption should be the power related to the actual density within the impeller region. This is comparable to what a solids concentration probe located near the vessel base would measure (Sec 4.1.1).

Referring to Fig 4.2.1-b, at low impeller speeds, the impeller digs a pit in the solids bed and the actual slurry density within the impeller region is less than the average density, therefore, equation 4.2.1 will overestimate the power requirement (eg 40% Wt curve in Fig 4.2.3) therefore the apparent power number becomes less.

As the impeller speed increases, the solid particles are partially suspended and concentrated at the lower half of the vessel. The slurry density at the impeller region will be higher than that the calculated average and therefore power will also be higher than would normally be estimated by equation 4.2.1. This phenomenon is commonly observed among axial flow impellers, for their energy dissipation is concentrated on the lower section of the vessel leaving a clear liquid layer at the top. Thus, the impeller tends to 'see' a much higher solids concentration than calculated. Fig 4.2.4 presents a plots of power numbers against impeller speed for a range of solids concentrations using a hydrofoil impeller. It is evident that it has a higher than expected corrected power number (i.e. ~ Po measured in water), when compared with the radial (Fig 4.2.3) and mixed flow impeller (Fig 4.2.5).

As the impeller speed increases even further, the solids are all fully suspended, the power will settle to a somewhat lower value than that which was calculated by using average slurry density. This is due to the centrifugal effect near the impeller and this phenomenon is more apparent with low solids concentration measurements (Fig 4.2.3). A similar observation of the effect of solids loading upon power number has been reported by Herringe (1979) except that he did not draw attention to the centrifugal effect at high impeller speeds (Fig 4.2.1).

The concept of interpreting the solid-liquid mixing power by the impeller carried mass is an important one. Another example is given in Fig 4.2.2, which presents plots of power numbers against impeller speeds for five pitched blade turbines at different clearances and pumping directions. Large upwards pumping PBTs at low clearance (Fig 4.2.2-d) demonstrated a drop in power numbers as the impeller speed increased (before air entrainment). Visual observations have confirmed that once the upflow has achieved a sufficiently high velocity, most solids are kept suspended in the upper part of the vessel and the carried mass of the impeller is reduced thus lowering the power numbers. In the case of downwards pumping impellers, the particles always follow a general circulation pattern near the impeller and thus give a relatively stable power number.

The effect of particle size on power number is similar to that of solids concentration - it increases the mixing duty. Fig 4.2.5-b and 4.2.8 present the corrected power number curves for 45° PBT4 (T/2,D/3.6) with 180 and 605 μm sand respectively. Fig 4.2.5-b shows that even with 40% wt of solids, the 180 μm particles are well distributed. Since the actual solids concentration carried by the impeller is somewhat less than the calculated average, the corrected power number for higher concentrations are less than water for reasons explained above. However, when a more demanding duty is imposed (i.e. bigger particles, Fig 4.2.8), the solids are only partially fluidised (Fig 4.2.1-b). The impeller is handling a higher than average concentration and this leads to higher corrected power numbers.

Additional experiments had been conducted to measured the local solids concentration near the impeller region and use the local slurry density to correlate the power data. This technique did not improve the correlation between data measured at different solids concentrations, and has the added difficulty of requiring local solids concentration measurements before power numbers can be calculated. The approach was eventually abandoned due to the extra effort and complexity involved.

4.2.2 Just Suspension Power and Power Index

The concept of just suspension power (P_{js}) is introduced to compare the suspension efficiency of an impeller. It is defined as the power delivered by an impeller into the vessel at the just suspension speed.

$$P_{js} = Po\ \rho_{av}\ N_{js}^3\ D^5 \qquad \text{...eqn(4.2.3)}$$

The just suspension power is a function of physical properties and geometrical configurations. Therefore, comparison can be made only if the suspension experiments are undertaken within the same test condition where the most efficient system will exhibit the lowest just suspension power. However, it is not always possible to do so and a common technique to compare impeller performance between different set-ups is to use the power index (Harnby et al 1985). This is essentially correcting the physical properties effects by substituting Zwietering's correlation into the Power number relationship:

The Zwietering correlation (eqn 2.1.2)

$$N_{js} = s\, \nu^{0.1} \left(\frac{g\, \Delta\rho}{\rho_L} \right)^{0.45} d_p^{0.2}\, X^{0.13}\, D^{-0.85}$$

Combined with the power number relationship from eqn 4.2.1

$$P = Po\, \rho_{av}\, N^3\, D^5$$

ie $P_{js} \propto Po\, N_{js}^3\, D^5$ ...eqn(4.2.4)

$$\propto Po\, D^5\, (\, s\, D^{-0.85}\,)^3$$

$$\propto Po\, s^3\, D^{2.45} = P_i$$ ...eqn(4.2.5)

The term $Po\, s^3\, D^{2.45}$ can be defined as a power index, P_i, of a geometry and used to compare the efficiencies of different set-ups. The lower the power index of a system, the more efficient it would be for solids suspension. One drawback of the power index concept is that the validity of the exponents in Zwietering's correlation has to be assumed.

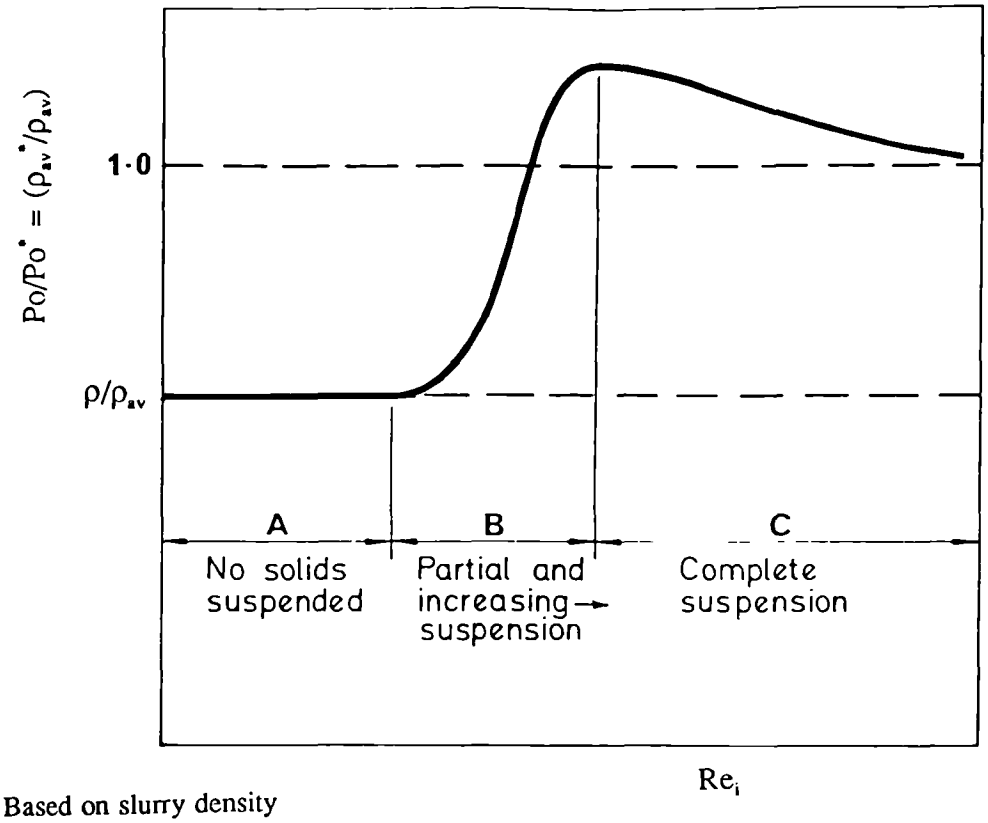

* Based on slurry density in impeller zone

Fig 4.2.1-a Expected Power Number Ratios for Solids Suspension (Herringe 1979)

Impeller digging a pit in the solids bed

$\rho_{actual} \leq \rho_{average}$, $Po_{predicted} \geq Po_{measured}$

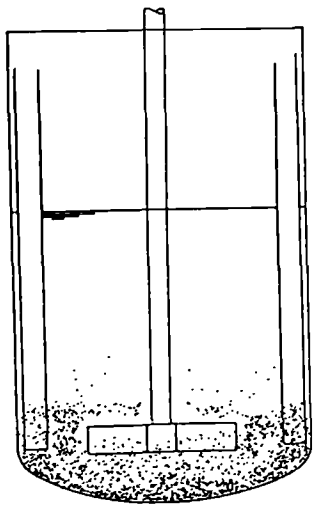

Particles are partially fluidised- concentrated at the lower region

$\rho_{actual} \geq \rho_{average}$, $Po_{predicted} \leq Po_{measured}$

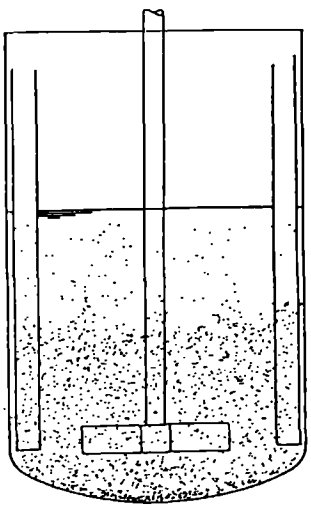

Particles are being suspended by the fluid upflow- concentrated at the upper region

$\rho_{actual} \leq \rho_{average}$, $Po_{predicted} \geq Po_{measured}$

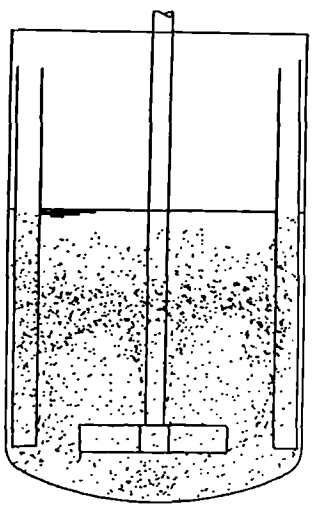

$$Po = \frac{P}{\rho_{av} N^3 D^5}$$

Fig 4.2.1-b Relating Particle Flow Pattern to Slurry Power No Prediction

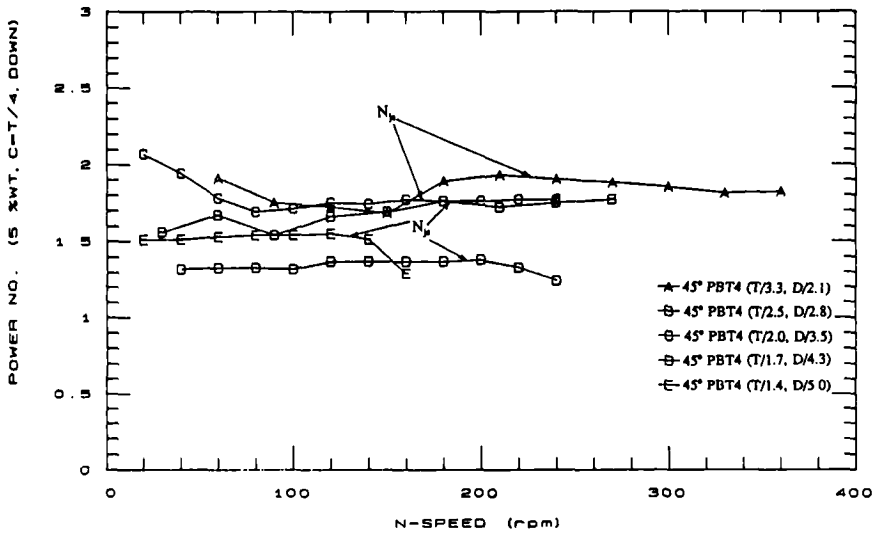

a) Downwards Pumping, C=T/4

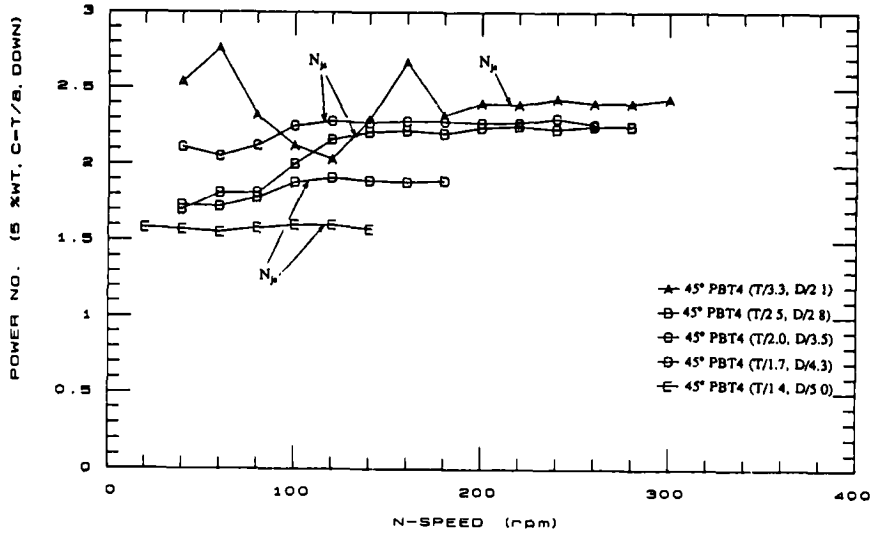

b) Downwards Pumping, C=T/8

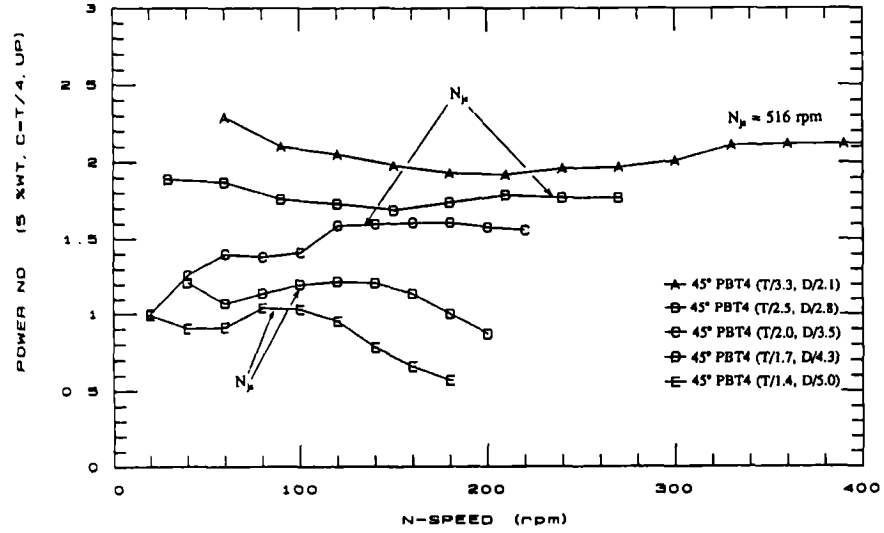

c) Upwards Pumping, C=T/4

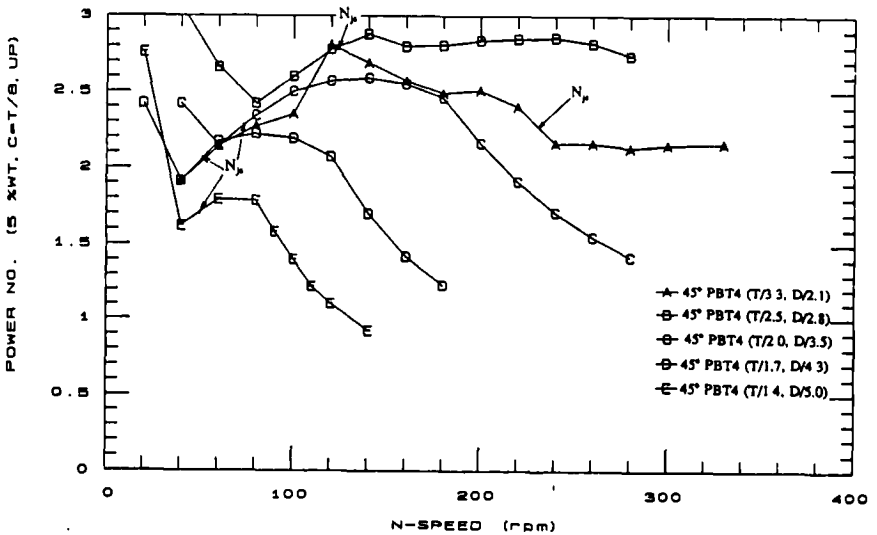

d) Upwards Pumping, C=T/8

Fig 4.2.2 Power Numbers for 5 Pitched Blade Turbines in T_{R1}

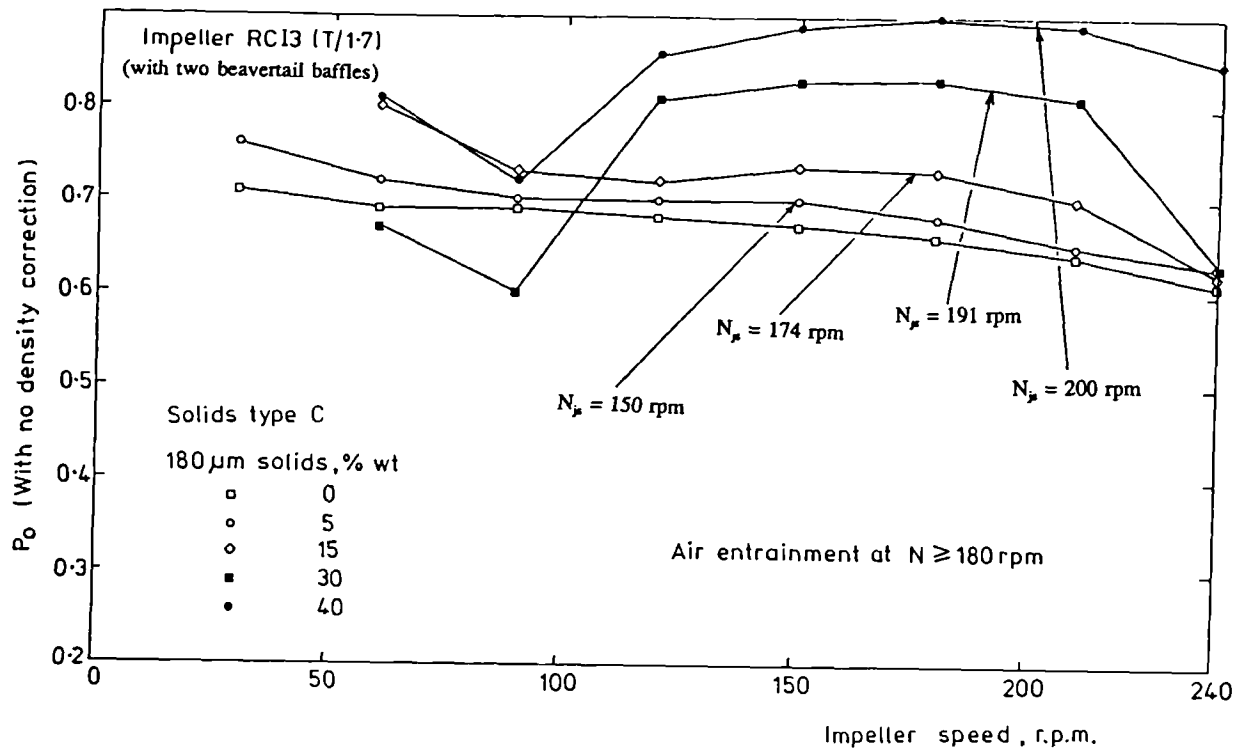

a) Without density correction

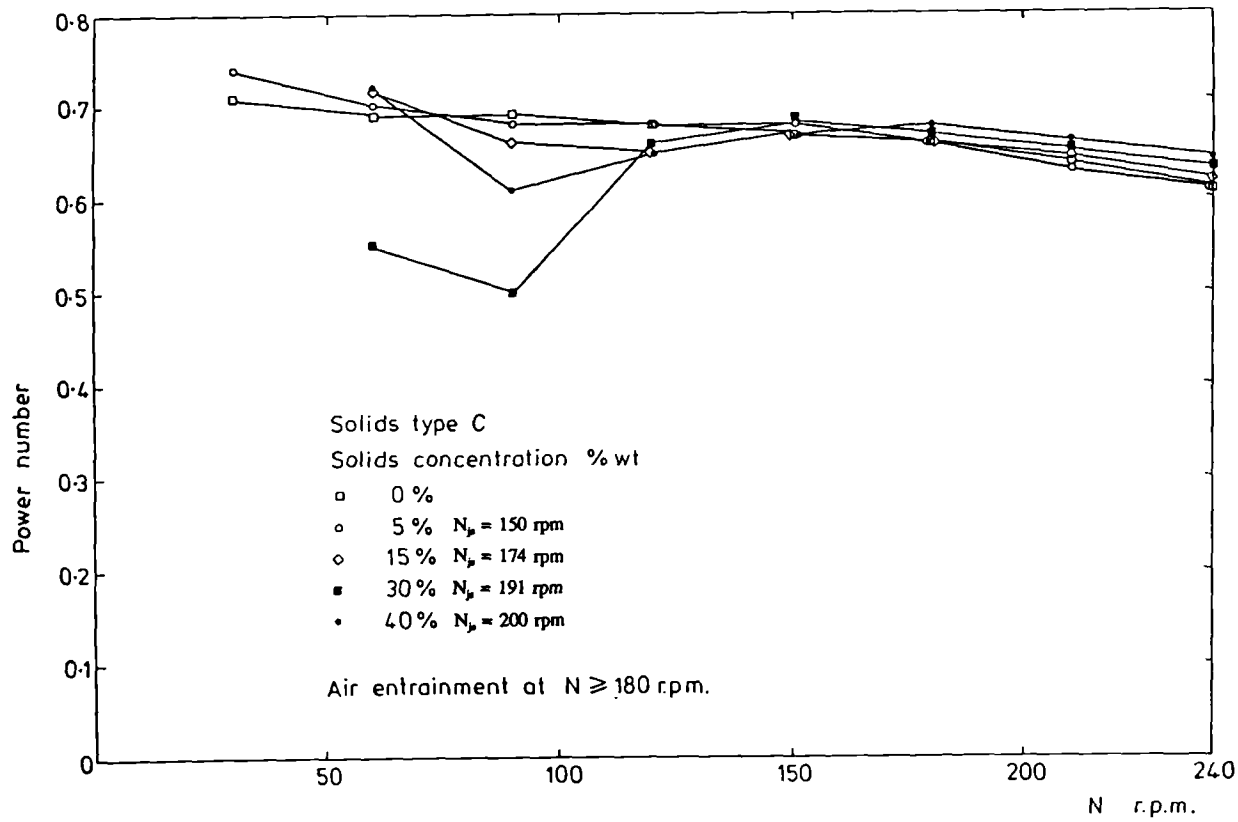

b) With density correction

Fig 4.2.3 Power Numbers for Retreat Curve Impeller in T_{61} (150-210 μm sand)

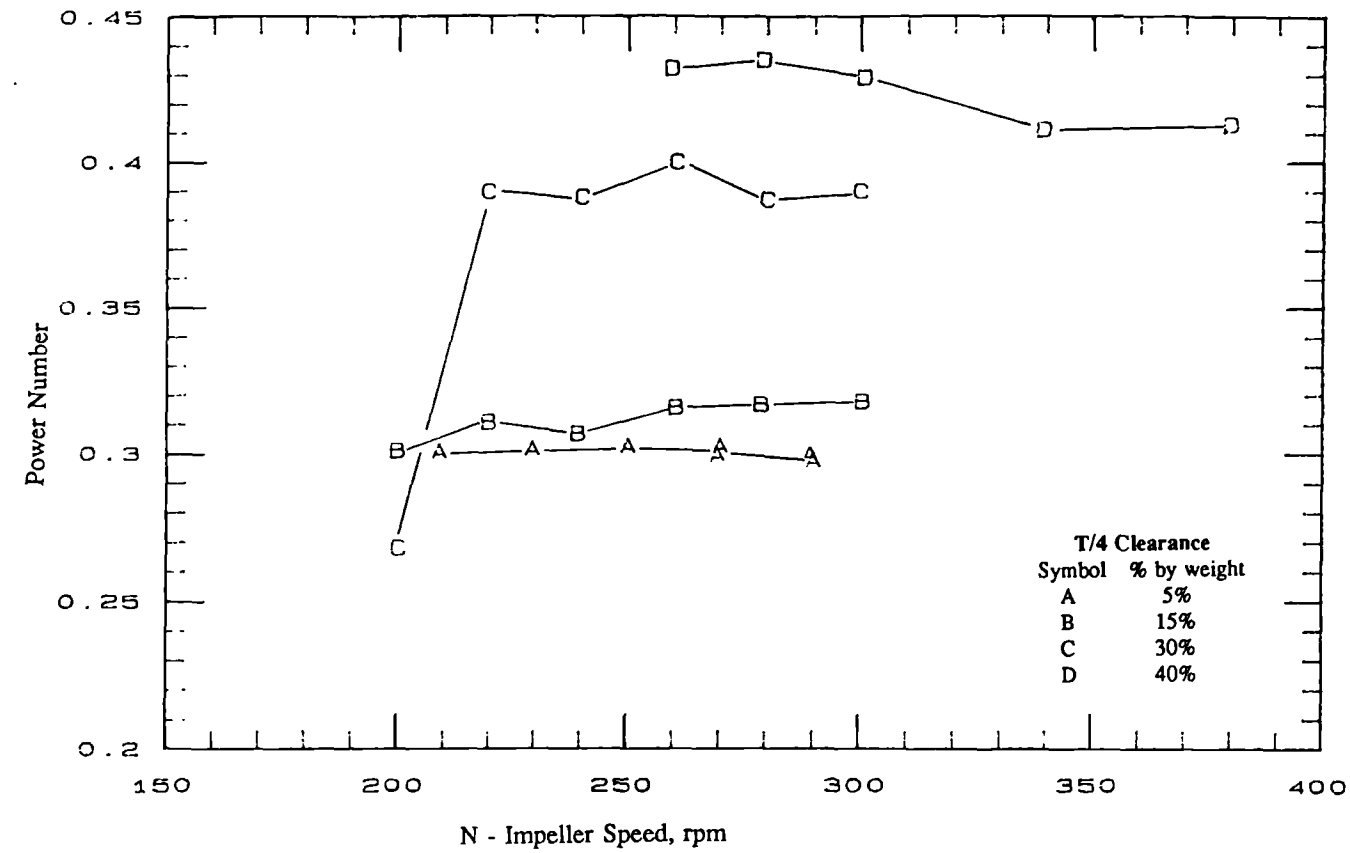

a) Without density correction

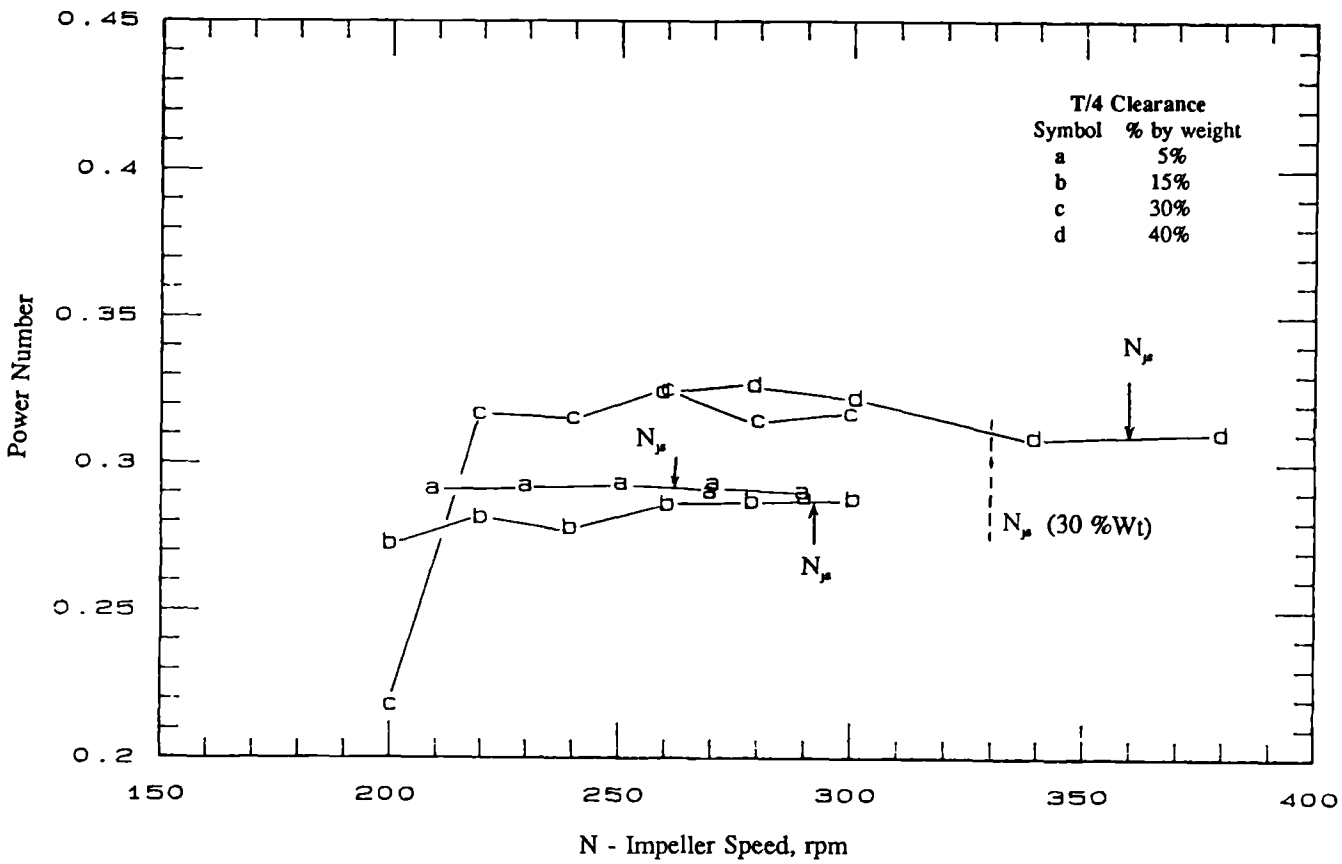

b) With density correction

Fig 4.2.4 Power Numbers for A310(T/2) in T_{61} (300-355 µm sand)

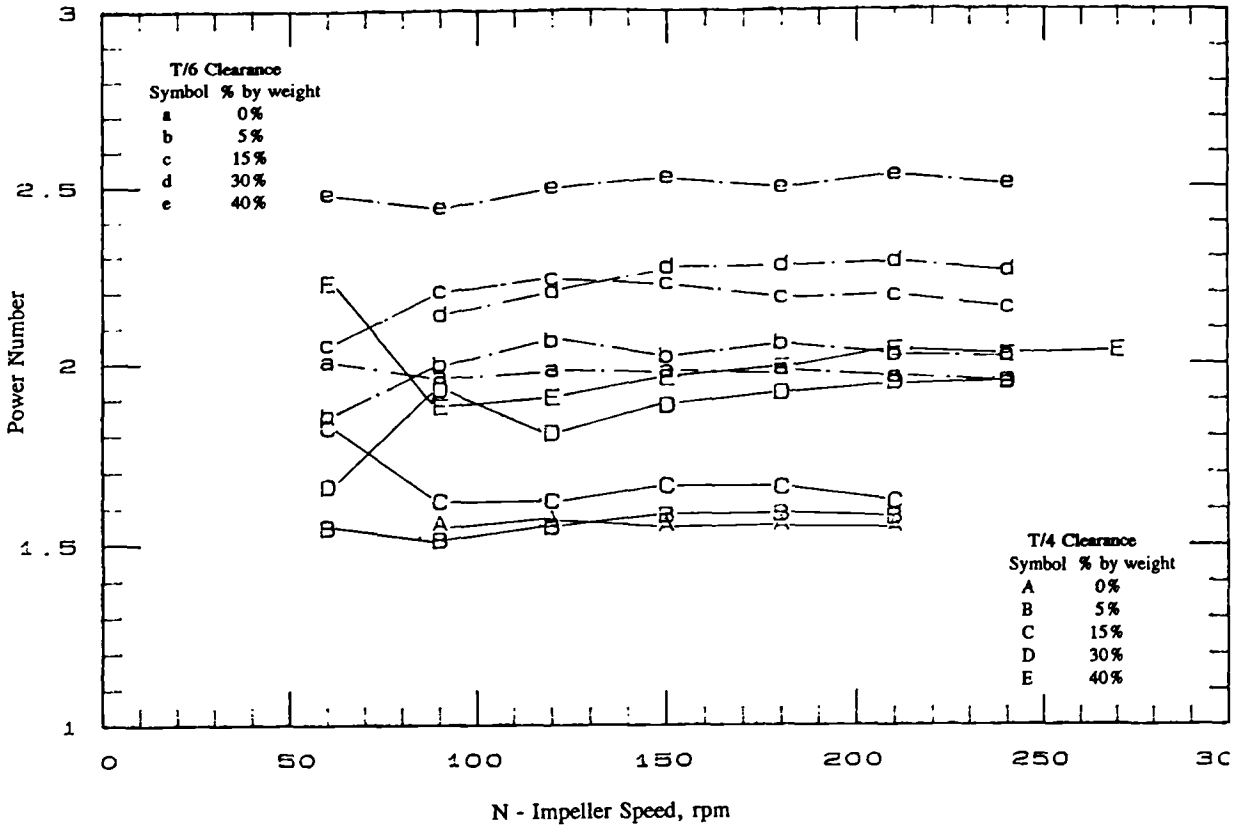

a) Without density correction

b) With density correction

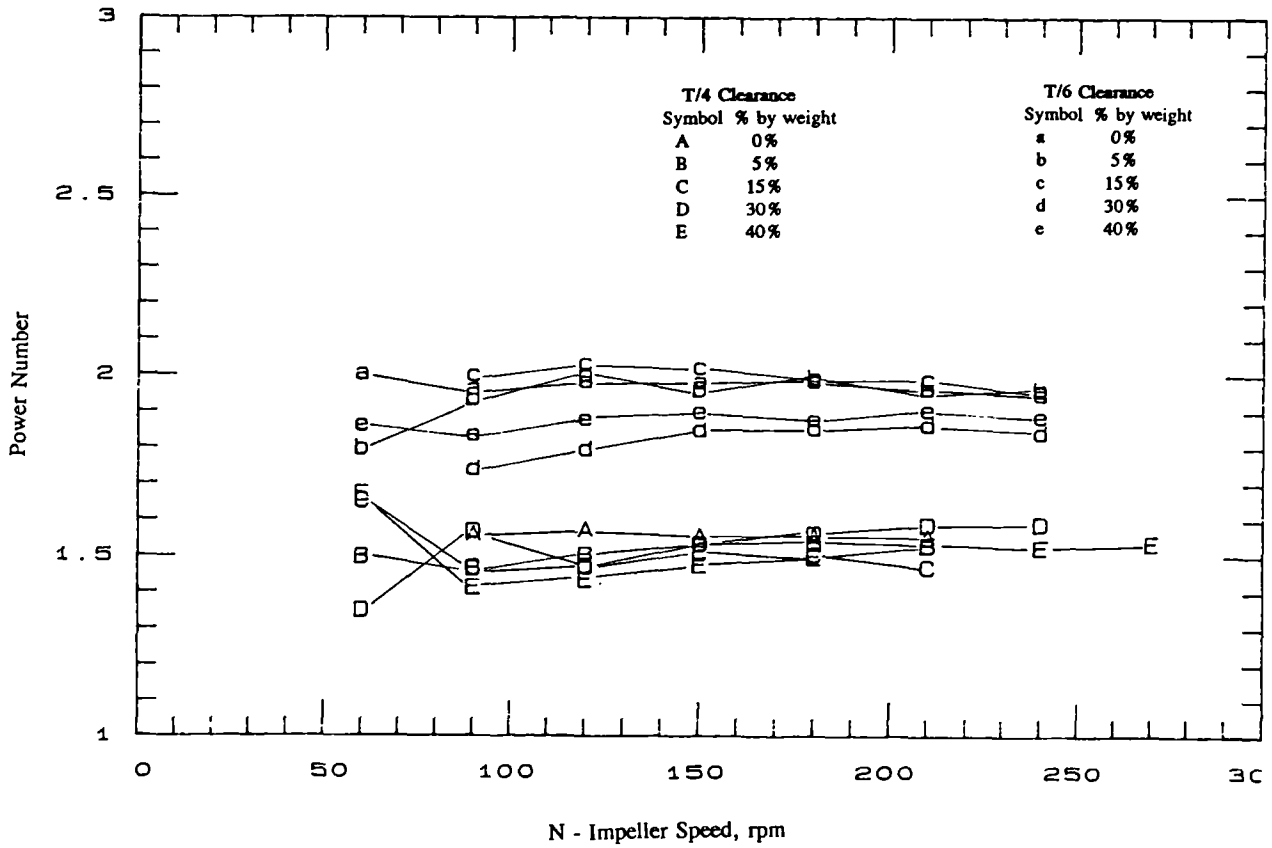

Fig 4.2.5 Power Numbers for 45° PBT4(T/2) at T_{61} (150-210 µm sand)

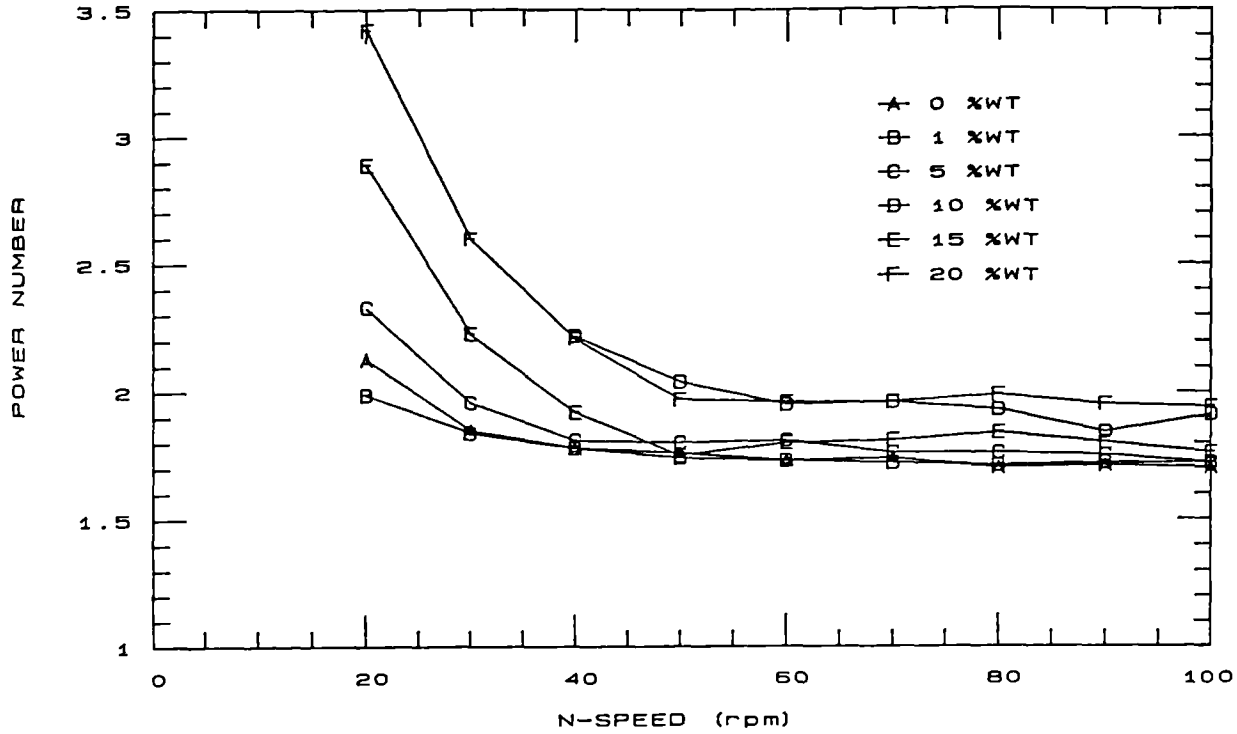

a) Without density correction

b) With density correction

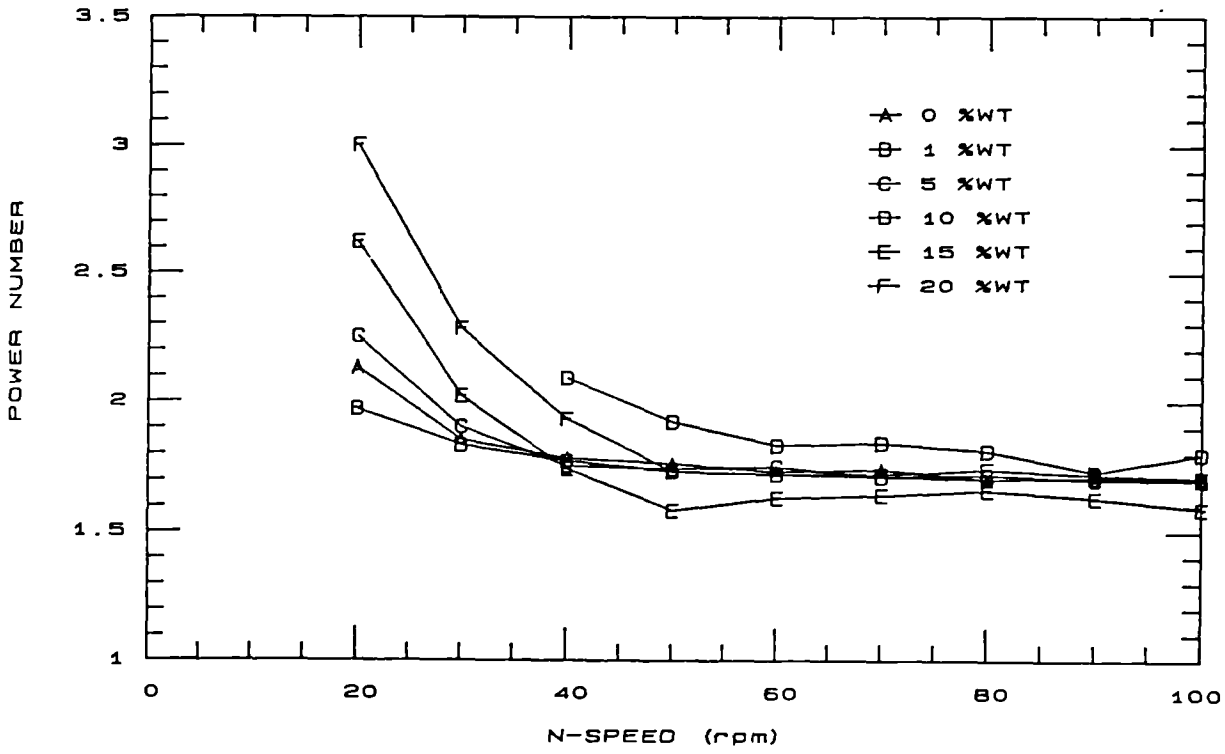

Fig 4.2.6 Power Numbers for 45° PBT4(T/2) at T_{183} (150-210 μm sand)

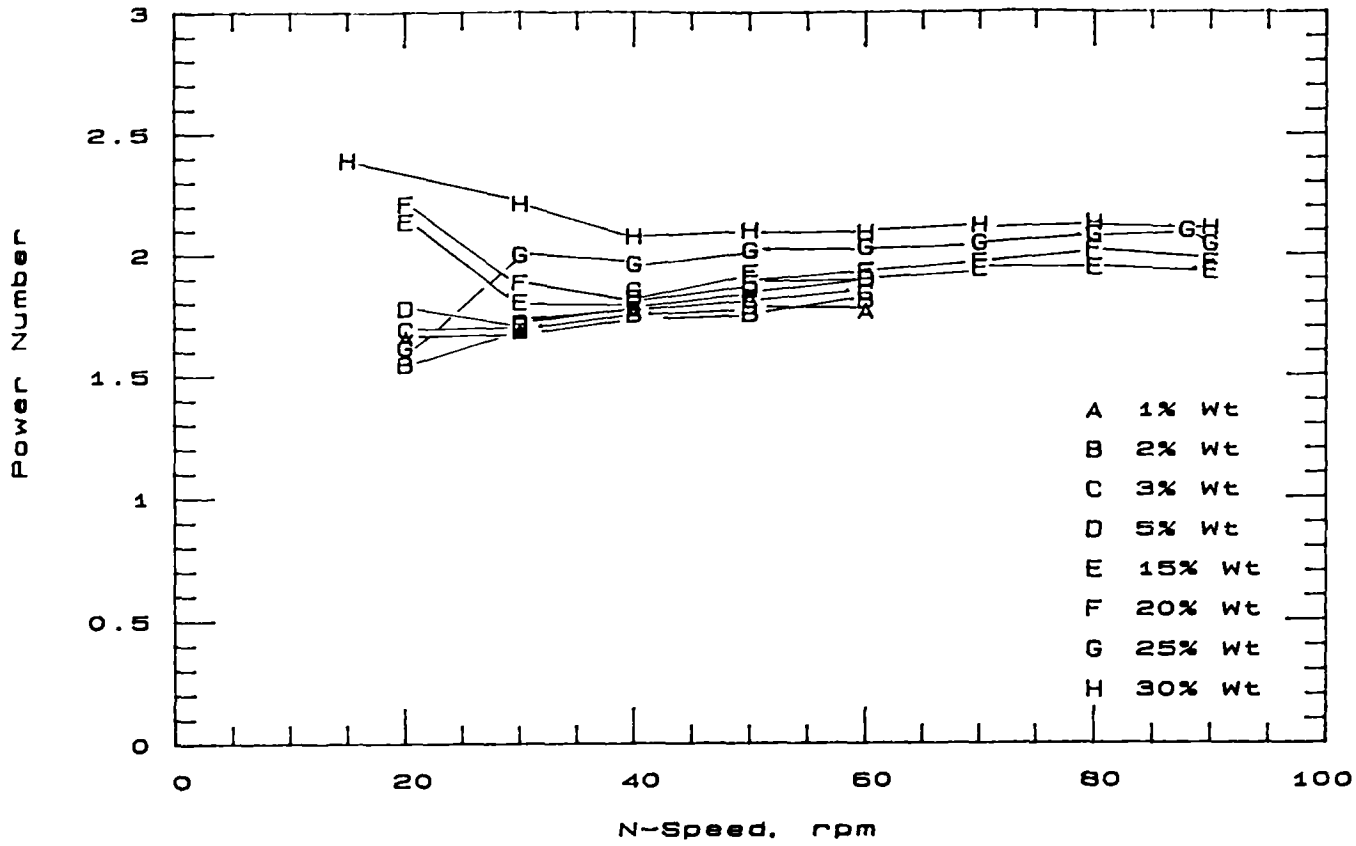

a) Without density correction

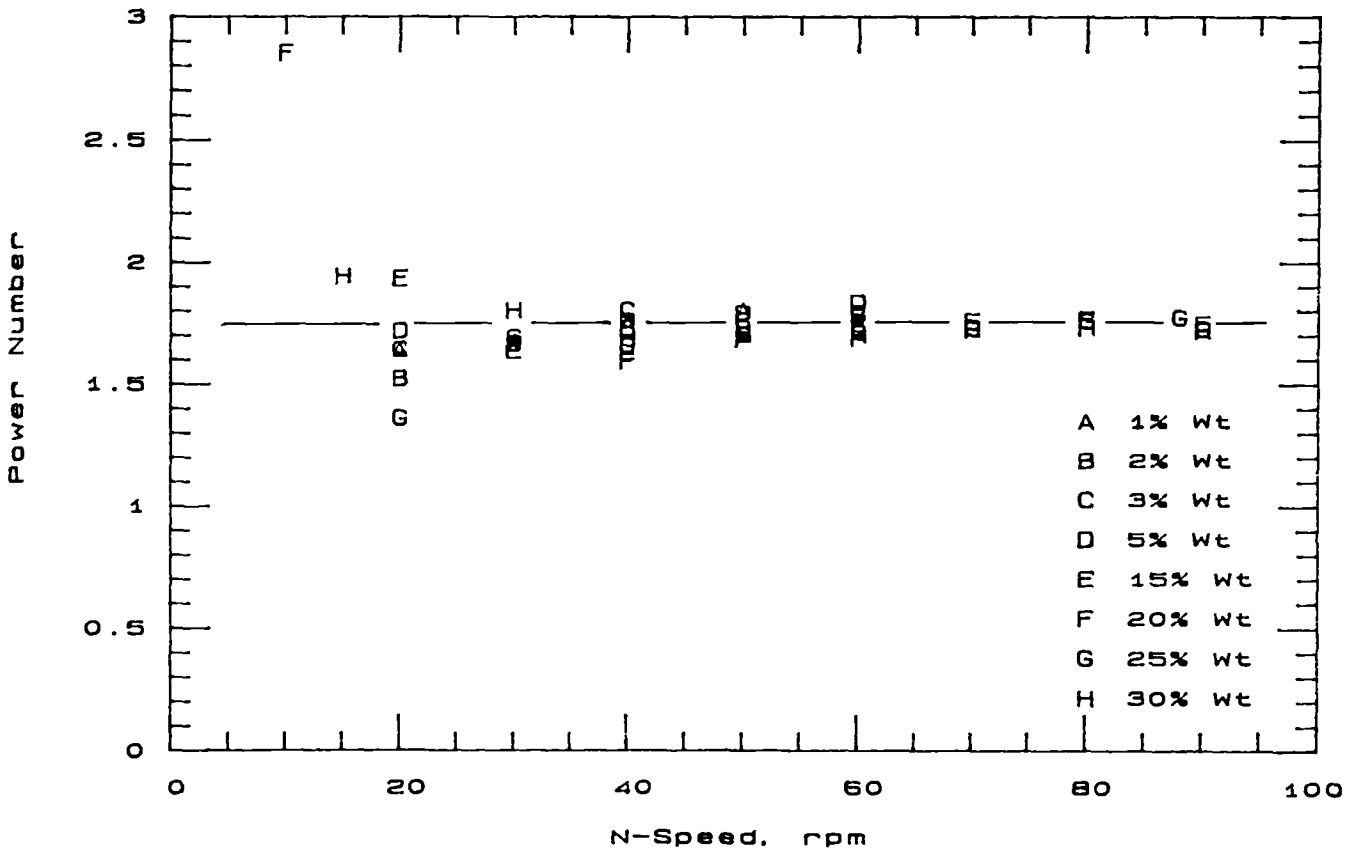

b) With density correction

Fig 4.2.7 Power Numbers for 45° PBT4(T/2) at T_{267} (150-210 µm sand)

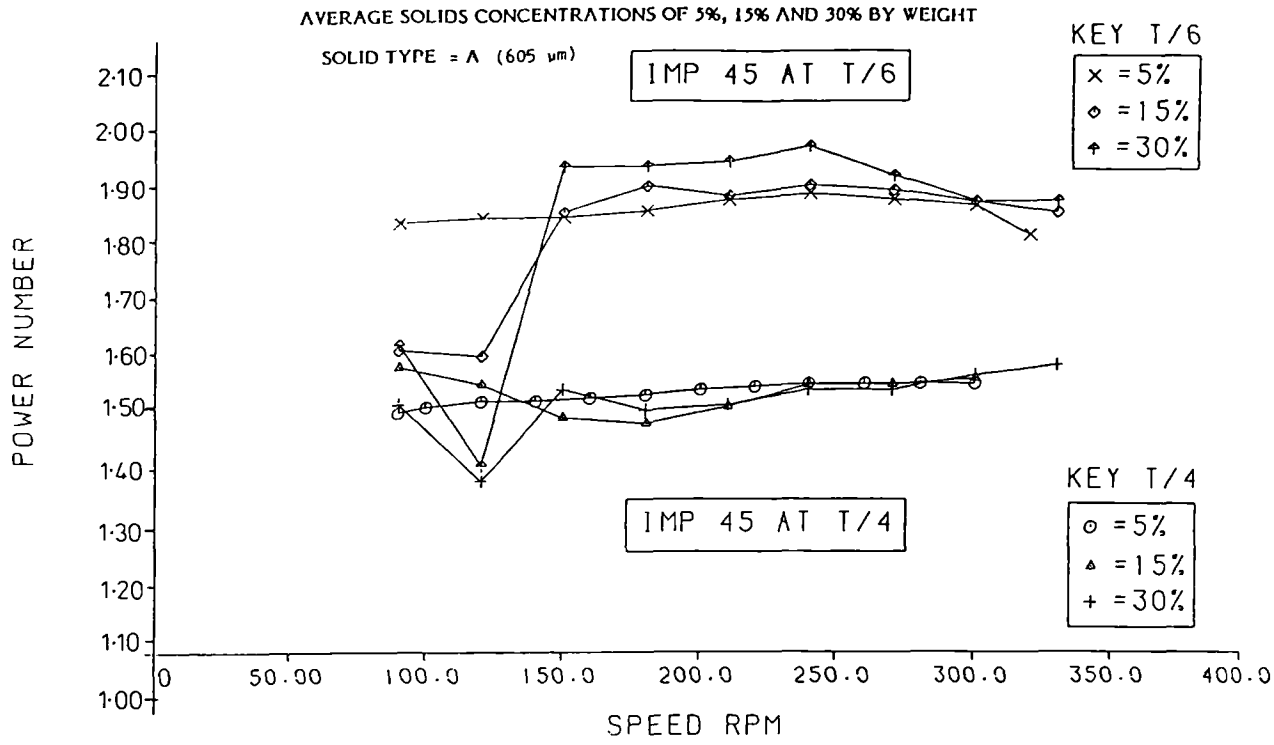

Fig 4.2.8 Power Number for 45° PBT4(T/2) at T_{61} (605 μm sand)

4.3 EFFECT OF IMPELLER SIZE

Solids suspension and distribution characteristics for a series of impellers in a 0.61 m dished based vessel have been measured (Mak 1987). The results showed that small diameter pitched blade turbines (PBTs) were more energy efficient than those of a larger diameter for solids suspension. In other words, the small diameter PBTs required less power to suspend solids than the larger ones. This result was greeted with some scepticism, since the accepted wisdom was that the reverse be true (eg Nienow 1968). The objective of this study is to examine the effect of impeller diameter on solids suspension and distribution.

4.3.1 Experimental Results

This section describes the results from a study of power input, solids suspension and solids distribution for three geometrically similar 4-bladed 45° pitched blade turbines. The impellers all have a constant diameter to blade width ratio of 3.5. The study was conducted in the 0.61 m (T_{61}) diameter torispherical based vessel. The impellers had a diameter of approximately 30% (T/3), 50% (T/2) and 60% (T/1.7) of the tank diameter. They were mounted at *T*/4, *T*/6 and *T*/8 clearances, measured from the centre bottom of the base to the centreline of the impeller. Mixtures of sand and water (150-210 μm sand, settling velocity of a single sand particle is 0.015 m s^{-1}) were used as the test media. Details of the geometries and experimental techniques are presented in Chapter 3. The dimensions of the impellers are summarised in Table 4.3.1.

Table 4.3.1 Impeller Dimensions for the 3 Geometrically Similar Impellers

Impeller Notation	No of Blades	α (°)	*D* (mm)	*W* (mm)	χ (mm)	Series No
45° PBT4 (T/3)	4	45	203	58	3.4	001-31-061
45° PBT4 (T/2)	4	45	298	86	3.3	021-45-061
45° PBT4 (T/1.7)	4	45	368	105	3.4	001-55-061

Power numbers for the three impellers at three clearances (T/4, T/6 and T/8) were measured in the turbulent region and corrected by average slurry density (Sec 4.2.1). The effect of clearance on power number was found to correlate better in terms of (C/D) than (C/T). Results are summarised in Table 4.3.2 and presented as a plot of Po against C/D in Fig 4.3.1.

Table 4.3.2 Po for the 3 Geometrically Similar PBTs

Impeller Clearance	Impeller					
	PBT4 (*T*/3)		PBT4 (*T*/2)		PBT4 (*T*/1.7)	
	C/D	Po	*C/D*	*Po*	*C/D*	*Po*
C = T/4	0.752	1.73	0.511	1.60	0.414	1.48
C = T/6	0.502	1.90	0.341	1.95	0.276	1.77
C = T/8	0.376	2.02	0.256	2.10	0.207	2.01

Regression Analysis :

D = T/3 : $Po = 1.62\ (C/D)^{-0.22}$ $r^2 = 0.999$

D = T/2 : $Po = 1.24\ (C/D)^{-0.40}$ $r^2 = 0.974$

D = T/1.7 : $Po = 1.00\ (C/D)^{-0.44}$ $r^2 = 0.998$

The flow pattern at the vessel base for the three geometrically similar PBTs follows the general observations described in section 4.1.2. As the impeller diameter increases, the radial flow region is reduced and the amount of circumferential flow increased. Similar trends were observed for a decrease in impeller clearance, which increases both the vortexing and circumferential flow regions. In all cases, the last suspension region was found on the centre bottom of the vessel base.

The just suspension speed was measured for all the three impellers at the three clearances (T/4, T/6 and T/8), with a solids concentration of 5% Wt (150-210 μm sand).

Previous work (Mak 1988a) has shown that Zwietering's correlation (1958) works well for solids concentration ($N_{js} \propto X^{0.13}$) and thus 5% Wt of sand was used for suspension experiments. This was to reduce the workload involved in experimentation. The results are given in Table 4.3.3 and also presented as plots of N_{js} against impeller diameter and clearance in Fig 4.3.2 and 4.3.3.

Solids concentration profiles for the three impellers at T/4 clearance were measured. Results are tabulated in Appendix A and also presented as plots of solids concentration profiles (Fig 4.3.12 to 4.3.17) and volumetric fraction of solids against impeller speeds at five axial positions (Fig 4.3.9).

Table 4.3.3 Summaries of N_{js}, "s" value and P_{js}

Impeller	Parameters	Nominal Clearance		
		$C = T/4$	$C = T/6$	$C = T/8$
PBT4 ($T/3$)	N_{js}	217	212	193
	P_{js}	29	30	24
	s	4.8	4.6	4.2
PBT4 ($T/2$)	N_{js}	171	139	123
	P_{js}	90	59	44
	s	5.2	4.2	3.7
PBT4 ($T/1.7$)	N_{js}	184	139	122
	P_{js}	298	154	118
	s	6.7	5.1	4.4

"s" is the geometrical constant in Zwietering correlation

4.3.2 Just Suspension Speed

For all three impellers tested, N_{js} decreases as the impeller clearance is reduced. This trend is more apparent with the two larger diameter impellers ($T/2$ and $T/1.7$). The lowest N_{js}

was given by the *T*/2 and *T*/1.7 impellers positioned at *T*/8 clearance (Fig 4.3.3). However, comparing the just suspension speed alone does not necessarily give the correct indication of the most efficient configuration. This is because even though the large diameter impeller has a relatively low N_{js}, its power input at N_{js} (i.e. P_{js}) could be higher than that of a smaller diameter impeller at N_{js} (eqn 3.8.2, $P_{js} \propto Po\ N_{js}^3\ D^5$).

Based on Zwietering's correlation for solids suspension, the geometrical constants "*s*" for various configurations were calculated. They are tabulated in Table 4.3.3.

Zwietering's Correlation :

$$N_{js} = s\ \nu^{0.1} \left(\frac{g\ \Delta\rho}{\rho_L} \right)^{0.45} d_p^{0.2}\ X^{0.13}\ D^{-0.85} \qquad \text{...eqn(4.3.1)}$$

The "*s*" value is a constant introduced in order to account for the geometrical effects. It is a function of impeller type, clearance and impeller diameter to tank diameter ratio. It can be used as a indicator to detect any change in flow pattern.

Zwietering (1958) suggested:

$$s \propto (T/D)^{\beta} \qquad \text{with } \beta = 0.82 \text{ for a propeller} \qquad \text{...eqn(4.3.2)}$$

By plotting the "*s*" value against (*T*/*D*), Zwietering found that the propellers exhibited a minimum at $D/T = 0.45$. He observed that for a $D < 0.45T$ propeller, the solid particles moved radially outward along the bottom and the last piles of particles occurred at the periphery. However, when $D > 0.45T$ the solids moved inward and centrally up into the propeller. This agrees well with our observed change in flow pattern from radial to circumferential flow as the impeller diameter is increased (Sec 4.1.2). A plot of "*s*" values against (*T*/*D*) for various *T*/*C* is presented in Fig 4.3.4, with the position of Zwietering's minimum at D=0.45T marked.

In this thesis, the effect of impeller diameter on N_{js} was studied. The results were firstly analysed by keeping the clearance constant. For the nine configurations tested, the

influence of impeller diameter on N_{js} is as follows:

T/4 Clearance	$N_{js} \propto D^{-0.32}$	$r^2 = 0.62$
T/6 Clearance	$N_{js} \propto D^{-0.76}$	$r^2 = 0.88$
T/8 Clearance	$N_{js} \propto D^{-0.82}$	$r^2 = 0.89$

The above relationships give an indication of the trends. The few data (only three points for each clearance) give a poor fit as shown by the low regression coefficient. The results suggest that the effect of impeller diameter on N_{js} is not a simple power law relationship. Further attempts were made to correlate data by including the effects of impeller clearance (C/D and C/T). No quantitative conclusion could be drawn based on statistical analysis as there were insufficient data points.

Impeller diameter has a greater effect on N_{js} at low clearance (i.e. C=T/8, $N_{js} \propto D^{-0.82}$) than at high clearance (i.e. C=T/4, $N_{js} \propto D^{-0.32}$). Rao (1988) suggested that this is because solids suspension is due to fluid flow and turbulence and the turbulence intensity decays along the length of the flow path. With an increase in the impeller diameter, less decay in the turbulence will occur because of a reduction in path length. Moreover, the liquid velocity also increases with an increase in the impeller diameter. The overall effect of increased liquid velocity and reduced decay in turbulence makes the dependence on the impeller diameter very strong. Furthermore, the power per unit volume below the impeller increases more rapidly with increasing impeller diameter at low clearances than at high clearances. This is because the actual volume underneath the impeller becomes smaller at low clearances.

It has been pointed out earlier that there is a change of flow pattern, from radially outwards to circumferential flow as the impeller diameter is increased. This change of flow pattern is reflected by the minima in Figure 4.3.4, where geometrical constants are plotted against (T/D). Similarly, a plot of N_{js} against impeller diameter for the three clearances shows that in all cases the just suspension speed decreases when the impeller diameter increases from T/3 to T/2, while a further increase in impeller diameter leads to either constant or slight increase in N_{js} (Fig 4.3.2). Regression analysis of the T/3 and T/2 diameter results for all three clearances suggests $N_{js} \propto D^{-1.02}$ with r^2 equal to 0.88.

Comparison was made between this result and the literature (Table 4.3.4). The

comparison is confined to the suspension of solids with axial or mixed flow impellers, i.e. propellers and pitched bladed turbines and most of the data were extracted from master and doctorate theses, in which the original data are accessible for analysis.

Referring to Table 4.3.4, there are two points which need to be resolved. Firstly, is there a minimum in the relationship between impeller diameter and N_{js}? Out of the eight references compared, three reported a minimum in their N_{js} results which were at D=0.36, 0.45 and 0.5T (Koutsakos 1989, Zwietering 1958 and Zolfagharian 1990 respectively). With the exception of Rao's results (1988), the three papers are among the highest D/T configurations tested. It is likely that the maximum (D/T) ranges in the others' work are too close to the transition point and therefore it is difficult to detect the minimum point as such.

The second question is, what is the effect of impeller diameter on just suspension speed? Excellent agreement is found between this work, which utilised a torispherical base ($N_{js} \propto D^{-1.02}$), and Koutsakos' ($N_{js} \propto D^{-1.06}$) where a profiled base was used. Table 4.3.4 showed that excluding Rao's value of -1.16, the exponent on D for a flat based vessel ranged from -1.5 (Chapman 1981) to -1.90 (Bujalski 1986). Rao's results should perhaps be treated with some caution because of the remarkable agreement between their data points and the Zwietering correlation. The author contacted Prof Joshi (Rao's co-author) two years ago, hoping to obtain their raw data for further analysis to resolve the above discrepancy and is still awaiting a reply.

The difference in the effect of impeller diameter on N_{js} between dished and flat based vessels has demonstrated the fact that the influence is a function of geometry. This leads to a fundamental question about the adequacy in the definition of just suspension speed. In other words, should there be different correlations for different geometries? Or, should there be another parameter to be included to account for the difference in geometries?

Power numbers were not included in the above analysis for it is difficult to obtain a good statistical fit with so few data. An overall regression in Section 4.7.1 shows that if power number were included (eqn 4.7.1), the exponent on D reduced to -0.89.

$$N_{js} \propto Po^{-0.33} \left(\frac{D}{T}\right)^{-0.89} T^{-0.79}$$

4.3.3 Just Suspension Power

From the power number relationship, $P = Po\ \rho\ N^3\ D^5$. If P, Po and ρ are constant, $N^3\ D^5$ is also a constant, and therefore $N \propto D^{-1.67}$. An exponent of -1.67 on the impeller diameter corresponds to just suspension power staying constant as the impeller diameter is increased, provided power number also remains constant:

$Po = constant,\ P_{js} \propto N_{js}^3\ D^5$

If the effect of impeller on N_{js} is: $N_{js} \propto D^{-1.67}$

Then, $P_{js} \propto (D^{-1.67})^3\ D^5,\ = constant$

It is well known that power number decreases slightly with increasing impeller diameter, a phenomenon again confirmed in this study (Fig 4.3.1). This, with the reported exponents of approximately -1.67 for flat vessel bases implies that just suspension power should decrease slightly with increasing impeller diameter. This is why large diameter impellers are recommended for solids suspension (eg Nienow 1988). However, the reported exponent on impeller diameter is less with a dished base when compared to that of the flat based vessels (This work: $N_{js} \propto D^{-1.02}$, Koutsakos: $N_{js} \propto D^{-1.06}$). This would suggest that the reduction in just suspension speed due to increased diameter is less with a dished base vessel and the reduction due to power number may or may not be able to compensate for the increase in diameter. Therefore, a closer look into the just suspension power is necessary.

$P_{js} \propto Po\ \rho\ N_{js}^3\ D^5$

And if $Po \propto (D/T)^{-\beta}$ and $N_{js} \propto (D/T)^{-\gamma}$

For constant T, $P_{js} \propto (D)^{-\beta}\ (D^{-\gamma})^3\ D^5$ ...eqn(4.3.3)

Therefore: $5-\beta-3\gamma > 0$, P_{js} increases with diameter

$5-\beta-3\gamma < 0$, P_{js} decreases with diameter

Since all the physical properties were kept constant during these experiments, just suspension power (P_{js}) becomes a sole function of impeller characteristics and configurations and the most efficient system will exhibit the lowest value. The just suspension power results are presented as plots of P_{js} against C/D in Fig 4.3.5 and P_{js} against D in Fig 4.3.6. For the nine configurations tested, the most energy efficient system was with impeller PBT4 (*T*/3) mounted at *T*/8 clearance. Compared at the same clearance, its just suspension power is 55% and 20% of impellers PBT4 (*T*/2) and PBT4 (*T*/1.7) respectively.

At the three clearances tested (*T*/4, *T*/6 and *T*/8), all impellers indicated that the best performance, in terms of just suspension power, is produced at a low impeller clearance (i.e. *T*/8, see Fig 4.3.5 and 4.3.6). This fits in well with the observation (Sec 4.4.3) that the most energy efficient clearance for 41° and 60° pitched blade turbines are *T*/6 and *T*/8 respectively. Of the three diameters tested, the smallest impeller appears to be the most energy efficient at all clearances.

The influence of impeller diameter on P_{js} are summarised as follows:

T/4 Clearance	$P_{js} \propto D^{3.80}$	$r^2 = 0.98$
T/6 Clearance	$P_{js} \propto D^{2.63}$	$r^2 = 0.96$
T/8 Clearance	$P_{js} \propto D^{2.54}$	$r^2 = 0.95$

Referring to the literature survey, it has been proposed that the velocity of the impeller discharge flow and its geometry play very important roles in the suspension performance of an impeller (Baldi 1978, Shamlou 1987). A calculation of the impeller average discharge velocity may be made by dividing the impeller outlet flow by the impeller area. If power number and flow number are assumed to remain constant as impeller diameter is increased, such a calculation shows that at constant average velocity, impeller power increases with the square of impeller diameter.

$$Po = \frac{P}{\rho N^3 D^5}$$

$$\text{and} \quad Fl = \frac{Q}{N D^3} \qquad \text{...eqn(4.3.4)}$$

For constant flow number, average discharge velocity can be assumed as:

$$\frac{Q}{A} \propto \frac{N D^3}{D^2} \propto N D \qquad \text{...eqn(4.3.5)}$$

and $$P \propto N^3 D^5 \propto (D^{-1})^3 D^5 \propto D^2 \qquad \text{...eqn(4.3.6)}$$

In the absence of any effects due to changes in the geometry of the discharge flow, we would expect just suspension power to increase with the square of impeller diameter, in order to maintain fluid velocities high enough for suspension directly beneath the impeller. This region beneath the impeller is the critical one where solids are most difficult to suspend for a PBT in a dished based vessel. In fact the just suspension power rises more rapidly than the square of impeller diameter, and thus, the effects due to changes in the geometry of the discharge flow cannot be ignored.

This result shows that small diameter impellers are more efficient for solids suspension while most of the literature suggested that suspension efficiency improves slightly, or at worst remains constant, with increasing impeller diameter. The most likely explanation for the apparent discrepancy is that the literature work has been carried out with flat based vessels, whereas this work was carried out with dished based vessels.

In a flat based vessel the region of last suspended solids may vary, occurring either in the centre of the vessel or in the corner between the vessel base and wall depending on circumstances such as impeller type and size. In a dished based vessel, the last suspended region is always found directly beneath the impeller.

Results obtained from this study can be explained by LDA measurements of impeller discharge flow. Fawcett (1989) conducted a series of flow measurements with pitched blade turbines of different diameter at various clearances. He showed that pitched blade turbines have a low flow velocity in their discharge directly below the centre of the impeller, which is where the last suspension is observed in this investigation. Moreover, as the diameter of the impeller is increased the angle of the discharge flow is deflected radially outwards away from the centre of the impeller (Fig 4.3.7). This reduces the effectiveness of the impeller in

the central region and therefore just suspension power becomes higher. Fawcett's results also confirm the observation that the amount of circumferential flow on the vessel base increases with impeller diameter.

Nagata (Fig 6.2, 1975) conducted a series of solids suspension tests in an unbaffled flat based vessel. He found that when the impeller diameter is too small, solid particles remain unsuspended at the periphery of the vessel despite the centre being clear. Conversely, when the impeller diameter is too large, solid particles are apt to remain undispersed in the centre of the vessel base while the periphery is clear. Therefore he proposed the optimum impeller diameter to be that size at which solids particles are fluidised in both the central and peripheral regions at the same speed.

A description of the suspension process for PBTs is that there is a critical region on the vessel base where there is a persistent region of unsuspended solids. The impeller speed must be high enough to suspend solids in this critical region, for example directly underneath the centre of the impeller. Changing the impeller diameter can improve the suspension efficiency by increasing local velocities in this critical region. However this is done at the expense of reduced velocities over other parts of the vessel base.

Eventually a point should be reached where the fluid velocities away from the critical region drop to such an extent that solids settle out elsewhere, for example in the periphery of the vessel. In other words, immediately below the just suspension speed there are two regions of unsuspended solids and therefore two critical regions. This situation will occur at the optimum impeller diameter for a given impeller geometry and this impeller diameter will be a function of clearance. So the reason for the increased efficiency of the small diameter pitched blade turbines is that they require less power to generate the same fluid velocities as the larger diameter impellers in the critical region of the vessel base, which is directly underneath the impeller in this case. Of course this is done at the expense of reduced velocities on the other areas of the vessel base. The results of this work imply that the optimum impeller geometry is less than $T/3$.

Table 4.3.4 Effect of Impeller Diameter - A Brief Survey

Reference	Impeller	Tank Size (mm)	Vessel Base	Clearance	D/T	Results	Transition Point	Remarks
Bujalski 1986	PBT6	290	Flat	C/T=0.25	0.33-0.52	$N_{js} \propto D^{-1.9}$	Nil	Similar relationship for disk turbine (up to T=0.61m)
Koutsakos 1989	PBT4	225-445	Profiled	0.22≤C/T≤0.69	0.23-0.57	$N_{js} \propto D^{-1.06}$ 0.36≤C/T≤0.52	D=0.36T	-
Susanto 1989	Propeller	188	Flat	C=constant	0.34-0.41	$N_{js} \propto D^{-1.69}$	Nil	$N_{js} \propto D^{-1.68}$ includes other turbines
DeRitter 1990	PBT6	292	Flat	0.5≤C/D≤1	0.22-0.35	$N_{js} \propto D^{-1.74}$, C/D=0.5 $N_{js} \propto D^{-1.68}$, C/D=1	Nil	-
Zolfagharian 1990	Propeller PBT4	240-297	Flat	C/T=0.25	0.20-0.63	$N_{js} \propto D^{-1.66}$	0.5	-
Zwietering 1958	Propeller	154-600*	Flat	C/T=0.25, 0.4	~ 0.16-0.63	$N_{js} \propto D^{-1.67}$	D=0.45T	-
Rao 1988	PBT6	570-1000	Flat	0.17≤C/T≤0.5	0.16-0.66	$N_{js} \propto D^{-1.16}$	Nil	-
Chapman 1981	PBT4	560	Flat	C/T=0.25	0.25-0.50	$N_{js} \propto D^{-1.5}$	Nil	$N_{js} \propto D^{-2.35}$ for disk turbines

* It was not clear which vessels were used to study the effects of impeller diameter

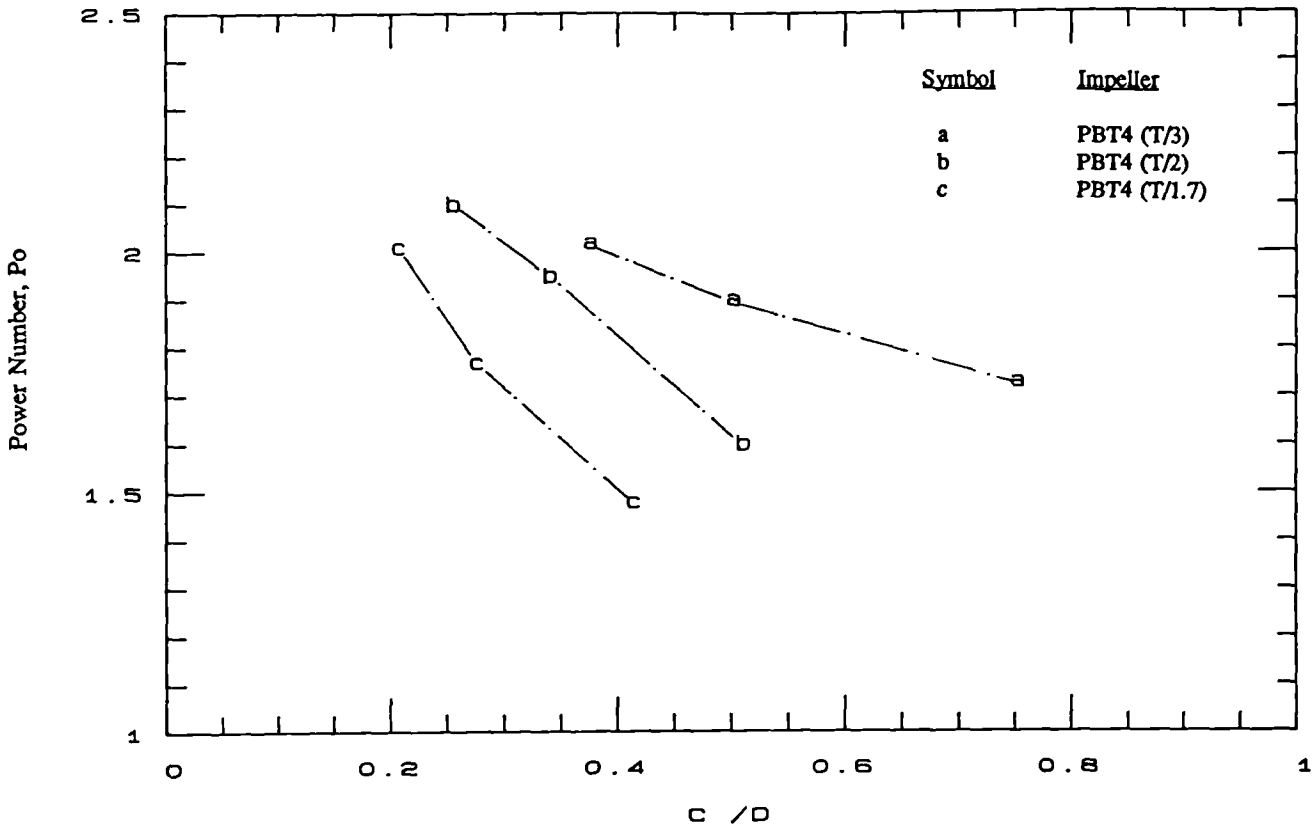

Fig 4.3.1 Po against (C/D) for the 3 Geometrically Similar PBTs

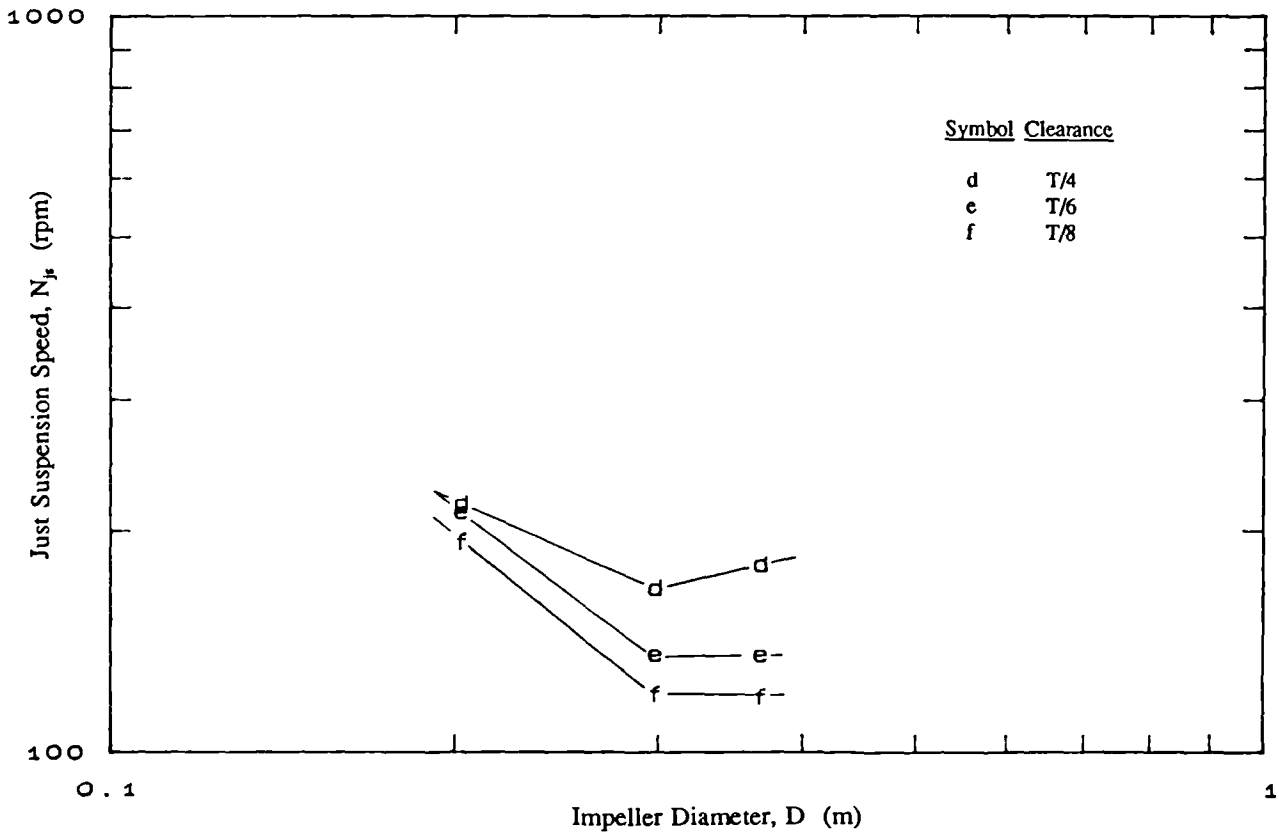

Fig 4.3.2 Effect of Impeller Diameter on Just Suspension Speed

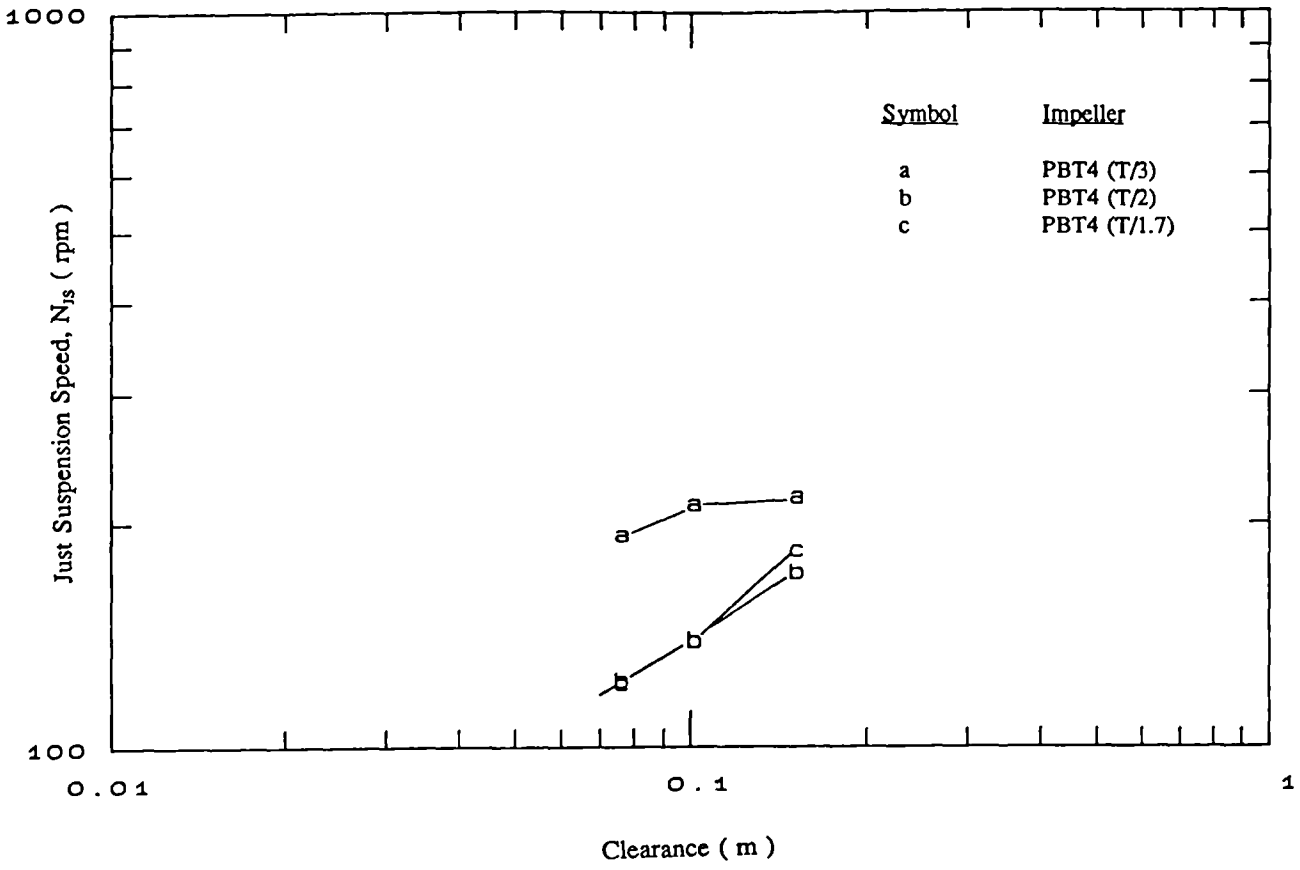

Fig 4.3.3 Effect of Impeller Clearance on Just Suspension Speed

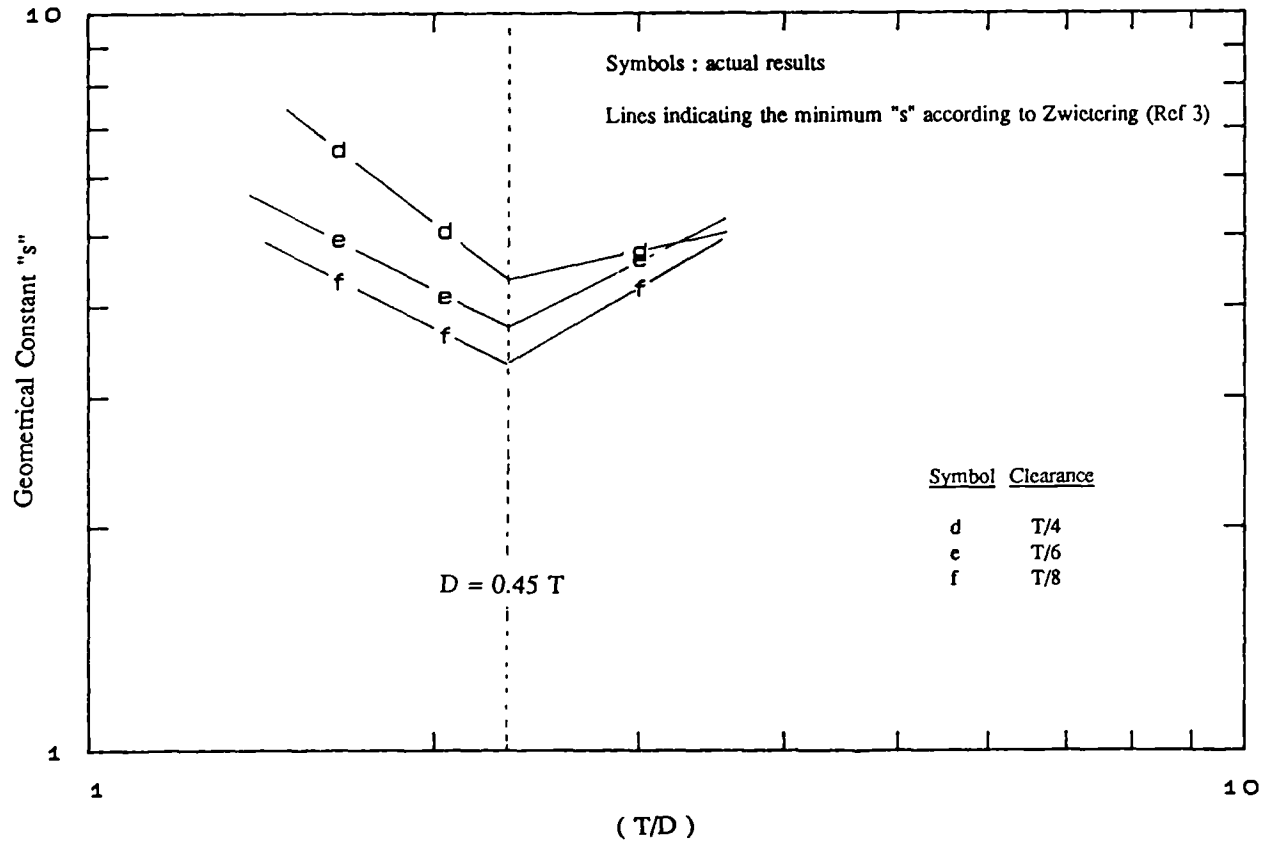

Fig 4.3.4 Plot of Geometrical Constant against (T/D)

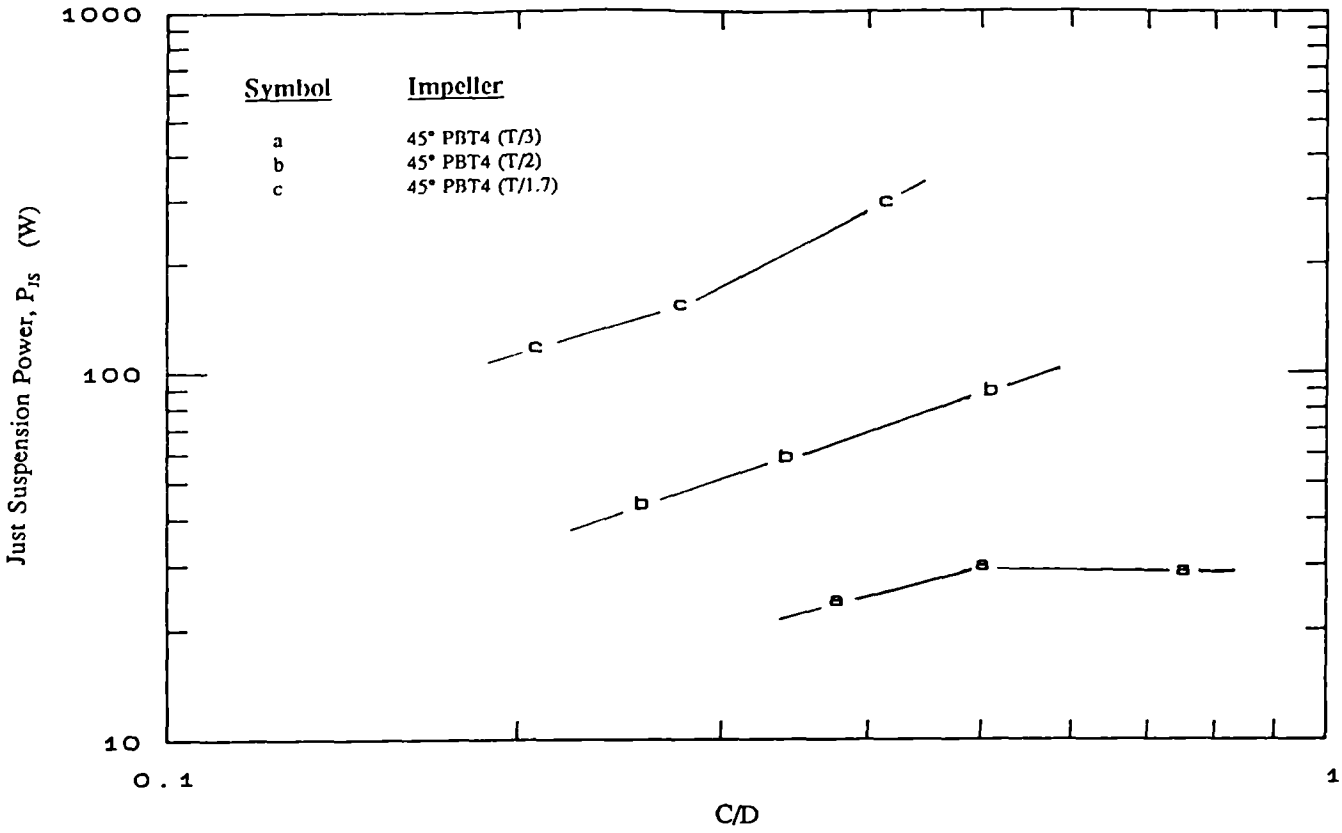

Fig 4.3.5 P_{js} against (C/D) for the 3 Geometrically Similar Impeller

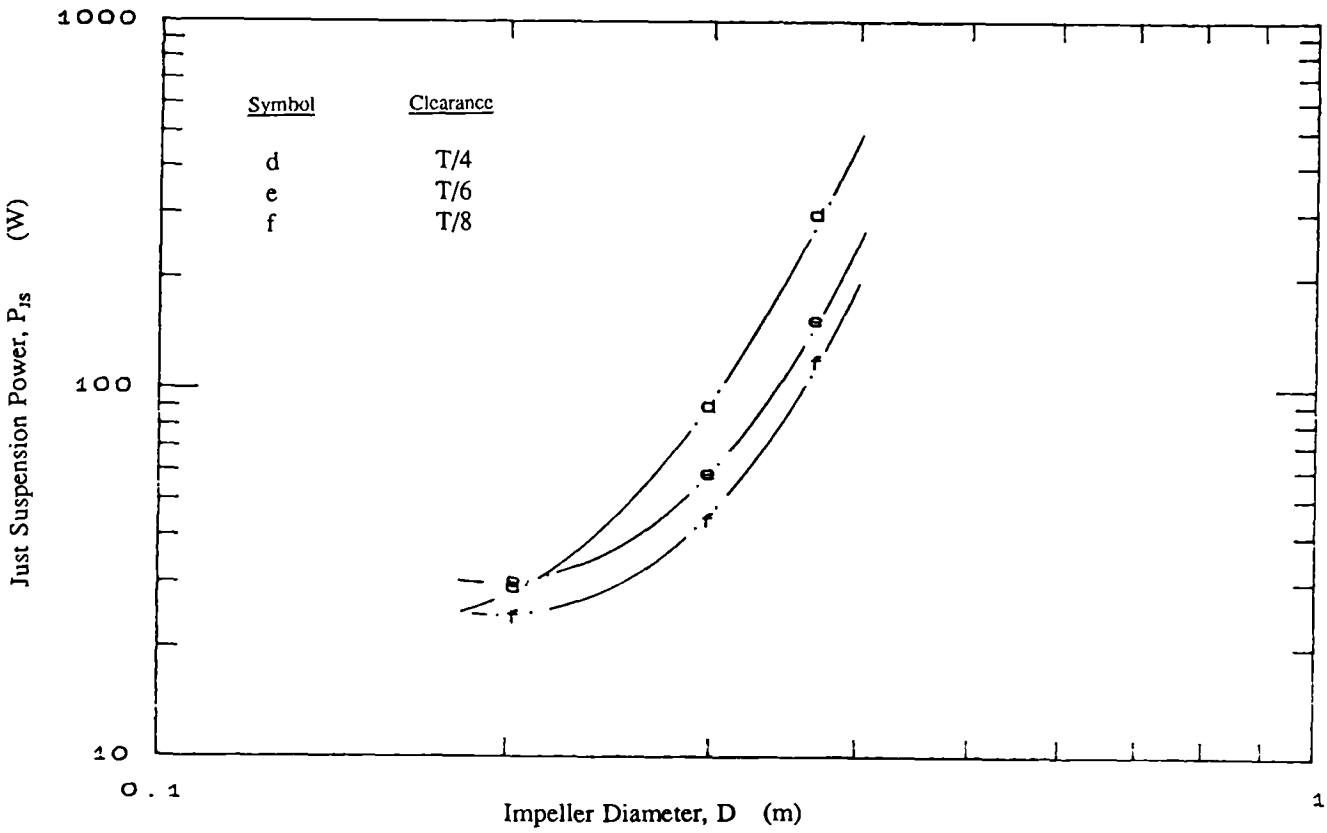

Fig 4.3.6 Effect of Impeller Diameter on P_{js}

4.3.4 Solids Distribution

In the previous sections, it was shown that small diameter PBTs are more energy efficient for suspending solids in dished based vessels, than those of large diameter. This section focuses on the influence of impeller diameter on solids distribution. Solids concentration measurements were made with three geometrically similar PBTs (D=T/3, T/2 & T/1.7, dimensions are summarised in Table 4.3.1) mounted at T/4 clearance. The results are tabulated in Appendix A. Fig 4.3.9 presents a plot of local solids concentration against impeller speed for the five sampling positions. This is taken from the 45° PBT4(T/2) results. However, all three impellers exhibited a similar trend and they confirmed the overall flow pattern generalised from visual observation (Sec 4.1.1).

Relative standard deviation at different speeds (RSD, eqn 2.2.1) is employed to quantify the level of homogeneity achieved by agitation. RSD for the three pitched blade turbines are plotted against impeller speed and are presented in Fig 4.3.10. As expected from flow visualisation, the degree of homogeneity increases as agitation is increased (hence RSD is decreased). The value of RSD goes through a minimum (RSD_{min}) and any further increase in impeller speed gives rise to an increase in RSD. This is believed to be caused by solids redistribution due to centrifugal forces (Bohnet and Niesmak 1980).

Referring to Fig 4.3.10, the speed required by the impeller to produce RSD_{min} is highest for the T/3 impeller and lowest for the T/1.7 impeller. In other words, the large diameter impeller achieves its minimum relative standard deviation at lower impeller speed than the small diameter impeller. A similar pattern is displayed in the plot of RSD against power input (Fig 4.3.11) which again suggests that large diameter PBTs achieve their RSD_{min} at a lower power input than small diameter PBTs. The difference in power input at individual RSD_{min} is very significant. The T/3, T/2 and T/1.7 PBTs required 217, 125 and 57W to achieve their RSD_{min} respectively. In other words, the T/3 PBT needed 3.8 times more power than T/1.7 PBT to achieve its point of maximum homogeneity. However, this trend is in reverse order when compared to the effect of impeller diameter on N_{js}, i.e. T/3 PBT is most energy efficient impeller for suspension (Sec 4.3.2).

To explain this rather interesting finding, N_{js} for the three impellers at 30% Wt are calculated based on the 5% Wt results. The concentration effect is corrected according to

Zwietering's correlation (i.e. $N_{js} \propto X^{0.13}$). The results are then marked on the same plot to facilitate the analysis (Fig 4.3.10). For the large diameter PBTs, RSD_{min} is achieved at a lower impeller speed than its corresponding just suspension speed whereas, for the small diameter impeller, the opposite is the case. Large diameter impellers generally produce more "top to bottom" flow than small diameter impellers for the same power input. It is the bulk flow which is primarily responsible for the distribution of the solid particles. Thus, large diameter PBTs achieve RSD_{min} at lower power input than that of small diameter PBTs. Moreover, the direction of the discharge flow between impellers of different diameter are not the same (Fawcett 1989). Due to the influence of vessel base on flow profiles, large diameter PBTs produce a higher level of radial component flow than the small diameter PBTs (Fig 4.3.7), whereas the discharge flow of a small PBT is less radial and targeted directly on the last suspension region on the vessel base which gives rise to its low N_{js} (Fig 4.3.8).

To prove the hypothesis quantitatively, concentration profiles at impeller speeds close to N_{js} for the three impellers are presented in Fig 4.3.15 to 4.3.17. In case of the small diameter impeller (T/3 PBT), the calculated just suspension is at 285 rpm. The concentration profile at 250 rpm (below N_{js}) shows that of the 5 measuring positions, the top sampling point is 50% of the average concentration while the lower 4 sampling points all exhibit very similar concentrations and they are approximately 30% higher than the average. At 300 rpm (above N_{js}), the five sampling positions still have a concentration approximately 8% higher than the theoretical average, indicating that a portion of clear liquid still exists at the top. Further increase in impeller speed (eg 350 rpm) still shows improvement in the concentration profile (further reduction in RSD). In cases of the two large diameter PBTs (T/2 and T/1.7, Fig 4.3.16 and 4.3.17), concentrations measured at the top sampling position are similar to the predicted average. Moreover, the concentration profiles for impeller speed around N_{js} are very similar and an increase in impeller speed above N_{js} does not improve the homogeneity of the particles, showing that the solids are already well distributed. This once again confirmed the results which show that just suspension speed occurs at lower power input than RSD_{min} and vice versa with large diameter PBTs.

Despite the fact that the large diameter impeller (eg D=T/1.7) achieves its RSD_{min} at a lower impeller speed than that of a small diameter impeller (eg D=T/3), the absolute value of RSD_{min} is lower (more homogeneous) in the case of the small diameter impeller. This is achieved at the expense of high power input (Fig 4.3.11).

Concentration profiles for the three impellers at various power inputs are presented in Fig 4.3.12 to 4.3.14. They are plotted as height from vessel base against solids concentration for the three impellers at low, medium and high power inputs. At low power inputs (Fig 4.3.12), the concentration profile of the T/3 PBT shows that there is more than one third of the vessel height of clear liquid in the vessel, the solids concentration beneath the clear layer is much higher than average and that there is little difference in concentration beneath the clear liquid region. On the other hand, the T/1.7 PBT does not have any clear liquid layer on the top of the vessel (at least according at the top most measuring point) but there is considerable variation in concentration within the profile itself when compared to the T/3 PBT. At medium power input (Fig 4.3.13), the clear liquid layer in the upper region for T/3 PBT has disappeared and the deviation from the mean concentration gradient within the vessel is still less than that of the large diameter impellers. At high power input (Fig 4.3.14), the concentration profile for T/3 PBT improves still further (more homogeneous) while redistribution starts to occur in the large PBTs (Sec 4.1.1) and this increases the magnitude of RSD.

Therefore, uniformity of solids distribution is not a good parameter to assess the condition of solids suspension and vice versa. Moreover, the use of homogeneity data as the criterion for just suspension speed determination should be interpreted with great care, as some impellers attain N_{js} before their most homogeneous points. For other impellers, just suspension speed requires higher speed or power input than RSD_{min}.

4.3.5 Verification of Tip Speed Criterion

Most theoretical models developed for solids distribution are based upon one dimensional dispersion analysis and the impeller tip speed (πND) is normally assumed to counterbalance the particle settling velocity (Sec 2.2.2). This gives rise to a constant tip speed criterion for impeller diameter as well as scale-up effect. Fig 4.3.18 is a plot of RSD against ND for the three geometrically similar impellers. Using ND = *constant* brings the three curves closer to each other but a stronger diameter effect is required to match them.

Brodkey (1988) suggested an expanded pumping number including the impeller to tank ratio (D/T) to be more useful:

$$Fl = \frac{Q\ (D/T)^{0.5}}{N\ D^3} \qquad \text{...eqn(4.3.7)}$$

$$Q \propto Fl\ N\ D^3 \left(\frac{D}{T}\right)^{-0.5}$$

The relative pumping rate can be estimated according to Nagata's correlation (1975):

$$Fl \propto \left(\frac{D}{T}\right)^{-2.5} \left(\frac{W}{T}\right) Po^{0.7} \qquad \text{...eqn(4.3.8)}$$

A plot of RSD against relative discharge rate is presented in Fig 4.3.20 and the data does not seem to correlate in this format.

Regression analysis gives a poor regression coefficient but suggests a diameter effect close to ND^2 (Fig 4.3.19), which is similar to the Thrust number as proposed by ITT Flygt (Karslen 1992).

Thrust force generated by an impeller:

$$F \propto \rho\ Q\ V \qquad \text{...eqn(4.3.9)}$$

$$\propto \rho\ (N\ D^3)\ (N\ D)$$

$$\propto \rho\ N^2\ D^4$$

And the Thrust number (Ft) is defined as:

$$Ft = \frac{F}{\rho\ N^2\ D^4} \qquad \text{...eqn(4.3.10)}$$

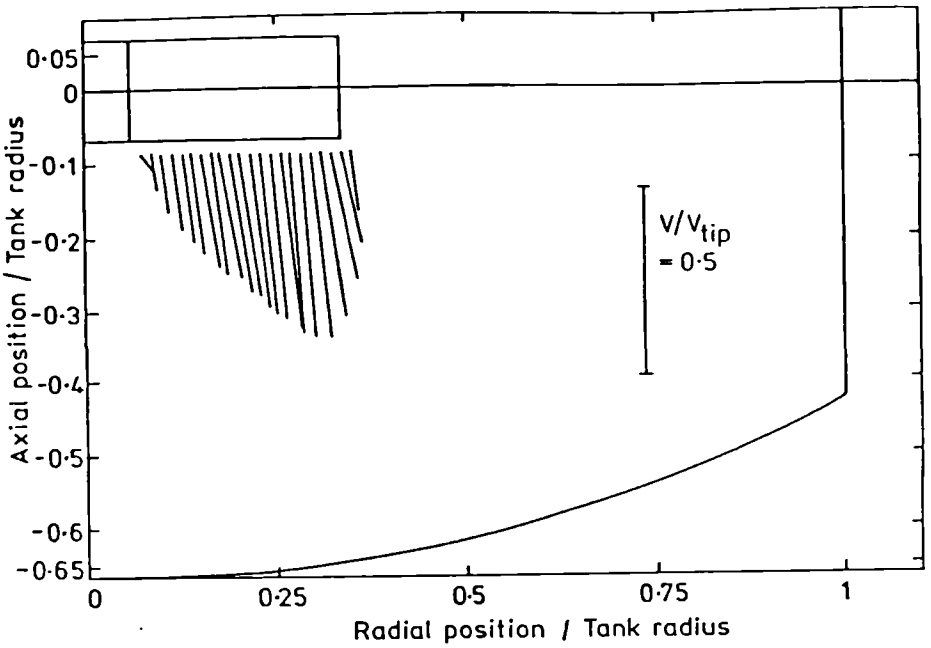

D=T/3, C=T/3

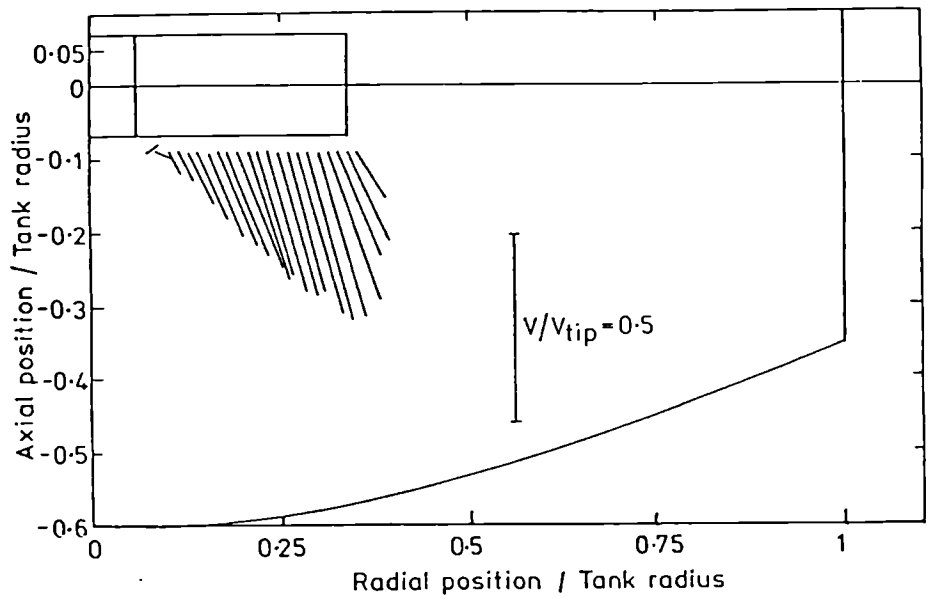

D=T/3, C=T/3.33

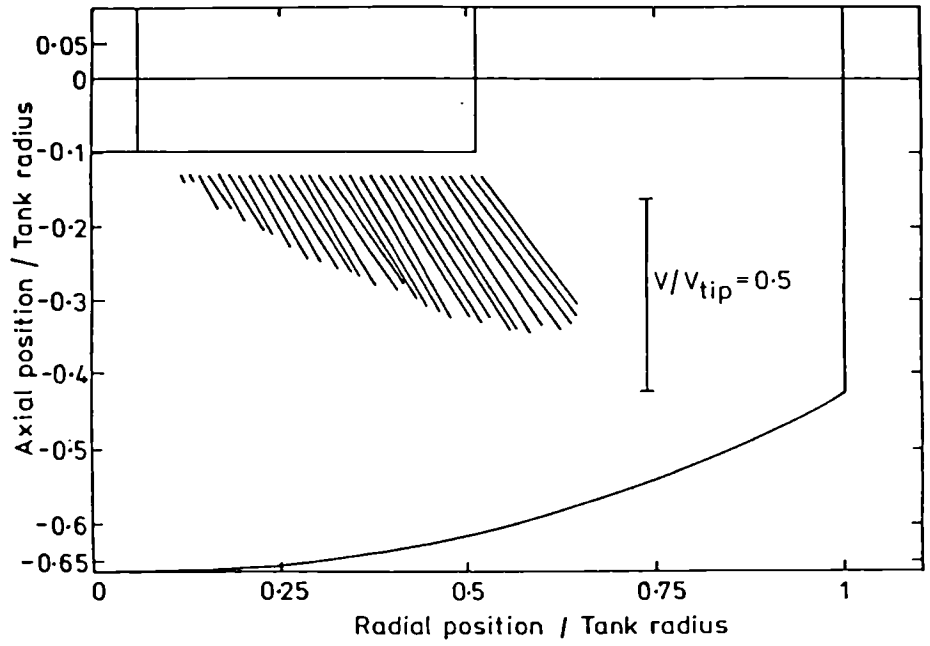

D=T/2, C=T/3

Fig 4.3.7 V_r, V_z Vectors Comparison for Pitched Blade Turbines (Fawcett 1989)

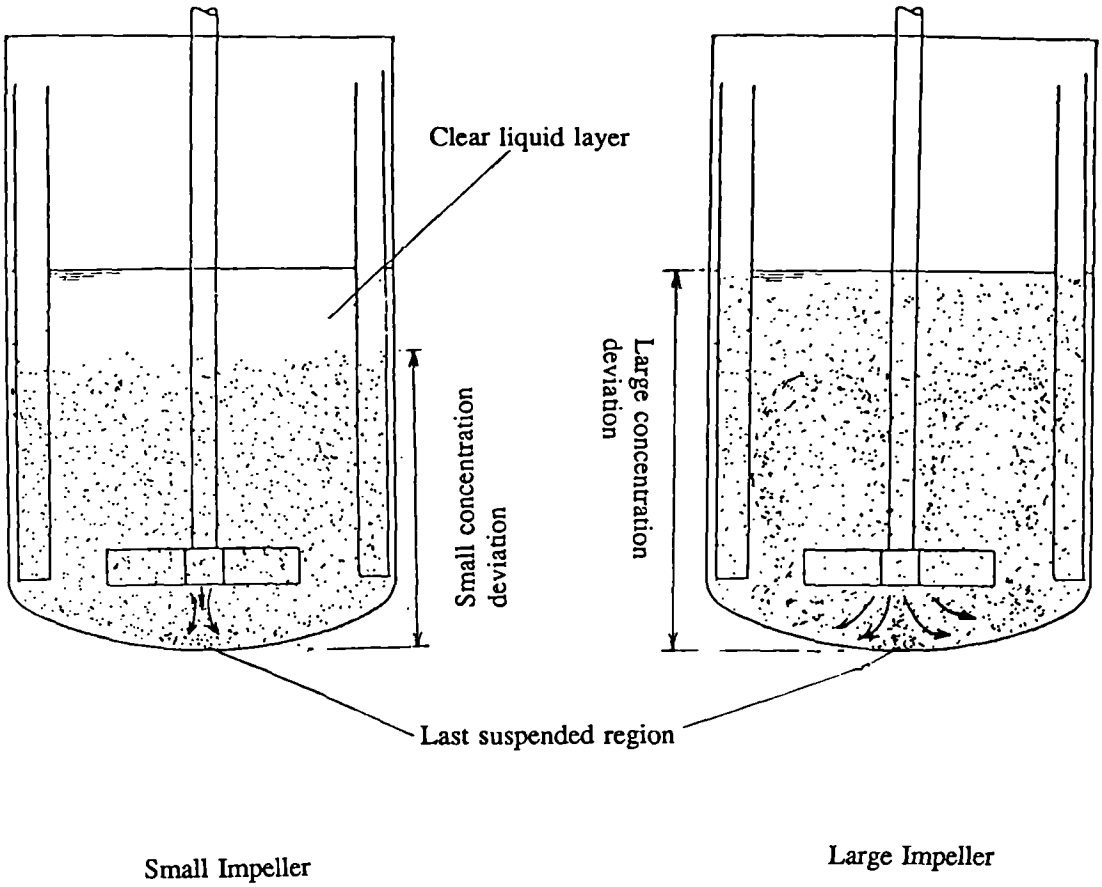

Fig 4.3.8 Comparison of Suspension and Distribution Characteristics between Small and Large Diameter PBTs

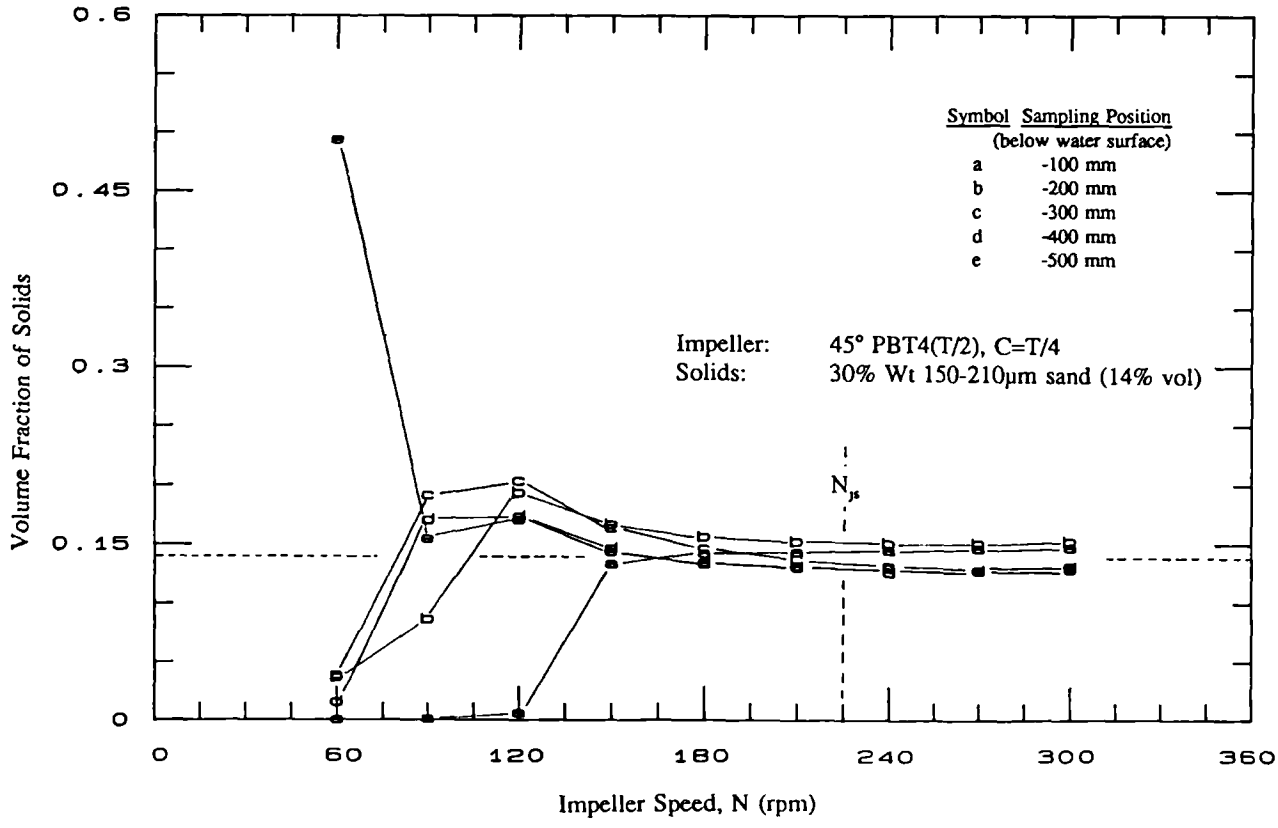

Fig 4.3.9 Plot of Solids Concentration against Speed at different Sampling Location

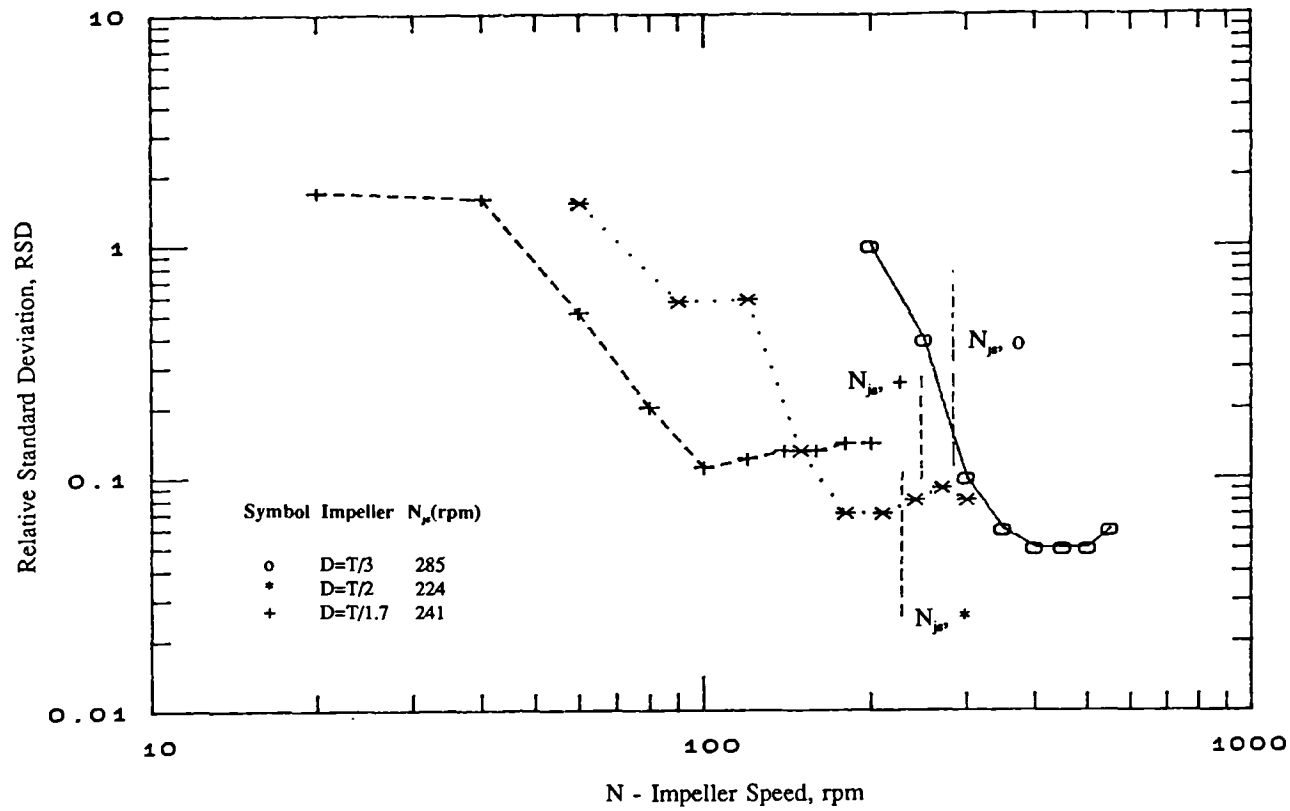

Fig 4.3.10 Effect of Impeller Diameter on RSD, Compared against Impeller Speed

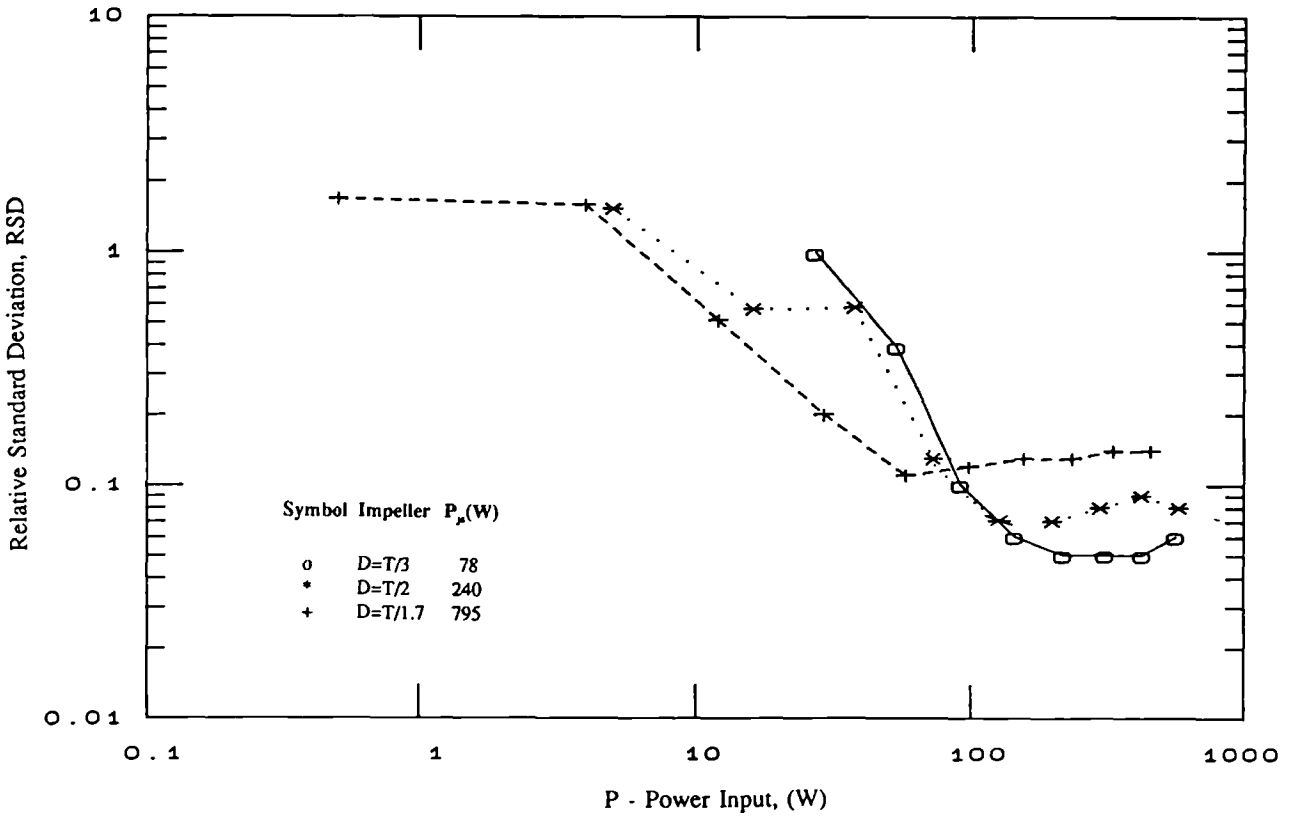

Fig 4.3.11 Effect of Impeller Diameter on RSD, Compared against Power Input

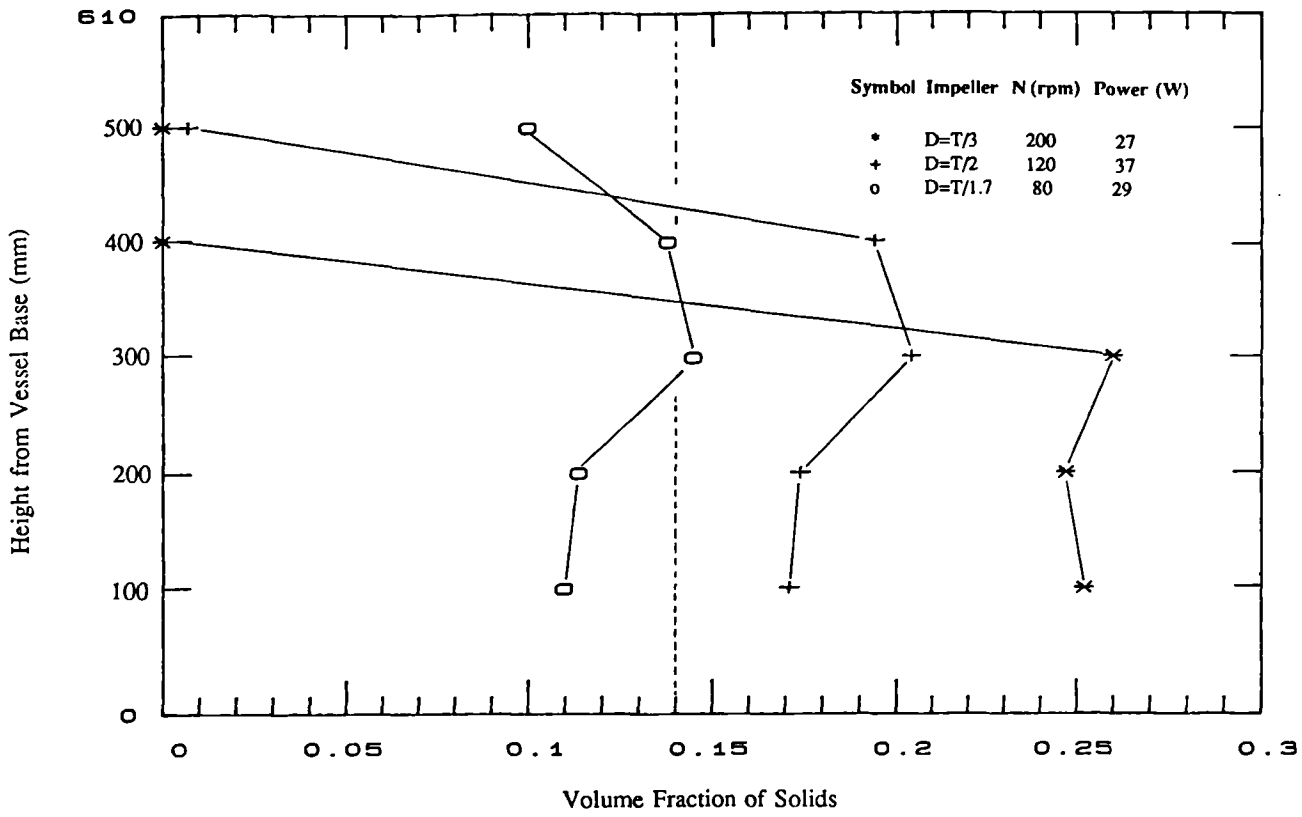

Fig 4.3.12 Concentration Profiles of the 3 PBTs at Low Power Input

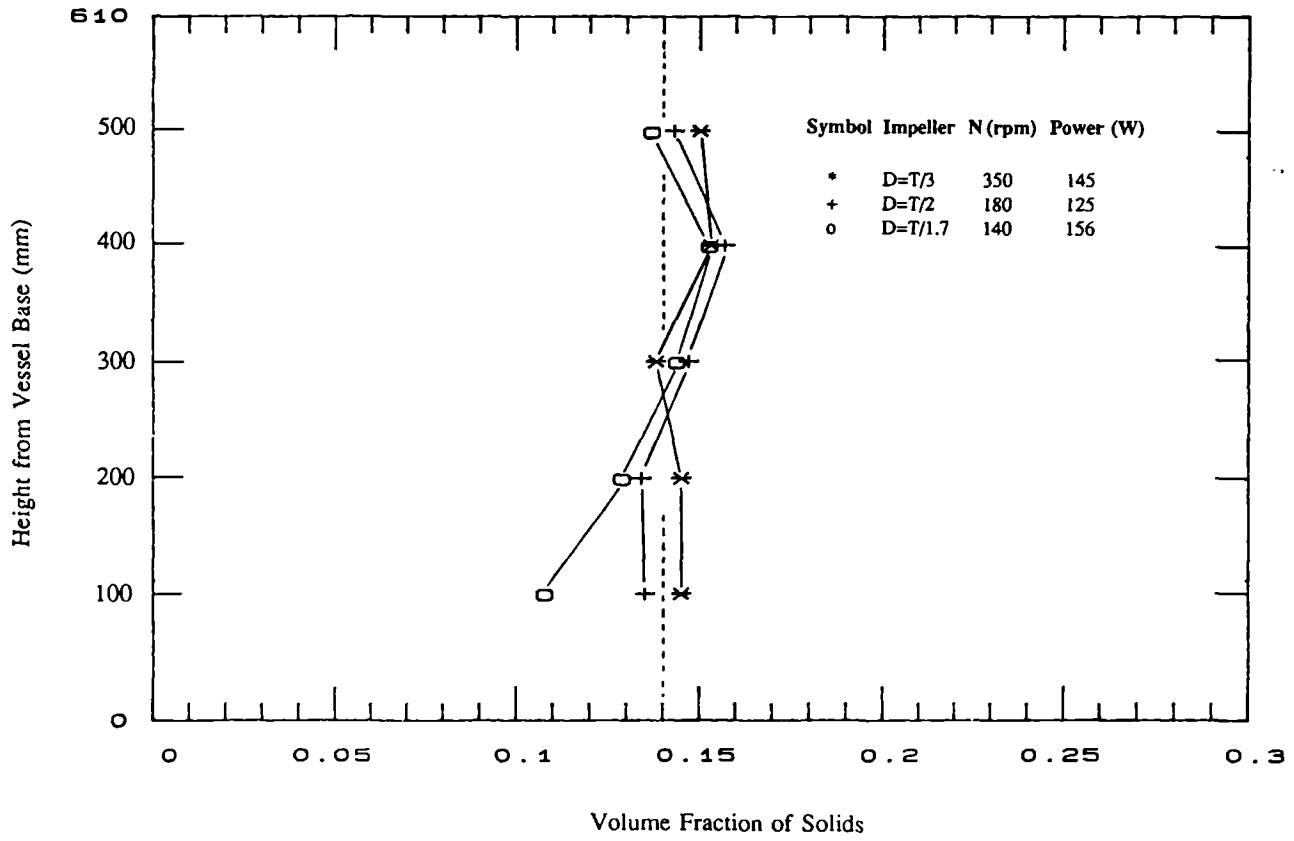

Fig 4.3.13 Concentration Profiles of the 3 PBTs at Medium Power Input

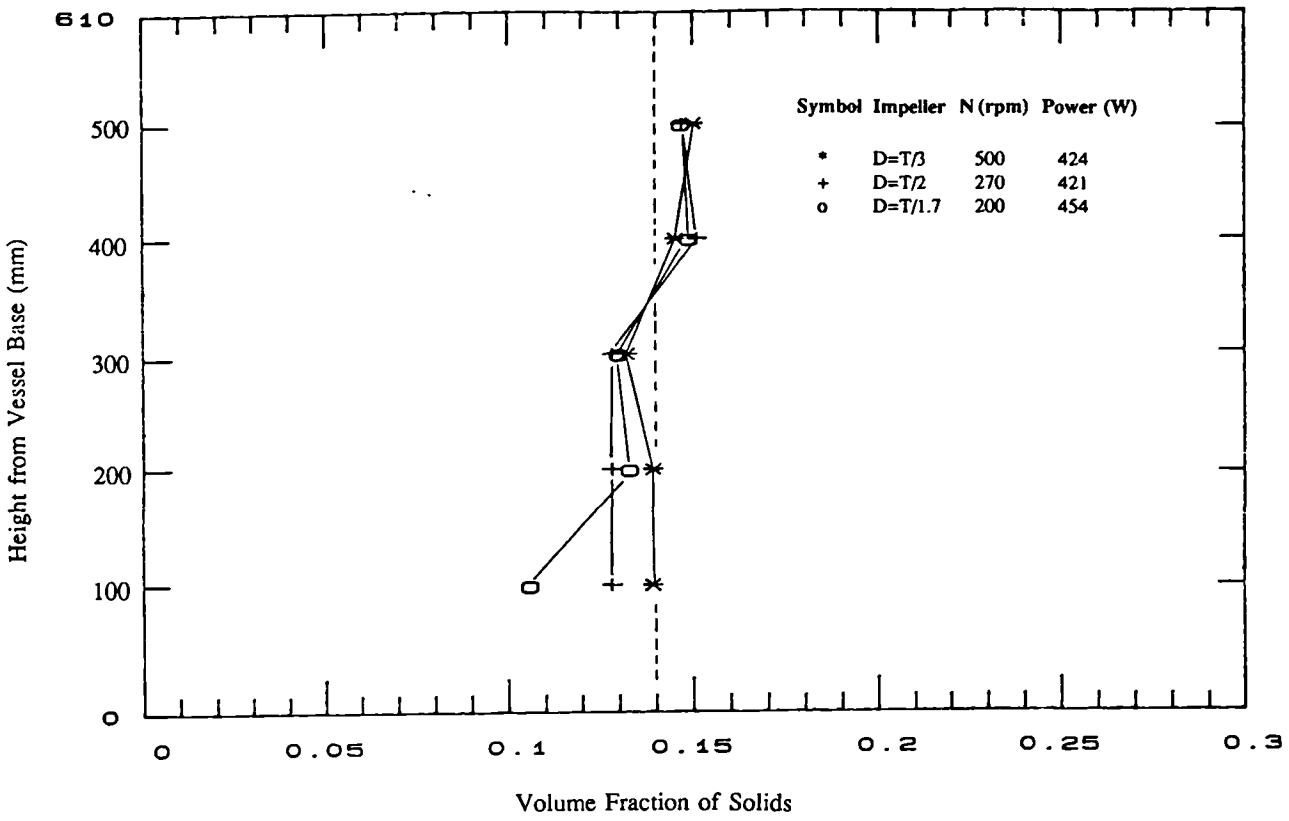

Fig 4.3.14 Concentration Profiles of the 3 PBTs at high Power Input

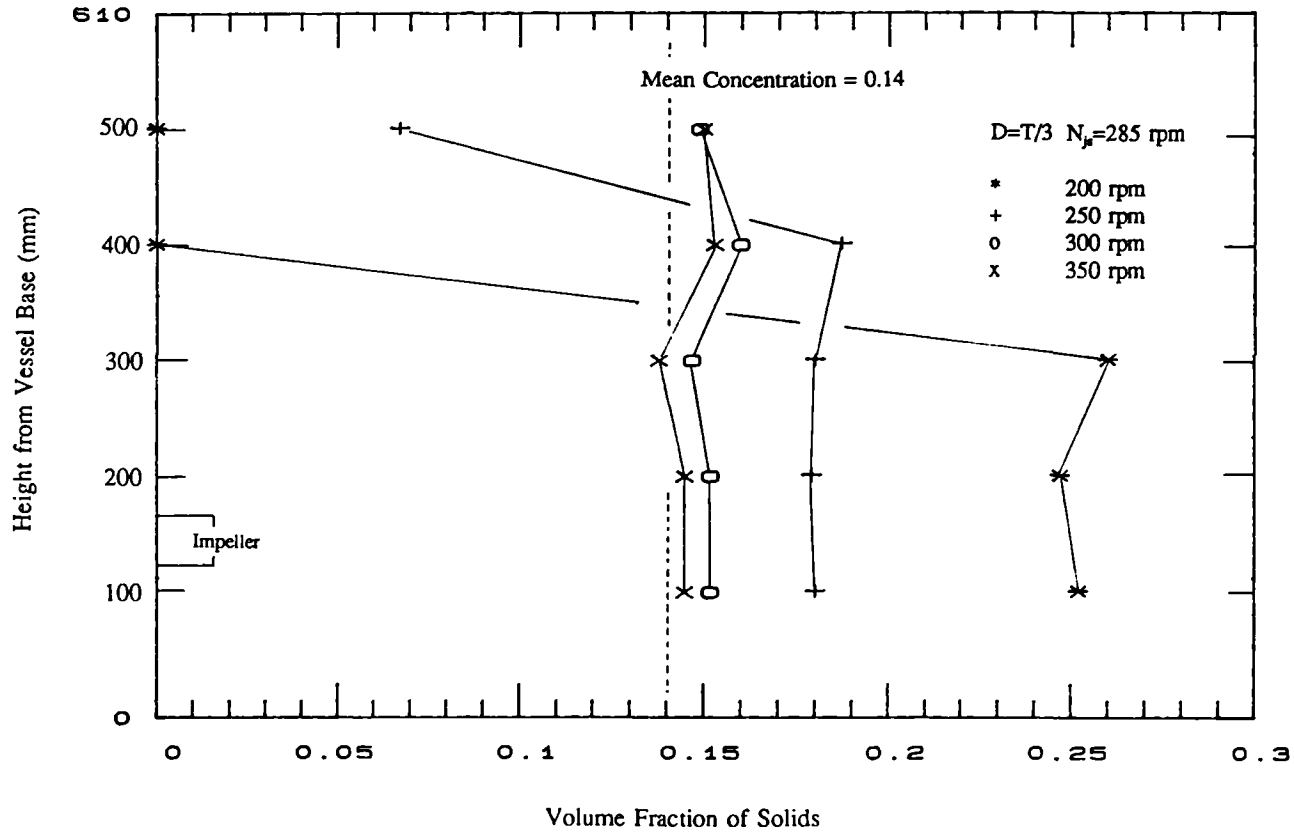

Fig 4.3.15 Concentration Profiles near N_{js} (T/3 PBT)

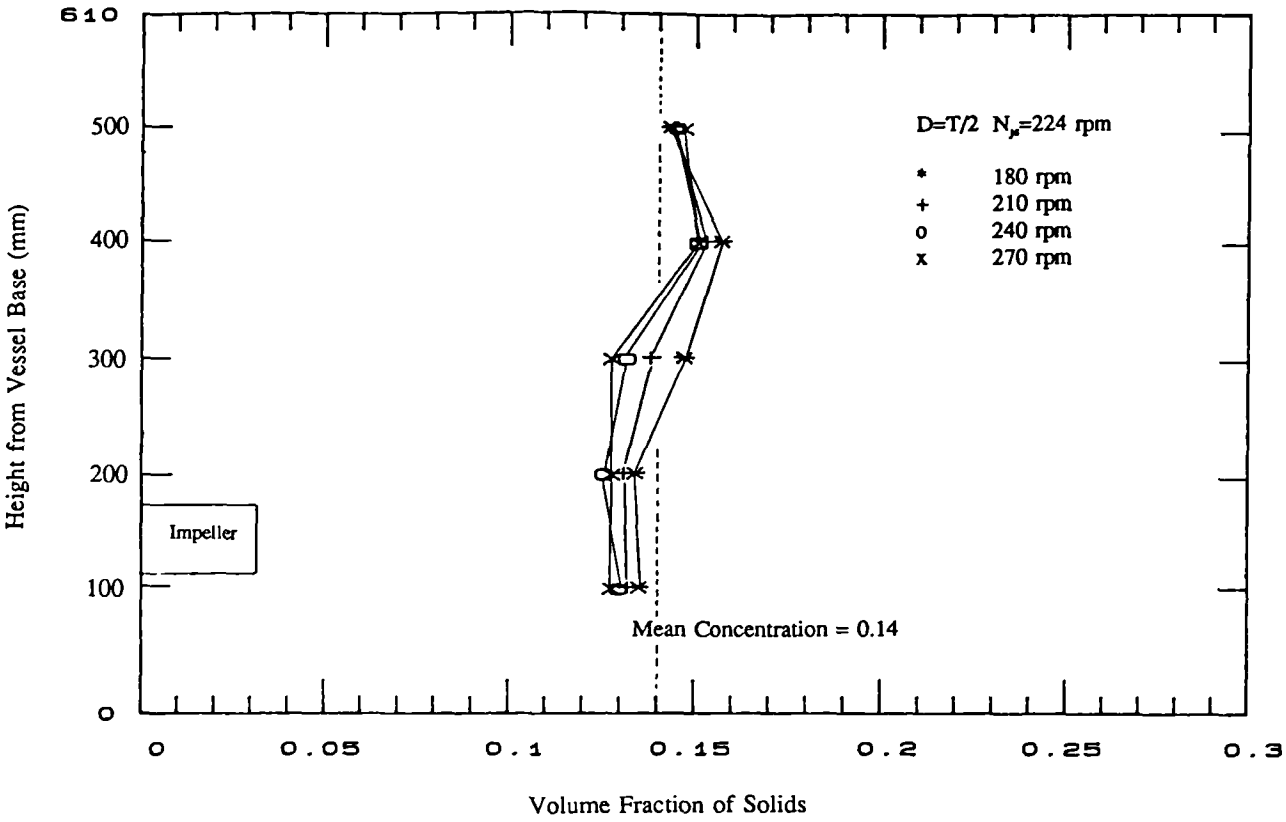

Fig 4.3.16 Concentration Profiles near N_{js} (T/2 PBT)

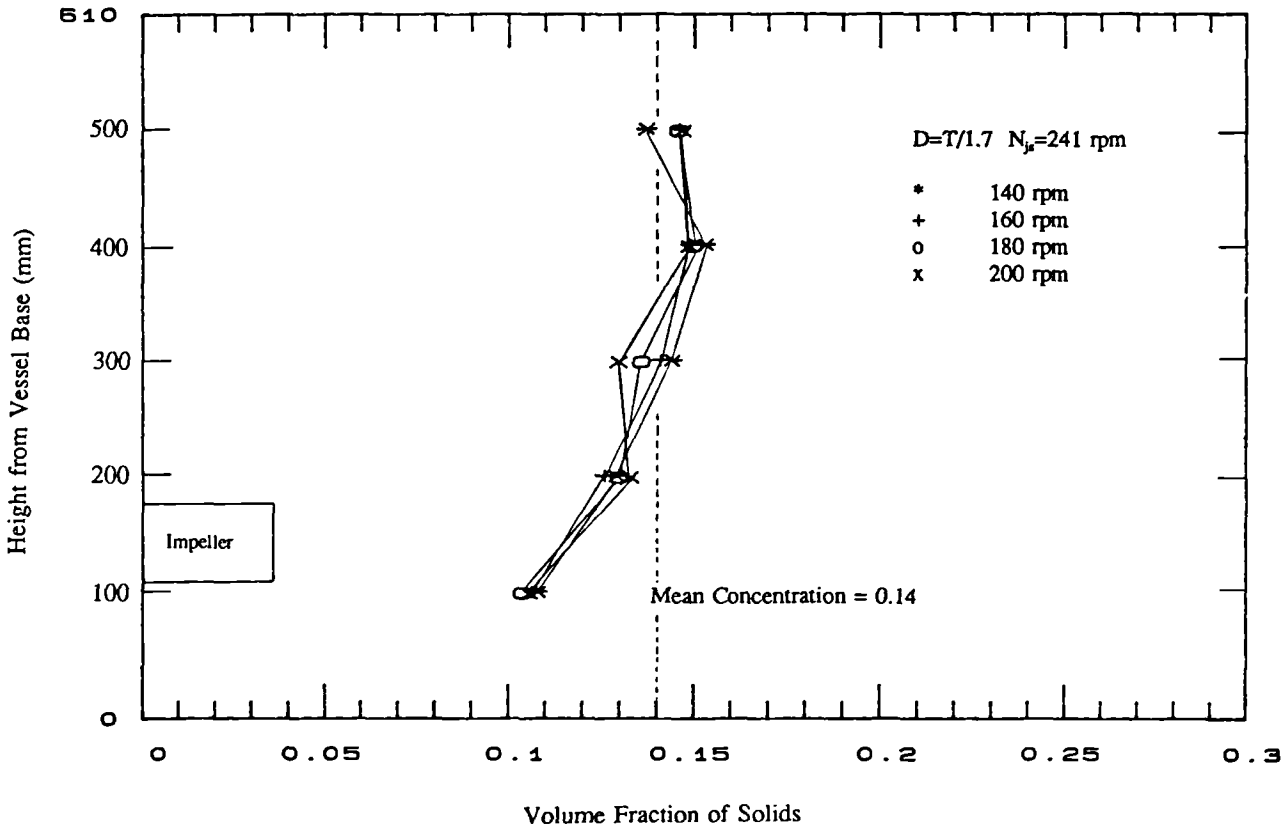

Fig 4.3.17 Concentration Profiles near N_{js} (T/1.7 PBT)

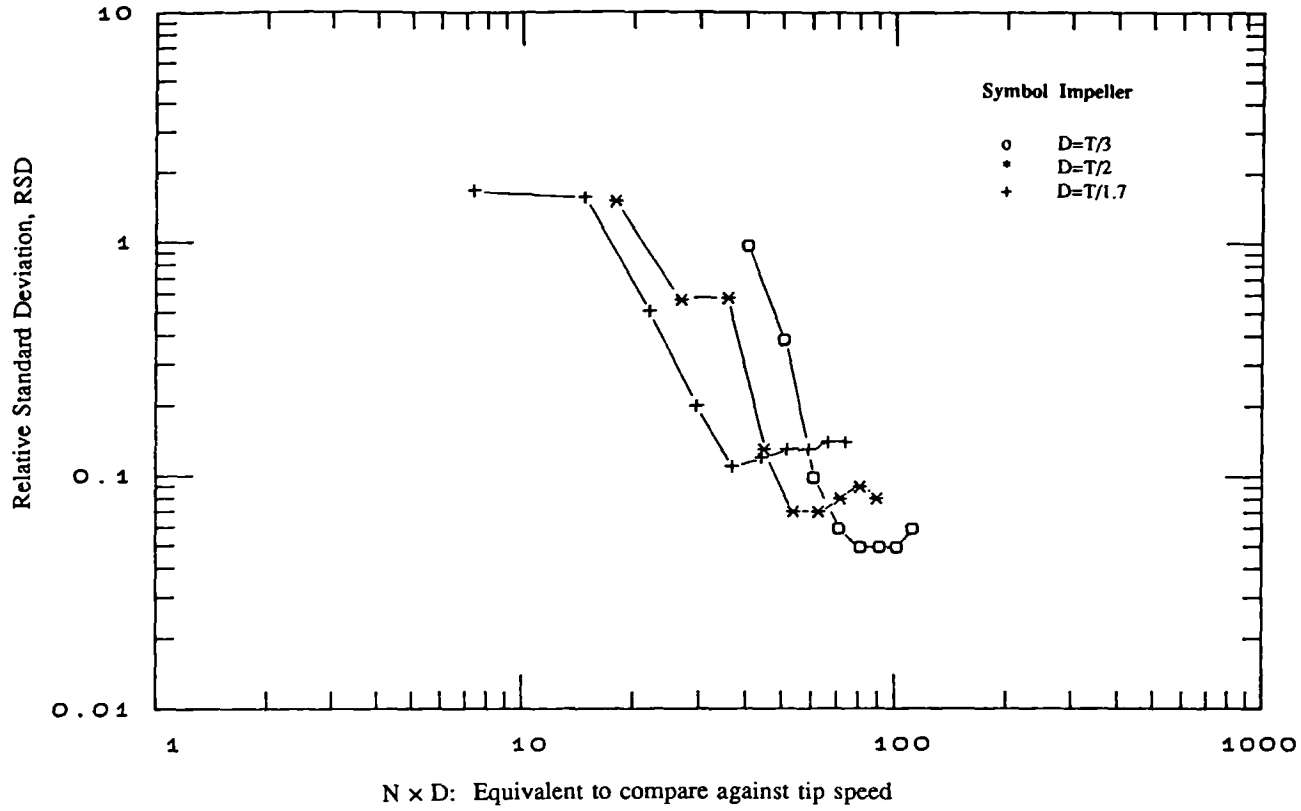

Fig 4.3.18 Comparing against Tip Speed Equivalent

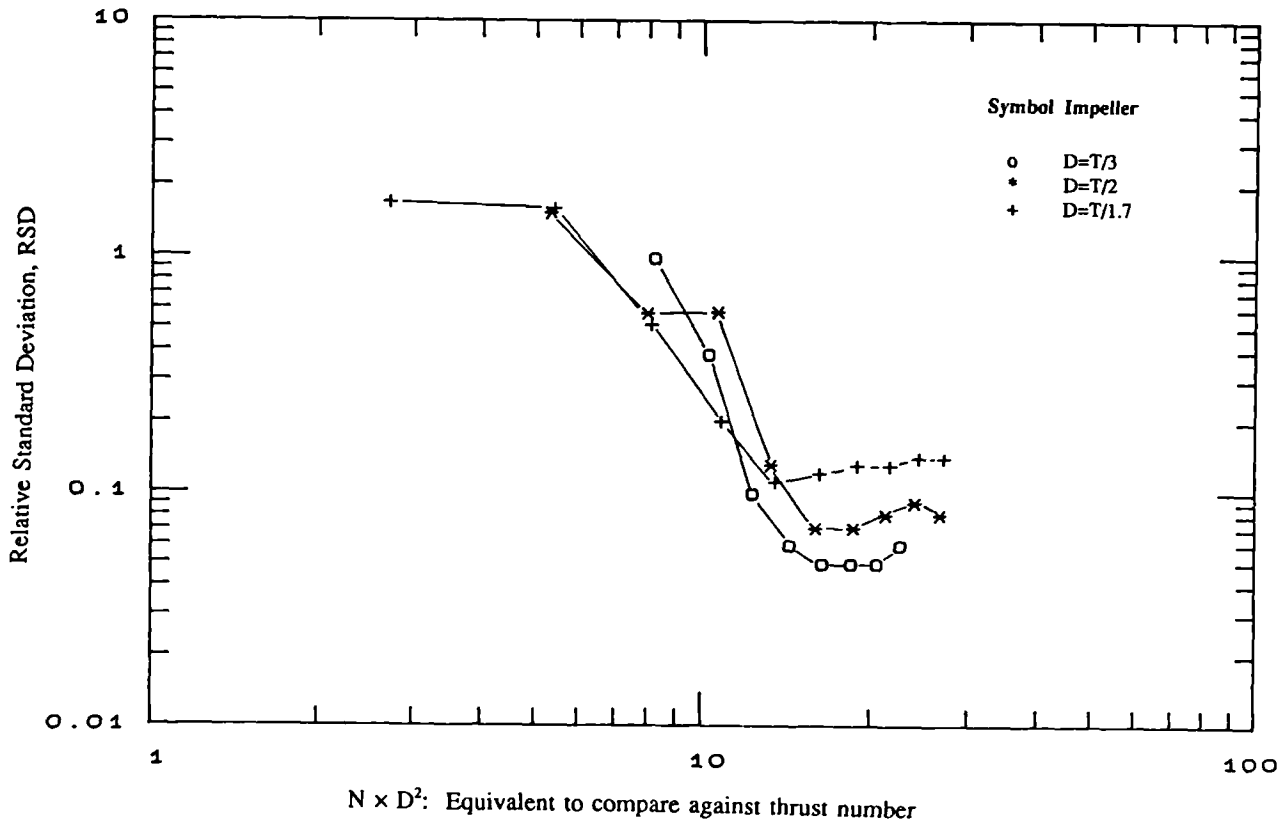

Fig 4.3.19 Comparing against Thrust Number Equivalent

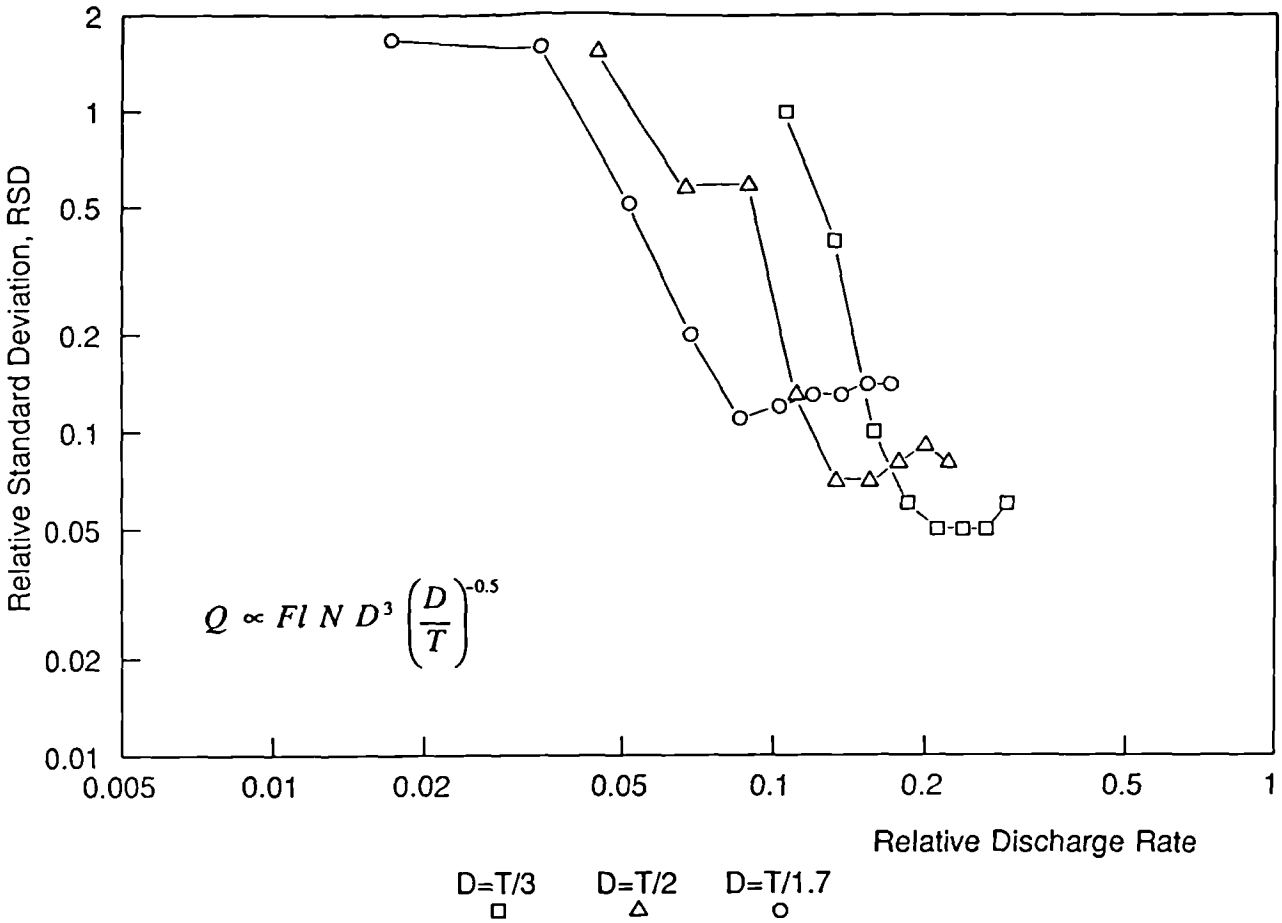

Fig 4.3.20 Plot of RSD against Relative Discharge Rate

4.4 EFFECT OF IMPELLER PITCH ANGLE

This section focuses on the effect of impeller pitch angle on solids suspension. The influence of impeller clearance was investigated simultaneously to establish if there was any associated change in the pitch angle effect similar to that which had been observed on the diameter effect. Four pitched blade turbines and a flat blade turbine were examined in the 0.61 m diameter vessel (T_{61}). The impellers all had diameters approximately one third that of the tank and their pitch angles were 30°, 41°, 45°, 60° and 90° to the horizontal. They were mounted at T/4, T/6 and T/8 clearances. Details of the impeller dimensions are presented in Table 4.4.1.

Table 4.4.1 Impeller Configurations

Impeller Notation	No of Blades	α (°)	*D* (mm)	*W* (mm)	W_p (mm)	χ (mm)	Series No
30° PBT4 (T/3)	4	30	202	82	41	3.4	023-46-061
41° PBT4 (T/3)	4	41	203	58	38	3.1	002-31-061
45° PBT4 (T/3)	4	45	203	58	41	3.4	001-31-061
60° PBT4 (T/3)	4	60	198	48	42	3.9	002-32-061
90° FBT4 (T/3)	4	90	203	41	41	3.3	008-37-061

Note that all the impellers tested have very similar projected blade width except 41° PBT4 (T/3)

4.4.1 Power Numbers

Power numbers in water were measured for the five impellers at all clearances (T/4, T/6 and T/8). The results are given in Table 4.4.2 and are also presented as plots of power number against the sine of pitch angle in Fig 4.4.1. Note that the 41° PBT4(T/3) data are slightly shifted from the general trend because the projected blade width of this impeller is smaller than that of the rest.

The results obtained indicate that the power number of an agitator increases in direct proportion to the blade inclination. Power numbers at different pitch angles are correlated in the form:

$$Po \propto (\sin \alpha)^c \qquad \text{...eqn(4.4.1)}$$

The exponent, c, is approximately 2.0 in all cases, i.e. c = 2.08, 2.04 and 1.87 for T/4, T/6 and T/8 clearances. Medek (1980) investigated a range of pitch angles from 10° to 90° at T/4 clearance in a flat based vessel. He presented the pitch angle effect on power number as a function of the impeller thickness to blade width ratio (ie χ/W) and for χ/W ratio of 0.05, the average exponent c in eqn 4.4.1 is equal to 1.97. Bates (1963) obtained an exponent of 2.5 at T/3 clearance. All these results are for impellers with constant projected blade width.

Table 4.4.2 Effect of Pitch Angle on Power Numbers

Impeller	sin α	Power Numbers		
		C=T/4	C=T/6	C=T/8
30° PBT4(T/3)	0.50	0.78	0.86	0.98
41° PBT4(T/3)	0.66	1.35	1.55	1.69
45° PBT4(T/3)	0.71	1.73	1.90	2.02
60° PBT4(T/3)	0.87	2.59	2.77	2.79
90° PBT4(T/3)	1	3.19	3.51	3.62

Warmoeskerken (1984) worked with six bladed pitched blade turbines with angles 30°, 40° and 60° mounted at T/2 clearance. The results with constant actual blade width, W, suggested $Po \propto (\sin \alpha)^3$. Similar findings was reported by Frijlink (1984). The dependency of power number on blade width at constant blade angle is reported by Muskett (1985) as:

$$Po \propto (W/D)^a \qquad \text{...eqn(4.4.2)}$$

Most workers report a value for "a" approximating to 1. Correction of Warmoeskerken and Frijlink's data for the effect of blade width gives a value for the exponent on sin α of approximately 2. A further regression analysis was conducted incorporating the (C/D) term to allow for the effect of clearance. The 95% confidence limits on the exponents of sin α and (C/D) are 1.89 to 2.11 and -0.32 to -0.14 which ties in well with published data reported by Muskett et al 1985: $Po \propto (C/D)^{-0.2}$. The exponent on (C/D) agrees well with the D=T/3 results reported in the previous section.

$$Po = 3.06\ (\sin \alpha)^{2.0}\ (C/D)^{-0.23} \qquad r^2 = 0.99 \qquad \text{...eqn(4.4.3)}$$

Further regression analysis was conducted for the seven impellers in T/4, T/6 and T/8 clearances {30° PBT4(T/3), 41° PBT4(T/3), 45° PBT4(T/3), 60° PBT4(T/3), 90° FBT4(T/3), 45° PBT4(T/2) and 45° PBT4(T/1.7)}. The power numbers correlate very well in the format:

$$Po = 3.19\ (\sin \alpha)^{2.23}\ (C/D)^{-0.29}\ (W/D)^{0.25}\ (D/T)^{-0.29} \qquad r^2 = 0.98 \qquad \text{...eqn(4.4.4)}$$

4.4.2 Flow Pattern

All three types of flow regimes on the vessel base which have been described in the previous sections (vortexing, radial and circumferential) were found in this series of experiments. In general, vortexing occurred only in the central region and the area dominated by this flow regime increases with decreasing impeller clearance. As the pitch angle increases, the radial flow region is reduced while the amount of circumferential flow increases (Fig 4.4.2). This can be explained by the relatively higher tangential velocity component in the impeller discharge flow of the 90° FBT4(T/3) as compared to the 30° PBT4(T/3).

When the operating speed is close to the just suspension speed, a layer of clear liquid with very low solids concentration surmounts the solid-liquid slurry. This clear liquid is deeper with a small pitch PBT than with a large pitch version, which indicates that the impellers with small pitched angle (eg 30°) are less efficient in generating bulk mixing.

4.4.3 Solids Suspension

Just suspension speed for the five impellers was measured at three clearances (T/4, T/6

and T/8), with a solids concentration of 5% Wt (150-210 μm sand). The results are given in Table 4.4.3 and are also presented as plots of N_{js} against clearance in Fig 4.4.3.

Table 4.4.3 Summaries of N_{js}, "s" value and P_{js}

Impeller	Parameters	Nominal Clearance		
		C=T/4, =0.75D	C=T/6, =0.5D	C=T/8, =0.38D
30° PBT4(T/3)	N_{js} (rpm)	291	325	328
	P_{js} (W)	31	48	56
	s	6.4	7.1	7.2
41° PBT4(T/3)	N_{js} (rpm)	217	202	207
	P_{js} (W)	23	21	25
	s	4.8	4.4	4.5
45° PBT4(T/3)	N_{js} (rpm)	217	212	193
	P_{js} (W)	29	30	24
	s	4.8	4.6	4.2
60° PBT4(T/3)	N_{js} (rpm)	204	192	171
	P_{js} (W)	32	28	20
	s	4.4	4.1	3.7
90° PBT4(T/3)	N_{js} (rpm)	200	189	186
	P_{js} (W)	42	39	38
	s	4.4	4.1	4.1

"s" is the geometrical constant in Zwietering correlation

At low clearances the solids on the vessel base are more likely to be entrained by the flow generated by the impeller. If the rotating impeller is to be considered as a momentum source, its power will decay gradually as it moves away from the impeller. Thus, not surprisingly, most values of N_{js} decrease gradually with decreasing clearance.

The 30° PBT4(T/3) is an obvious exception to this, with N_{js} increasing as clearance is decreased. An explanation for this anomaly will be given later on in this section. The general pattern of "s" values is expected to be very similar to that of N_{js}, since all physical and geometrical parameters were kept the same during the experiments and the impeller diameters are similar to each other. From eqn 4.3.1:

$$s \propto N_{js} \qquad \text{...eqn(4.4.5)}$$

The results obtained for just suspension power are also tabulated in Table 4.4.3. The impeller P_{js} at different clearances do not follow any obvious trend. These suggest that all the impellers have an optimum clearance. The most energy efficient clearance for 30°, 41°, 45°, 60° and 90° turbines are T/4, T/6, T/8, T/8 and T/8 respectively (Fig 4.4.4). Nienow and Miles (1978) examined the effects of impeller/tank configuration on solids suspension in flat based vessels. The influence of geometries such as impeller diameter and clearance on the suspension performance of the 45° pitched blade turbine were investigated. They found that the results did not follow any obvious trend.

Among the fifteen impeller/clearance configurations tested, 30° PBT4(T/3) and 60° PBT4(T/3) at T/8 clearance gave the highest and lowest just suspension power. In other words, they are the least and most efficient configurations for solids suspension. The effect of impeller clearance on just suspension varies from one impeller to another. The ratios in P_{js} between the worst and best mounting clearances are 1.81, 1.19, 1.25, 1.60 and 1.11 for the 30°, 41°, 45°, 60° and 90° turbines respectively. The 41° and 45° PBTs give the best overall performance while the 30° and the 60° PBTs are most sensitive to the effect of clearance.

The general pattern of results may be explained by the particle flow pattern on the vessel base. Different types of flow patterns (Sec 4.4.2) were displayed by the particles on the vessel base near N_{js} and these patterns are functions of the impeller characteristics and its interactions with the surroundings. Just suspension power for the 30° PBT increases with decreasing clearance. It is axial flow dominated (i.e. radially outwards after impinging on the vessel base) and is analogous to a liquid jet pointing downwards. In general, the radial component of the impeller discharge (which translates to circumferential flow on the vessel base) increases with decreasing impeller clearance but this occurs at the expense of reducing the axial component in the discharge. As the impeller clearance is reduced, the radial flow

on the vessel base, which in this case, is what the solid particles rely on for suspension also reduces. The corresponding increase in circumferential flow is insufficient to pick up the same amount of solids, so the efficiency of the impeller decreases with clearance. This result also ties in with jet mixer design which recommends a maximised path length for improved efficiency.

The fact that both 41° and 45° impellers are less sensitive to clearance can be explained by their mixed flow nature. Solid particles being picked up by these impellers rely on a mixture of different mechanisms and a slight change in relative proportions is unlikely to affect performance.

As the impeller pitch angle is increased, the amount of circumferential flow on the vessel base increases (Fig 4.4.2). For the 60° PBT, solid particles are mainly shifted by circumferential flow, which is generated by the radial component of the impeller discharge (Fig 4.1.6). An increase in impeller clearance will reduce the amount of radial component in the impeller discharge hence the circumferential flow. Again, following the same argument as for the 30° PBT, the efficiency of the impeller in picking up the solids is reduced.

In case of the 90° PBT, the radial component in the impeller discharge is so strong that any increase due to clearance (to T/4) is not high enough to upset the flow pattern. Thus, impeller clearance has virtually no effect on the impeller performance within the test range.

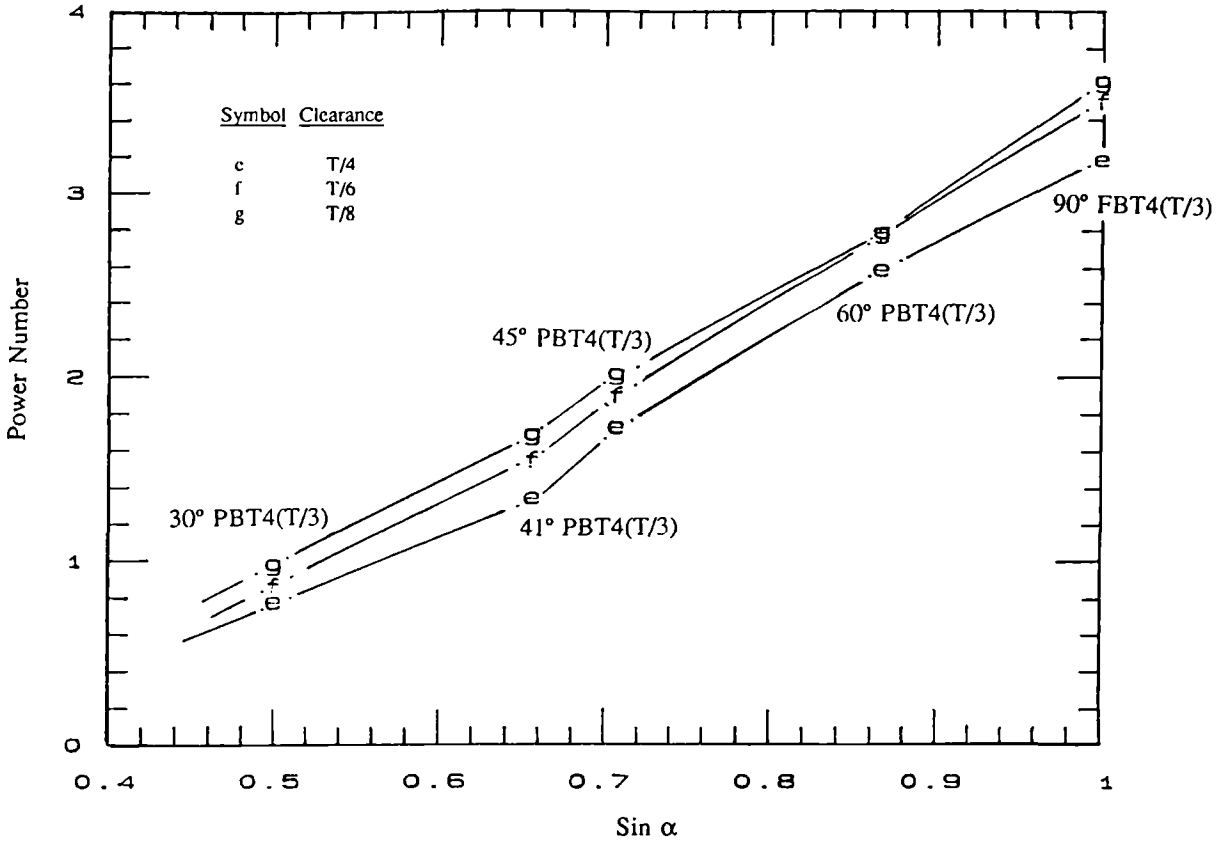

Fig 4.4.1 Power Number against the Sine of Pitched Angles
(Po are measured in turbulent region)

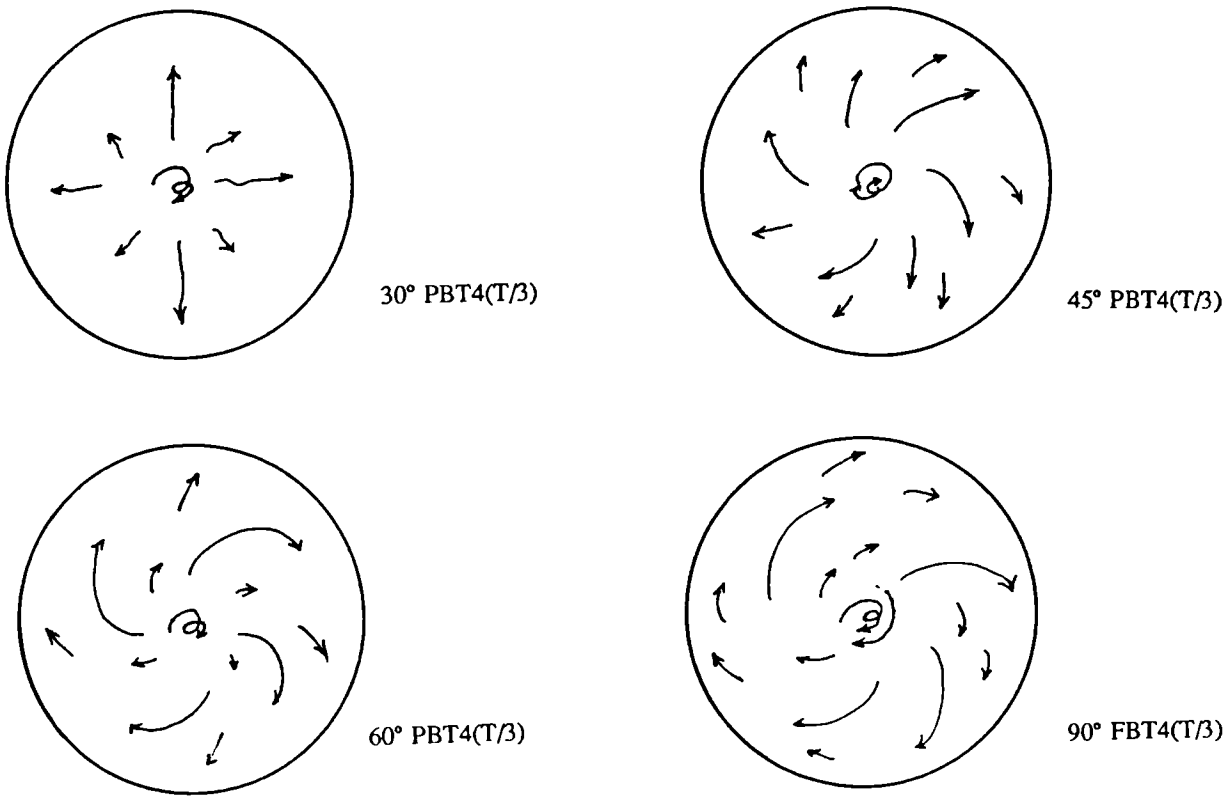

Fig 4.4.2 Particle Flow Pattern Approaching N_{js} - viewing from the base

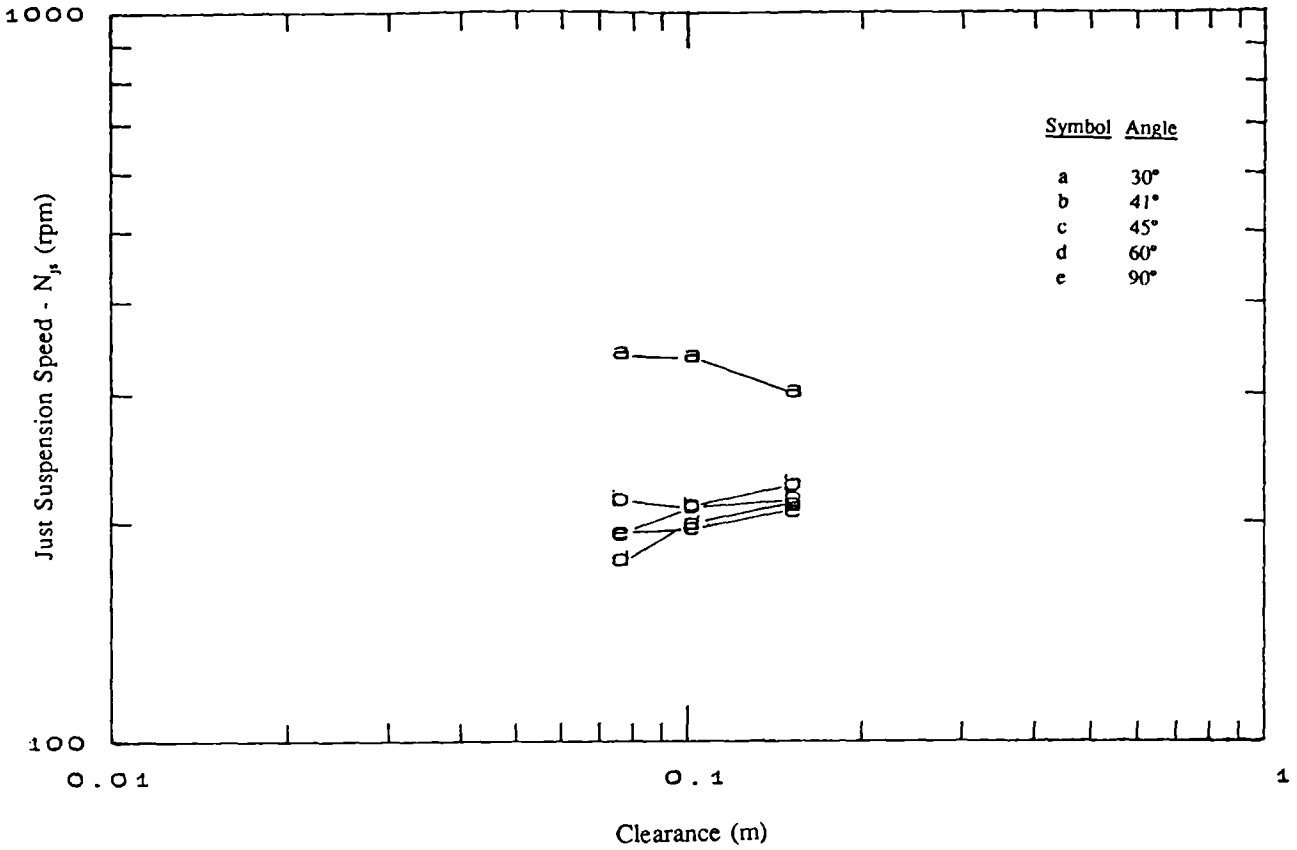

Fig 4.4.3 Just Suspension Speed for the 4 Impellers at 3 Clearances

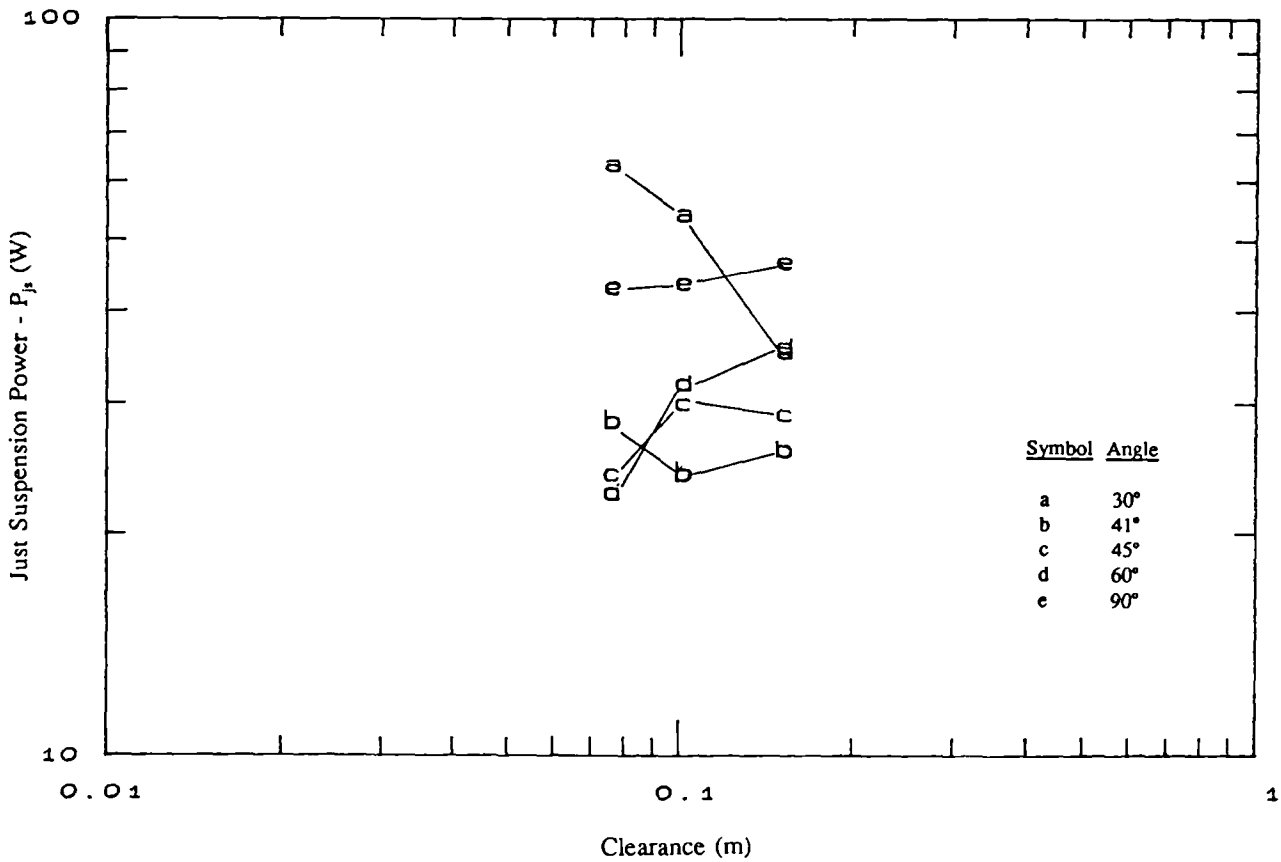

Fig 4.4.4 Just Suspension Power for the 4 Impellers at 3 Clearances

4.4.4 Solids Distribution

This section summarises the solids distribution results obtained from three T/3 PBTs of pitch angles 30°, 45° and 90° to the horizontal. In all cases, the impellers were mounted at T/4 clearance. Details of the impeller dimensions are shown in Table 4.4.1. The test media used was 30% Wt of 150-210 μm sand in water. The data are tabulated in Table A.1, B.1 and B.2 in the Appendices.

The pattern of the RSD curves are very similar to those which have been reported in section 4.3.4. These tests have covered a wide enough range of speeds to pick up various distribution regions within the RSD curve (Fig 4.4.5). At low impeller speeds, most of the solids settle on the vessel base with a clear liquid layer above. At this stage, RSD decreases very slowly with increasing impeller speed (Region A). As the impeller speed increases further, towards the point of maximum homogeneity (Region B), RSD decrease rapidly as the solids are being entrained and distributed by the fluid. Further increase in impeller speed (Region C) showed very little improvement in RSD (i.e. reduction) and subsequently, RSD would increase again due to solids redistribution.

Fig 4.4.6 presents a plot of RSD for the three impellers against speed. Since the three impellers are all T/3 in diameter, it is similar to plot RSD against impeller tip speed. At most impeller speeds, before approaching the point of maximum homogeneity, the 45° PBT gave the lowest RSD. This is because the 45° PBT is capable of generating good overall bulk mixing when compared with the other two impellers.

For the three impellers tested, the 30° PBT gave the lowest RSD_{min}. Despite the fact that the 30° PBT possessed the lowest RSD, it redistributed the solids rapidly once beyond RSD_{min} and its RSD at higher speeds (eg ≥ 500 rpm) were higher than that of the 45° PBT. Great care should be taken if the 30° PBT is to be used to achieve a low standard deviation, due to its sensitivity to the operating conditions.

It is interesting to note that the three RSD versus speed curves have virtually the same $N_{RSD,\,min}$. They all have their points of maximum homogeneity at approximately 385 rpm. It is possible that impellers with same (D/T) ratio, will also have their RSD_{min} at the same impeller speed (or tip speed). The magnitude of the relative standard deviation will depend

on the pumping rate and power input of the system. This is going to be discussed in more detail in the forthcoming sections.

The just suspension speeds for the three impellers are also marked in the same plot (Fig 4.4.6). The 30° PBT is the only impeller where N_{js} and RSD_{min} occur at similar speeds. For the other two impellers, N_{js} is lower than RSD_{min} and thus, distribution is the limiting factor for design.

Fig 4.4.7 compares the RSD of the three PBTs against power input. The 30° PBT achieved the lowest RSD at all power inputs until it reached its minimum value. It also gives the most rapid fall in RSD against power input. On the other hand, the 90° FBT required higher power input than the other two impellers, in order to achieve the same degree of homogeneity.

Barresi et al (1987) deduced from their theoretical analysis on power dissipation that RSD is proportional to $Po^{-1/3}$. Unfortunately their experimental results did not seem to confirm this. This can be shown by overlaying two of their plots (Fig 4.4.8). It is clear that the impeller with a higher power is "over-corrected" by the exponent on Po. Magelli et al (1990) studied the effect of power number on RSD based on experimental data only. They covered a 1.9-fold change in power numbers and their empirical correlation suggested $RSD \propto Po^{-0.09}$.

Results from this study also implied a negative effect of power number on RSD (Fig 4.4.7). In other words, impellers of high power numbers are less efficient for solids distribution. Regression analysis was conducted with RSD, Po and N (Fig 4.4.11):

$$RSD \propto Po^{-0.14} N^{-1.91} \qquad r^2 = 0.71 \qquad \text{...eqn(4.4.6)}$$

The regression analysis gives a poor fit for the RSD curves covering more than one flow regime. It is included here for indication purpose only, its sole purpose is to show that the effect of power number on RSD is not as strong as proposed by Barresi ($RSD \propto Po^{-1/3}$).

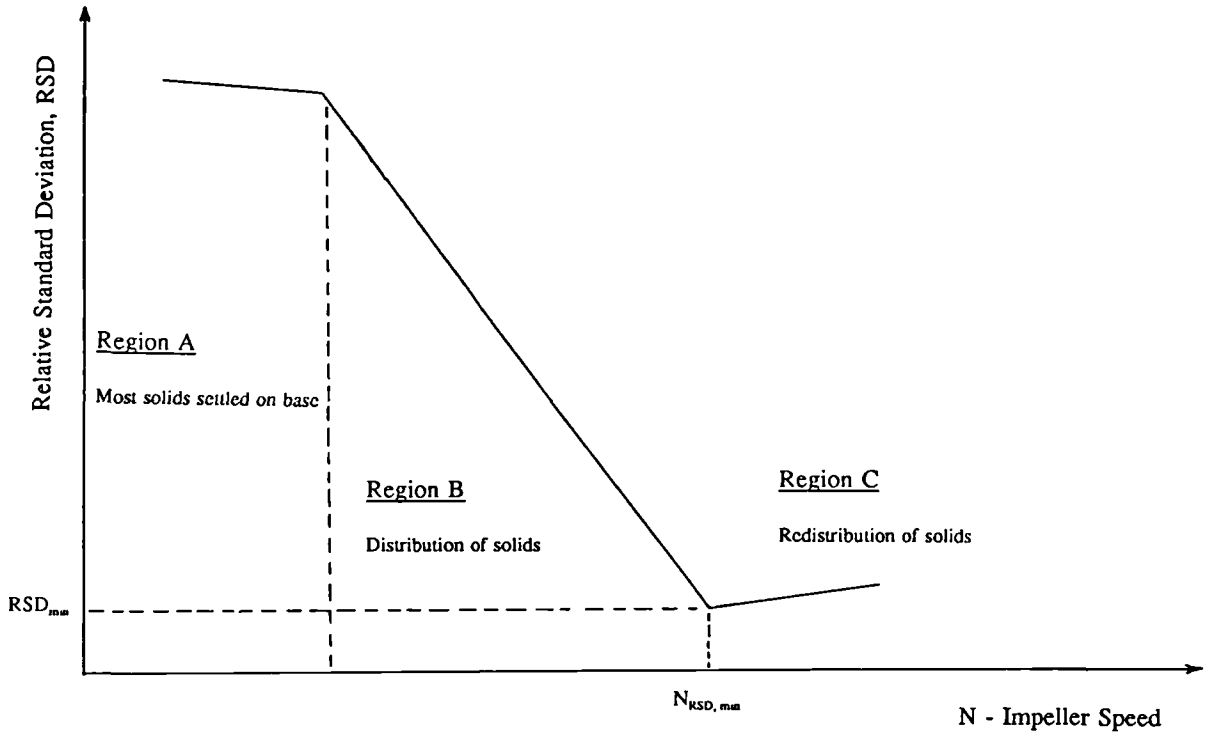

Fig 4.4.5 Generalised Pattern of the RSD Curve

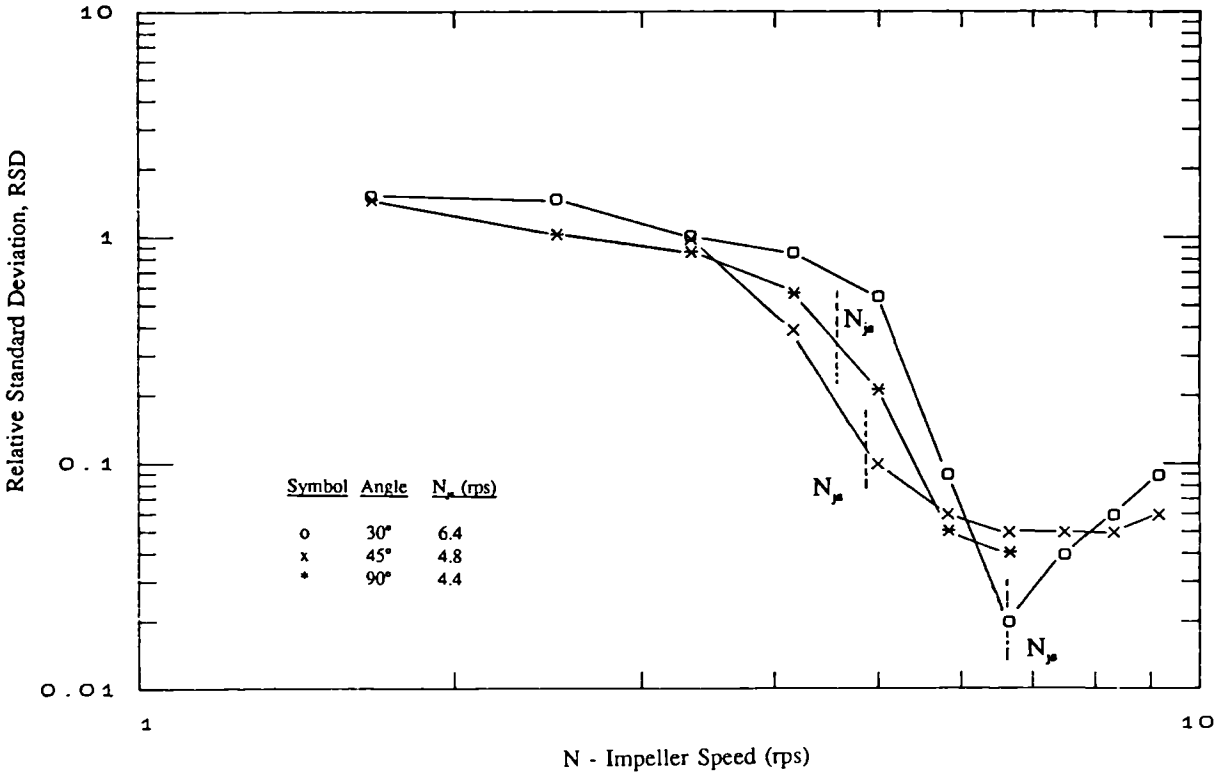

Fig 4.4.6 Effect of Pitch Angle on RSD, Compared against N

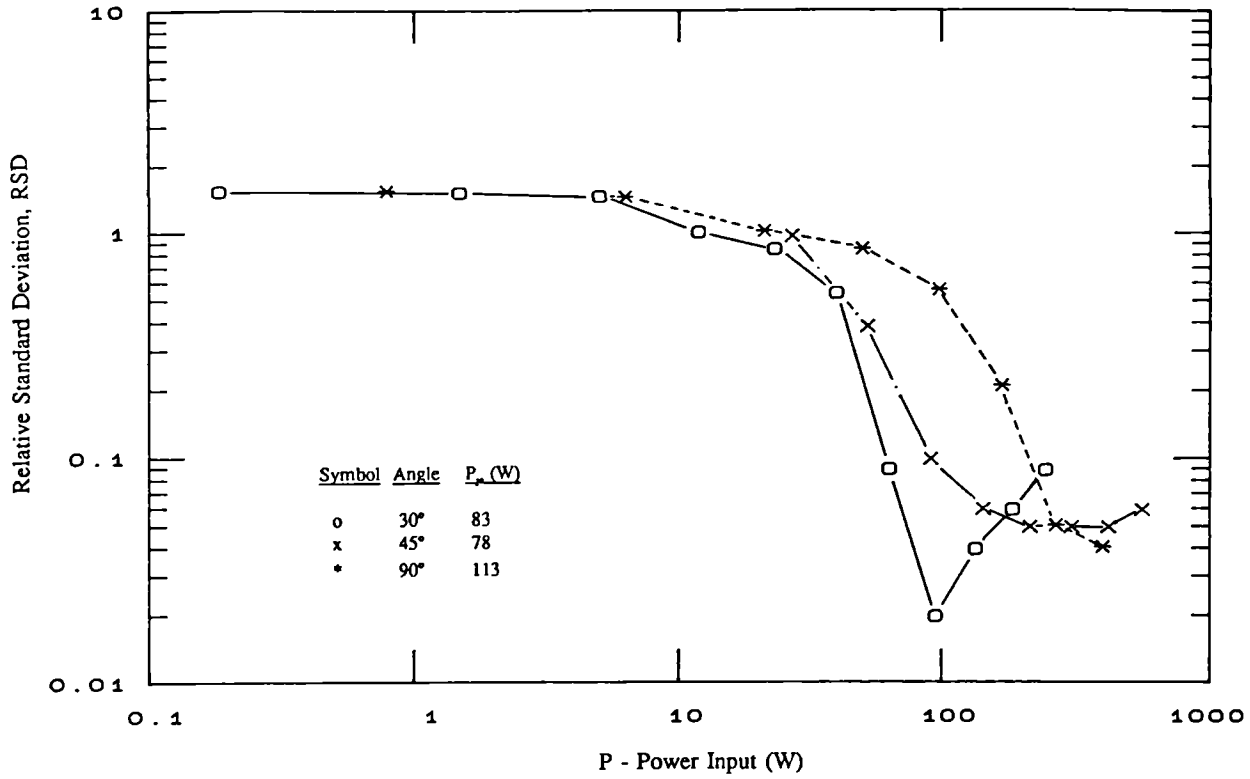

Fig 4.4.7 Effect of Pitch Angle on RSD, Compared against Power Input

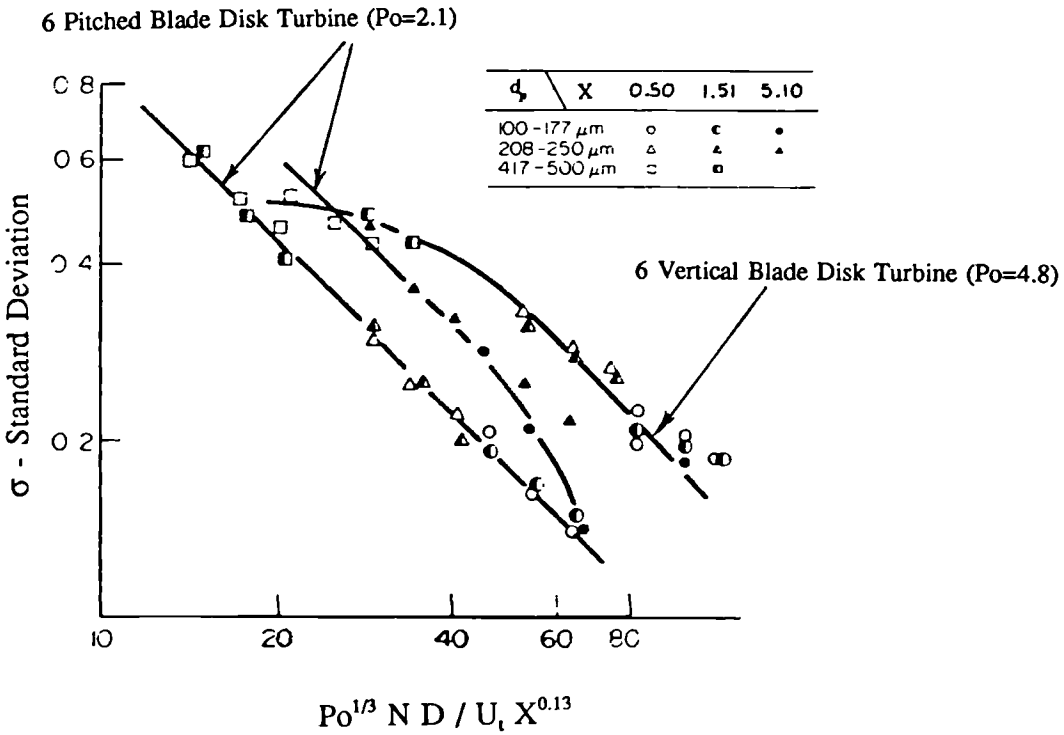

Fig 4.4.8 Influence of Power Number on Solids Distribution (Barresi et al 1987)

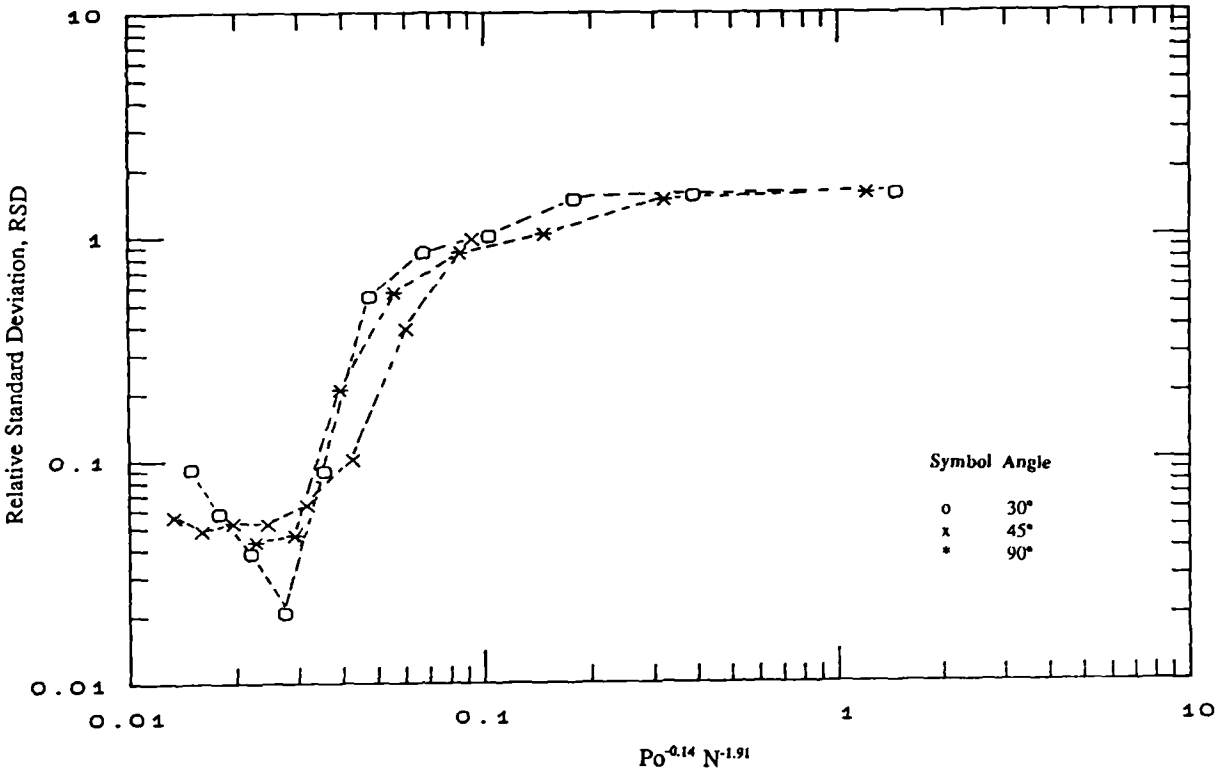

Fig 4.4.9 Plot of RSD against $Po^{-0.14}\ N^{-1.91}$

4.5 DUAL IMPELLER SYSTEMS

Multiple impeller configurations are often adopted in stirred tank designs especially where aspect ratios (i.e. H/T) are greater than one. It is generally believed that an additional impeller will enhance the overall mixing of the vessel, the upper impeller helping to distribute the solids throughout the tank and ease the suspension duty of the bottom impeller. Therefore, the solids suspension and distribution performance should be improved.

However, despite the wide use of multiple impeller systems in industry, design information is limited and research effort in the area has been small. For example, there is no standard impeller spacing for solids suspension design and the improved performance with an additional impeller has yet to be quantified. This section looks into the effects of an extra impeller on solids suspension and distribution with the following objectives:

- To compare the performance between a variety of dual impeller configurations and also with that of single impellers.

- To generalise the suspension and distribution results and to use the results to improve knowledge of the solid-liquid mixing process.

- To make recommendations for future research, based on this initial work.

Two dual impeller systems, dual pitched and flat/pitched were included in this study. They are all downward pumping. The three impellers were all T/3 in diameter and geometrical details can be found in Table 4.4.1. Configurations examined in this test program are summarised in Table 4.5.1.

	Lower impeller	Upper Impeller
System 1	41° PBT4(T/3) No. 002-31-061	41° PBT4(T/3) No. 003-31-061
System 2	90° FBT4(T/3) No. 008-37-061	41° PBT4(T/3) No. 003-31-061

In all experiments, the bottom impeller position was fixed at a low clearance (C=T/8) where it is likely to give good solids suspension performance and will allow mixing to

continue even when the tank is being drained during a process. The position of the upper impeller was varied through a wide range of clearances from close to the bottom impeller to close to the fluid surface, with the slurry depth kept at H=T level. Two single impeller systems, single PBT and FBT at fixed T/8 clearance were studied and were used as a reference to assess the performance of the dual impeller systems. Round grained sand (sieved to a particle size range of 150-210 μm, settling velocity of 0.015 m s^{-1}) and water were used as the test media.

Table 4.5.1 Summary of Test Configurations

Upper Impeller Clearance	Pitched/Pitched Combination			Flat/Pitched Combination		
	N_{js} (5% Wt)	Po (in water)	RSD (30% Wt)	N_{js} (5% Wt)	Po (in Water)	RSD (30% Wt)
0.30T		*	*	*	*	*
0.40T				*	*	
0.45T	*	*				
0.50T	*	*	*	*	*	*
0.55T	*	*				
0.60T	*	*		*	*	
0.65T	*	*				
0.70T	*	*	*	*	*	*
0.75T	*	*				
0.80T	*	*		*	*	

4.5.1 Power Consumption

Two dual impeller systems, dual pitched {41° PBT4(T/3)} and pitched-flat {41° PBT4(T/3) & 90° FBT4(T/3)} were included in this study. The three impellers used all have a nominal diameter of T/3 and the effect of combined power was examined by fixing the lower impeller at T/8 clearance with the upper impeller mounted at different clearances. Their

combined power numbers are tabulated in Table 4.5.2 and 4.5.3 and presented graphically in Fig 4.5.1. The power dissipation of a dual impeller system depends upon two parameters; impeller type and spacing between the two impellers. Fig 4.5.1 shows that the total power drawn by the dual impeller combinations is always smaller than the sum of power of the two impellers at T/8 and T/3 clearance (C=T/3 was highest upper clearance tested).

Bates et al (1963) examined the power characteristics of three dual impeller systems, namely dual flat, pitched-flat and dual pitched. Results were plotted in terms of power ratio, which was the combined power divided by power of a flat bladed turbine, against impeller spacing (Fig 4.5.2). In all cases, the combined power approached some constant values, which were either equal to (pitched-flat) or less than (dual flat and dual pitched) the summation of the two single impeller powers when the spacings were greater than one impeller diameter. However, the dual flat combination developed a total power almost 25% greater than the sum of the two when the spacing was less than one diameter. This could due to the fact that the two flat bladed turbines behaved as one when they were close together and the effect of blade width on power is greater than linear proportionality (i.e. doubling the blade width increases the power number by a factor of more than two).

In the forthcoming sections, solids suspension and distribution performance will be compared in terms of power input. Instead of using the combined power numbers, which is based on the nominal diameter, actual power input will be used. Since $P = Po\ \rho\ N^3\ D^5$, plotting power input against N^3 should give a straight line with slope of k and $k = Po\ \rho\ D^5$ (Fig 4.5.3-4). Therefore, just suspension power of a configuration can be given as $k\ N^3$.

4.5.2 Flow Pattern

The flow pattern of solids on the vessel base was examined by placing a mirror below the vessel. It can differ dramatically from a single impeller system, depending on the impeller clearances. Generally speaking, in the pitched-pitched configuration, radial flow is dominant on the base (Fig 4.1.5-b). Increasing the spacing between the two impeller introduces slow moving regions both at the centre and the circumference (eg Fig 4.5.6 C_t=0.7T). Circumferential flow dominates in the pitched/flat combination. As the upper impeller (pitched) is moved upwards, the central vortexing region increases and a certain amount of radial flow between the central vortexing region and outer circumferential region is observed

(eg Fig 4.5.8 C_t=0.7T). Detailed sketches of the particle flow pattern on the vessel base are presented in Fig 4.5.6 and 4.5.8.

Flow visualisation tests of the whole vessel were conducted using PVC particles as flow followers. In the case of dual pitched bladed turbines, if the two impellers were placed very close together (eg < D apart), they behaved as a single unit but with an improved pumping effect (Fig 4.5.13). If the pitched blade turbines were spaced further apart, circulating zones as well as swirls were observed (Fig 4.5.15). The swirls were rotating anti-clockwise looking inwards and were located somewhere between the two impellers. Their exact position depended largely on impeller type and clearance between them. The swirls are thought to be caused by interactions between the outflow of upper and lower impeller in which the discharge from the upper impeller baulks the circulation pattern of the lower impeller. This is likely to be the reason why an additional impeller does not necessarily reduce the just suspension speed (Sec 4.5.3).

The situation in a system equipped with a flat bladed turbine (lower) and a pitched bladed turbine (upper) is similar except that the circulation zones are less apparent (Fig 4.5.13-15). This is attributed to the lower pumping capacity with a flat bladed turbine as compared to a pitched bladed turbine. Therefore, one can expect that the combined flow pattern of a dual hydrofoil or upwards/downwards pumping pitched blade turbine systems would be very different from that which has so far been examined (Fig 4.5.16-17).

4.5.3 Solids Suspension

The Po, N_{js} and P_{js} data at 5% Wt solids concentration are tabulated in Table 4.5.2 for pitched/pitched combination and in Table 4.5.3 for flat/pitched combination. The just suspension results are also presented graphically in Fig 4.5.5 and 4.5.7. The just suspension speeds at 30% Wt are referred to in the solids distribution section. They are calculated from the 5% Wt and used Zwietering's correlation to correct for solids concentration: $N_{js} \propto X^{0.13}$.

Pitched/pitched Configuration

Referring to Fig 4.5.5, for most of the top impeller clearances tested, N_{js} results are unexpectly higher than that of a single PBT at T/8 clearance (i.e. bottom impeller only).

There is a reduction in N_{js} only when the impeller spacing between the upper and lower impellers exceeds 1.7 times the impeller diameter. The lowest dual impeller N_{js} is recorded when the upper impeller is mounted at the highest clearance tested (0.8T) where there is 3.5% reduction in N_{js}. Since the power drawn by a dual impeller system is approximately equal to the summation of power consumed by the upper and lower impellers (section 4.5.1), it can be seen that an increase in efficiency through using dual impellers is possible only when the reduction in N_{js} is greater than 21%.

Since $P = Po\ \rho\ N^3\ D^5$

i.e. $P_{js} \propto Po\ N_{js,\ single}^{\ 3}$

Power number for pitched/pitched combination is roughly twice that of the single pitched. In order to make the power input between the systems comparable, N_{js} in the dual impeller system has to be reduced:

$$P_{js} \propto 2\ Po\ N_{js,\ dual}^{\ 3}$$

$$\left(\frac{N_{js,\ dual}}{N_{js,\ single}}\right) \propto \left(\frac{1}{2}\right)^{1/3} = 0.79$$

Fig 4.5.9 presents a plot of just suspension power of dual pitched configuration at different upper impeller clearances. The corresponding power for a single PBT at T/8 clearance (25 W) is marked on the same plot for comparison. At all impeller clearances tested, P_{js} for dual pitched configuration is higher than that of a single PBT, even when the upper impeller is mounted near the fluid surface at which dual N_{js} is less than that of single N_{js}. In other words, the reduction in N_{js} with dual pitched configuration cannot outweigh the increase in power consumption.

Since $P = 2\ \pi\ \tau\ N$, i.e. $P \propto \tau\ N$ ...eqn(4.5.1)

As the increase in just suspension power is higher than the reduction in just suspension speed, that means the impeller torque required to produce just suspension is greater in the dual pitched configuration.

Table 4.5.2 N_{js}, "s", Po and P_{js} Results for Pitched/Pitched Configurations at 5% Wt

Upper Impeller Clearance	Parameters			
	N_{js} (rpm)	"s"	Po_c	P_{js}
0.45T	245	5.4	2.33	57
0.50T	243	5.4	2.30	54
0.55T	243, 246	5.4	2.31	57
0.60T	228	5.0	2.52	50
0.65T	215, 217	4.7	2.84	48
0.70T	206	4.5	2.74	40
0.75T	200, 203	4.4	2.85	39
0.80T	200	4.4	2.95	39

Single PBT at T/8 clearance:

N_{js}: 207 rpm

Po: 1.69

"s": 4.5

P_{js}: 25 W

Single PBT at T/3 clearance:

Po: 1.22

The increase in N_{js} and P_{js} with the dual pitched/pitched configurations is believed to be caused by flow interactions between the upper and the lower PBTs. Flow visualisation (Fig 4.5.13-15) confirmed that somewhere between the two impellers where the outflow from the lower impeller meets the discharge of the upper, eddies were clearly visible. The formation of eddies would absorb some of the energy that was originally available for solids suspension. Moreover, as these two flow streams are opposing each other, the fluid circulations of both impellers are being 'throttled' and hence the impeller effectiveness is reduced.

Only when the impeller spacing becomes sufficient to eliminate interference between the flow loops is there a reduction in N_{js}, compared to a single PBT. It occurs when the upper impeller is sufficiently apart from the lower, to supplement the bottom impeller flow loop

instead of distorting it (Fig 4.5.15).

The plot of Po_c versus impeller clearance for the pitched/pitched configuration (Fig 4.5.1) consists of two nearly flat portions (below top impeller clearances of 0.55T and above top impeller clearance of 0.65T) with a transition in between. The positions of the flat regions and the transition correspond almost exactly to the flat regions and transitions in the N_{js} plot (Fig 4.5.5). It is likely that as the upper impeller clearance is increased there is a change of flow pattern and this change affects both power number and N_{js}.

Flat/Pitched Configuration

Referring to Fig 4.5.7, the behaviour of the flat/pitched configuration is very different from that of the pitched/pitched configuration. Over the entire range of clearances tested (0.3 to 0.8T), the just suspension speed for the flat/pitched configuration is less than that of a single flat blade turbine at T/8 clearance. It starts at a relatively low value when the two impellers are close together (i.e. 0.5D apart), rises to a maximum when they are approximately one impeller diameter apart and then falls again as the spacing increases still further.

A possible explanation of the flat/pitched N_{js} results is that the two impellers behave as one when they are in close proximity to each other. Their combined axial and radial flows complement each other which facilitates the suspension of solids (Fig 4.5.8 C=0.3T to C=0.5T and Fig 4.5.13). As the upper impeller clearance is increased, a recirculating loop forms between the top and bottom impeller (Fig 4.5.14) which would undoubtedly absorb some of the energy available for suspension. Any reduction in N_{js} would obviously depend upon how much of the bottom impeller's suction is being throttled and how much "help" the top impeller can contribute to the suspension. As the upper impeller is raised, the recirculating loop moves further away from the lower impeller and hence its influence is reduced. Coincidentally, the suction of the upper impeller seems to entrain fluid from near the circumference of the vessel (Fig 4.5.15-b) and this augments the discharge flow of the lower impeller hence reducing the just suspension speed again.

Table 4.5.3 N_{js}, "s", Po and P_{js} Results for Pitched/Flat Configurations at 5% Wt

Upper Impeller Clearance	Parameters			
	N_{js} (rpm)	"s"	Po_c	P_{js}
0.30T	163	3.6	4.38	31
0.40T	176	3.8	4.49	40
0.50T	180	3.9	4.52	43
0.60T	173	3.7	4.73	40
0.70T	172	3.7	4.78	40
0.80T	164	3.6	4.77	35

Single FBT at T/8 clearance:

N_{js}: 186 rpm

Po_c: 3.62

"s": 4.1

P_{js}: 38 W

The just suspension power for this dual impeller configuration is about the same as the single FBT (38 W, Fig 4.5.10). A very slight reduction (10 to 15%) in P_{js} is achieved only when the two impellers are either very close to or highly separated from each other. However, since the FBT is a rather inefficient impeller to be used for solids suspension, remembering that P_{js} of FBT is approximately 50% higher than for the PBT. If we start with an inefficient single impeller it is easier to make improvements by adding a second impeller, even though the dual impeller system may still be inherently inefficient.

General

Summarising all the just suspension speed and power results, the best solids suspension performance is achieved using a single PBT at T/8 clearance. The performance of the two dual impeller systems are very similar when the upper impeller is mounted at a large clearance. If for any reason the top impeller must be mounted at a low clearance, then the flat/pitched configuration is recommended.

The results clearly suggest that just suspension speed is not simply a function of power input or impeller type but a careful matching of the impeller flow and the last suspension region. If a second impeller is to be used, it should be mounted in such a way that the flow loop of the bottom impeller can be enhanced. Fig 4.5.16(a) and 4.5.17(a) proposes two possible methods by which the above may be achieved.

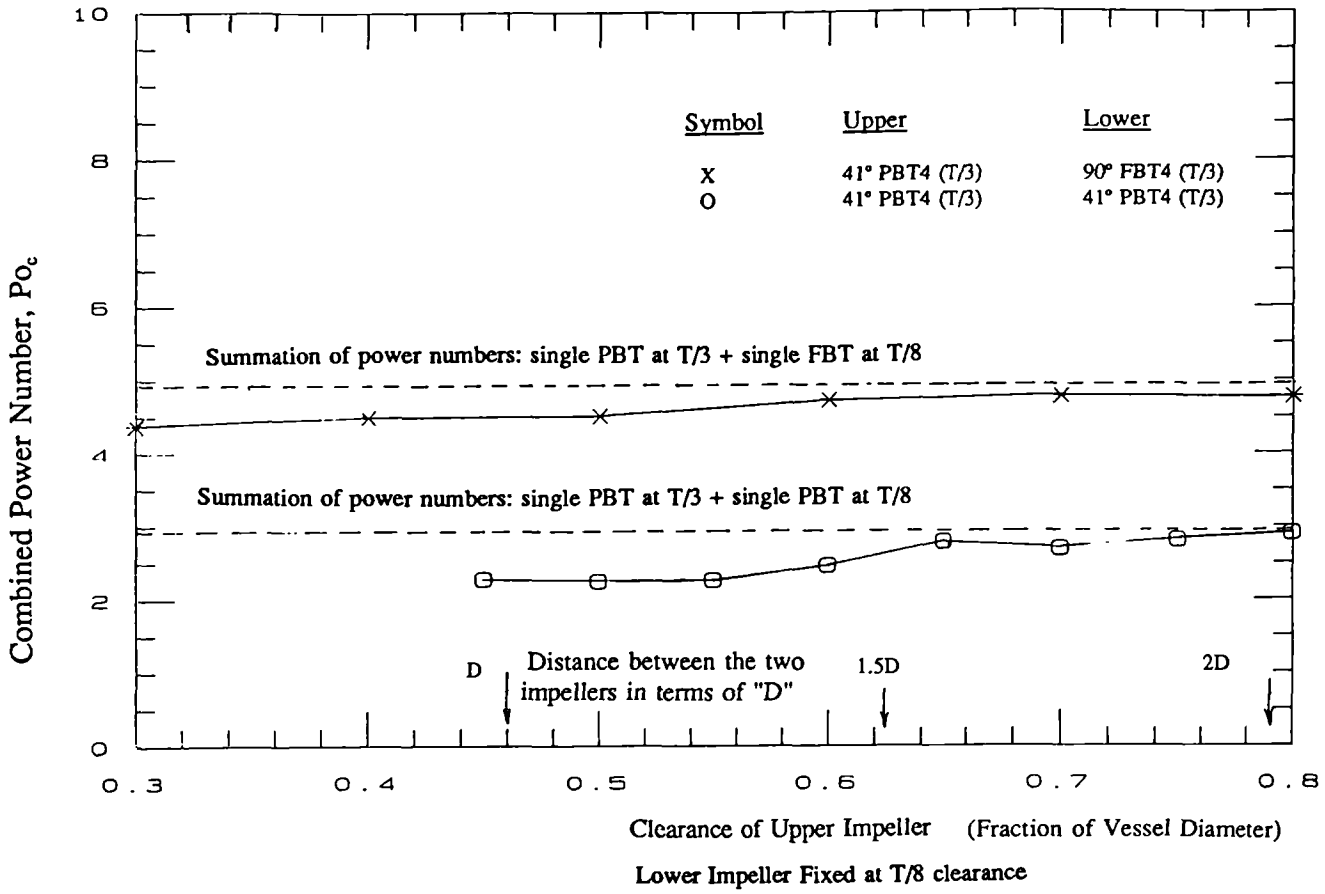

Fig 4.5.1 Power Numbers for Dual Impeller Systems

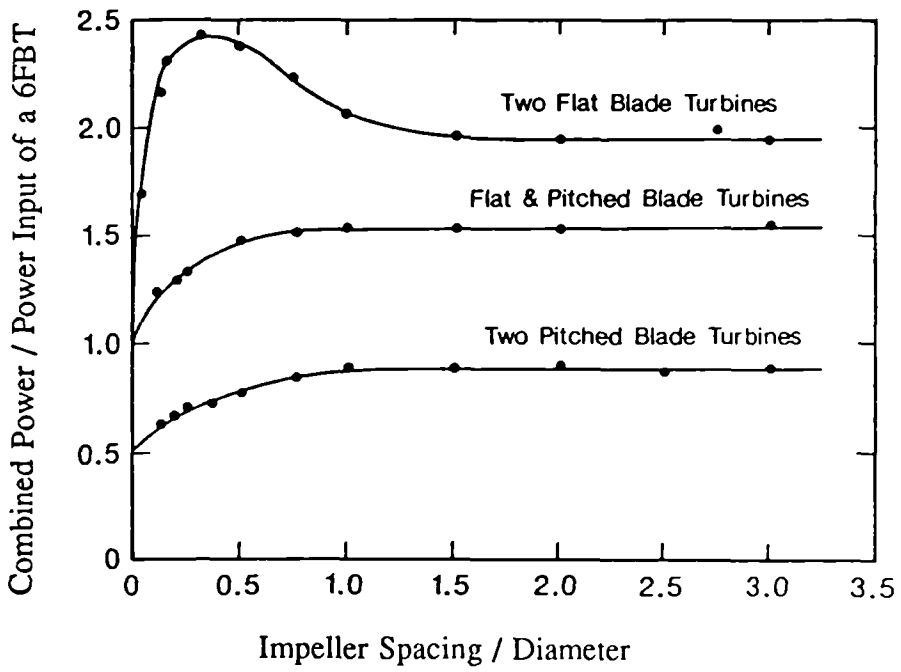

Fig 4.5.2 Power Characteristics of Three Dual Impeller Systems (Bates 1963)

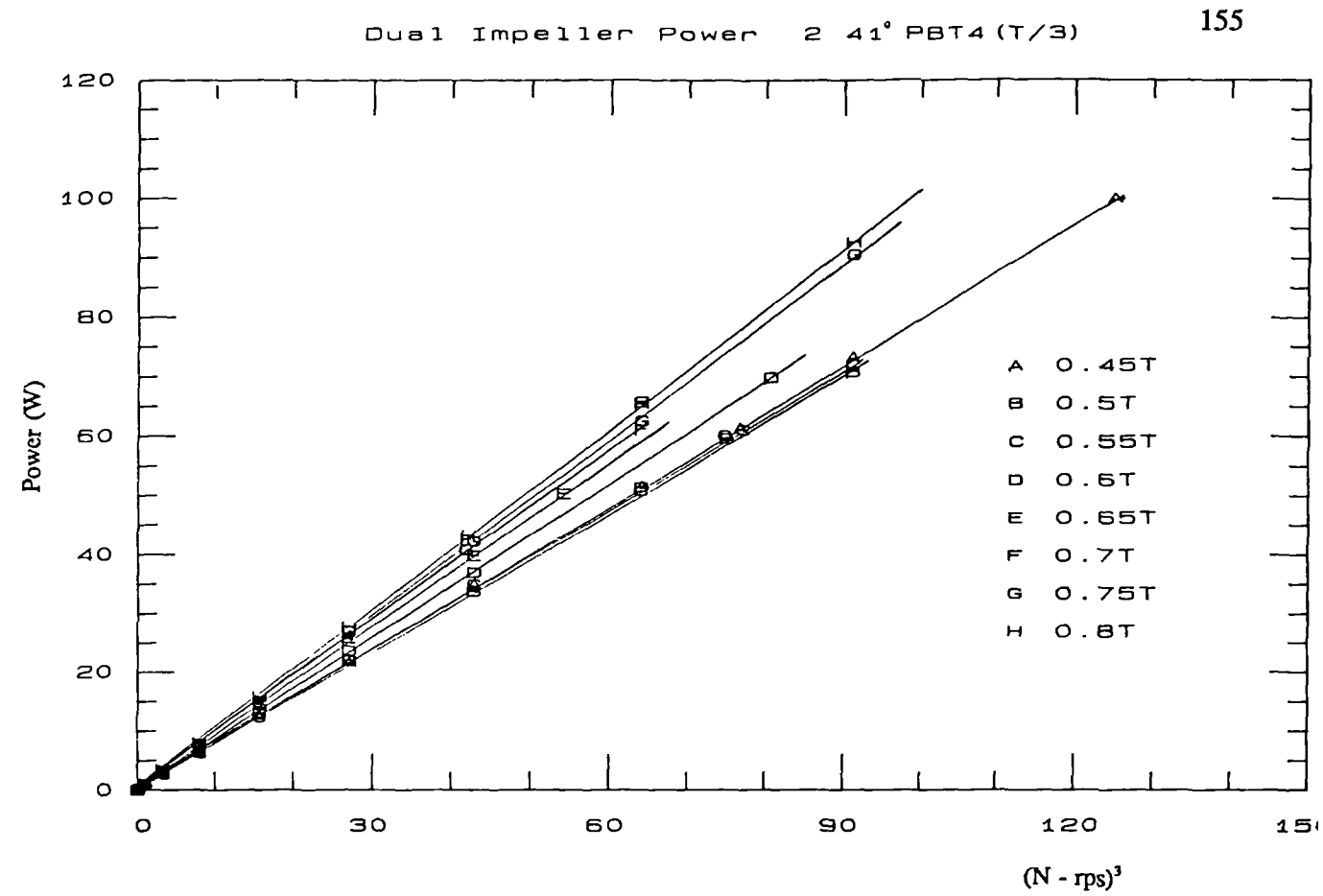

Fig 4.5.3 Power Input against N^3 for Pitched/Pitched Combinations

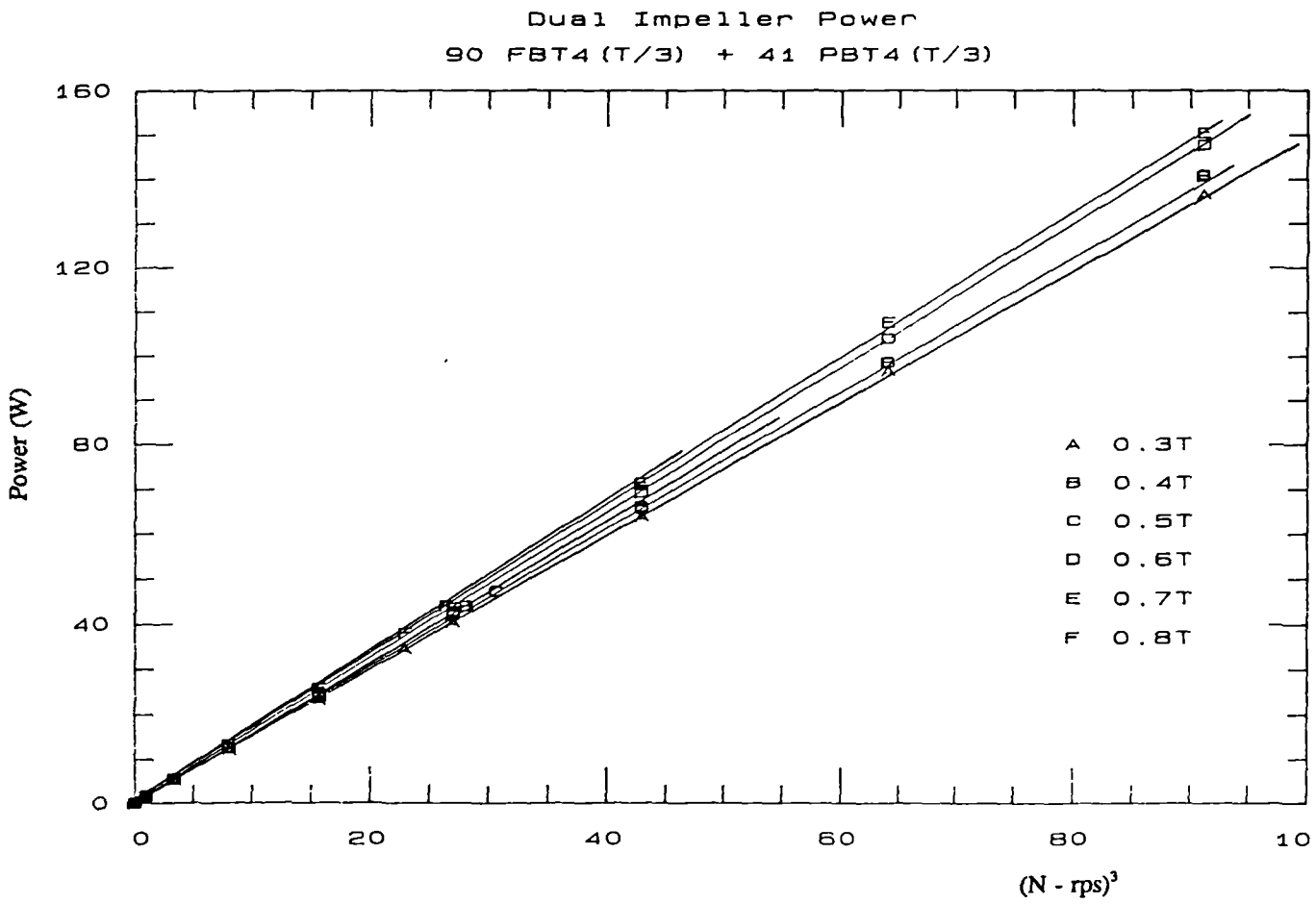

Fig 4.5.4 Power Input against N^3 for Pitched/Flat Combination

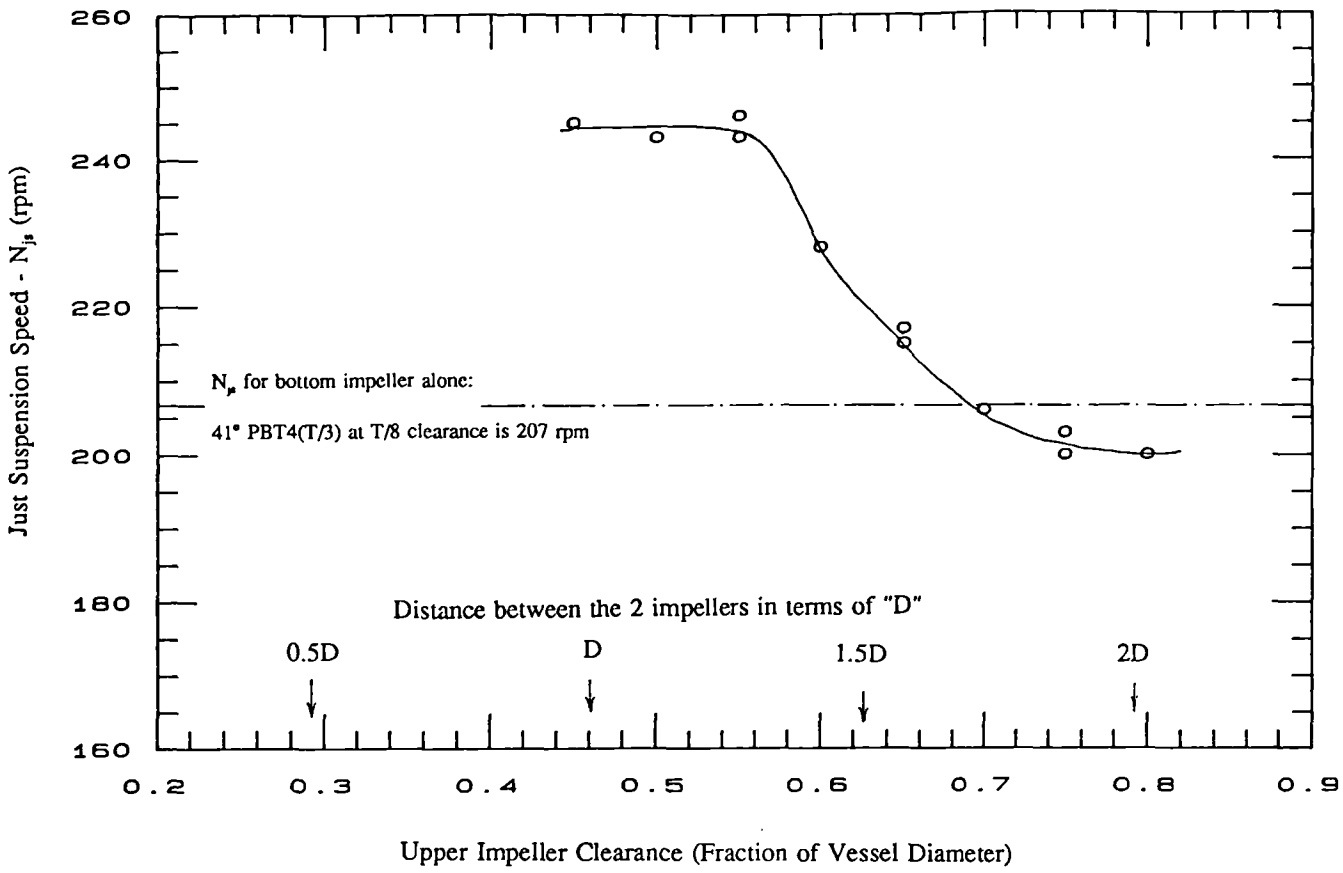

Fig 4.5.5 Just Suspension Speed for Pitched/Pitched Combination

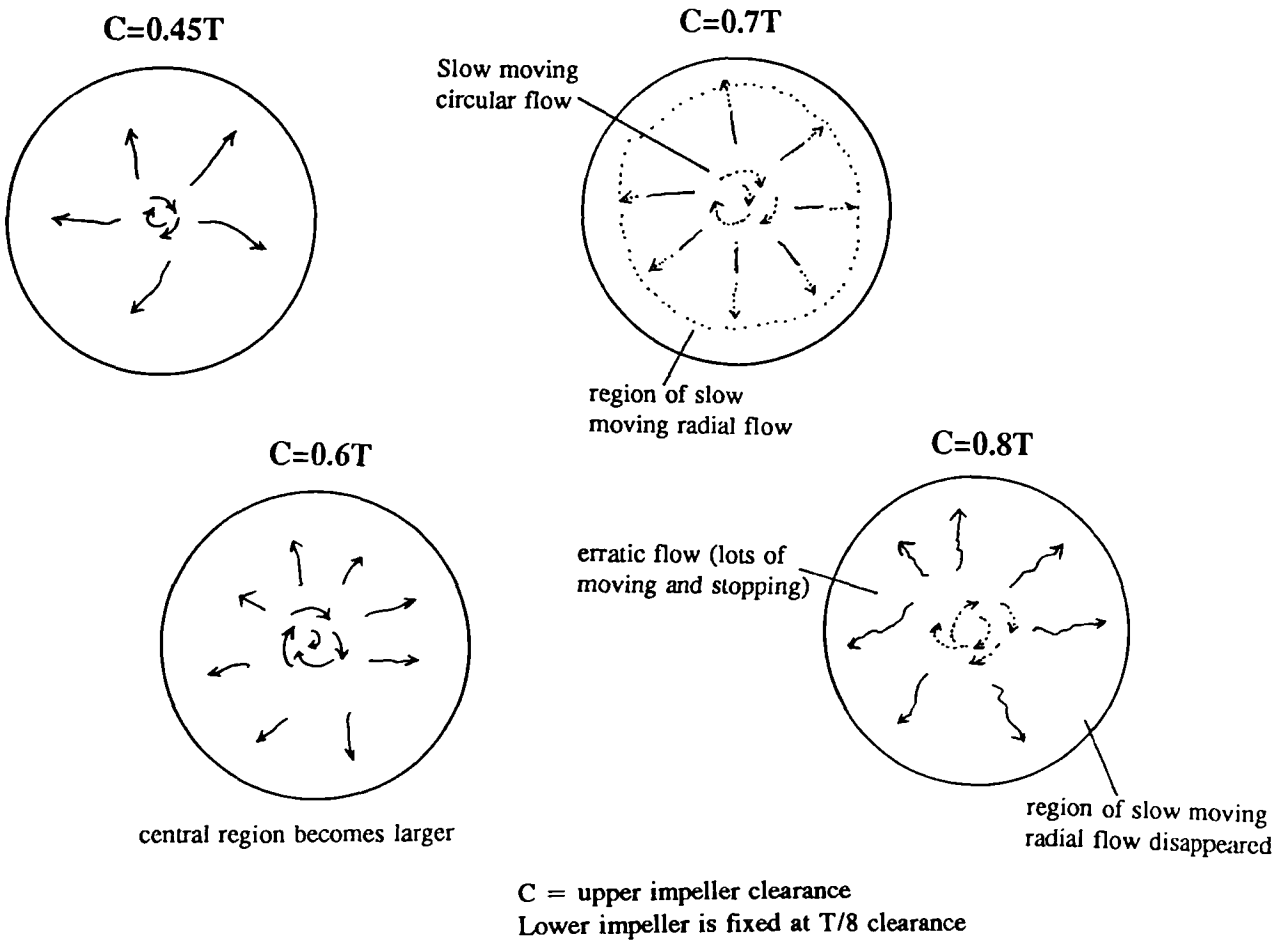

Fig 4.5.6 Particle Flow Pattern near N_{js} for Pitched/Pitched Combination

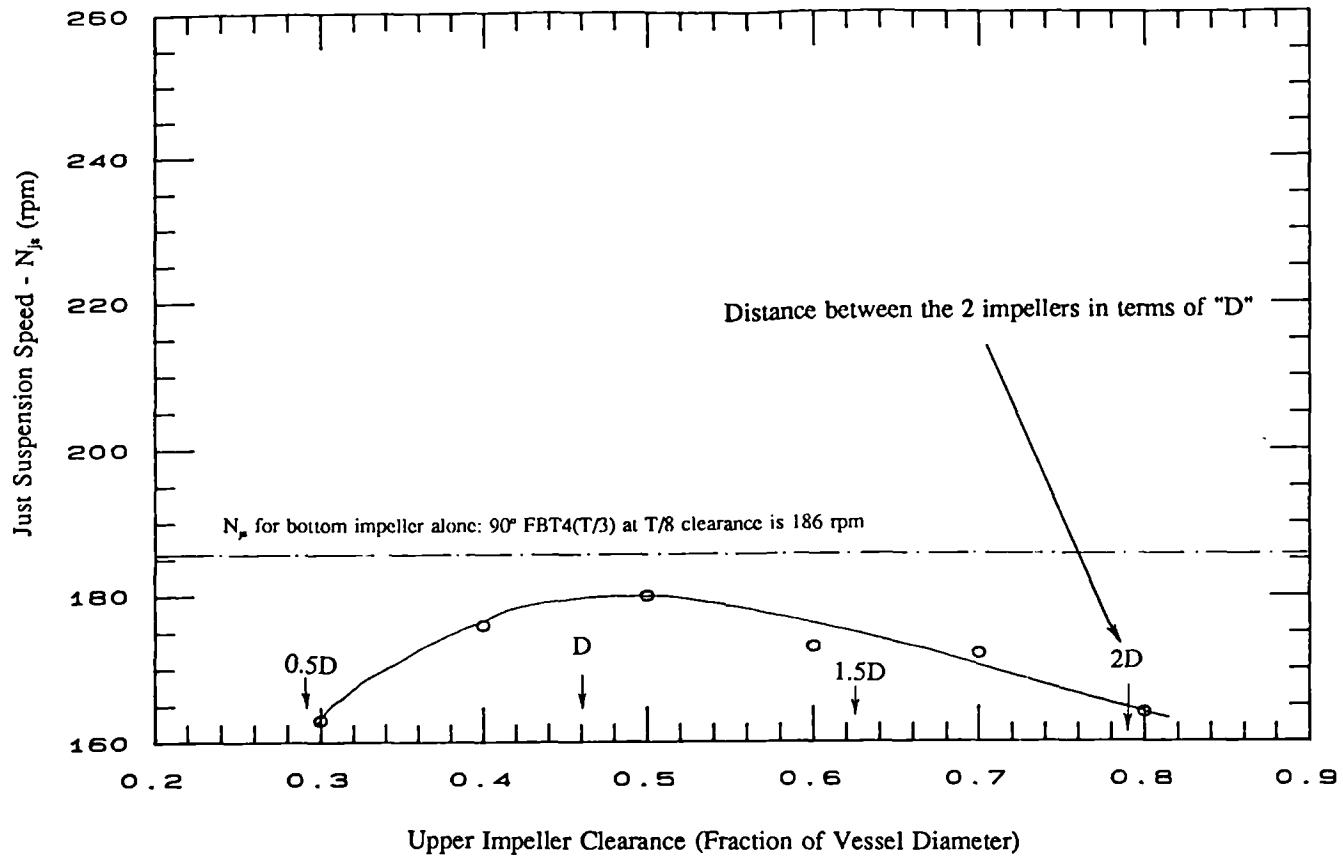

Fig 4.5.7 Just Suspension Speed for Flat/Pitched Combination

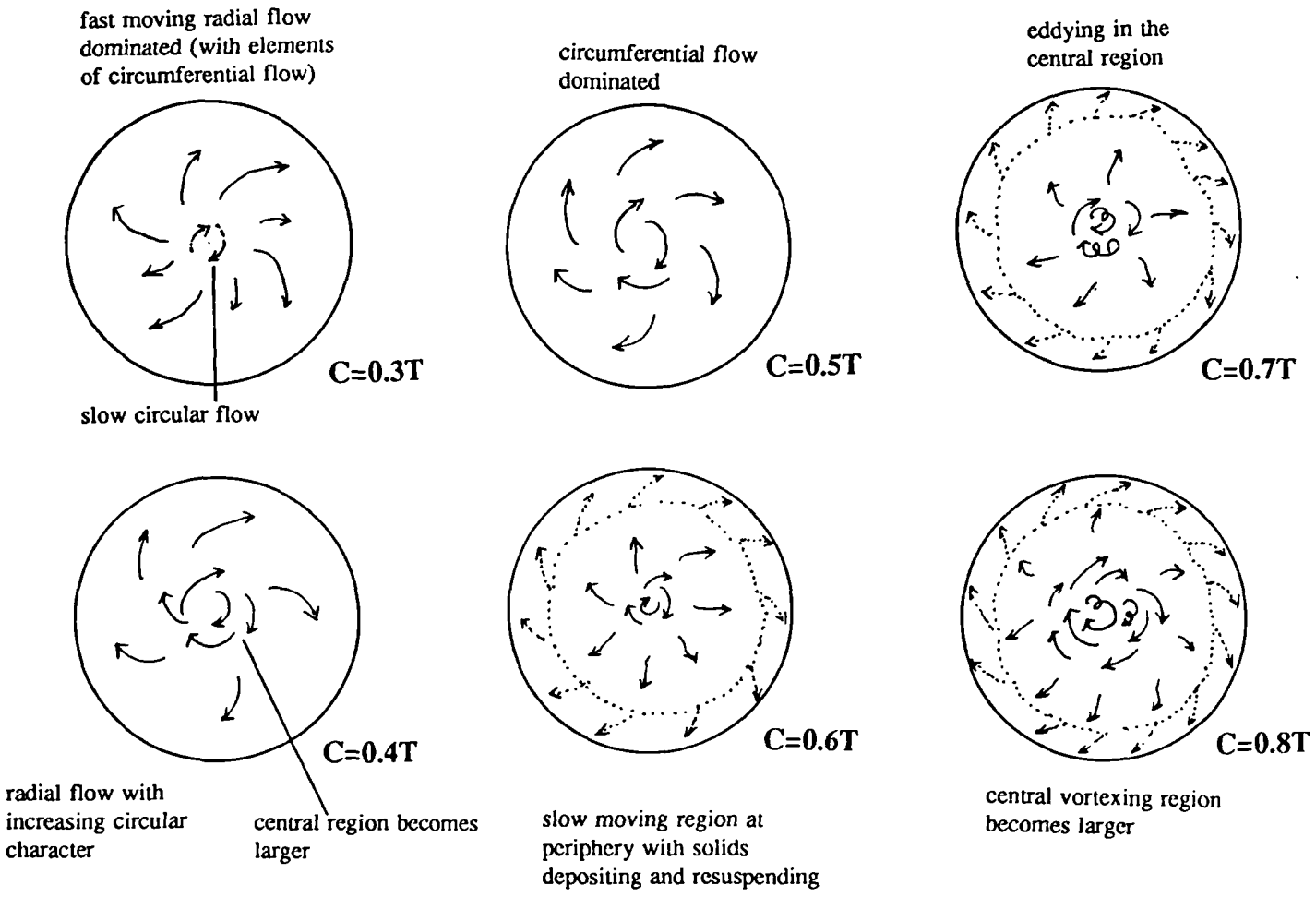

Fig 4.5.8 Particle Flow Pattern near N_{js} for Flat/Pitched Combination

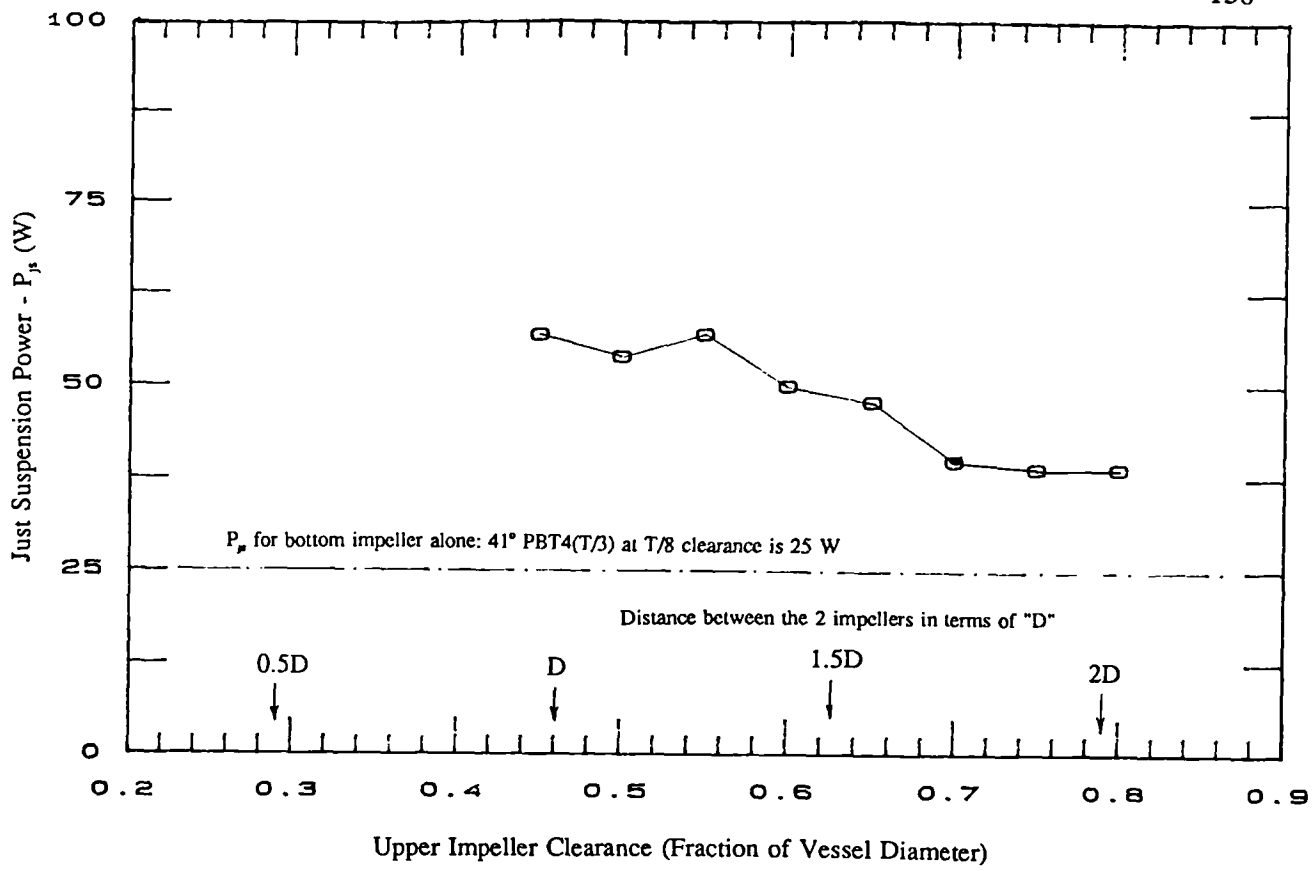

Fig 4.5.9 Just Suspension Power for Pitched/Pitched Combination

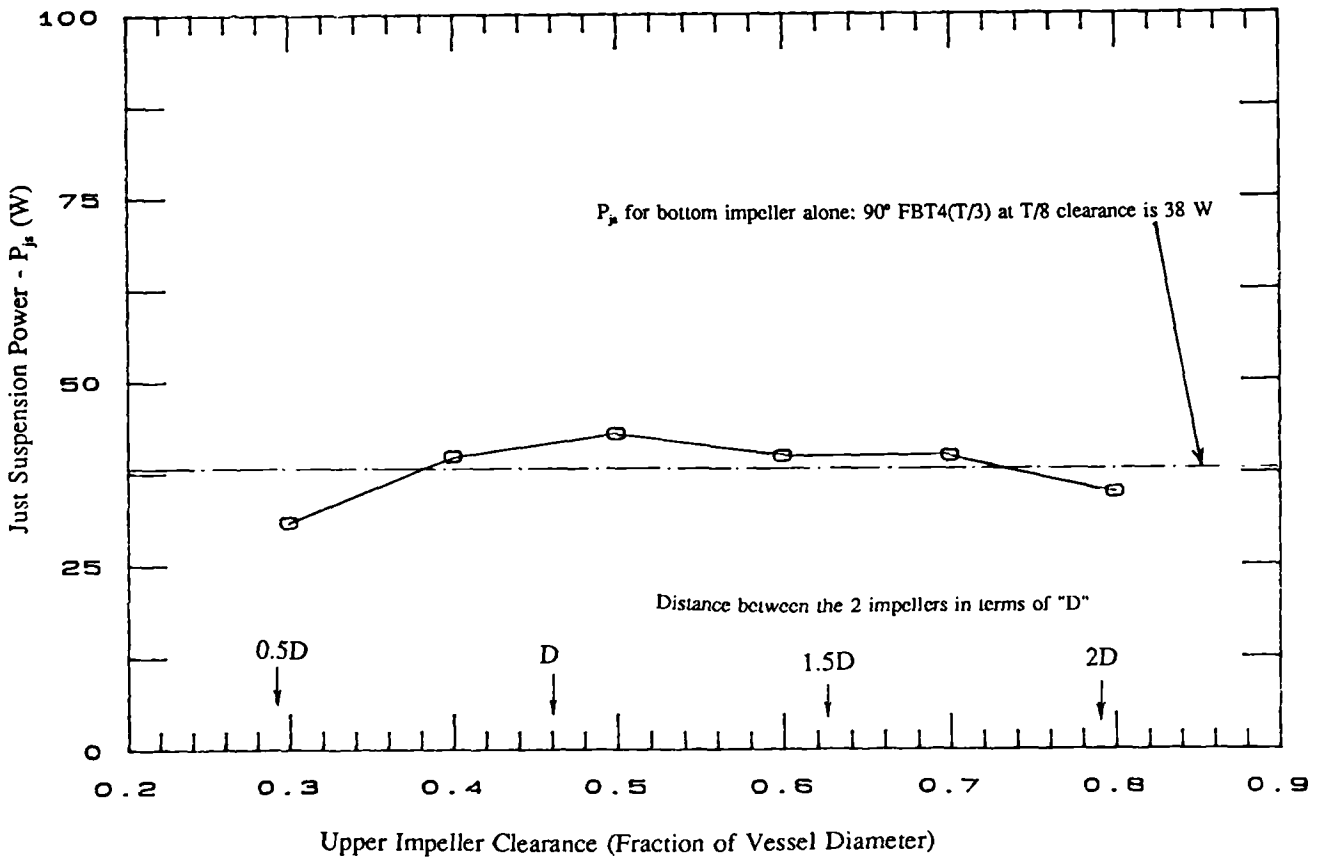

Fig 4.5.10 Just Suspension Power for Flat/Pitched Combination

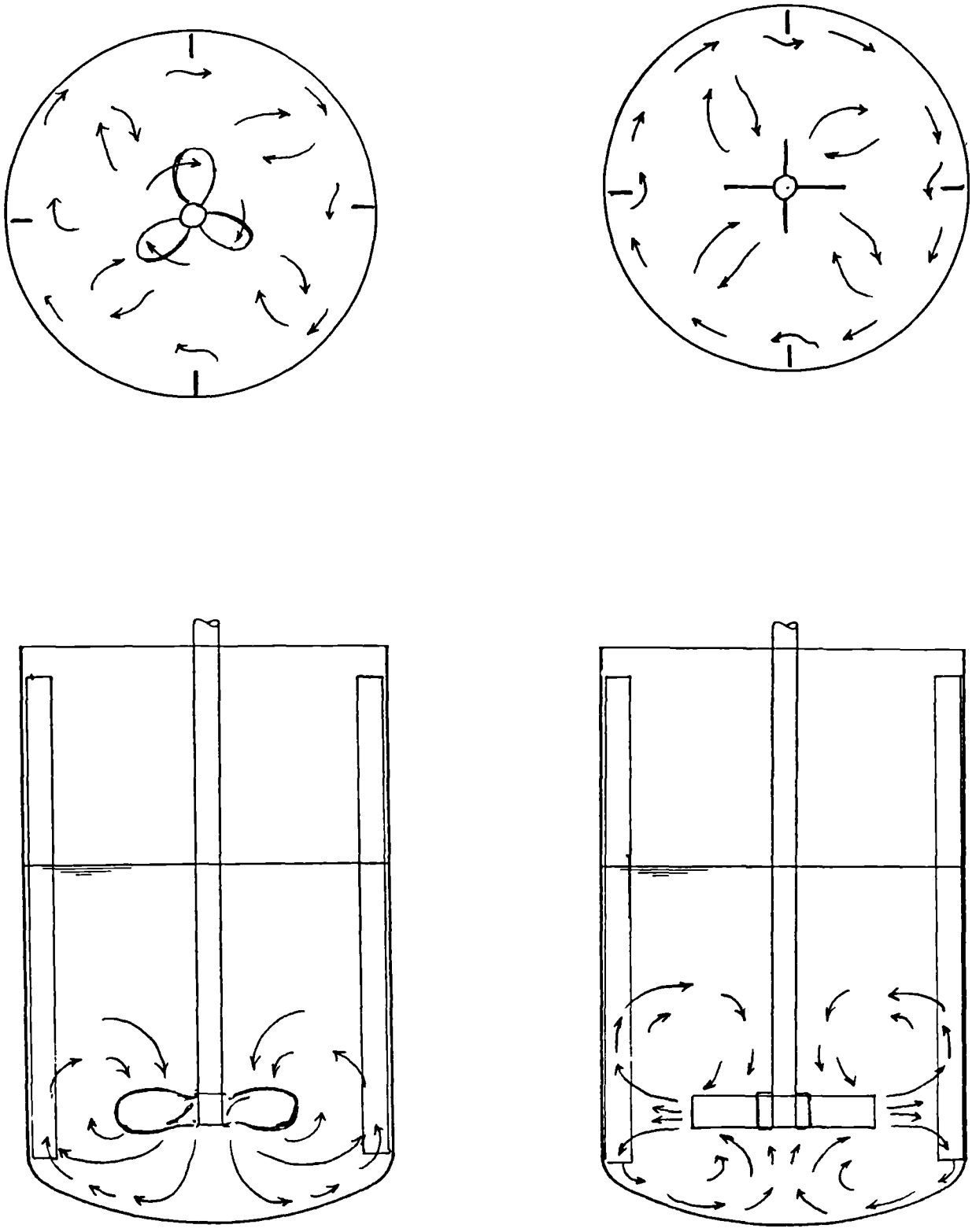

a) Axial/Mixed Flow Impeller

b) Radial Flow Impeller

Fig 4.5.11 General Flow Pattern

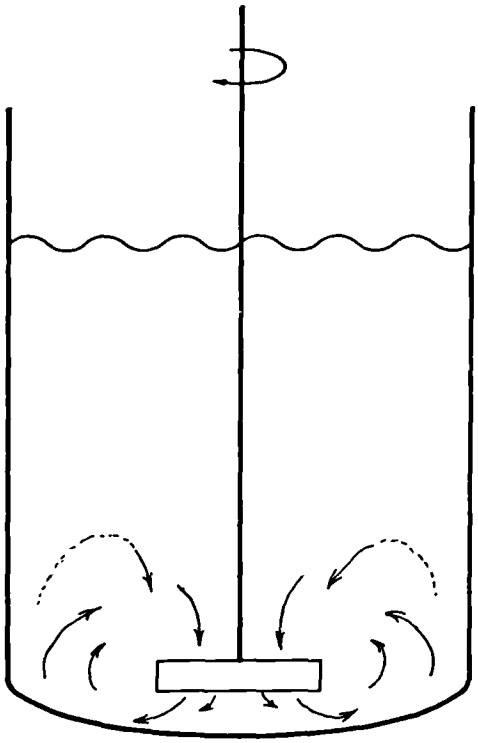

a) 41° PBT4(T/3)

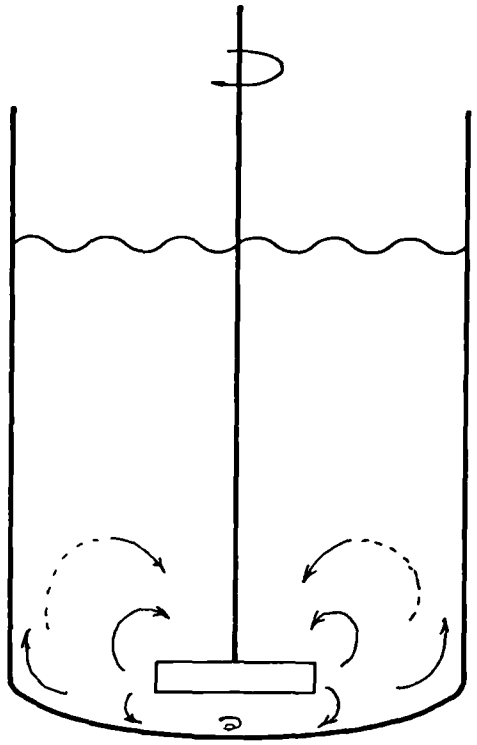

b) 90° FBT4(T/3)

Fig 4.5.12 Single Impeller, C=0.125T

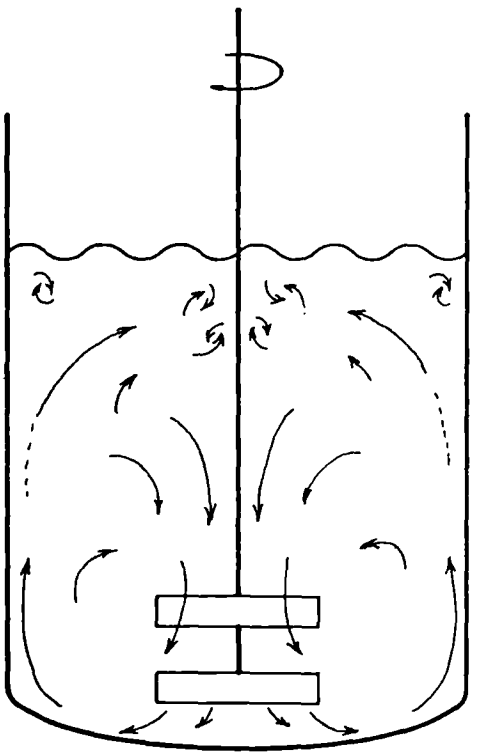

a) 2 × 41° PBT4(T/3)

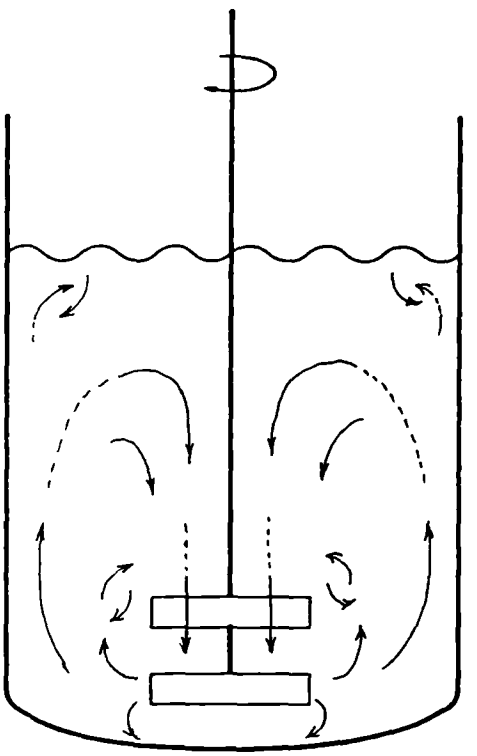

b) Upper: 41° PBT4(T/3)
Lower: 90° FBT4(T/3)

Fig 4.5.13 Upper: C=0.3T, Lower: C=0.125T Baffles not shown

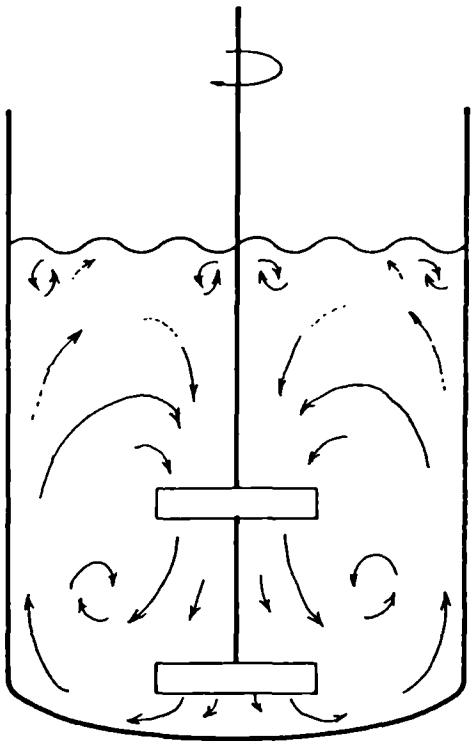

a) 2 × 41° PBT4(T/3)

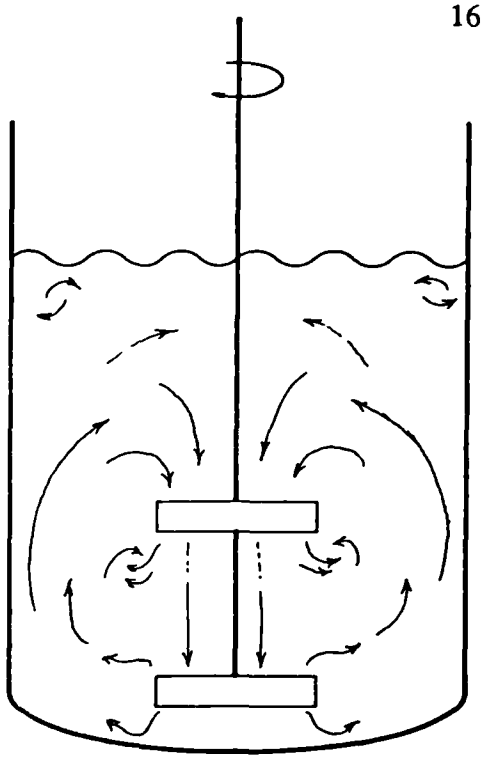

b) Upper: 41° PBT4(T/3)
Lower: 90° FBT4(T/3)

Fig 4.5.14 Upper: C=0.5T, Lower: C=0.125T

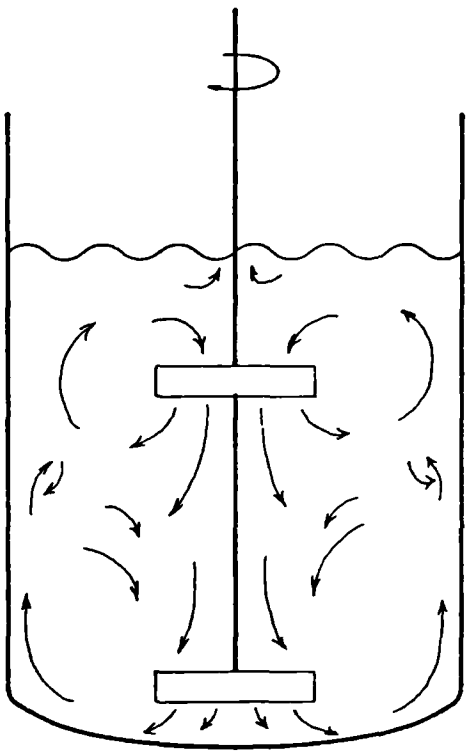

a) 2 × 41° PBT4(T/3)

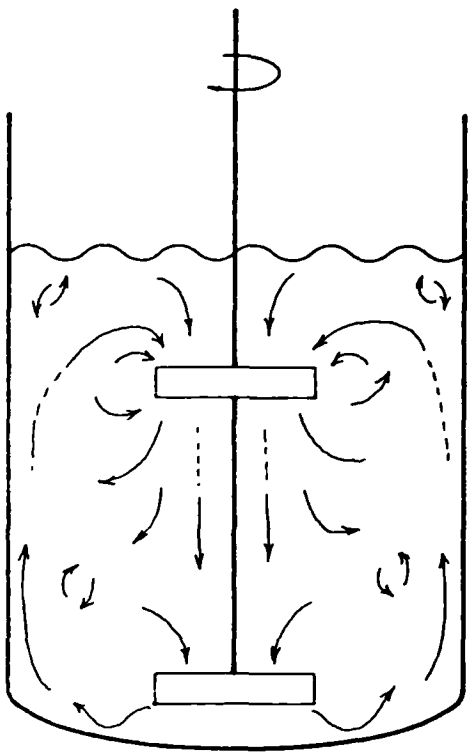

b) Upper: 41° PBT4(T/3)
Lower: 90° FBT4(T/3)

Fig 4.5.15 Upper: C=0.7T, Lower: C=0.125T Baffles not shown

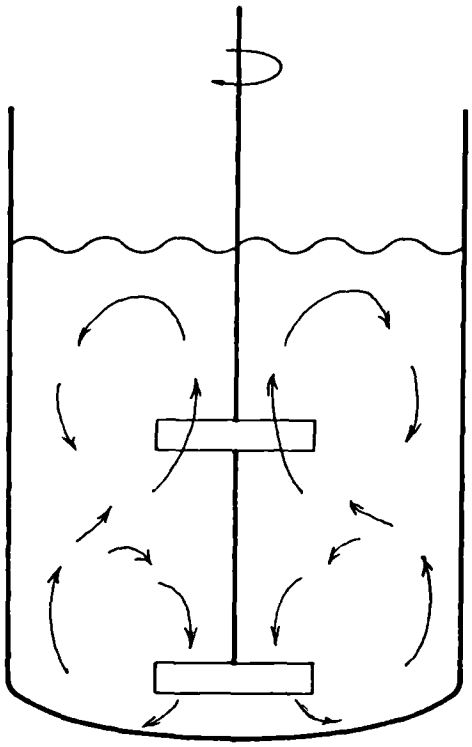

a) Upper: Upwards Pumping PBT
Lower: Downwards Pumping PBT

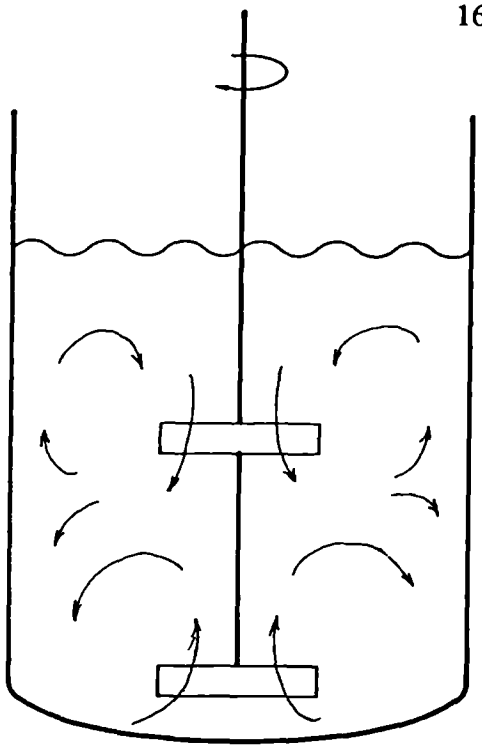

b) Upper: Downwards Pumping PBT
Lower: Upwards Pumping PBT

Fig 4.5.16 Predicted Flow Pattern

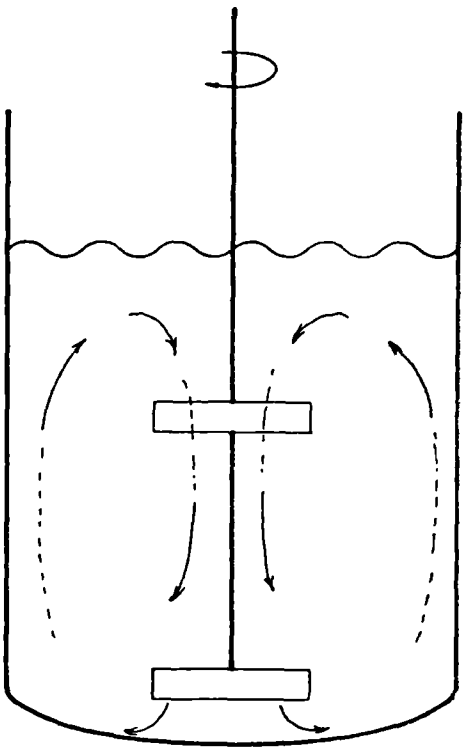

a) Two Hydrofoils

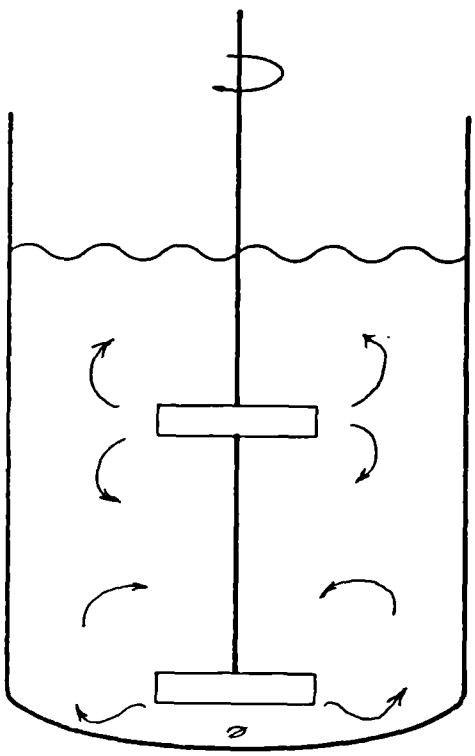

b) Two Disc Turbines

Fig 4.5.17 Predicted Flow Pattern Baffles not shown

4.5.4 Solids Distribution

Solids distribution for the two dual impeller systems was measured with the bottom impeller mounted at T/8 clearance and the top impeller at 0.3, 0.5 and 0.7T from the vessel base (Table 4.5.1). Results are tabulated in Appendix C. Graphs of RSD plotted against impeller speed are shown in Fig 4.5.18 and 4.5.19, and against power consumption in Fig 4.5.20 and 4.5.21. Graphs for the corresponding single impellers at T/8 clearance are also included in these figures for comparison.

Pitched/Pitched Configuration

The results follow a similar trend to that described in Sec 4.4.4 (Fig 4.4.5). However the transition point from distribution region A to B starts at a lower impeller speed with dual impeller systems than that of a single PBT. Thus, at most speeds compared (Region A and B), dual PBTs gave a much lower RSD than a single PBT set-up. This is due to the improvement in bulk mixing by the extra PBT. Of the three dual PBT combinations tested, the higher the top impeller clearance, the lower the RSD in the distribution region obtained.

None of the agitators could achieve perfect homogeneity (i.e. an RSD of zero), however a lower RSD_{min} could be achieved with the two dual pitched combinations (0.5T and 0.7T) than with the single impeller. RSD_{min} for C_t=0.3T configuration was higher than that of a single impeller. This is because at C_t=0.3T, the two impellers were sufficiently close together to behave as a single unit. For all top impeller positions, N_{js} for the dual impeller combination was equal to or higher than $N_{RSD,\,min}$. If good homogeneity is essential then for this combination operation above N_{js} is the limiting factor, rather than solids distribution (eg 0.5T curve).

Comparison of distribution efficiency was made by plotting RSD against power input for the various impeller combinations. In general, dual impeller combinations give better solids distribution than a single PBT at equal power input (Fig 4.5.20). Take a RSD requirement of 0.05 for example, the twin impeller configurations at C_t=0.3, 0.5 and 0.7T will require a power input of 86, 49 and 77 W respectively whereas 157 W is required for a single PBT (extrapolated from Fig 4.5.20). There is a 69% saving in power if a 0.5T pitched/pitched combination is used instead of a single pitched. The dual configurations also need much less

power (70 to 100 W) to reach the limiting RSD (i.e. RSD_{min}) than that required by the single PBT (200 W) although it should be remembered that their absolute values of RSD_{min} are not necessarily lower than that of the single PBT.

If it is not essential to achieve the best possible solids distribution, then it may be sufficient to operate at the point where the RSD begins to flatten out. Dual impeller configurations are the obvious choice for they require much less power to reach the RSD_{min} than the single PBT. However, in a situation where only just suspension speed is important, the single PBT is the best choice because its just suspension power is the lowest of all the configurations tested (Sec 4.5.3).

Flat/Pitched combination

The behaviour of the flat/pitched combination (Fig 4.5.19) was very similar to the pitched/pitched combination - the two systems have very similar RSD versus impeller curves. The main difference is that the flat/pitched configuration had a lower N_{js} but higher $N_{RSD,\,min}$ under the same conditions. Thus, for a flat/pitched combination, the limiting design factor for solid-liquid mixing would be distribution rather than suspension.

It is not surprising that dual impeller systems produce a better solids distribution than a single impeller when compared at similar rotational speeds. The dual impeller configurations produce a more uniform distribution of turbulence and velocity throughout the tank than the single impeller and they also pump a greater volume of fluid, hence increasing fluid velocities and turbulence levels in regions of the tank which are remote from a single impeller.

Fig 4.5.21 compares the distribution performance of a single flat bladed turbine against various flat/pitched combinations based on power input. An RSD curve for a single pitched is also included for comparison. In all the power ranges compared before solids start to redistribute, dual configurations performed better than the single flat bladed unit. However, the performance of the flat/pitched configurations were still worse than the single PBT. The only exception is with C_t=0.7T at low power input in which the dual configuration shows a more rapid fall in RSD than a single PBT. This feature is unlikely to be of any practical use.

The origin of the poor performance of the flat/pitched combination appears to lie in the inadequacy of the single FBT. Addition of a second impeller (upper PBT) improves the distribution, but not enough to match the single PBT (Fig 4.5.21). This is most likely due to the poor top to bottom flow generated by the FBT.

General

The RSD versus impeller speed curves of the two single impellers (PBT and FBT) and the two dual impeller configurations at C_t=0.3T are almost identical (Fig 4.5.22), even though the power inputs are very different in each individual configuration. This striking similarity was initially thought to be a coincidence. However, graphs of RSD against impeller speed for the FBT at T/4 and T/8 again shown a similar trend (Fig 4.5.23). What is even more surprising is that the speeds for maximum homogeneity for the three single impeller configurations are about 380 rpm, which is almost identical to the corresponding speeds for the 30° and 45° PBTs (Sec 4.4.4). It is possible that at constant impeller diameter and vessel size, RSD is a function of impeller rotational speed or tip speed.

Fig 4.5.24 and 4.5.25 presents the concentration profiles of all the impeller combinations at their RSD_{min}. In all cases, the typical inverted S-shaped profiles are displayed. Concentration profiles from dual impeller combinations were found to follow the same pattern as that of a single impeller. This implies the bottom impeller is always the one which controls the overall flow pattern.

If good distribution is to be achieved, a pitched/pitched combination with the upper impeller clearance equal to 0.7T should be adopted. N_{js} results showed that for dual impeller configurations, suspension efficiency improves with impeller separation. Therefore, it is logical to assume that a dual pitched configuration with high top clearance would give the best overall solid-liquid mixing performance. However, it must be remembered that such a configuration is likely to entrain air at higher rotational speeds.

If a modest solids distribution can be accepted, then a single PBT will give adequate performance and there is little to be gained by fitting a second impeller. The single PBT should be operated at a point between N_{js} and where the RSD versus power curve begins to flatten out (Fig 4.5.20). Although the pitched/pitched combination can achieve the same RSD

at lower power consumption, for some combinations it would have to operate below its N_{js} (eg C_t=0.7T), leaving a persistent region of unsuspended solids on the vessel base. To remove these unsuspended solids requires a larger power input which subsequently may cause solids redistribution.

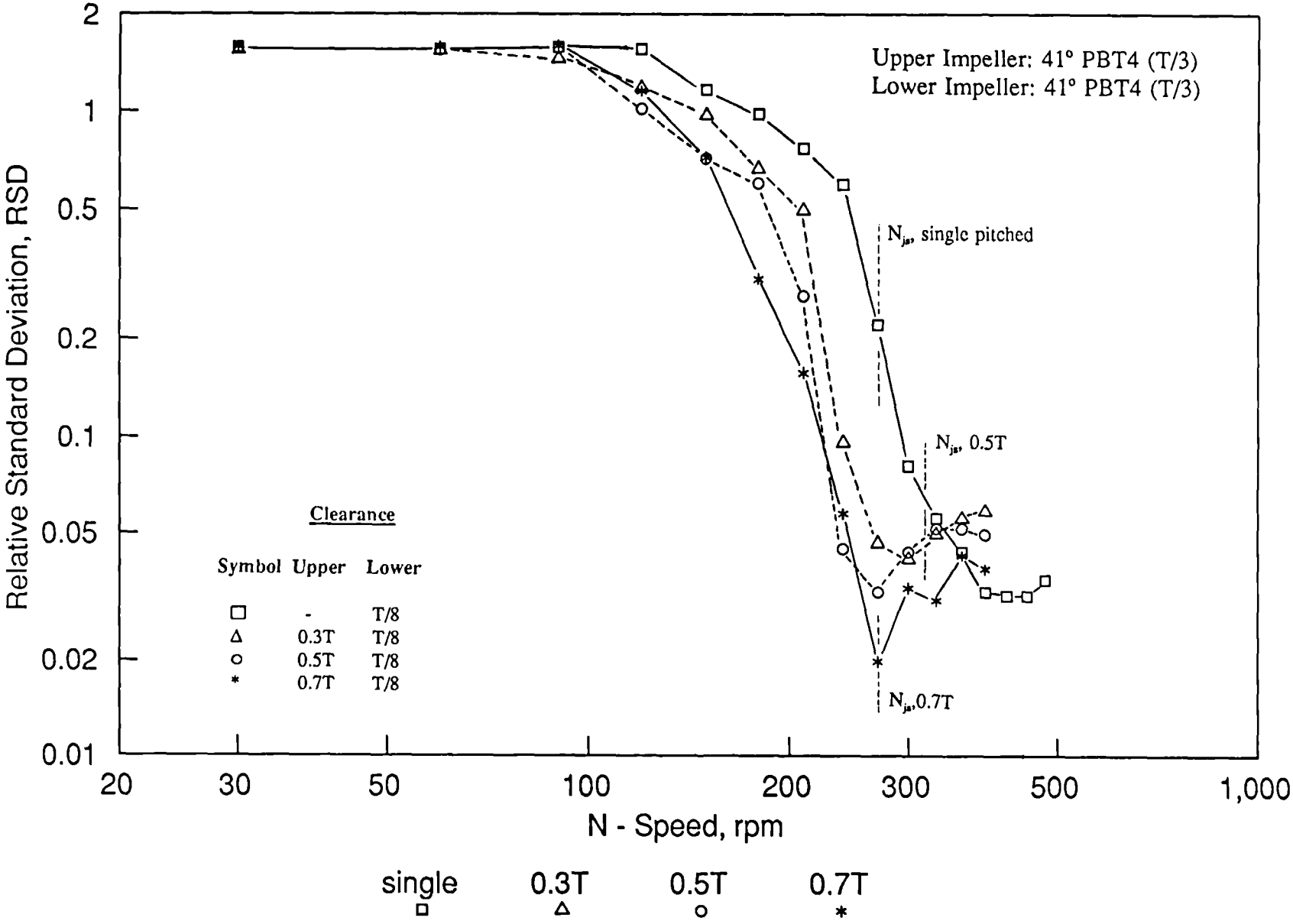

Fig 4.5.18 RSD against Impeller Speed for Pitched/Pitched Combination

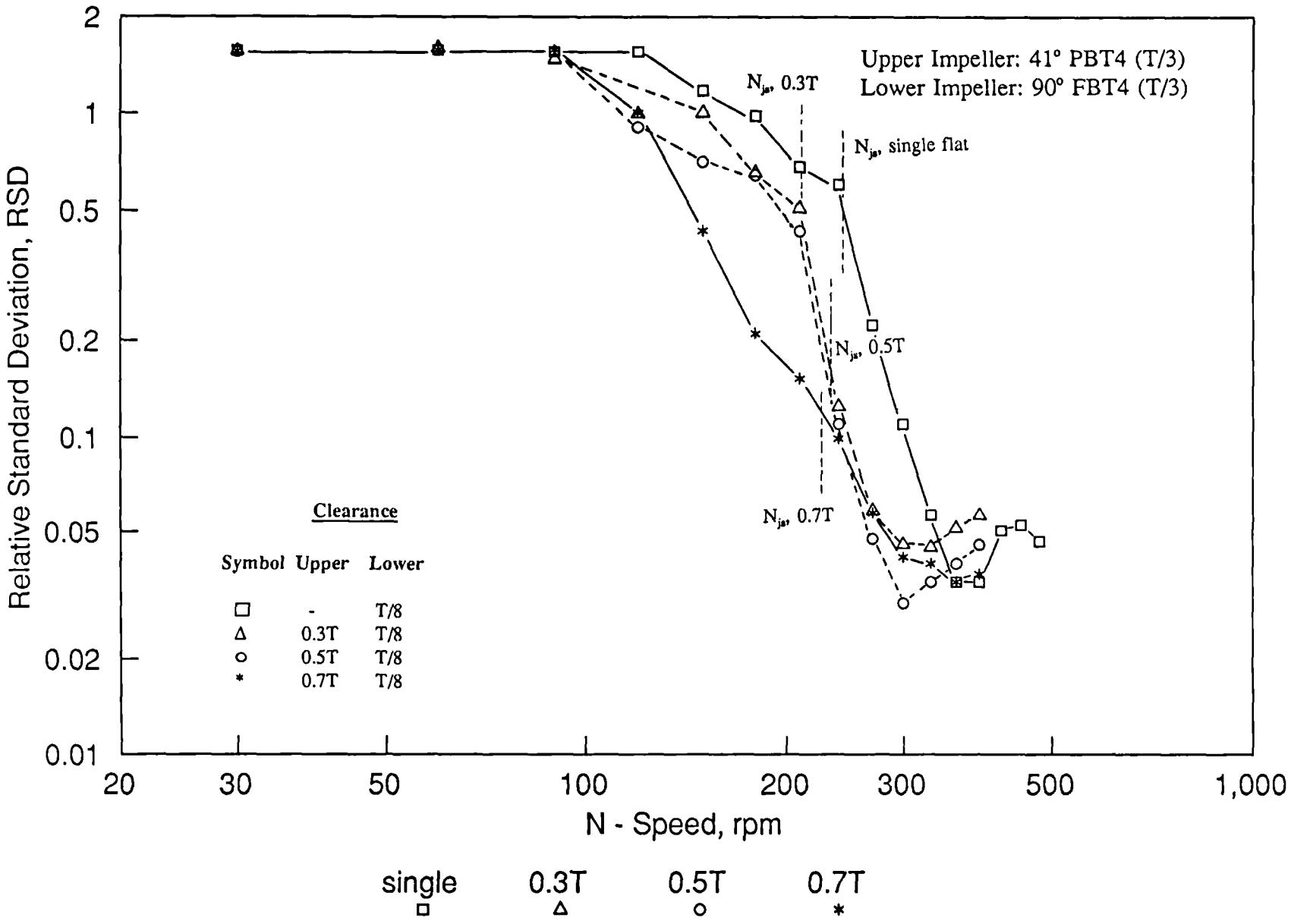

Fig 4.5.19 RSD against Impeller Speed for Flat/Pitched Combination

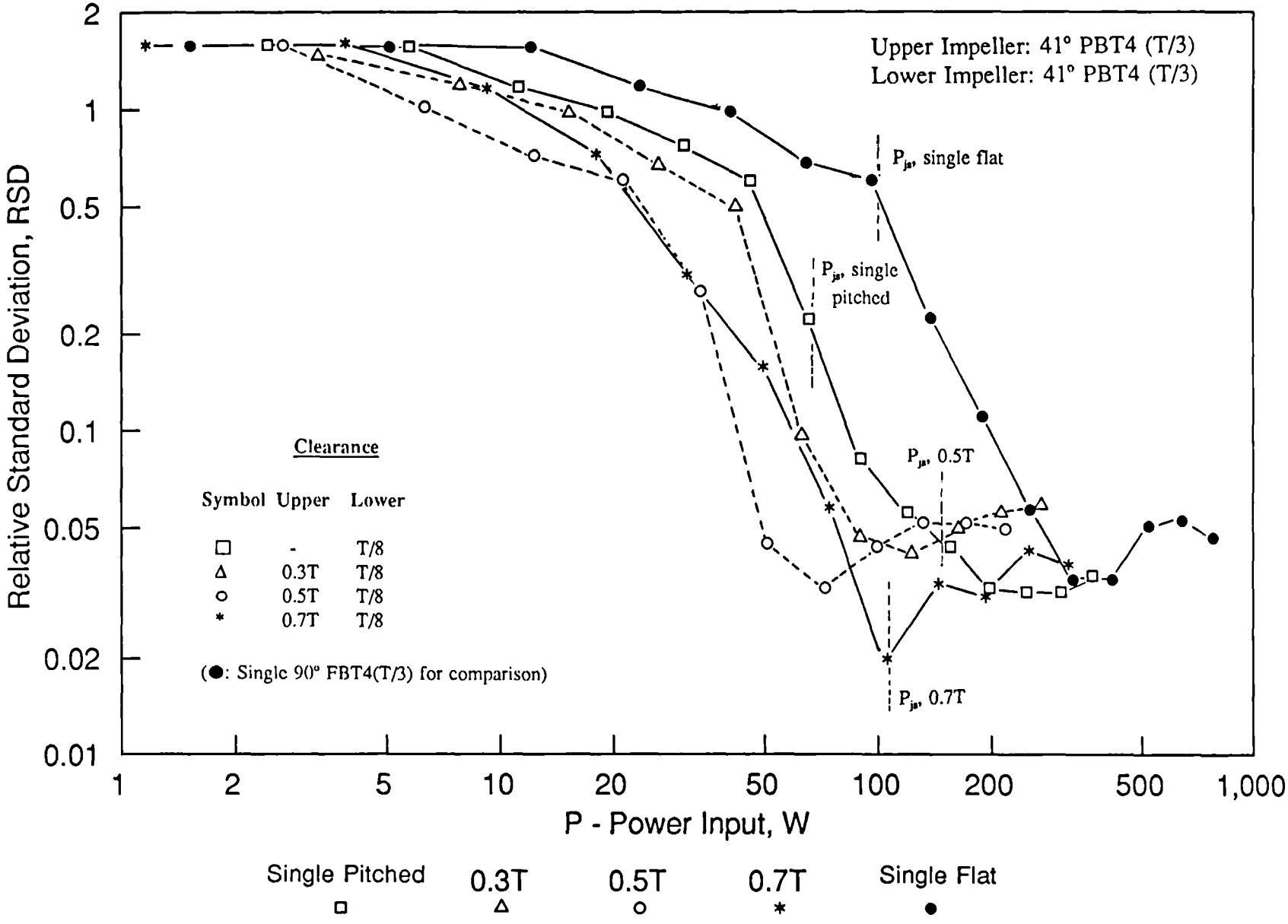

Fig 4.5.20 RSD against Power Input for Pitched/Pitched Combination

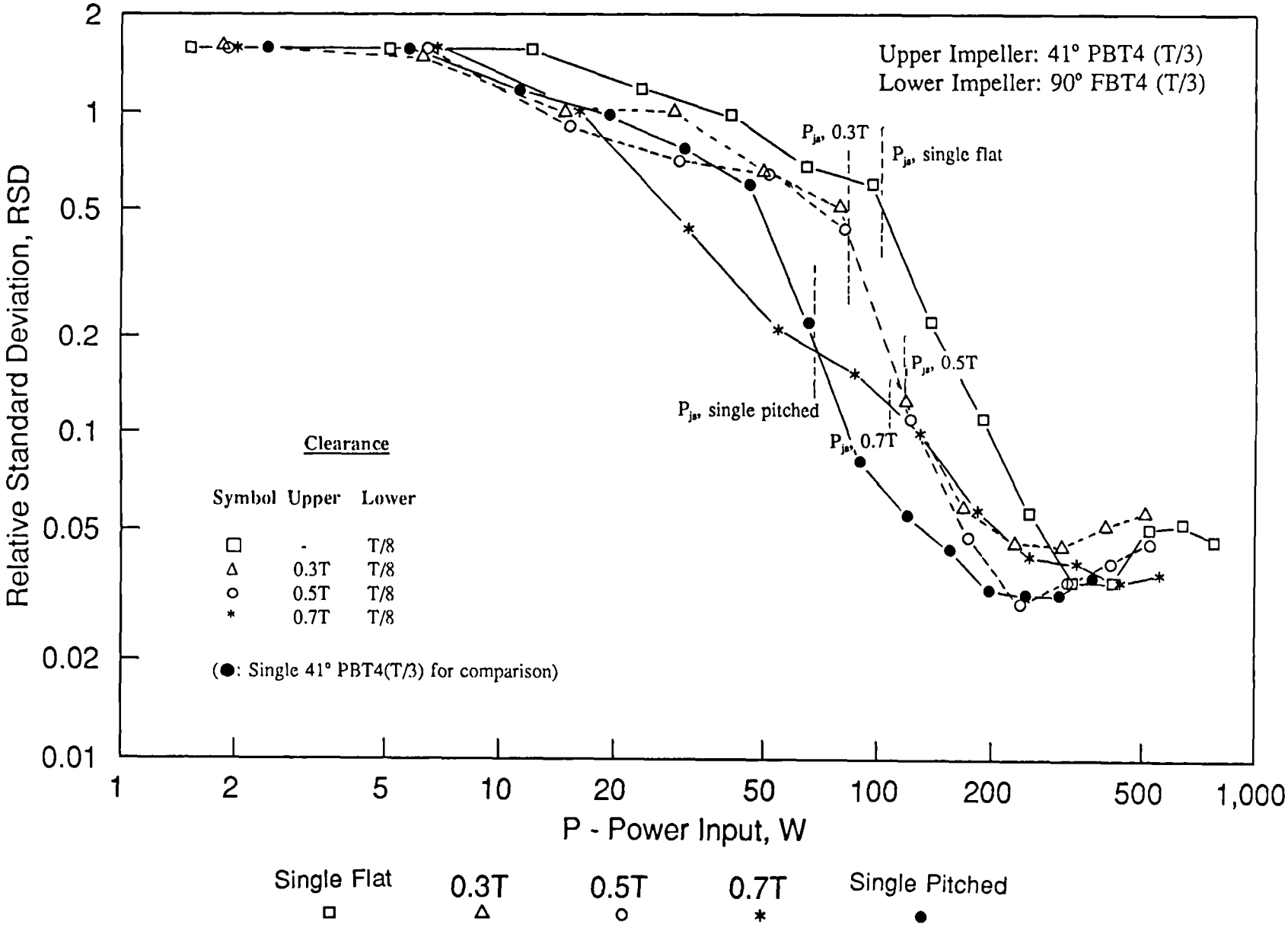

Fig 4.5.21 RSD against Power Input for Flat/Pitched Combination

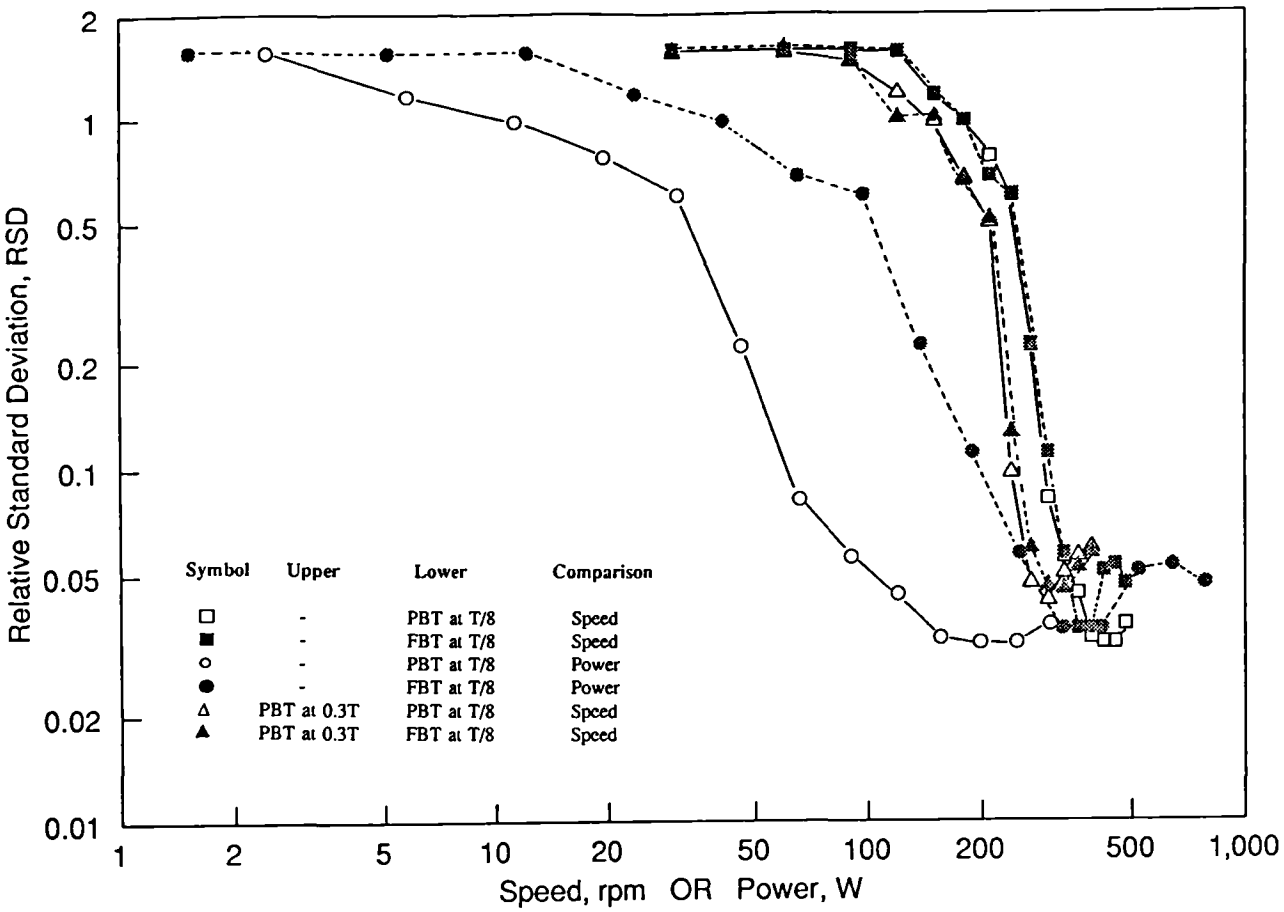

Fig 4.5.22 Comparison of RSD Profiles

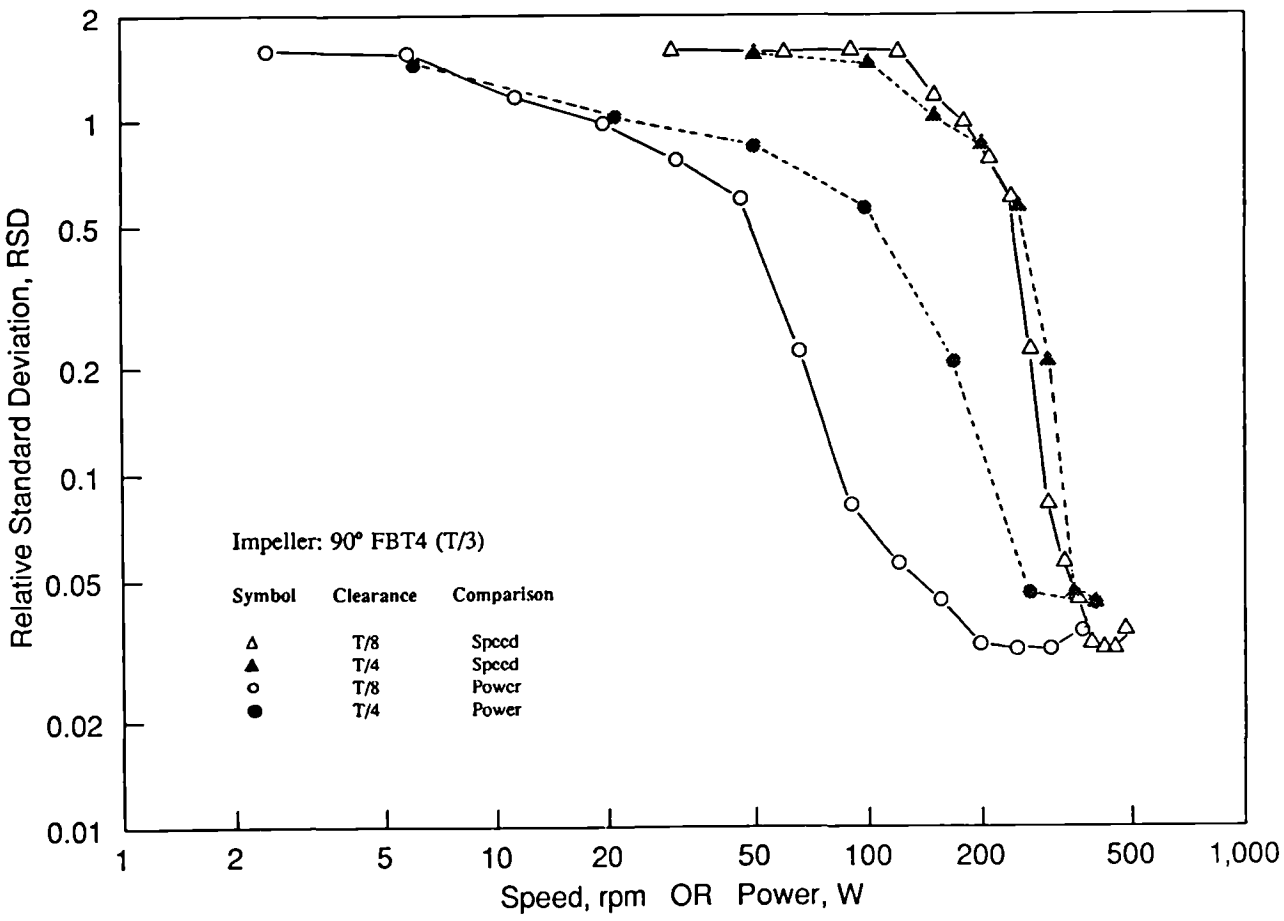

Fig 4.5.23 Comparison of RSD Profiles

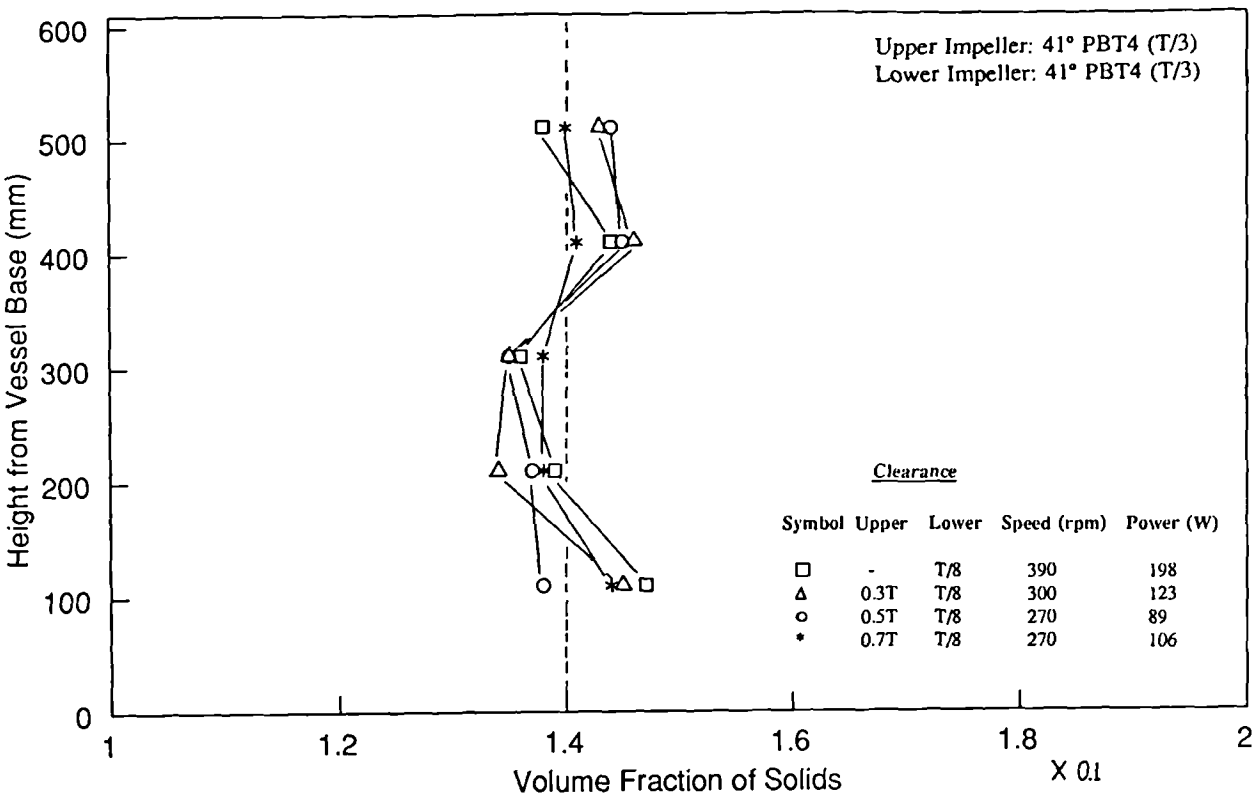

Fig 4.5.24 Concentration Profiles at RSD_{min} for Pitched/Pitched Combination

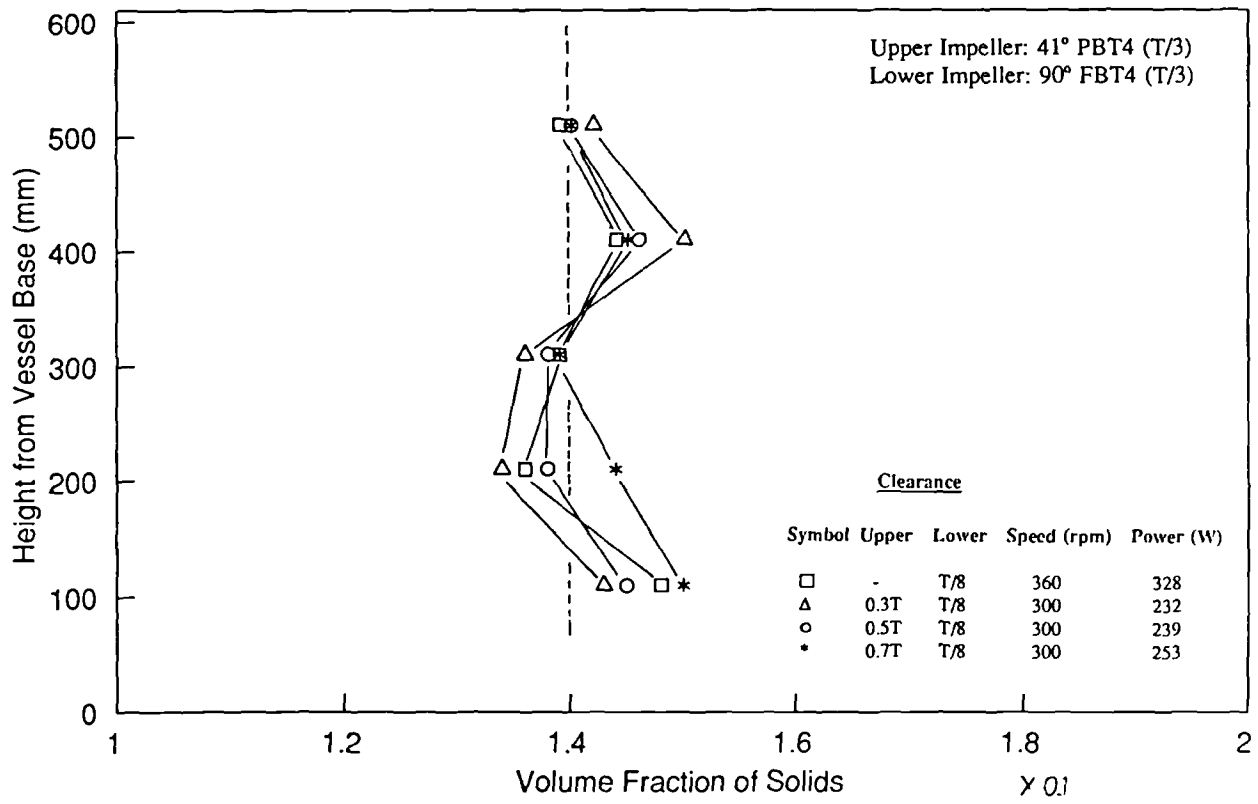

Fig 4.5.25 Concentration Profiles at RSD_{min} for Flat/Pitched Combination

4.6 SCALING UP

Scaling up plays an important role in stirred vessel design because mixing characteristics are often determined in a small and more flexible pilot plant before a full scale unit is built. However as this design technique can only be truly successful if an accurate prediction of the effect of scale is known, it is essential to develop a reliable criterion to ensure similar performance between the two scales. The literature survey in this thesis has already demonstrated that scale-up criteria for both solids suspension and distribution are far from being conclusive and the differences due to individual criteria are large enough to cast doubt on our present beliefs on scale-up (Sec 1.2).

This section describes the scale-up investigation undertaken in four geometrically similar stirred vessels (T_{31}, T_{61}, T_{183} and T_{267}). The four vessels provide a linear scale of 9:1 and cover vessel sizes up to those widely used in industry. Power, solids suspension and distribution measurements were made with a 45° downward pumping pitched blade turbine {45° PBT4(T/2,D/3.6)} mounted at T/4 clearance. Mixtures of water and sand (150-210 μm) were employed as the test media. An additional impeller {45° PBT4(T/2,D/5.2)}, which has a narrower blade width than the former, was also used to verify the scale-up relationship for solids distribution.

4.6.1 Power Numbers

Power number measurements were made with water and various solids concentrations at three scales. Results for T_{61}, T_{183} and T_{267} are presented as plots of power numbers against impeller speeds in Fig 4.2.5 to 4.2.7. It can be seen that power numbers with density correction (eqn 4.2.1) gave similar values to those measured in water, justifying the use of average density concept for solid-liquid power prediction.

The power numbers measured at T_{61}, T_{183} and T_{267} scales are found to be equal to 1.52, 1.75 and 1.75 respectively. Power number from T_{31} is not available and an estimated value of 1.52 is assumed (Palmer 1987). Power numbers in T_{183} and T_{267} were found to be 15% higher than the corresponding measurements in T_{61}. This could have very serious implications on the interpretation of the results so the geometries of the vessels were checked and the torque measurement repeated. No deviation from the standard geometry was found and the

same power numbers were obtained on retesting. It has been reported in the literature (Bujalski 1986) that power numbers of pitched blade turbines increase with scale. Evidence was also found in Mackinnon (1987)'s report, who carried out power measurements in the same vessel but with different impellers. For the two other 45° pitched blade turbines tested, power numbers in T_{183} are 11 and 14% higher than the corresponding value in T_{61} (Table 4.6.1).

Table 4.6.1 Comparison of Power Numbers at T_{61} and T_{183}

Reference	Impeller	Clearance	Po at T_{61}	Po at T_{183}	% increase
This work	45° PBT4(T/2,D/3.6)	T/4	1.52	1.75	15
Mackinnon 1987	45° PBT4(T/3,D/3.5)	T/3	1.62	1.80	11
Mackinnon 1987	45° PBT4(T/3,D/5.2)	T/3	1.12	1.28	14
Bujalski 1986*	45° PBT6(T/2,D/5)	T/4	1.66	1.72	4

* Po at T_{45} = 1.57

4.6.2 Solids Suspension

Just suspension speed measurements were made in four scales (T_{31}, T_{61}, T_{183} and T_{267}) with a solids concentration range of 0.1 to 40% Wt. Raw data are tabulated in Appendix D. A regression analysis was conducted on the complete set of data and the following correlation was obtained:

$$N_{js} \propto X^{0.125} D^{-0.824} \qquad r^2 = 0.99 \qquad \text{...eqn(4.6.1)}$$

Previous work (Mak 1988a) has confirmed that as long as the solids concentration is within the unhindered settling regime, the effect of solids concentration on N_{js} is as proposed by Zwietering (1958), i.e. $N_{js} \propto X^{0.13}$. A further regression was therefore conducted with exponent on X retained as 0.13 (Fig 4.6.2):

$$N_{js} = K X^{0.13} D^{-0.83} \qquad r^2 = 0.99 \qquad \text{...eqn(4.6.2)}$$

The constant K is equal to 0.85 with a relative standard deviation of ± 5%. The 95% confidence limits on the exponent of D range from -0.81 to -0.85. This result confirms the applicability of the Zwietering correlation for solids suspension scale-up up to vessels of 2.67 m in diameter. Results from this investigation are also correlated in Zwietering format and presented in Fig 4.6.3. A comparison between the measured and predicted N_{js} with 95% confidence intervals for prediction is given in Fig 4.6.4.

The previous section (Sec 4.6.1) reported an increment in power numbers with scale. If power were included in the regression analysis:

$$P_{js}/M \propto X^{0.372}\, T^{0.392} \qquad r^2 = 0.95 \qquad \text{...eqn(4.6.3)}$$

Since $P_{js}/M \propto N_{js}^3\, D^2$, and $D \propto T$

$$N_{js} \propto X^{0.12}\, D^{-0.80} \qquad \text{...eqn(4.6.4)}$$

The 95% confidence limits on the exponent of D ranged from -0.82 to -0.78. The exponent on D is slightly lower than the former analysis (eqn 4.6.2). The 95% confidence ranges on the exponent of D for eqn 4.6.2 and 4.6.4 overlap with each other and in view of the similarity between the two equations, they can be taken to be the same for design purpose. However, a rather philosophical question thus arises - which of the two approaches provides a better description of the results? This resolves to how confident are we in predicting the effect of geometric scale on power number? Power number is a measure of pressure forces producing flow against inertial force and is analogous to a drag coefficient. It remains constant only when the ratio of the hydrodynamic parameters are the same between small and large scales.

Table 4.6.1 shows that there is a tendency for power number to increase with scale but it does not seem to follow any obvious trend. For example, there is no apparent change in Po between T_{183} and T_{267} scales. Not until the effect of scale on power number is thoroughly understood can the approach adopted in deriving eqn 4.6.4 be generally applicable.

One may argue that the difference in power number may be due to the fact that the vessels are not geometrically similar. It has already been stated in the last section that the

dimensions and instrumentation chain were double checked and found to be correct, leaving us with the conclusion that power number does in fact either change with scale or is effected by very delicate geometrical influence such as surface roughness of the vessel. On the other hand, if Po is so incredibly sensitive to geometry that one could not detect any difference when the geometry was being checked in this carefully planned scale-up experiments, the chance of getting the geometries right will be even less in an industrial environment. Provided that the exact power numbers between the plant and pilot scales are known, the analysis adopted in eqn 4.6.2 is superior.

Both analyses indicate a lower exponent (in magnitude) on D than Zwietering's. If the Zwietering correlation is to be retained dimensionless for scaling purpose, other exponents in the correlation must be altered in order to make provision for the new exponent on D. The most suitable candidate is the particle diameter for it is the only other parameter consisting of a length scale alone.

The Zwietering Correlation :

$$N_{js} = s\,\nu^{0.1}\left(\frac{g\,\Delta\rho}{\rho_L}\right)^{0.45} d_p^{0.2}\,X^{0.13}\,D^{-0.85} \qquad \text{...eqn(4.6.5)}$$

Fig 4.6.1 presents examples of the diverse scale-up rules presented in open literature. Proposed criteria ranged from $P/V \propto T^{0.5}$ (power per unit mass increasing with scale) to $P/V \propto T^{1}$ (power per unit mass decreasing with scale). For 100-fold change in scale, the two extremes give 1000-fold difference in power requirement prediction. It was felt that some discrepancy is due to the fact that many of the literature results were based on small scale experiments where minor errors may affect the delicate scale-up results. An added disadvantage of extrapolating scale-up rules from very small set-ups is that they are further away from the actual sizes where the rules applied. Moreover, if the scale-up rules are scale/mechanistic dependent, results derived from small scale will be of very little practical value.

Comparison was made between this investigation and the literature (Table 4.6.2), confined to those with experimental set-ups equal to or larger than one metre in diameter.

Zwietering's results (1958) is also included by virtue of its popularity. It was found that with the exception of Chudacek (1986)'s results on flat base vessels, all the exponents on scale lie roughly between -0.85 (Zwietering's correlation) and -0.67 (constant power per unit mass). Chudacek's flat base results ($N_{js} \propto D^{-0.53}$) look somewhat doubtful because his correlation predicted a particle size effect of $d_p^{0.56}$ on N_{js}, which is higher than that is generally quoted in the literature. Most results exhibited a change in exponent due to scale, impeller type, concentration and particle sizes (eg Zwietering, Herringe, Chudacek and Bujalski). This change is likely to be hydrodynamic/mechanistic driven. Results from this study are also presented as plot of $N_{js}/X^{0.13}$ against impeller diameter, with Zwietering, constant tip speed and constant power input scale-up rules marked on the same plot for comparison.

Chudacek suggested that in the ideal case, mean upward velocity should be kept constant in geometrically similar vessels, implying that constant tip speed should be used for scaling up. Deviation from the ideal case decreases as the recirculation flow in a mixed tank becomes structured so that systems with draft tubes approach the ideal scale up relationship.

Table 4.6.2 Effect of Geometrical Scale on Solids Suspension

Reference	Tank Size (m)	Vessel Base	Impeller	C	Conc (% Wt)	d_p (μm)	ρ_s (kg m^{-3})	Exponent on D	Remarks
Zwietering 1958	0.15-0.60	Flat	various	various	0.5-20	150-850	2600	-0.85	actual exponent ranged from -0.78 to -0.91, impeller type dependent
Herringe 1979	0.15-1.0	Flat	PTD6(T/3)	T/3	14-46	300	2650	-0.71	actual exponent varies with scale, concentration and particle size
Chapman 1981	0.29-1.83	Flat	DT, PTD4	T/4	1	300-710	2650	-0.76	H=0.92T in T_{183}, bottom window design casts doubt on results
Buurman 1985	0.48-4.26	Dished	PTD4(T/2.5), PTU4(T/2)	T/3	1-30	~157	2650	-0.67	probe located off-centre in large scale[1]
Chudacek 1986	0.5-1.0	Flat, cone & fillet	Propeller, PTD6	various	14-39	77-290	2650	-0.53 to -0.68	scale-up exponent dependent on mechanisms
Bujalski 1986	0.29-1.83	Flat	PTD6(T/2)	T/4	0.1	440-530	2950	-0.76	T_{183} results off the trend, comments on Chapman's set-up also applied here
Molerus 1986	0.19-1.5	Dished	T/3 Propeller	T/3	0.5-30% Vol	34-1937	2480-7841	Ar≤40, -0.89 Ar>40, -0.64	Solids conc has no effect on N_{js} when Ar ≤ 40
Rao 1988	0.3-1.5	Flat	PTD6(T/3)	T/3	0.7-11.3	100	2520	-0.82	
This work	0.31-2.67	Dished	PTD4(T/2)	T/4	0.1-40	150-210	2630	-0.83	Po changes with scale, results from large scales (T_{183} & T_{267}) give a lower exponent

Impellers: DT=Disc turbines, PT(U/D)n=n bladed (upward/downward pumping) pitched blade turbine [1] Private communication with the Author

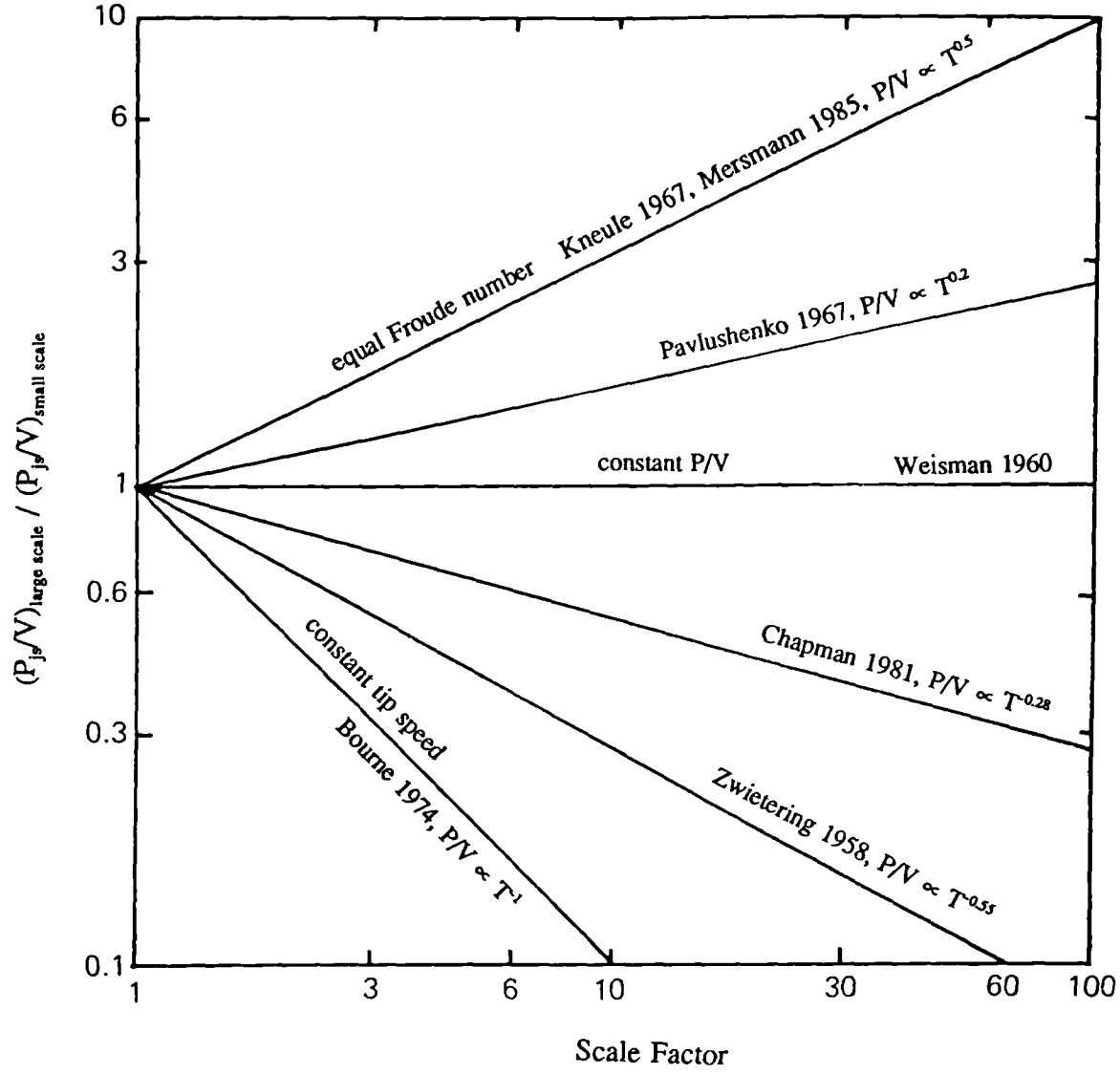

$$\frac{P_{js}}{V} \propto \frac{N_{js}^3 D^5}{T^3} \propto N_{js}^3 D^2, \quad for\ D \propto T$$

$$If\ N_{js} \propto D^{-\gamma}$$

$$\frac{P_{js}}{V} \propto D^{(2-3\gamma)}$$

Fig 4.6.1 Examples of Suspension Scale-up Rules Published in Literature

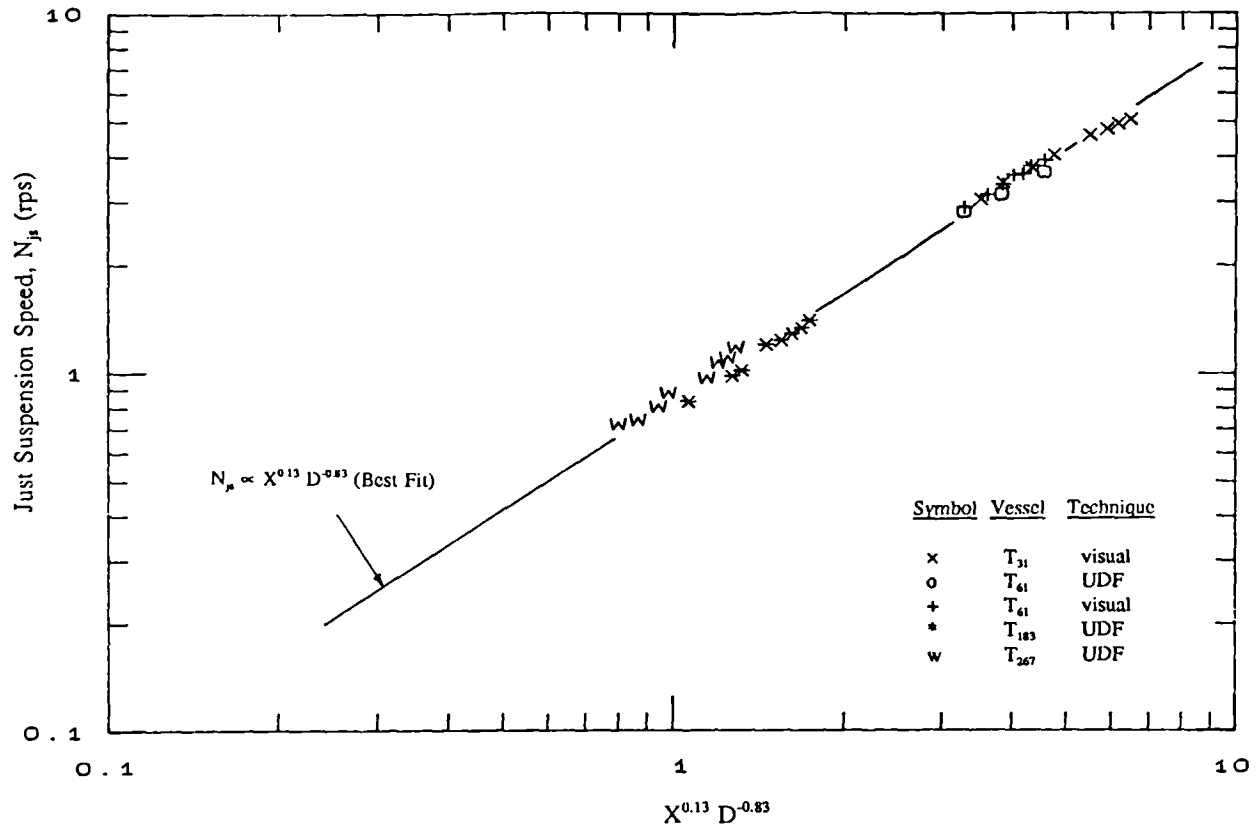

Fig 4.6.2 Best Fit for all Scale-up Data

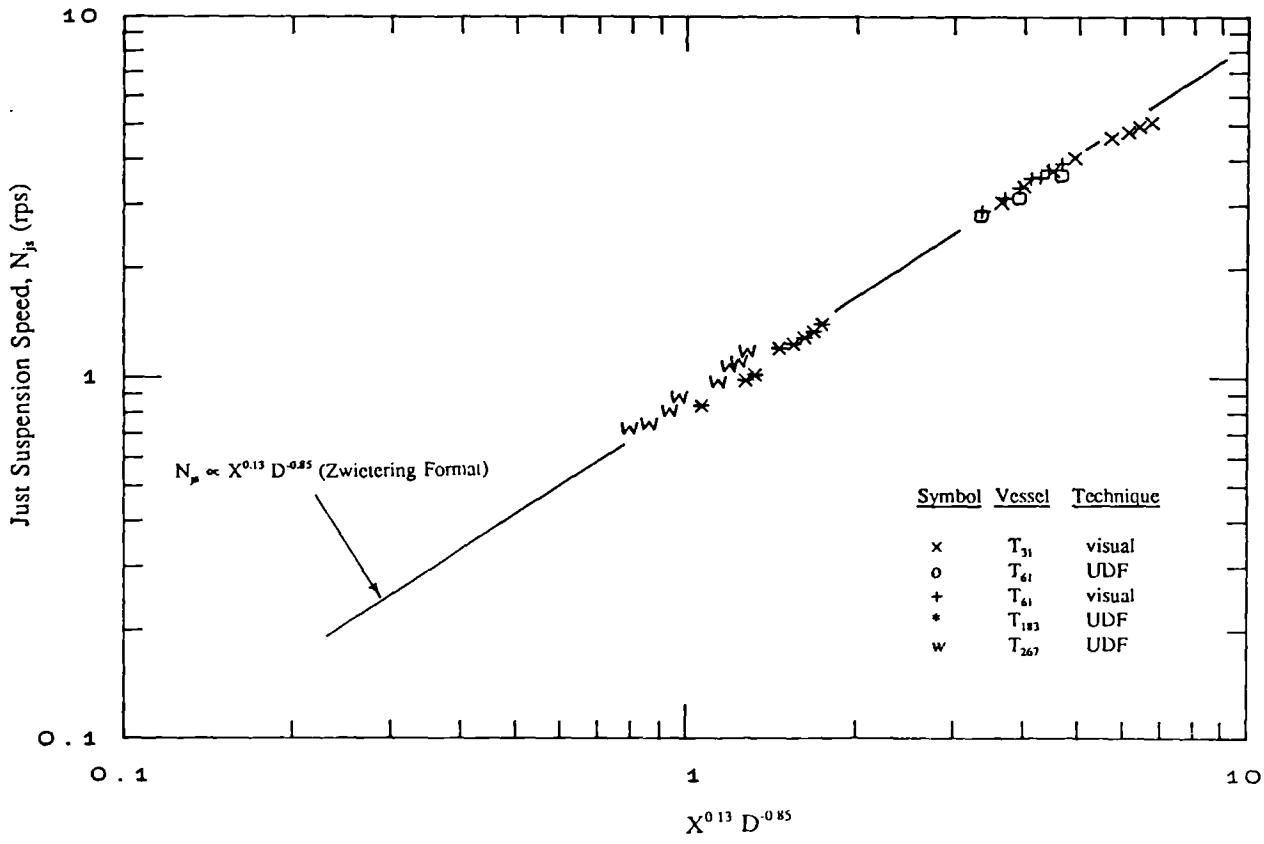

Fig 4.6.3 Scale-up Data Presented in Zwietering's Format

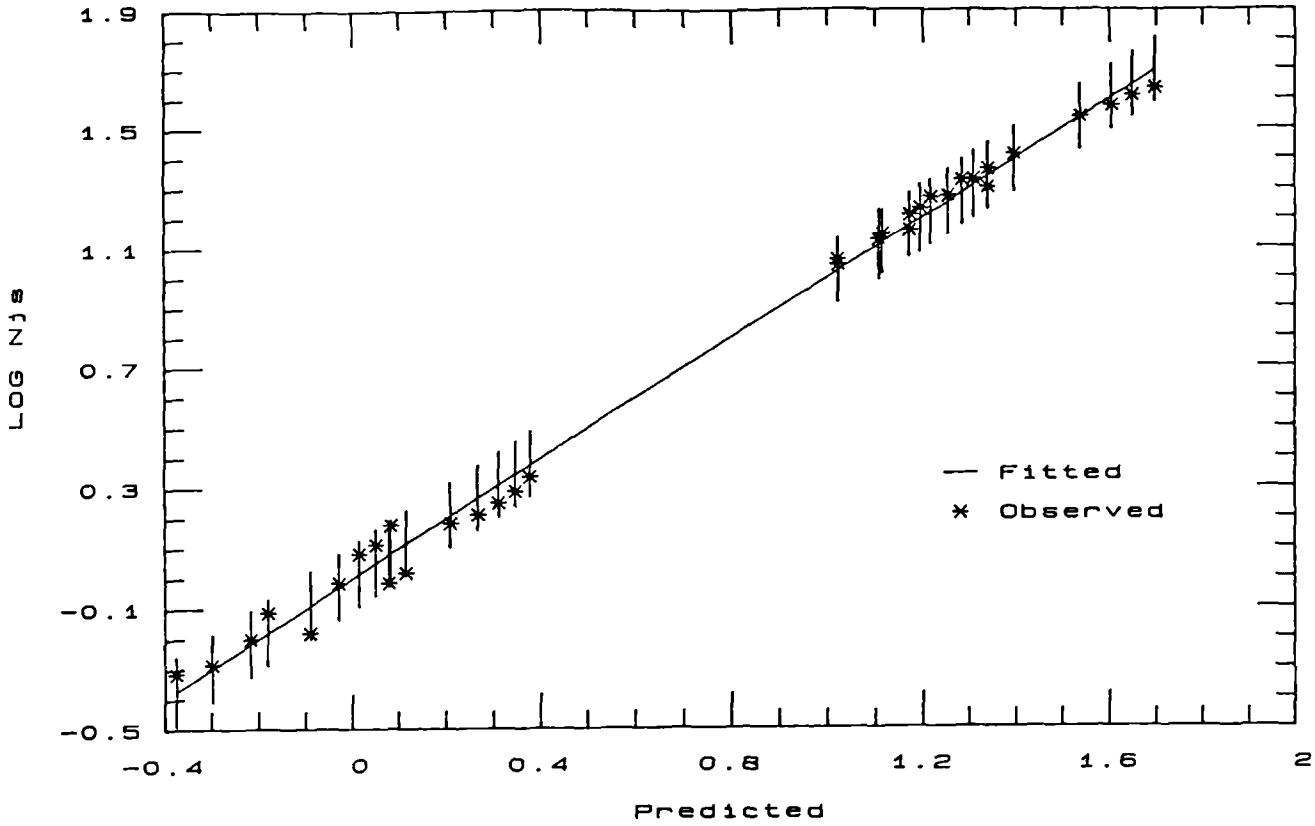

Fig 4.6.4 Scale-up Data Presented in Zwietering's Format - Comparing Predicted and Observed Values with 95% Confidential Intervals for Predictions

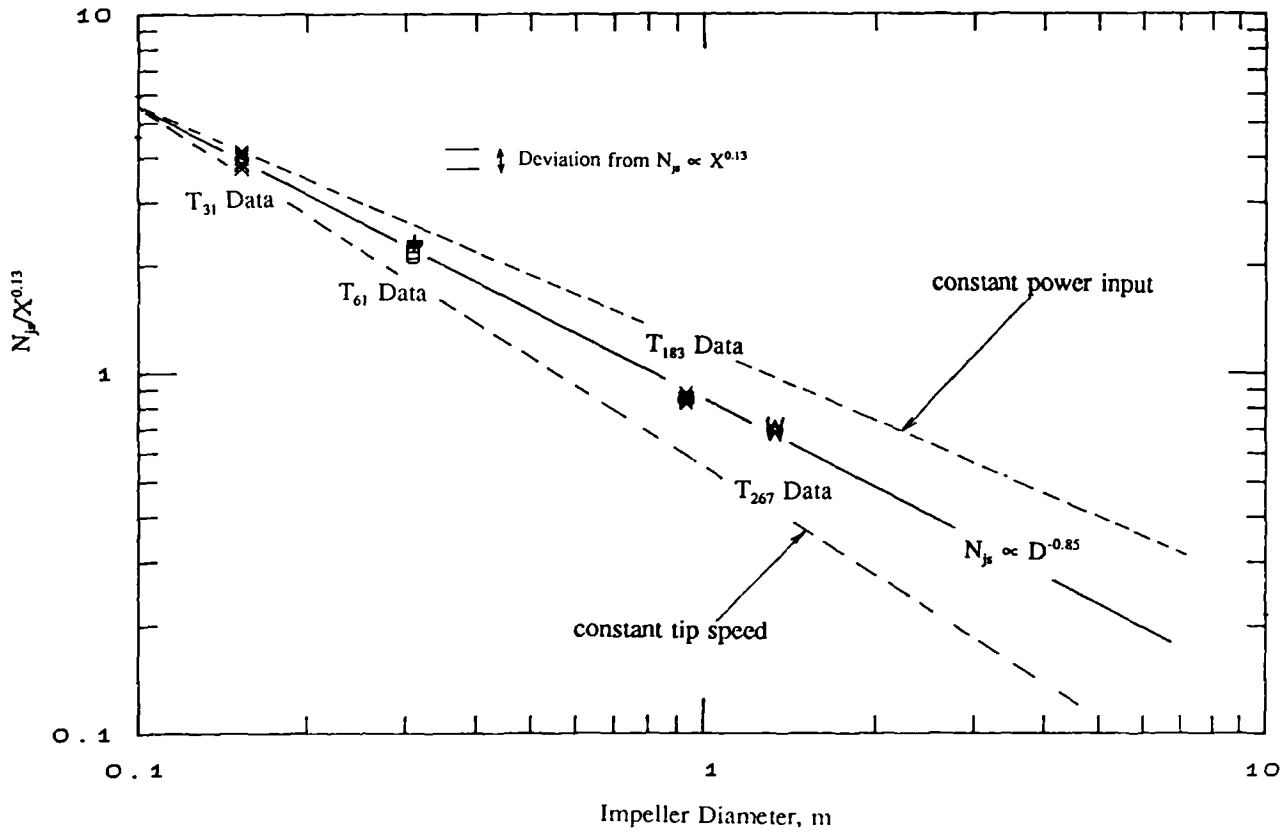

Fig 4.6.5 Effect of Geometrical Scale on Solids Suspension

4.6.3 Solids Distribution

Solids distribution measurements were conducted with two 45° T/2 PBTs in three scales (T_{61}, T_{183} and T_{267}) and a solids concentration range of 15 to 30% Wt. In all cases, it covered five standard axial positions {T/6.1 (0.1, 0.3, 0.45), T/3.1 (0.2, 0.6, 0.9), T/2.0 (0.3, 0.9, 1.35), T/1.5 (0.4, 1.2, 1.8) and T/1.2 (0.5, 1.5, 2.25)} at a fixed radial position of T/6 from the vessel wall (Sec 3.10.3). The three numbers in brackets indicate the actual probe locations in metres below the fluid surface at the three scales being studied. Details of the results are tabulated in Appendix E.

In order to check the radial concentration profiles, three additional radial positions (T/4, T/12 and T/60 from the vessel wall) were also studied in T_{183}. It was not possible to measure the solids concentration further towards the centre of the tank, due to the presence of the gearbox. Results are presented as plots of volume fraction of solids against probe radial position at constant axial position, for a range of impeller speeds (Fig 4.6.6a-e).

The radial concentration profiles were flat, the only exception being when the probe was at the clear liquid/solid-liquid interface. This happened when the probe was mounted towards the top of the vessel, with the impeller running at relatively low speed - some solids are rotating in a "wave form". The results suggest that the potential effect on radial solids distribution caused by the up and down flow loops is negligible. The flatness of the radial profiles has already been reported by other researchers (eg Barresi 1987, Shamlou 1989) but their results were established from vessels of limited sizes (T=0.39 and 0.225 m). It is encouraging to have the results confirmed in vessel of much larger scale. Thus, the one-dimensional steady state model is a reasonable representation of the distribution process and comparisons conducted in this work, which focus on one radial position, i.e. T/6 from vessel wall, is therefore justified.

The influence of geometric scale on solids distribution was investigated by comparing the results obtained from two impellers, three concentrations and three scales. They are presented as plots of relative standard deviation against the equivalent of tip speed (ND), power per unit volume (N^3D^2) and Froude number (N^2D) (Fig 4.6.8 to 4.6.15). Similar analyses were carried out with power numbers incorporated into the dependent variables in order to account for its effect on scale-up relationship (Fig 4.6.10). All results suggested that

the use of constant tip speed ($N_{RSD} \propto D^{-1}$) as scale-up criterion for solids distribution under-estimated the power requirement in large scales (Fig 4.6.8 and 4.6.12), while constant Froude number criterion ($N_{RSD} \propto D^{-0.5}$) over-estimated the power requirement in large scales (Fig 4.6.11 and 4.6.15). Equal power per unit volume ($N_{RSD} \propto D^{-0.67}$) is the recommended criterion for solids distribution scale-up (Fig 4.6.9-10 and 4.6.13-14).

Unlike solids suspension, which has attracted considerable attention in the past, there have been few quantitative studies in solids distribution. Table 2.2.1 presents a summary of existing solids distribution models. Three out of the four models reported are based on a one-dimensional dispersion approach, which leads to a constant tip speed criterion for solids distribution scale-up. Unfortunately, these studies were restricted to a single scale at relatively low solids concentrations. This work and Buurman's (1985) are the only two systematically planned solids distribution investigations that cover industrially sized vessels. His turbulent model suggested the modified Froude number should be greater or equal to 20 in order to achieve maximum solids homogeneity, indicating a scale-up relationship of $N_{RSD} \propto D^{-0.78}$. Scale-up results from this study were plotted in terms of RSD against N $D^{0.78}$ and presents in Fig 4.7.4 to verify Buurman's model for solids distribution. It is found that his model slightly underestimates the power requirement at large scales.

4.6.4 Comparison between the Two Scale-up Rules

Previous results (Sec 4.3.2) have shown that some impellers (eg T/3 PBT4s) attained just suspension condition before the point of maximum homogeneity. For some other impellers (eg T/2 PBTs), just suspension speeds were higher than $N_{RSD,\,min}$ (eg Fig 4.3.10). However, scale-up relationships were found to be different for solids suspension and distribution (i.e. $N_{js} \propto D^{-0.83}$, $N_{RSD} \propto D^{-0.67}$). These findings have interesting design implications. Take a small diameter impeller for example, for which the impeller speed for suspension is lower than that of maximum homogeneity (eg Fig 4.3.10). If N_{js} were to be used as a scale-up criteria, the solids distribution in the vessel will be worse as the scale increases. Conversely, if the same process is scaled up according to solids homogeneity, the suspension quality will improve with scale. This is illustrated graphically in Fig 4.6.16.

a) 300 mm below fluid surface

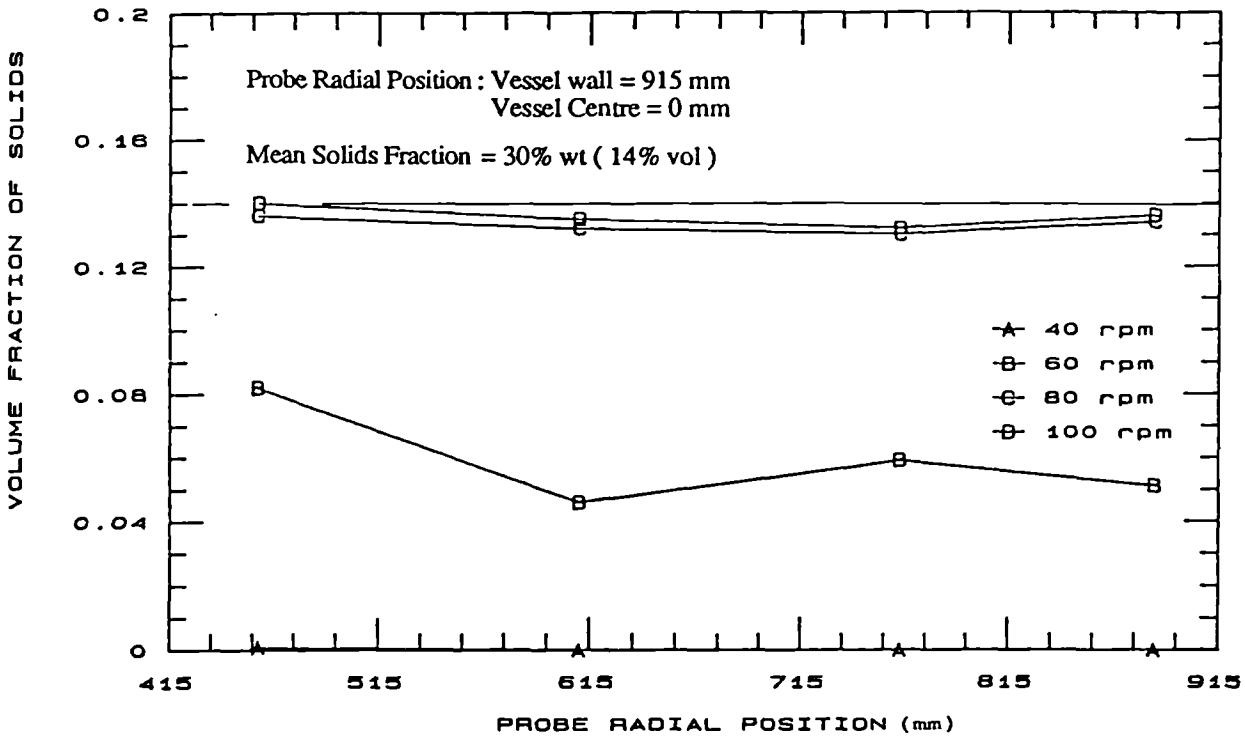

b) 600 mm below fluid surface

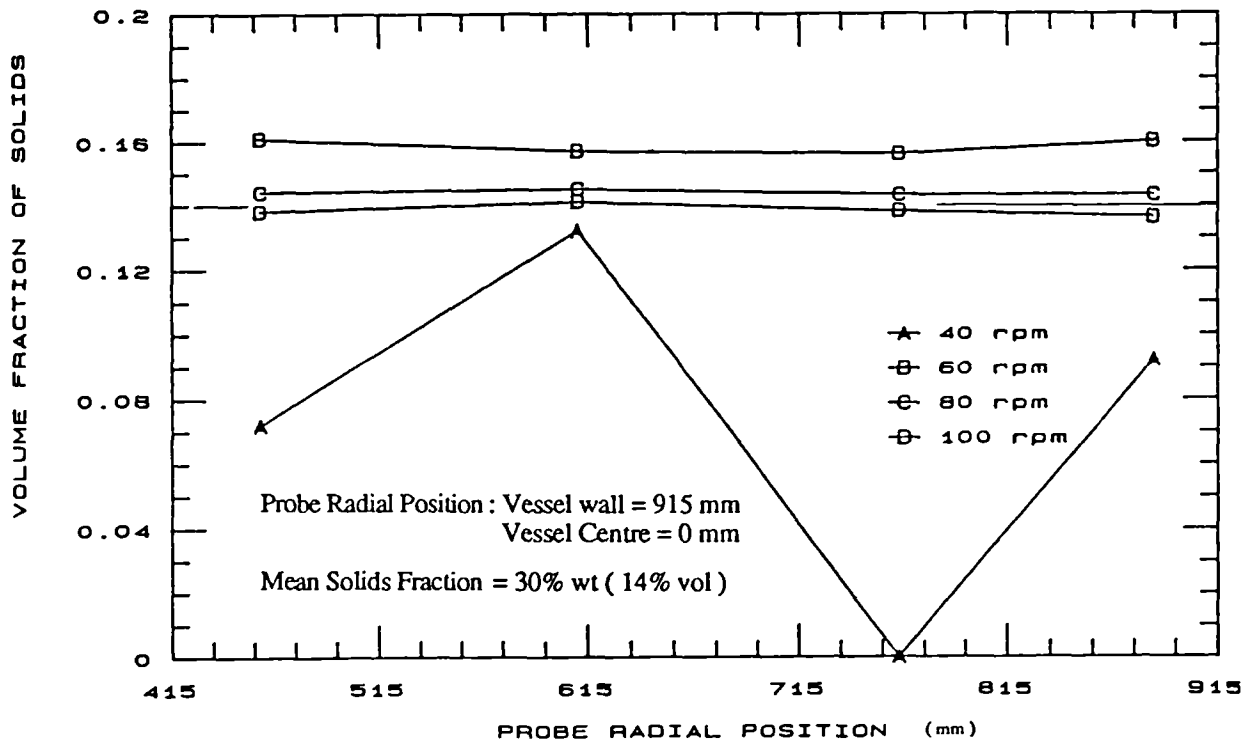

Fig 4.6.6 Radial Solids Distribution for 45° PBT4(T/2, D/3.6) in T_{183}

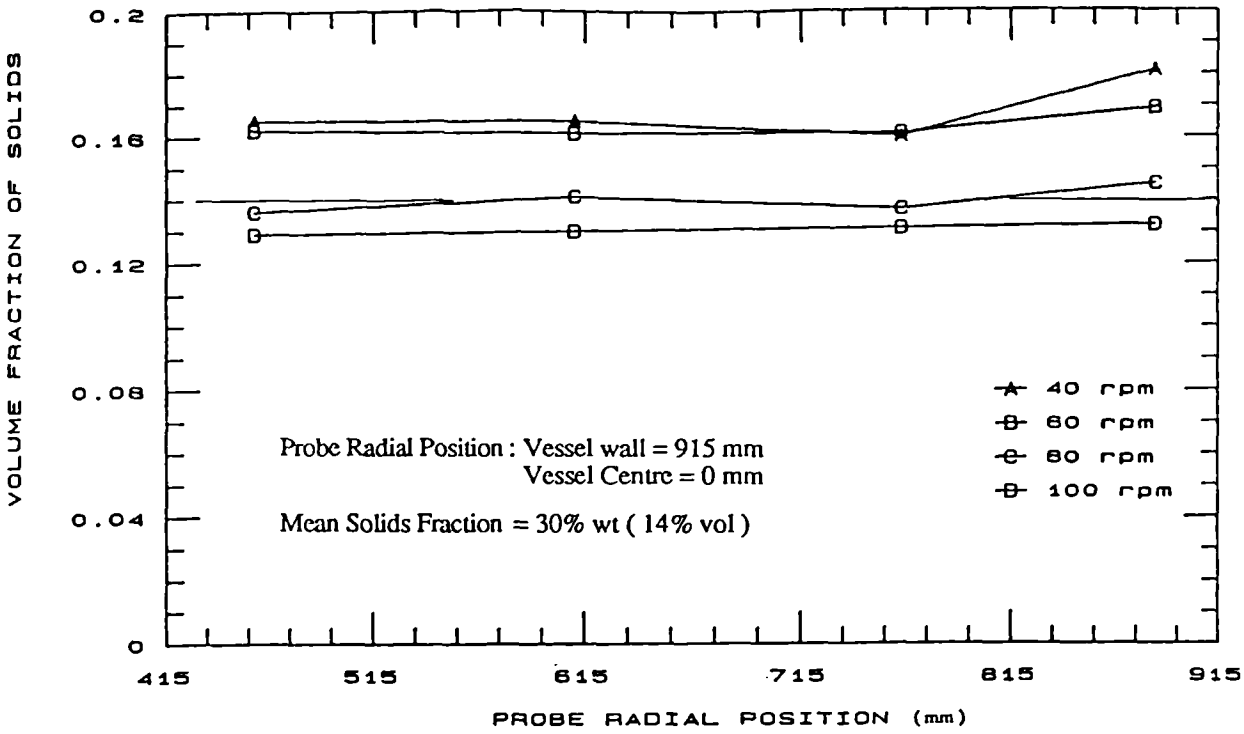

c) 900 mm below fluid surface

d) 1200 mm below fluid surface

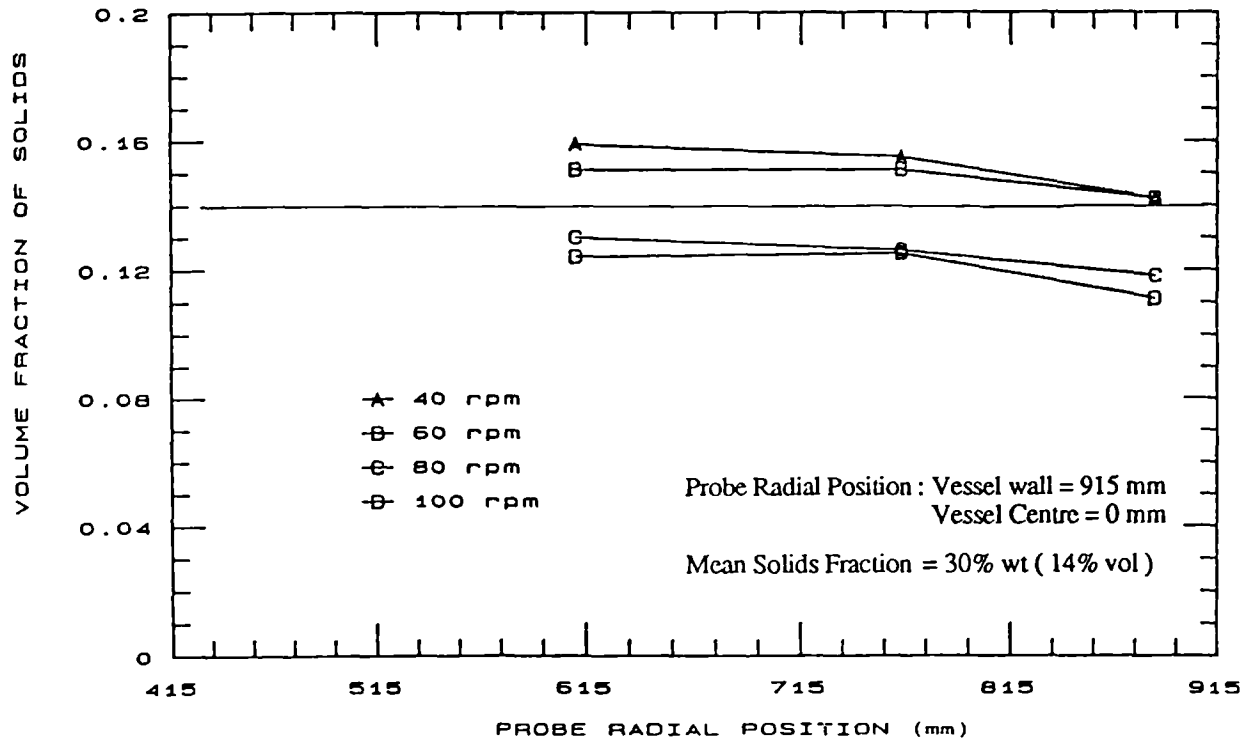

Fig 4.6.6 Radial Solids Distribution for 45° PBT4(T/2, D/3.6) in T_{183}

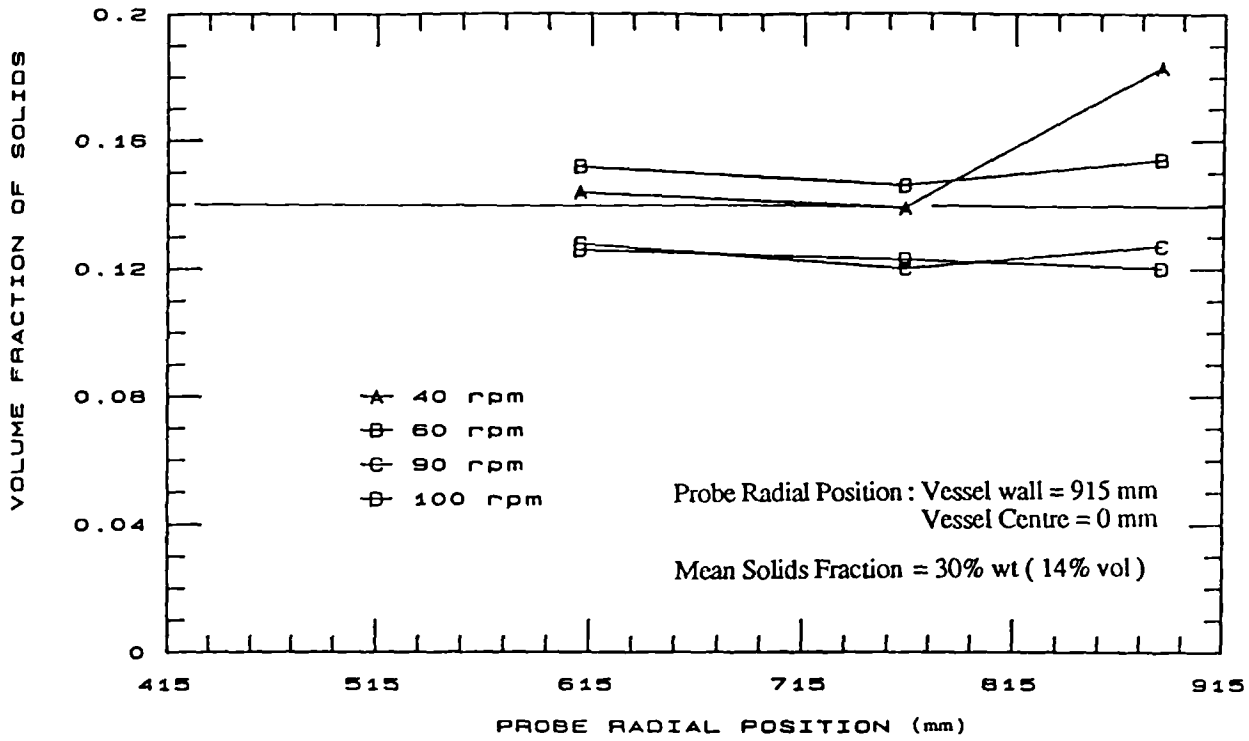

Fig 4.6.6 Radial Solids Distribution for 45° PBT4(T/2, D/3.6) in T_{183}

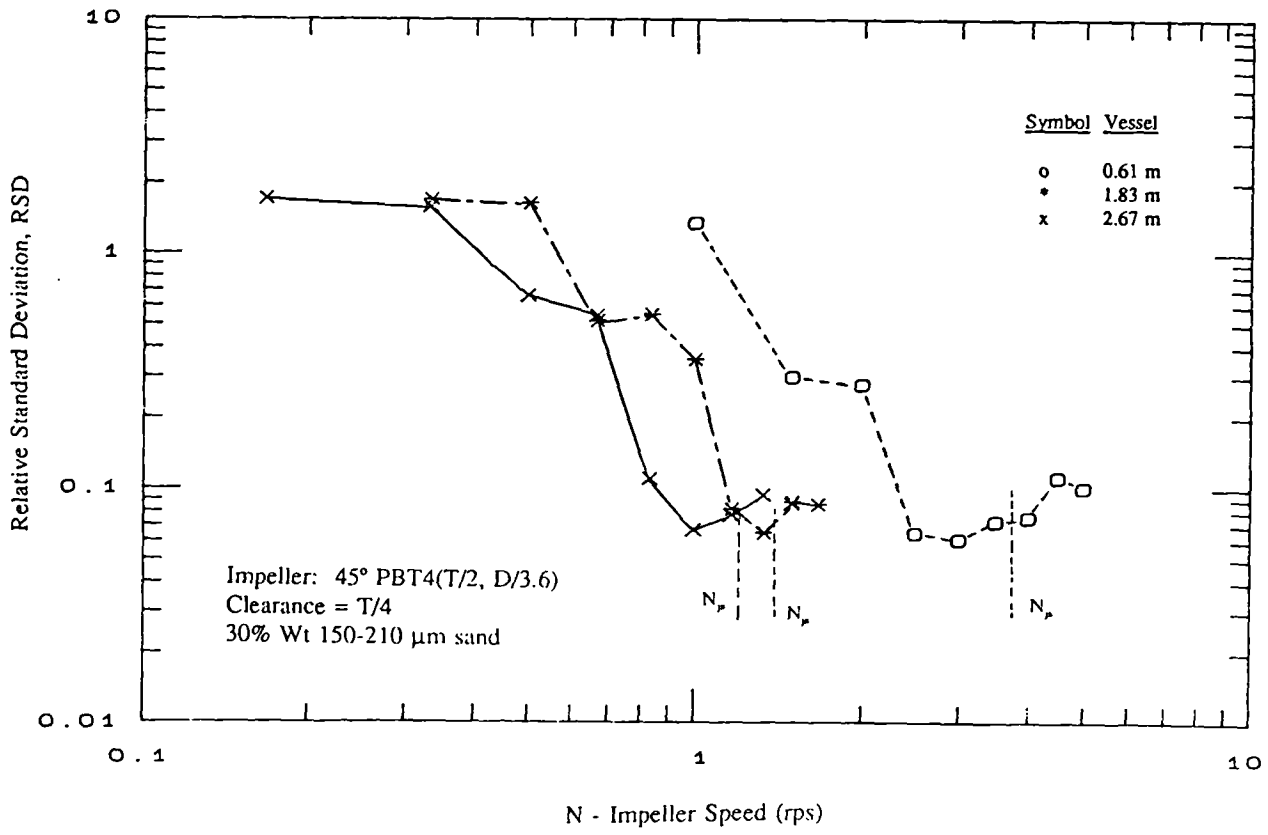

Fig 4.6.7 Plot of RSD against Impeller Speed for 3 Scales

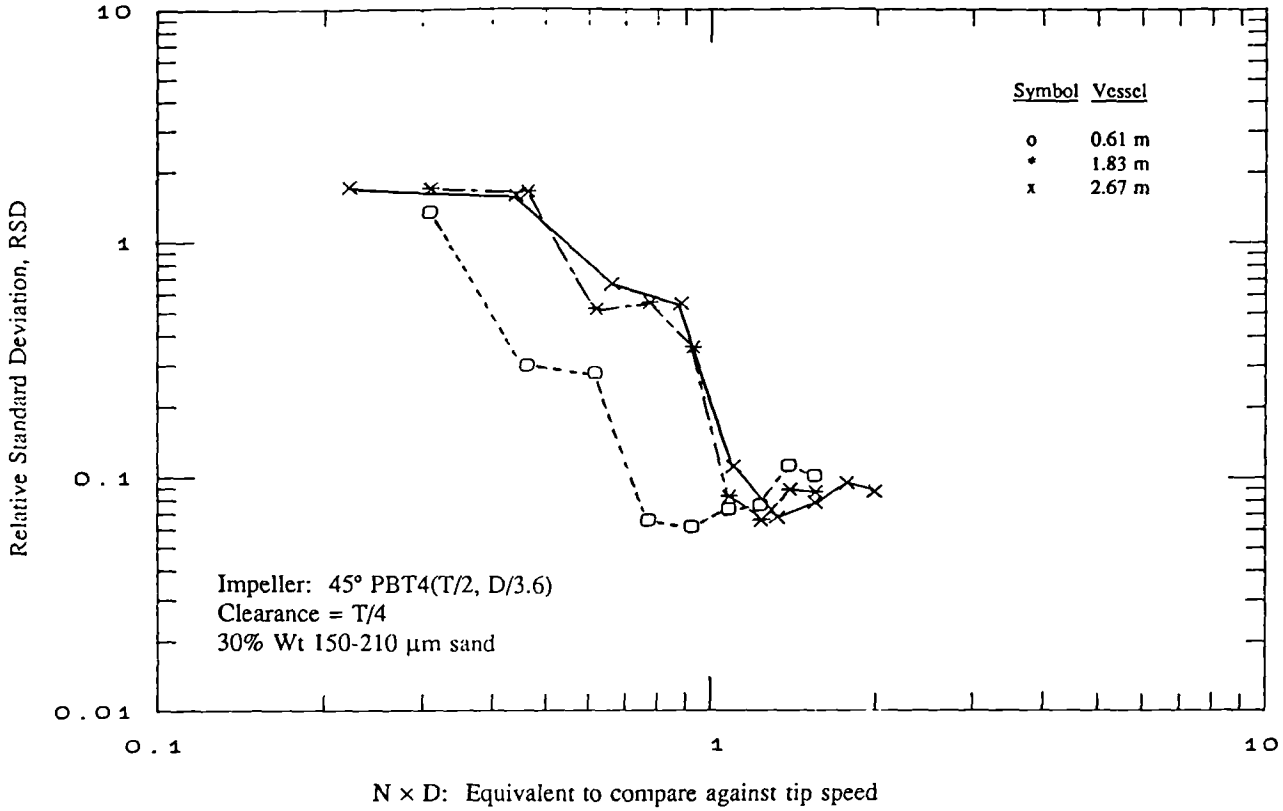

Fig 4.6.8 Scale-up Data: comparing against impeller tip speed

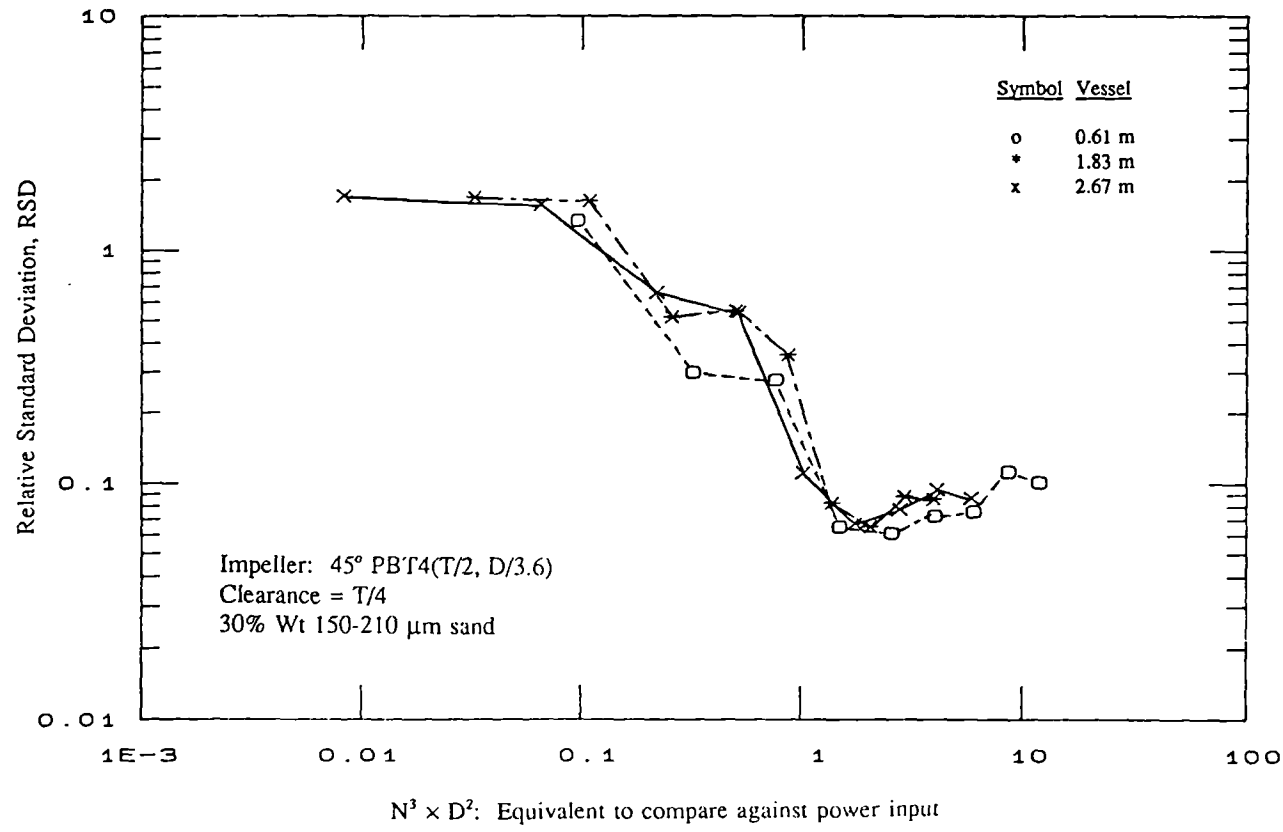

Fig 4.6.9 Scale-up Data: comparing against power input (assuming constant Po)

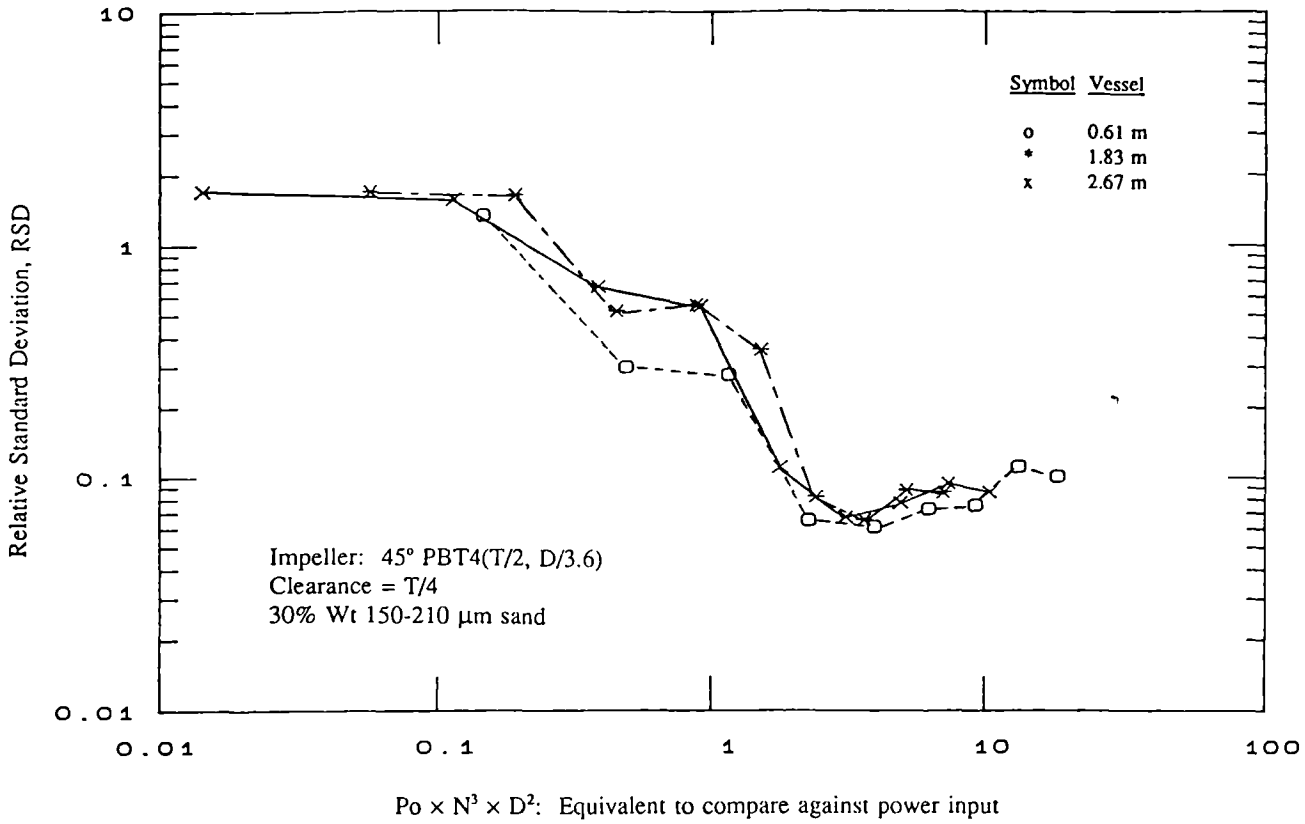

Fig 4.6.10 Scale-up Data: comparing against power input

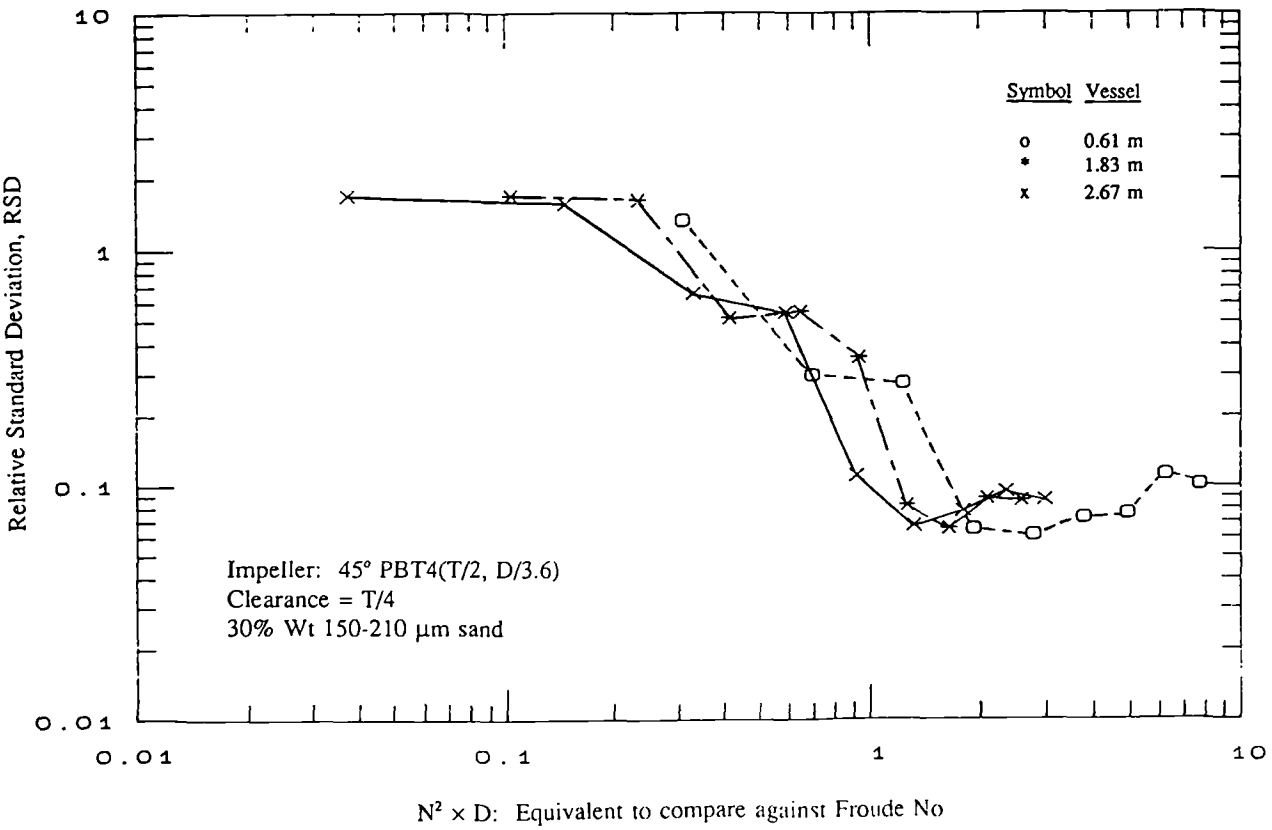

Fig 4.6.11 Scale-up Data: comparing against Froude No

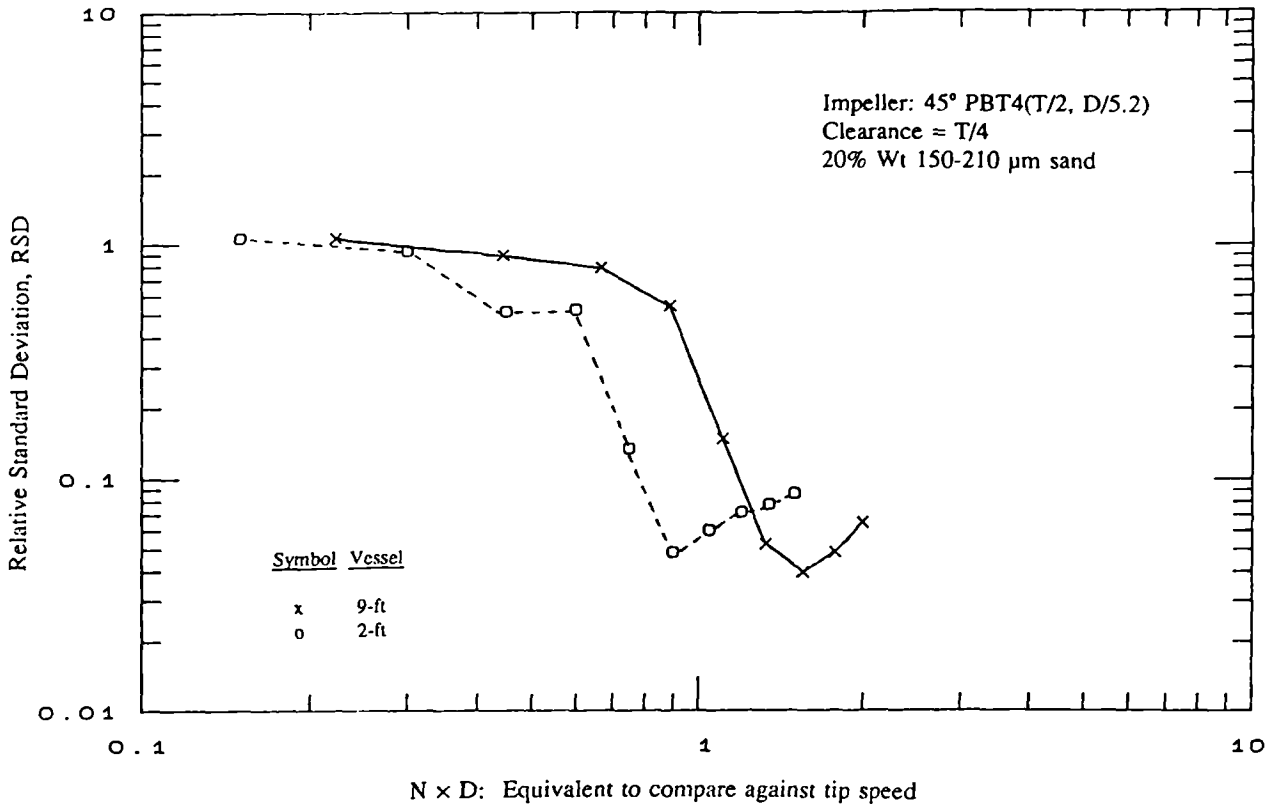

Fig 4.6.12 Scale-up Data: comparing against impeller tip speed

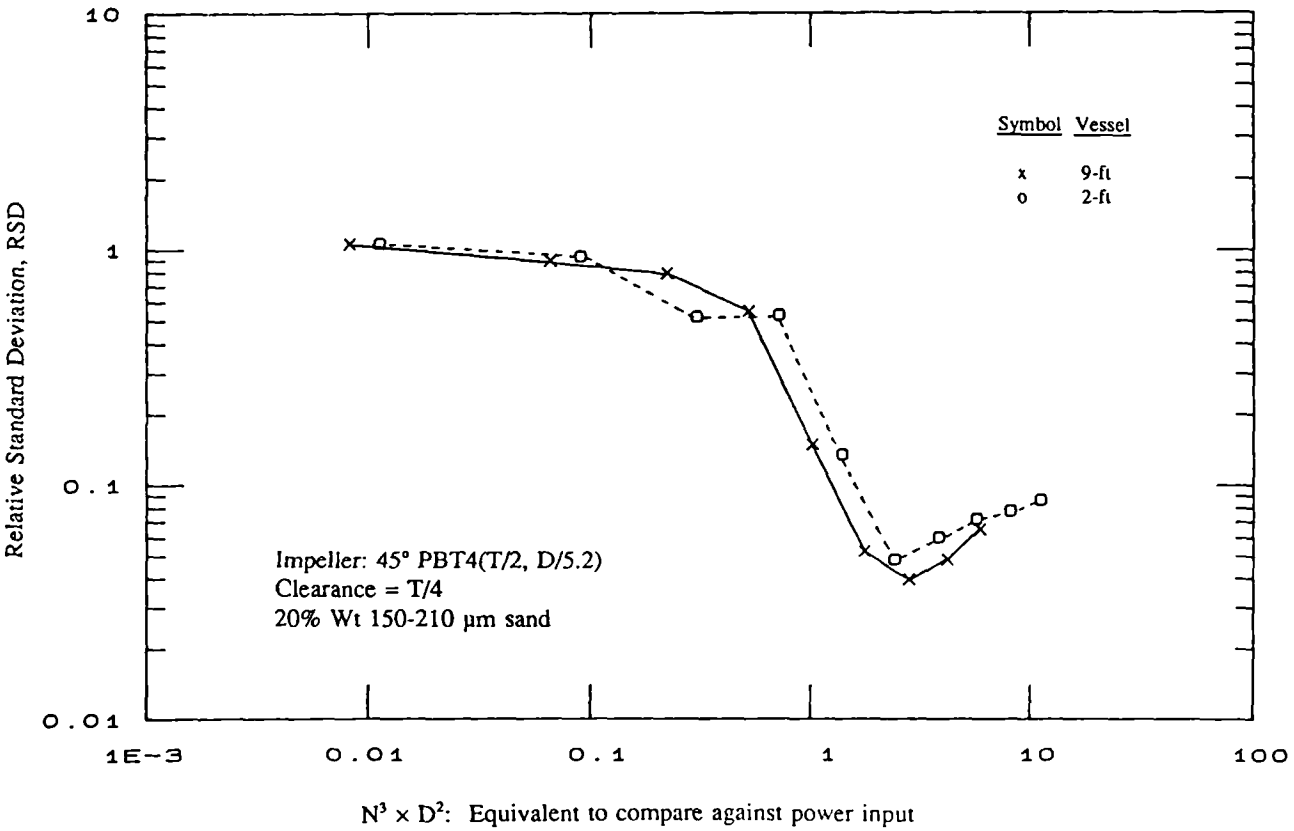

Fig 4.6.13 Scale-up Data: comparing against power input

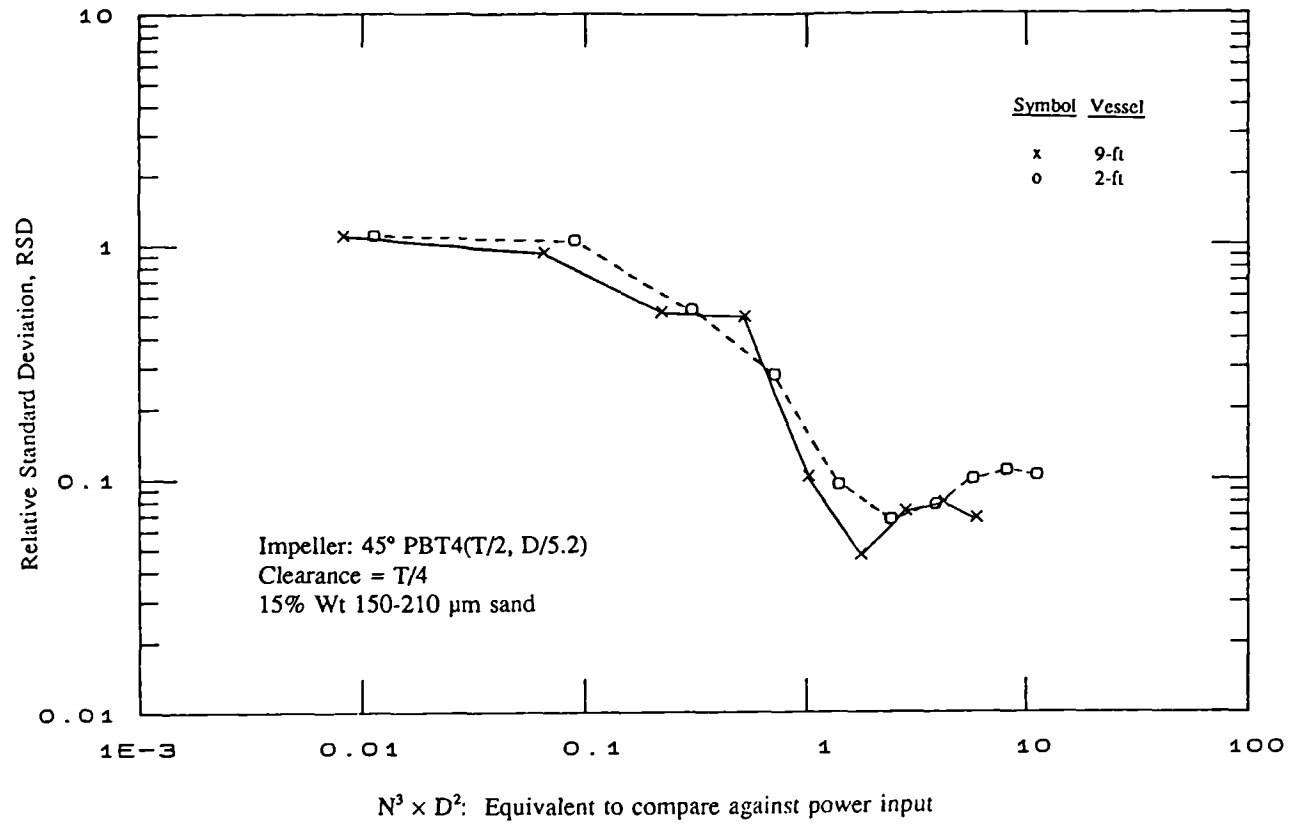

Fig 4.6.14 Scale-up Data: comparing against power input

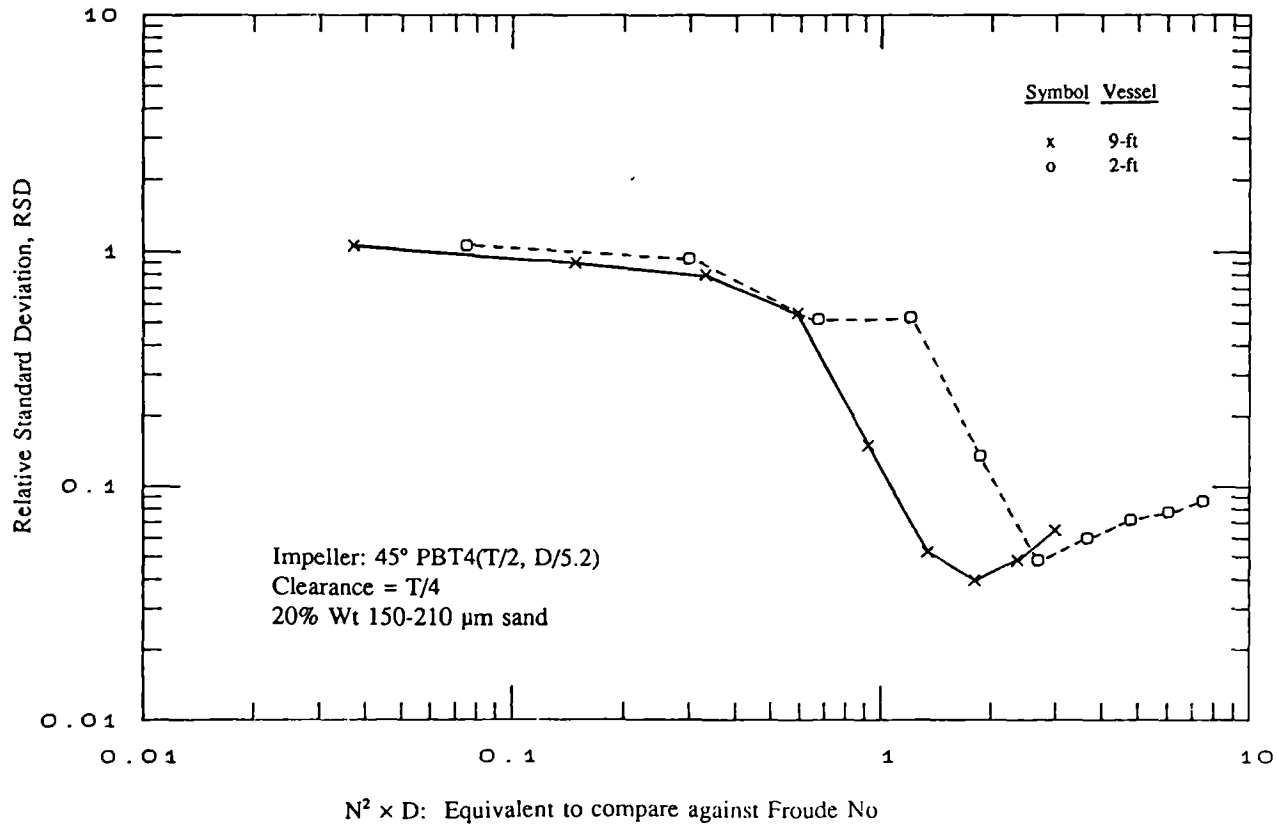

Fig 4.6.15 Scale-up Data: comparing against Froude No

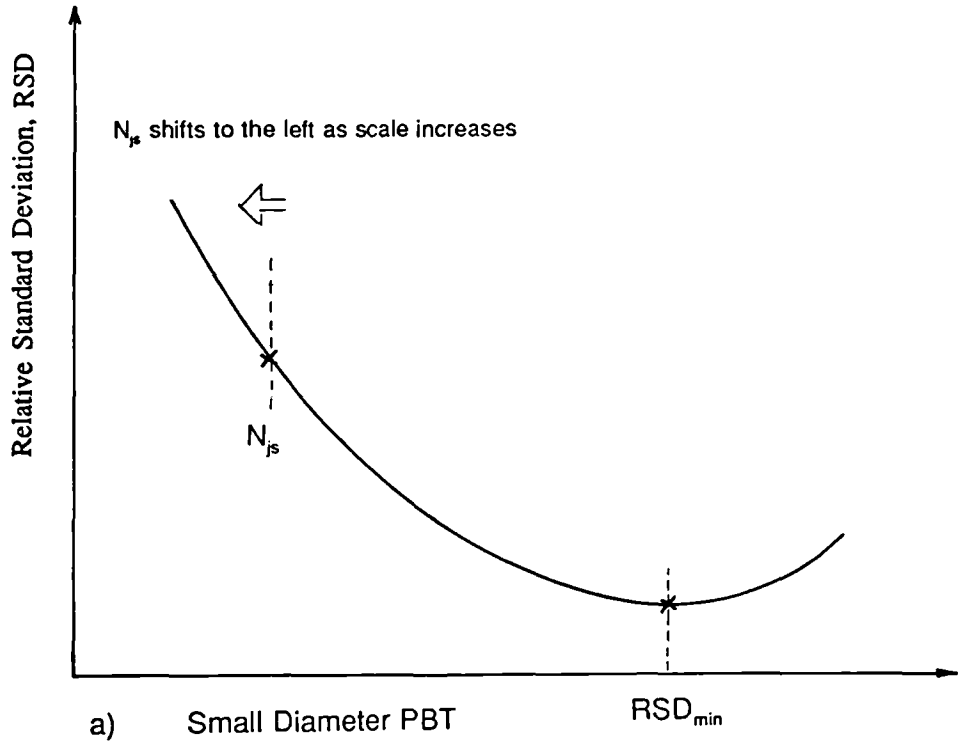

$N_{js} \propto D^{-0.85}$ $N_{RSD} \propto D^{-0.67}$

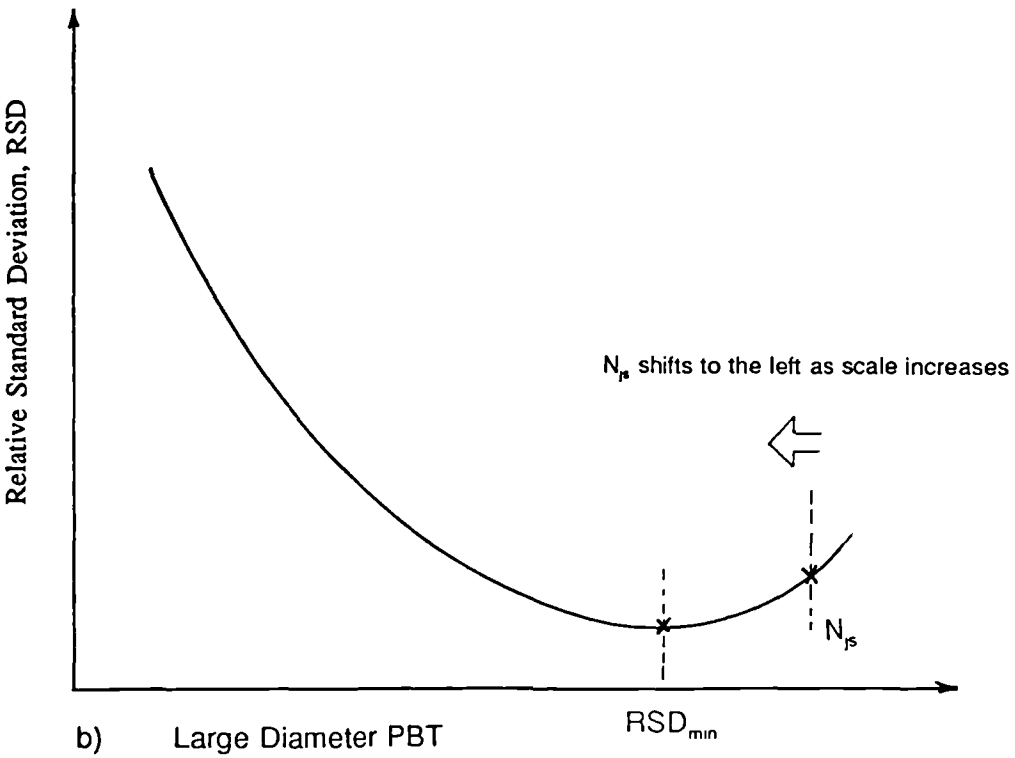

Fig 4.6.16 Effect of Scale on the Relative Position of N_{js} and RSD_{min}

4.7 FURTHER DISCUSSION

Further to the literature survey in Chapter 2, it is felt that sufficient modelling work has already been carried out by the other researchers. This thesis takes on the role of understanding the mixing behaviour by comparing geometries which are commonly used. Knowledge so gathered will be used to verify and improve on the existing models. Currently, measurements of power, flow pattern, solids suspension and distribution in a wide range of geometries have been carried out (Sec 4.1 to 4.6). Results so gathered will be used to compare the validity of the models.

There are three objectives in this section. It verifies/improves the existing solids suspension and distribution models, engineering solutions for solid-liquid mixing design will be proposed and areas for further study will be highlighted as a result of this study.

4.7.1 Overall Suspension Results

The just suspension data were analyzed by performing a multiple regression of N_{js} on Po, X, (D/T) and T. All the N_{js} results in this study were included, together with results from previous work (Appendix F). The result of the regression is:

$$N_{js} \propto Po^{-0.33}\, X^{0.13} \left(\frac{D}{T}\right)^{-0.89} T^{-0.79} \qquad \text{...eqn(4.7.1)}$$

The correlation coefficient, r^2, is 97% and F-ratio is 759 for 84 data points. The individual t-values for the exponents of Po, X, (D/T) and T are 10.1, 10.9, 16.0 and 39.0 and they have all satisfied the 95% standard t-test. The constant for eqn 4.7.1 is equal to 0.95 with a standard deviation of ± 10%. A plot of the regression line is presented in Fig 4.7.1. The 95% confidence intervals for the coefficient estimated are given in Table 4.7.1.

It would be useful also to check the sensitivity of the scale-up exponent based on the accuracy of the measurements. For a typical just suspension speed measurement of 200 rpm in T_{61} and 57 rpm in T_{267}, just suspension speeds are repeatable up to ± 5 and ± 2 rpm respectively. This would give a D exponent range of -0.79 to -0.87, with a mean value of -0.83. This is comparable to the 95% confidential intervals proposed in Table 4.7.1.

Table 4.7.1 95% Confidence Intervals for Parameters in Eqn 4.7.1

Parameter	Exponents on Parameter		
	Lower Limit	Upper Limit	Average
Po	-0.40	-0.27	-0.33
X*	0.10	0.14	0.12
(D/T)	-1.00	-0.78	-0.89
T	-0.83	-0.75	-0.79

* $N_{js} \propto X^{0.13}$ is forced fitted

N.B. If power number is assumed constant, analysis of the scale-up results gives $N_{js} \propto T^{-0.83}$, 95% confidence limits on the exponent of T ranged from -0.81 to -0.85 (Sec 4.6.2).

4.7.2 Comparing to the Suspension Models

Referring to Section 2.1.8, the theoretical models which have been reviewed so far can generally be classified into two categories; namely those in which particles are believed to be picked up by turbulent eddies (eg Baldi 1978, Ditl 1985) and those in which particles are believed to be picked up by fluid flow (eg Shamlou 1987, Wichterle 1988). There is a third category in which the suspension model is not based on an independent mechanism, but is simulated by another phenomenon of which the researchers had more modelling experience, such as pump flow and fluidisation (Molerus 1987).

According to the nature of the models, they can be further subdivided into three groups but these groups do not seem to bear direct relationship to the mechanisms on which they are based. The first group relies on single correlations to describe the influence of physical parameters and geometrical configurations on N_{js} (eg Zwietering 1958, Buurman 1985 and Shamlou 1987). The second group of models suggests that particles are suspended by two different mechanisms. There exist critical parameters which determine which of the two mechanisms is governing the suspension, they can be a function of diameter ratio (d_p/T,

Mersmann 1985), Archimedes number (Molerus 1987) and particle diameter to eddy size (Ditl 1985). The final group suggests that there is a continual variation of exponents on the individual parameters (Wichterle 1988).

Results from this thesis are initially compared to those of authors who have produced single correlations to describe the suspension phenomena (Table 4.7.2). Later the results will be checked against other models to see if the suspension correlation can best be described by more than one correlation and if the proposed critical parameters are sufficient to distinguish them.

(i) Single Correlation Models

Table 4.7.2 Single Correlation Models

Reference	Correlation	Remarks
Zwietering 1958	$N_{js} = s\, \nu^{0.1} \left(\frac{g\, \Delta\rho}{\rho_L} \right)^{0.45} d_p^{0.2}\, X^{0.13}\, D^{-0.85}$	"s" depends on (T/D), (T/C) and impeller type
Buurman 1985	$N_{js} \propto \left(\frac{g\, \Delta\rho}{\rho_L} \right)^{1/2} d_p^{1/6}\, D^{-2/3}$	
Shamlou 1987	$N_{js} = A\, Po^{-1/3} \left(\frac{g\, \Delta\rho}{\rho_L} \right)^{1/2} d_p^{1/6}\, C_v^{1/3}\, T\, D^{-5/3}$	"A" is equal to 3.4 for (D/T) $\leq$ 0.5 (Zolfagharian 1990)

Suspension results from this study compare favourably with Zwietering's correlation (Table 4.7.2). Analysis of Zwietering's data for axial flow turbines (propellers) shows that $s \propto (D/T)^{-0.82}$. Combining with the scale effect on just suspension speed, i.e. $N_{js} \propto D^{-0.85}$, eqn 4.6.5 can be re-arranged as:

$$N_{js} \propto \left(\frac{D}{T}\right)^{-0.82} D^{-0.85} \qquad \text{...eqn(4.7.2)}$$

The exponent on (D/T) from this work is -0.89, which compared well with Zwietering's -0.82 for propellers. The slight increase in the exponent could be attributed to the presence of radial flow in pitched blade turbines. Evidence for this can be found in Zwietering results where a much higher exponent for disc turbines is quoted $\{s \propto (D/T)^{-1.5}\}$. For constant (D/T) ratio, the dependence of N_{js} on length scale according to eqn 4.7.1 and 4.7.2 are $N_{js} \propto T^{-0.79}$ and $N_{js} \propto D^{-0.85}$ respectively. The exponent on D (scale-up effect) in the Zwietering correlation was an average over a range of test conditions: the actual exponent ranged from -0.78 to -0.91 and is impeller dependent. This again compares well with the exponent of -0.79 suggested by this study.

There is very little difference between Buurman and Shamlou et al's model, except Shamlou's model covered more physical parameters than the former. Shamlou proposed a diameter and scale effect of:

$$N_{js} \propto \left(\frac{D}{T}\right)^{-1} D^{-2/3} \qquad \text{...eqn(4.7.3)}$$

Their correlation suggested a weaker (D/T) ratio effect but a stronger scale effect on N_{js} than either this study or Zwietering's. However, the overall effect on impeller size (i.e. varying impeller diameter in a fixed diameter vessel) remains the same as that in eqn 4.7.2 (i.e. $N_{js} \propto D^{-1.67}$). Their model suggests a $N_{js} \propto D^{-2/3}$ relationship, which implies a power per unit volume rule for scale up. This has exceeded the 95% confidential limits of the scale effect results (-0.67 as against -0.83 to -0.75 in Table 4.7.1). In other words, results from this investigation cannot be described satisfactorily by their model.

The author derived the $N_{js} \propto D^{-2/3}$ relationship by relating the energy dissipation rate at the vessel base to the fluid force acting on the particles. He further assumed that the total energy dissipation rate is proportional to that of close to the vessel base. Therefore, for constant power input:

$$P/V \propto N^3 D^5/T^3$$

i.e. $N \propto D^{-2/3}$

The three single model correlations presented in Table 4.7.2 show a very similar density effect (i.e. ρ_L and $\Delta\rho$ on N_{js}). However, Shamlou's model predicts a $Po^{-1/3}$ and $C_v^{1/3}$ effect. These two proposed parameters are of different format from that of Zwietering's and will be the subjects of the following discussion.

It has been widely postulated that the fluctuating velocity of the eddies (turbulent model) or the total fluid force acting on the particles (flow model) is proportional to the rate of energy dissipation (i.e. power input) which naturally leads to a $N_{js} \propto Po^{-1/3}$ relationship. Results from this thesis have clearly confirmed the above relationship (Sec 4.7.1). Thus, power number can be included in the suspension correlation to improve confidence in N_{js} prediction.

Traditionally, the solid to liquid mass ratio, X is used to account for the effect of solids concentration on N_{js}. This came about when Zwietering first adopted the parameter in 1958 and it has described the concentration effect satisfactorily ever since. The deficiency of this parameter is that it carries little physical significance. N_{js} results obtained from the four scales (T_{31}, T_{61}, T_{183} and T_{267}) are used to verify the two different ways of correlating the data (i.e. Zwietering: $N_{js} \propto X^{0.13}$, Shamlou: $N_{js} \propto C_v^{1/3}$). Results are presented as plots of N_{js} against $X^{0.13}$ (Fig 4.7.2) and $C_v^{1/3}$ (Fig 4.7.3). It is clear that the former approach gives a much better fit to the results. From statistical analysis, if C_v is to be used, the best fit line is given by $N_{js} \propto C_v^{0.13}$. More detailed comparison between these two approaches would be valuable, especially for mixing processes with extreme solids concentrations (i.e. $C_v > 20\%$ or $C_v < 0.1\%$), where the solid to liquid mass ratio approach is likely to break down.

To conclude, suspension results from this study compare favourably with Zwietering's correlation. The power number term (i.e. $Po^{-1/3}$) can be incorporated into the equation. The solids to liquid mass ratio, X correlates the concentration effect satisfactorily. The Zwietering correlation is still recommended for general use:

$$N_{js} = s\, \nu^{0.1} \left(\frac{g\, \Delta\rho}{\rho_L} \right)^{0.45} d_p^{0.2}\, X^{0.13}\, D^{-0.85} \qquad \text{...eqn(4.7.4)}$$

Results from this study based on Zwietering's format are recommended for pitched blade turbines:

$$N_{js} = s_1 \, Po^{-0.33} \, \nu^{0.1} \left(\frac{g \, \Delta\rho}{\rho_L} \right)^{0.45} d_p^{0.14} \, X^{0.13} \left(\frac{D}{T} \right)^{-0.89} T^{-0.79} \qquad \text{...eqn(4.7.5)}$$

$$s_1 = 3.6$$

Note that the exponent on d_p has been modified in order to keep eqn 4.7.5 dimensionless. The exponent on d_p is unlikely to follow a single power law relationship (Mak 1988b). Zolfagharian's thesis (1990) covered a very impressive range of particle size effect, the results of which can be used to build in an extra safety margin if necessary. Analysis of hydrodynamics range on drag coefficient may shed light on the understanding of the particle size effect.

(ii) Correlations with a Critical Dividing Parameter

Table 4.7.3 presents a summary of models in which the authors believed that solids suspension involves more than one mechanism. Therefore two correlations are required to describe the suspension process and they can be distinguished by a critical parameter.

For all the models listed, the exponent on ρ_L and $\Delta\rho$ are very similar. The major difference lies on the exponents of d_p (-0.07 by Ditl to 0.56 by Molerus) and D (-0.5 by Mersmann to -0.89 by Molerus). It is interesting to note that the critical parameters so proposed by different researchers differ markedly from each other. Mersmann's critical parameter is geometrically based (i.e. d_p/T) while Molerus uses the physical properties based on Archimedes number. Ditl uses a combination of physical properties, geometrical parameters as well as power number to establish the dividing criteria.

Neither of Mersmann's models satisfy the 95% confidential limits on D exponent (Table 4.7.1) and therefore are rejected. Results from this study give an Archimedes number of 72 (i.e. Ar > 40). However, Molerus' correlation for Ar > 40 does not fit in with concentration and scale-up results from this study (i.e. Molerus: $N_{js} \propto C_v^{0.36} \, T^{0.64}$).

Table 4.7.3 Correlations with Critical Dividing Parameter

Reference	Correlation	Range in this work
Mersmann 1985	$(d_p/T) < 10^{-3}$: $N_{js} \propto \left(\frac{g\ \Delta\rho}{\rho_L}\right)^{0.5} d_p^{0.5}\ D^{-1}$	$6.0 \times 10^{-4} \le (d_p/T) \le 6.7 \times 10^{-5}$
	$(d_p/T) > 10^{-3}$: $N_{js} \propto \left(\frac{g\ \Delta\rho}{\rho_L}\right)^{0.5} D^{-0.5}$	
Molerus 1987	Ar ≤ 40: $N_{js} \propto \left(\frac{d_p\ g\ \Delta\rho}{\rho_L}\right)^{0.56} \nu^{-0.11}\ D^{-1}\ T^{0.11}$	Ar = 72
	Ar > 40: $N_{js} \propto (g\ \Delta\rho)^{0.5} \left(\frac{d_p}{\rho_L}\right)^{0.14} (C_v\ H)^{0.36}\ D^{-1}$	
Ditl 1985	$(d_p/\eta_t) \ge 32$: $N_{js} \propto \nu^{0.1}\ d_p^{-0.07} \left(\frac{g\ \Delta\rho}{\rho_L}\right)^{0.45} \left(\frac{D}{T}\right)^{-0.86} D^{-0.58}$	$(d_p/\eta_t) < 6$
	$(d_p/\eta_t) < 32$: $N_{js} \propto \nu^{0.1}\ d_p^{0.1} \left(\frac{g\ \Delta\rho}{\rho_L}\right)^{0.45} \left(\frac{D}{T}\right)^{-0.69} D^{-0.75}$	

Note: $$Ar = \left(\frac{d_p^3\ g\ \Delta\rho}{\nu^2\ \rho_L}\right) \qquad \text{...eqn(4.7.6)}$$

$$\frac{d_p}{\eta_t} = \left(\frac{4\ Po}{\pi}\right)^{1/4} \left(\frac{d_p}{D}\right) \left(\frac{N\ D^2\ \rho_L}{\mu}\right)^{3/4} \left(\frac{T}{D}\right)^{-3/4} \qquad \text{...eqn(4.7.7)}$$

Results from this work are analysed according to Ditl's critical particle diameter (i.e. d_p/η_t) and it was found that in all cases (d_p/η_t) is small than 6. According to Ditl the following correlation applies:

$$(d_p/\eta_t) < 32: \quad N_{js} \propto \nu^{0.1}\, d_p^{0.1} \left(\frac{g\ \Delta\rho}{\rho_L}\right)^{0.45} \left(\frac{D}{T}\right)^{-0.69} D^{-0.75} \qquad \text{...eqn(4.7.8)}$$

The exponent of D lies within the 95% confindential interval of this analysis while the exponent of (D/T) is outside the limits (Table 4.7.1). Further statistical analysis was conducted by substituting the experimental data from this investigation into eqn 4.7.8. A relative standard deviation of ± 16% is given, as against ± 10% in eqn 4.7.1.

Although it is possible that the particles are suspended by two mechanisms according to a critical parameter, the correlations presented are inadequate to describe the data produced in this study. Another concern is that the critical parameters adopted by the various authors are of a very diverse physical nature and this is reflected by the contradictory theories of solids suspension mechanism.

(iii) Models with a Continual Variation of Exponents

Some researchers suggested that there is a continual variation of exponents in the suspension correlation. The models so established are not fully proven. Baldi et al (1978) used a turbulent model and from an analogy of the decay of turbulence behind a grid, they deduced a similar correlation to Zwietering's when C is equal to D (eqn 2.1.7). They commented that if the (C/D) ratio is changed the exponents in their correlation will also change. The exponents at (C/D) of 1 were determined experimentally and no theoretical relationship between the (C/D) ratio and predicted exponents were given in his paper. It is interesting to note that the critical parameter adopted by them (i.e. C/D) is again different from what had been reviewed previously.

Wichterle's model suggested that the exponents on physical properties will change according to Archimedes number but a single-power function $N_{js} \propto (D/T)^{4/3}\, D^{2/3}$ applies. However, his assumed exponent on scale does not agree with the results from this study.

Wichterle proposed:

$$N_{js}^{*} = N_{js}\,\mu^{-1/9}\,(g\,\Delta\rho)^{-4/9}\,\rho_L^{5/9}\,D^2\,T^{-4/3} = f\,(\,d_p^{*}\,) \qquad \text{...eqn(4.7.9)}$$

In the current study:

$$d_p^{*} = d_p\left(\frac{g\,\Delta\rho\,\rho_L}{\mu^2}\right)^{1/3} = constant$$

Therefore:

$$N_{js} \propto \nu^{1/9}\left(\frac{g\,\Delta\rho}{\rho_L}\right)^{4/9}\left(\frac{D}{T}\right)^{-4/3} D^{-2/3} \qquad \text{...eqn(4.7.10)}$$

4.7.3 A Final Remark on Solids Suspension Modelling

This study has demonstrated qualitatively and quantitatively that more than one mechanism is involved in suspending particles in a stirred vessel. The occurrence of a certain mechanism is geometry (Sec 4.1.2, Fig 4.1.6, Table 4.1.1 and 4.1.2) and physical property (Fig 4.1.9) dependent. Evidence is found in literature of a diverse range of exponents on d_p (eg 0 to 0.52 in Zolfagharian 1990) and D (Table 4.6.2).

A review of solids suspension models indicates that theoretical models can generally be classified into two categories; those in which particles are believed to be picked up by turbulent eddies and those where particles are picked up by fluid flow. Although both of these theories display considerable merit, there remains a number of questions to be resolved (Sec 2.1.8). To complicate the matter further, results from this study show that the suspension is also geometry dependent. Examples include flow interaction in dual impeller systems (Sec 4.5.3) and the removal of the central dead zone by a pitched blade turbine which depends on the impeller discharge and the curvature of the vessel base.

The added difficulty in modelling these complicated influences is that they are inter-related so that it is virtually impossible to study each effect in isolation. Until models are developed which can take account of these complex mechanisms, it is unlikely that any purely

theoretical model will be able to correlate the available experimental data. The suspension phenomenon is best described by empirical or semi-empirical models.

4.7.4 Modelling of Solids Distribution

Fig 4.4.5 has described the general behaviour of a RSD curve. In order to model a distribution process successfully, it is felt that two types of inter-related models are required, first one to identify the point of maximum homogeneity and second, a method of describing the rate of decreasing RSD relating to impeller speed/power input, for a given condition (Region B, Fig 4.4.5).

Results from this study show that power per unit volume has to remain constant in order to maintain the same degree of homogeneity across scales. A review of the available distribution models shows that most imply a constant tip speed scale up criterion (eg Barresi 1987, Shamlou 1989, Sec 2.2.2). Buurman measured the height of the slurry liquid interface and his model indicates a scale-up relationship of $N_{RSD} \propto D^{-0.78}$.

$$N_{RSD} \geq 4.47 \left(\frac{g\ \Delta\rho}{\rho_L} \right)^{0.5} \left(\frac{d_p}{D} \right)^{0.275} D^{-0.50} \qquad \text{...eqn(4.7.11)}$$

His model comes the closest in describing the results from this study (i.e. $f(Fr^*)$ results presented in the Appendices) but it still underestimates the power requirement for scaling up (Fig 4.7.4).

A basic distributed model can be established to predict the distribution quality (Region B, Fig 4.4.5) based on the results from this study:

Analysis of the scale-up results indicates a constant power per unit volume criterion. Therefore, the impeller speed required to achieve a certain degree of homogeneity, N_{RSD} can be given as:

$$N_{RSD} \propto T^{-2/3} \qquad \text{...eqn(4.7.12)}$$

Distribution tests with the three geometrically similar impellers showed that the results are neither correlated in terms of tip speed nor power input but are best described by the thrust number (Sec 4.3.5), thus:

$$N_{RSD} \propto \left(\frac{D}{T}\right)^{-2} \qquad \text{...eqn(4.7.13)}$$

Combining with eqn 4.7.12:

$$N_{RSD} \propto \left(\frac{D}{T}\right)^{-2} T^{-2/3} \qquad \text{...eqn(4.7.14)}$$

It is interesting to note that results from tests with the 30°, 45° and 90° PBT produce a regression line of $RSD \propto Po^{-0.14} N^{-1.91}$ (Fig 4.4.9), indicating a power number dependence of $Po^{0.07}$ on N_{RSD}. This is comparable to Magelli's (1991) suggestion of $N_{RSD} \propto Po^{0.08}$. However, as the effect of Po on N_{RSD} is relatively small when compared with other parameters, it is excluded from the distribution correlation to be established.

Further analysis of single impellers (PBT and FBT) at two clearances (T/4 and T/8) and dual impeller systems (upper at C=0.3T, lower at C=0.125T) showed that for constant impeller and vessel diameter the distribution quality is a function of impeller speed or tip speed only (Sec 4.5.4). This agrees with eqn 4.7.14.

Referring to the summary of distribution models in Table 2.2.1, Buurman proposed that $N_{RSD} \propto (g\ \Delta\rho/\rho_L)^{0.5}$ and all the other researchers also suggested that $N_{RSD} \propto U_t$, which is proportional to $(d_p\ \Delta\rho/\rho_L)^{0.5}$ in Newton's Law range. With this information, eqn 4.7.14 becomes:

$$N_{RSD} \propto d_p^{0.5} \left(\frac{g\ \Delta\rho}{\rho_L}\right)^{0.50} \left(\frac{D}{T}\right)^{-2} T^{-2/3} \qquad \text{...eqn(4.7.15)}$$

The assumption of $N_{RSD} \propto d_p^{0.5}$ is close to a preliminary result reported previously ($N_{RSD} \propto d_p^{0.6}$, Mak 1988a).

All results measured in the distributing region (Region B, Fig 4.4.5) were analyzed by performing a multiple regression of RSD on N, (D/T), T and C_v. The result of the regression is:

$$RSD = 0.007\ C_v^{0.18}\ N^{-3.67} \left(\frac{D}{T}\right)^{-7.53} T^{-2.52} \qquad \text{...eqn(4.7.16)}$$

The correlation coefficient, r^2, is 81% and F-ratio is 49 for 49 data points. The constant has a relative standard deviation of ± 14%. The individual t-values for exponents of C_v, N, (D/T) and T are 0.8, 13.9, 11.3 and 11.3. With the exception of the concentration effect (i.e. C_v), all exponents satisfied the 95% standard t-test.

Eqn 4.7.16 can be re-arranged into the following format:

$$RSD^{0.27}\ N = 0.26 \left(\frac{D}{T}\right)^{-2.05} T^{-0.69} \qquad \text{...eqn(4.7.17)}$$

To maintain a specific distribution quality, RSD = constant:

$$N_{RSD} \propto \left(\frac{D}{T}\right)^{-2.05} T^{-0.69} \qquad \text{...eqn(4.7.18)}$$

This confirms the deduction given by eqn 4.7.15. Distribution results employed for the regression are presented in Fig 4.7.5 according to eqn 4.7.15.

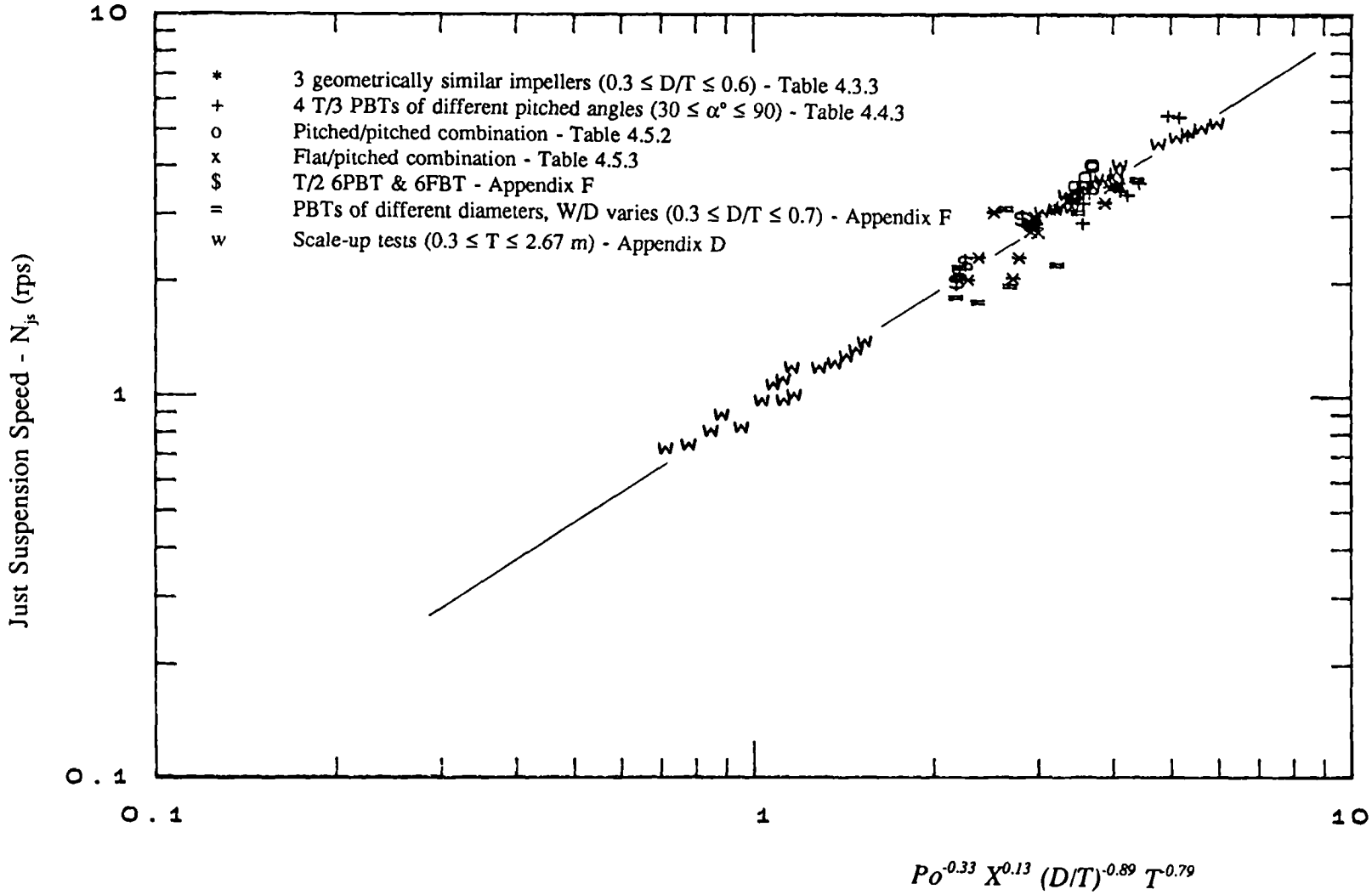

Fig 4.7.1 Overall Regression of all Suspension Data

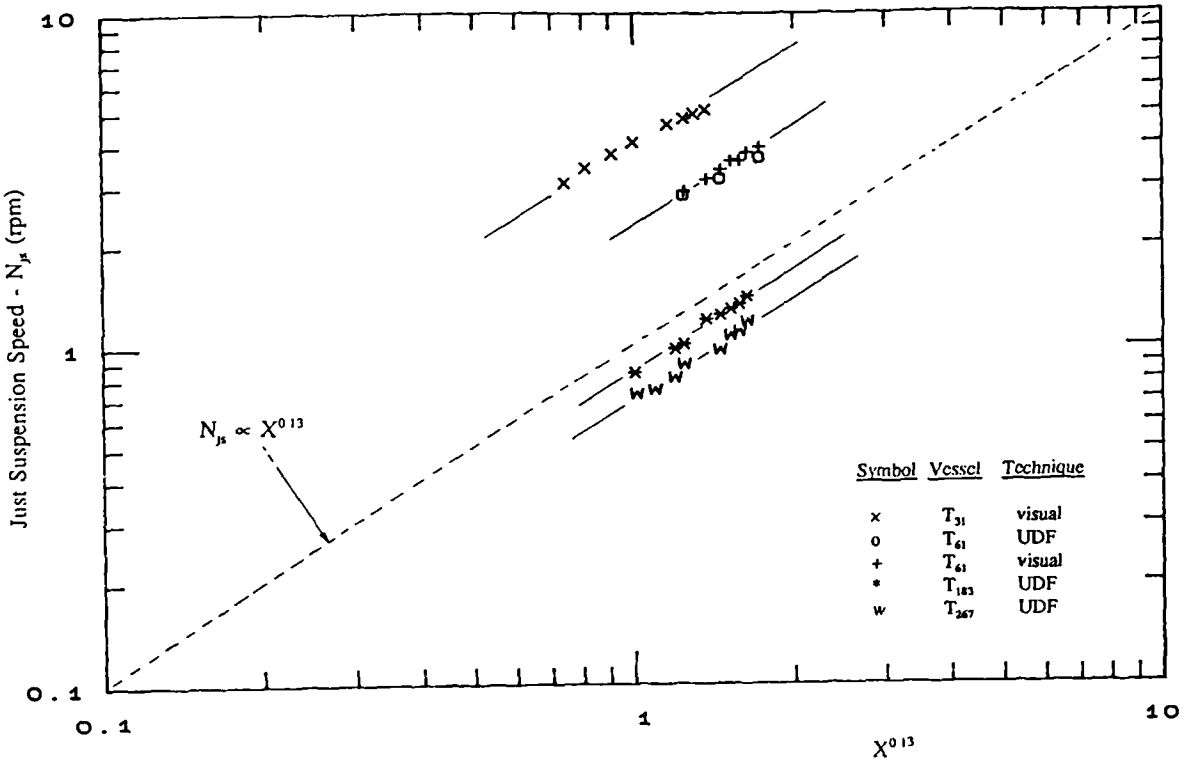

Fig 4.7.2 Plot of N_{js} versus $X^{0.13}$

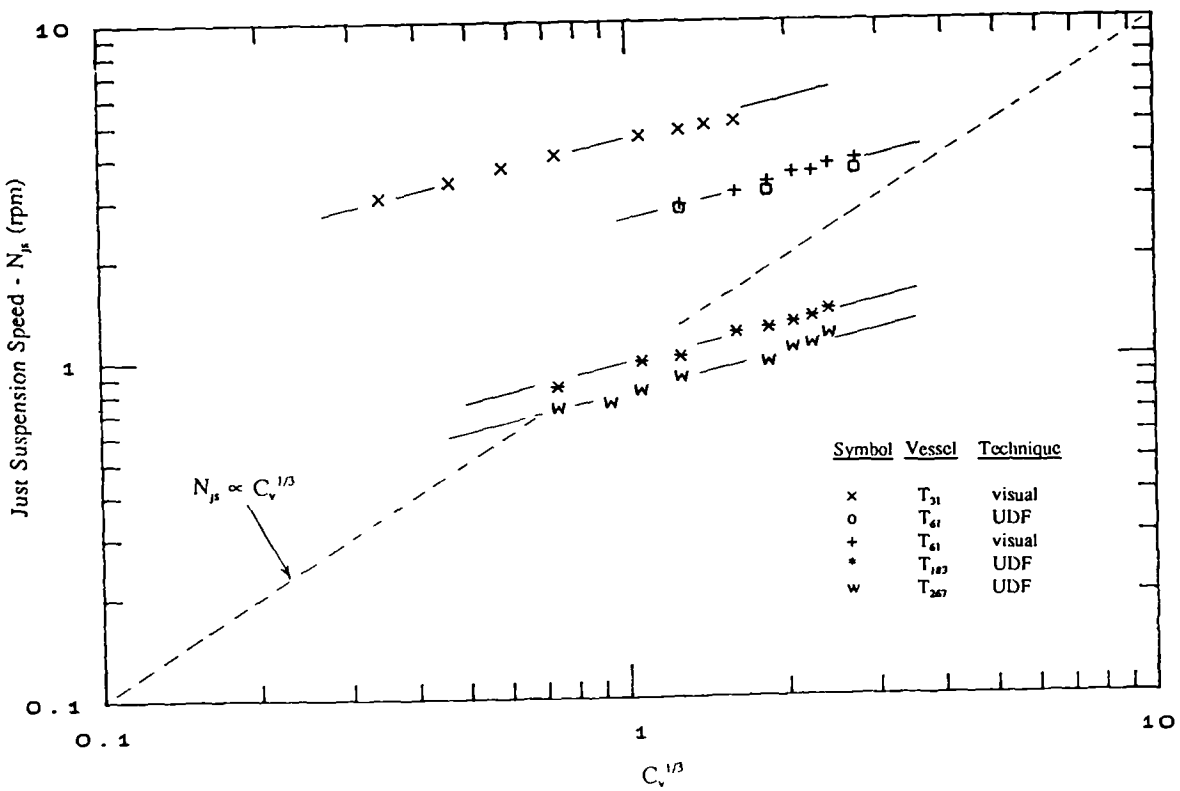

Fig 4.7.3 Plot of N_{js} versus $C_v^{1/3}$

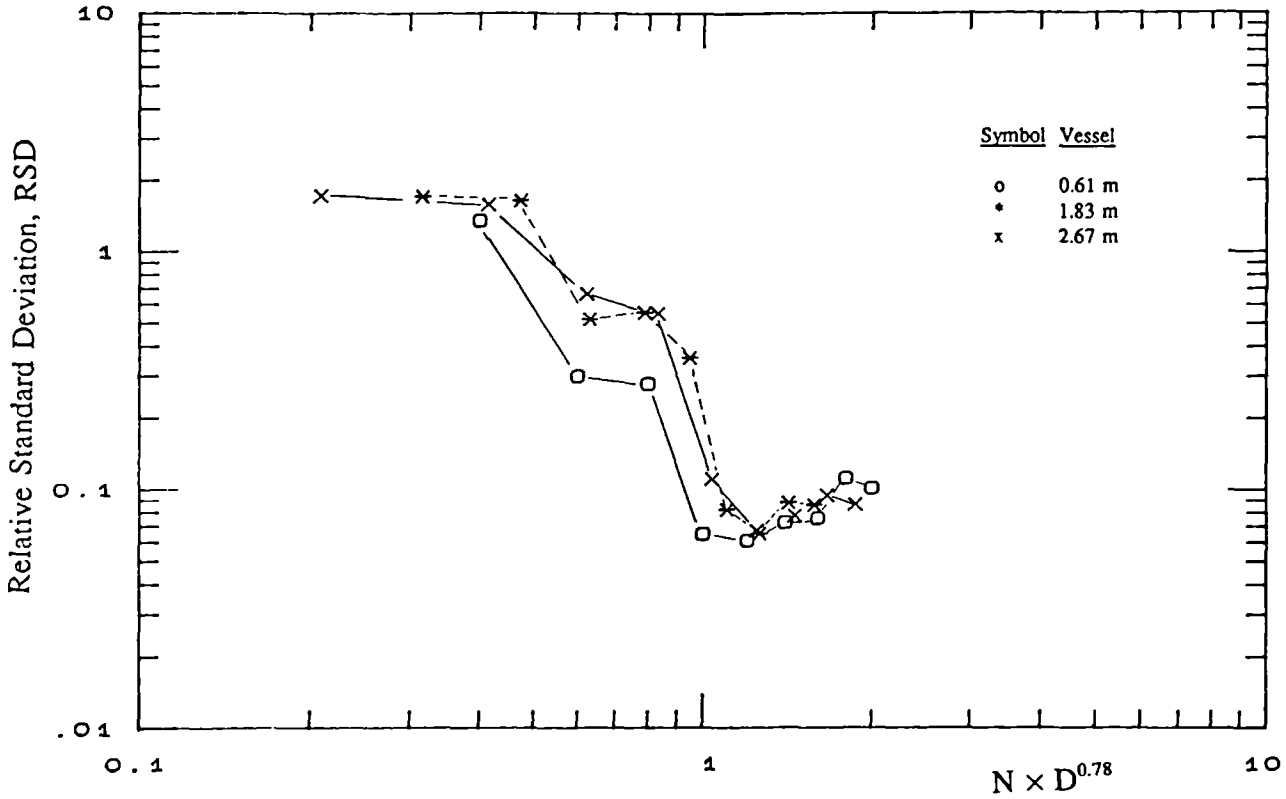

Fig 4.7.4 Scale-up Data According to Buurman's Model ($N_{RSD} \propto D^{-0.78}$)

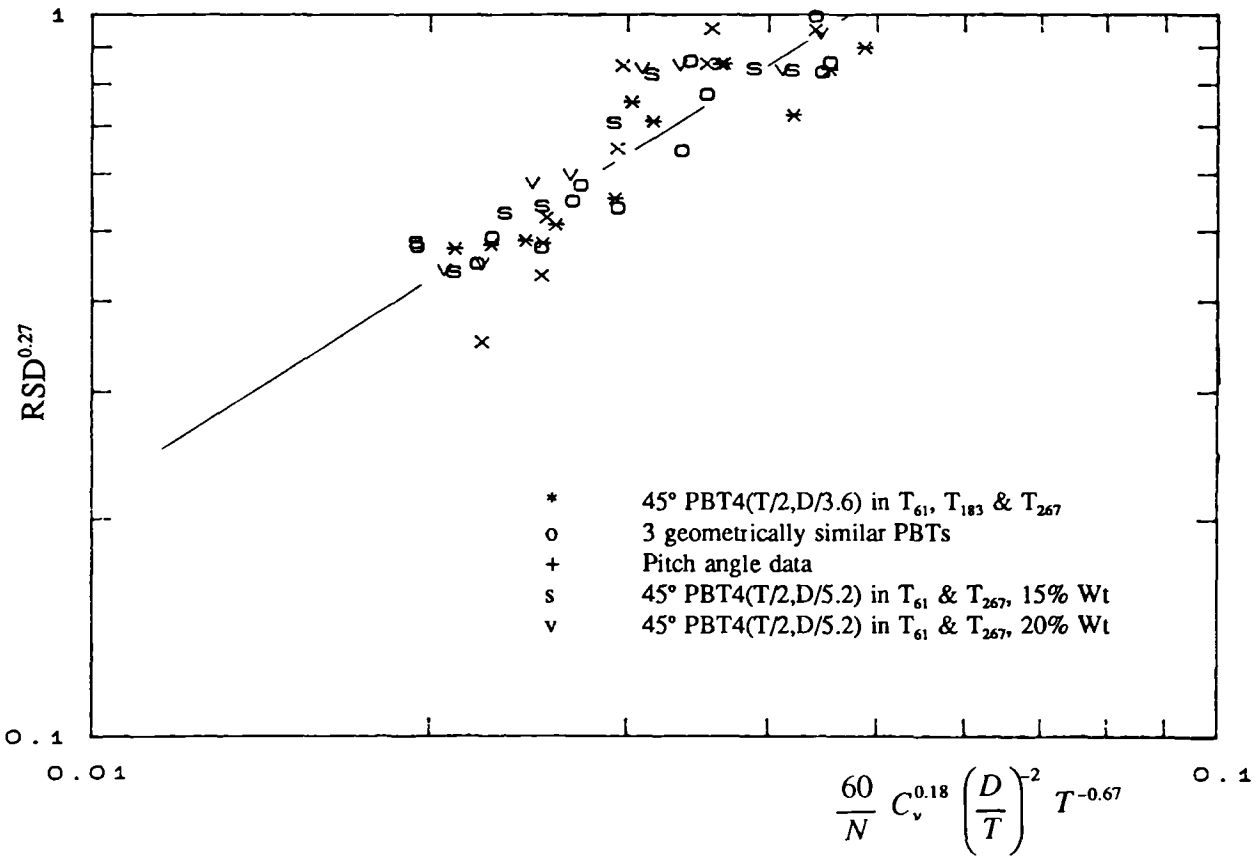

Fig 4.7.5 Distribution Data According to Eqn 4.7.15

CHAPTER 5: CONCLUSIONS AND RECOMMENDATIONS

5.1 CONCLUSIONS

This research has concentrated on the study of flow pattern, power inputs, solids suspension and distribution in stirred vessels. Data have been obtained for three geometrically similar pitched blade turbines ($0.3 \leq D/T \leq 0.6$, $T/4 \leq C \leq T/8$), five turbines with pitch angles ranging from 30° to 90° ($T/4 \leq C \leq T/8$), two dual impeller systems (dual pitched and flat/pitched) and four vessel sizes ($0.31 \leq T \leq 2.67$ m). The following conclusions can be drawn:

Three types of particle flow pattern have been identified on the vessel base; vortexing is found at the centre, circumferential flow takes place at the outermost regions with radial flow in between (Fig 4.1.6).

The use of average density to allow for the presence of solids in estimating the solid-liquid mixing power requirement has been validated up to 2.67 m scale (T_{267}), with a solids concentration of 1 to 40% Wt.

The effect of solids concentration on N_{js} was examined in four scales and a solids concentration range of 0.1 to 40% Wt. The results show good agreement with Zwietering's recommendation (i.e. $N_{js} \propto X^{0.13}$).

Small diameter PBTs are more efficient for solids suspension than those of larger diameter in dished based vessels. This can be explained by differences in direction of impeller discharge flow. Results show that the T/1.7 PBT required between 5 and 10 times the power of a T/3 PBT for the same suspension duty.

The effect of impeller diameter on N_{js} is found to be vessel base dependent. Results from this study obtained in the 0.61 m diameter vessel show good agreement with work reported with similar geometries.

i.e. $N_{js} \propto D^{-1.02}$

Just suspension data from the pitch angle impellers show that for each angle there is an optimum clearance.

Both dual impeller combinations tested in this study require significantly more power to just suspend solids than the single impeller. This is believed to be caused by the interaction between the flow patterns of the upper and the lower impeller.

The scaling effect put forward by Zwietering for solids suspension has been confirmed by this study up to vessel diameters of 2.67 m.

The overall correlation for N_{js} based on data from this study (with Po) is given as:

$$N_{js} \propto Po^{-0.33}\ X^{0.13} \left(\frac{D}{T}\right)^{-0.89} D^{-0.79}$$

for dual impeller systems, Po should be replaced by Po_c.

Compared with just suspension speed, impeller power number appears to have less influence on solids distribution.

Distribution tests with the three geometrically similar impellers show that the results are neither correlated in terms of tip speed nor power input but are best described by the thrust number (i.e. $N^2 D^4$).

In general, dual impeller systems improve solids distribution compared with those of a single impeller.

The radial concentration profiles measured in T_{183} were flat, except when the probe was at the clear-liquid/solid-liquid interface. Although the flatness of radial profile has already been reported by other authors, it is the first time this result has confirmed in vessel of industrial scale. The use of a one-dimensional steady state model by other researchers is therefore justified.

The use of constant tip speed as the scale-up criterion for solids distribution underestimates the power requirement. This study indicates that equal power per unit

volume is required to achieve the same degree of homogeneity.

Summarising all the distribution results, the following equation can be used to describe the speed requirement to match a specific RSD:

$$N_{RSD} \propto d_p^{0.5} \left(\frac{g\ \Delta\rho}{\rho_L} \right)^{0.50} \left(\frac{D}{T} \right)^{-2} T^{-2/3}$$

This study has shown that some impellers (eg D/T=0.3) attained the just suspension condition before the point of maximum homogeneity. For some other impellers (eg D/T=0.5), just suspension speeds are higher than $N_{RSD,\ min}$. Therefore, the use of homogeneity data as the criterion for N_{js} should be interpreted with care.

The scale-up relationships were found to be different for solids suspension and distribution (i.e. $N_{js} \propto D^{-0.83}$ and $N_{RSD} \propto D^{-0.67}$). If the just suspension condition was used as the scale-up criterion, the solids distribution quality will be worse as the scale increases.

In addition to these conclusions, the following improvements on experimental techniques were made:

The ultrasonic Doppler flowmeter technique initiated by Buurman in 1985 to measure the just suspension speed was adopted in this study. Back to back comparisons were made between the visual and UDF techniques and the following relationship was obtained:

$$Visual\ N_{js} = k\ UDF\ N_{js}, \qquad k = 1.07 \pm 0.01$$

Application of such a correction factor to the visual observation allowed direct comparison of N_{js} over the full range of scales.

Local solids concentrations were measured by a solids concentration probe developed by BHR Group Ltd from a design used at the Warren Spring Laboratory. The initial

calibration was largely conducted by Ruszkowski (1985). This study has demonstrated the suitability of this technique to large scale work and overcomes the problem of limited concentration range encountered by optical techniques.

5.2 SUGGESTIONS FOR FUTURE WORK

In conducting the present research programme a number of important questions arose which could not be answered as part of this work. It is recommended that the following could form part of any future investigation into the area of solid-liquid mixing:

It appears that there is more than one mechanism responsible for solids suspension. It would be valuable to design experiments in which only one mechanism is controlling and hence study the suspension behaviour accordingly. In addition, laser measurements of velocity and energy distribution at vessel base are recommended. This information aid to clarify the nature of suspension mechanism(s) at just suspension condition.

The flow pattern of an impeller has been shown to have a substantial influence on solids suspension and distribution but these effects are virtually impossible to quantify by normal experimental means. A computational fluid dynamics study on flow interactions and their effects on solid-liquid mixing may be the most effective way of clarifying this area.

In view of the similarities between the suspension of particles, fluidisation, transportation of sediments and solids, a comparative study of present knowledge in these processes would be a fruitful exercise.

This study demonstrates that power number increases with vessel sizes. This does not affect the validity of the scale-up rules as long as geometrical similarity is assumed. However, it will certainly affect the choice of motor and gear box. Further study is necessary to clarify the effect of scale on power number.

REFERENCE

Al-Dhahir, L., "Solids Suspension in Viscous Newtonian and Non-Newtonian Liquids" PhD Thesis, University College London, Nov 1990

Barresi, A. and Baldi, G., "Solid Dispersion in an Agitated Vessel" Chem Eng Sci, Vol 42, No 12, pp 2949-2956, 1987

Barresi, A. and Baldi, G., Shorter Communication : "Solid Dispersion in an Agitated Vessel: Effect of Particle Shape and Density" Chem Eng Sci, Vol 42, No 12, pp 2969-2972, 1987

Bates, R. L., Fondy, P. L. and Corpstein, R. R., "An Examination of Some Geometric Parameters of Impeller Power" I & E C Process Design and Dev, Vol 2, No 4, pp 310-314, Oct 1963

Brodkey, R. S. and Hershey, H. C., "Transport Phenomena - A Unified Approach" McGraw-Hill, 1988

Bohnet, M. and Niesmak, G., "Distribution of Solids in Stirred Suspensions" German Chem Eng, Vol 3, pp 57-65, 1980

Bourne, J. R. and Sharma, R. N., "Suspension Characteristics of Solid Particles in Propeller-agitated Tanks" 1st European Conf on Mixing and Centrifugal Separation, Cambridge, England, BHRA. Paper B3 (9-11 Sept 1974)

Bujalski, W., "Three Phase Mixing: Studies of Geometry, Viscosity and Scale" PhD Thesis, University of Birmingham, Dec 1986

Buurman, C., Resoort, G. and Plaschkes, A., "Scale-up Rules for Solids Suspension in Stirred Vessels" 5th European Conf on Mixing, Wurzburg, W Germany, BHRA. Paper 5 (10-12 June 1985)

Buurman, C., "Stirring of Concentrated Slurries: A Semi-empirical Model for Complete Suspension at High Solids Concentrations and 5 m^3 Verification Experiments" Fluid Mixing IV, I Chem E Symposium Series No 121, pp 343-350, Sept 1990

Chapman, C. M., "Studies of Gas-Liquid-Particle Mixing in Stirred Vessels" PhD Thesis, University College London, Sept 1981

Chudacek, M. W., "Solids Suspension Behaviour in Profiled Bottom and Flat Bottom Mixing Tanks" Chem Eng Sci, Vol 40, No 3, pp 385-392, 1985

Chudacek, M. W., "Relationship between Solids Suspension Criteria, Mechanism of Suspension, Tank Geometry and Scale-up Parameters in Stirred Tanks" Ind Eng Chem Fundam, Vol 25, pp 391-401, 1986

Conti, R. and Baldi, G., "Complete Suspension of Particles in Mechanically Agitated Vessels : Effect of System Geometry" Int Sym on Mixing, Faculte Poly de Mons, Paper B2, 21-24th Feb 1978

DeRitter, G. R., "Multiphase Solid-liquid-liquid Mixing in Stirred Tanks" MSc Thesis, New Jersey Institute of Technology, 1990

Ditl, P. and Rieger, F., "Suspension of Solid Particles" -Letter to the Editors, Chem Eng Sci, Vol 35, pp 764-765, 1980

Ditl, P. and Rieger, F., "Suspension of Solids Particle - Relative Velocity of Particles in Turbulent Mixing" 5th European Conf on Mixing, Wurzburg, W Germany, BHRA. Paper 8 (10-12 June, 1985)

Einenkel, W. D., "Influence of Physical Properties and Equipment Design on the Homogeneity of Suspensions in Agitated Vessels" Ger Chem Eng, Vol 3, pp 118-124, 1980

Einenkel, W. D. and Mersmann, A., "Erforderliche Drehzahlen zum Suspendieren in Rührwerken" Verfabrenstechnik (Mainz), Vol 11, No 2, pp 90-94, 1977

Fawcett, N. S. J., "The Mean Flow Field in the Discharge of Pitched-blade Turbines" FMP Interim Report 1046, BHRA, October 1989

Frijlink, J. J., Kolijn, M. and Smith, J. M., "Suspension of Solids with Aerated Pitched Blade Turbines" IChemE Sym Series No 89, Fluid Mixing II, Bradford, 1984

Hamby, N., Edwards, M. F. and Nienow, A. W., "Mixing in the Process Industries" Butterworths, 1985

Hepworth Minerals and Chemicals Limited, Private communication with The Technical Department of Building Materials Division, July 1992

Herringe, R. A., "The Behaviour of Mono-size Particle Slurries in a Fully Baffled Turbulent Mixer" 3rd European Conference on Mixing, York, England, BHRA Paper D1, 4-6th April 1979

Hirsekorn, F. S. and Miller, S. A., "Agitation of Viscous Solid-Liquid Suspensions" Chem Eng Prog, Vol 49, No 9, pp 459-466, 1953

Hockey, R. M., Nouri, J. M. and Pinho, F., "Flow Visualisation of Newtonian and Non-Newtonian Fluids in a Stirred Reactor" Proceedings of the 5th Int Sym on Flow Visualization, Prague, Czechoslovakia, Hemisphere Publishing Corp, pp 976-987 (21-25th August, 1989)

Holmes, D. B., Voncken, R. M. and Dekker, J. A., "Fluid Flow in Turbine-stirred, Baffled Tanks, I. Circulation Time, II. Dispersion during Circulation" Chem Eng Sci, Vol 19, pp 201-213, 1964

Karslen, H., Private communication with Flygt ITT Fluid Technology Corporation, Solna, Sweden, June 1992

Kneule, F. and Weinspach, P. M., "Suspendierenvon Feststoffpartikeln im Rührgefäß" Verfahrenstechnik, No 12, pp 531-540, 1967

Kolar, V., "Studies on Mixing X - Suspending Solid Particles in Liquids by means of Mechanical Agitation" Coll Czech Chem Comm, Vol 26, pp 613-627, 1961

Koutsakos, E., "Solids Suspension in Mechanically Agitated Vessels" PhD Thesis, University College London, April 1989

Machon, V., Fort, I. and Skrivanek, J., "Local Solids Distribution in the Space of a Stirred Vessel" 4th European Conf on Mixing, Noordwijkerhout, The Netherlands, BHRA (27-29 April 1982)

Mackinnon, C., "Research Review: Comparative Mixing times" FMP 029, April 1987, BHRA

Magelli, F., Fajner, D., Nocentini, M. and Pasquali, G., "Solids Concentration Profiles in Slurry Reactors Stirred with Multiple Impellers: Recent Results" Engg Foundation Mixing XI, New Hampshire, USA, 2-7 August, 1987

Magelli, F., Fajner, D., Nocentini, M. and Pasquali, G., "Solids Concentration Distribution in Slurry Reactors Stirred with Multiple Axial Impellers" Engg Foundation Mixing XII, Potosi, USA, 6-11 August, 1989

Magelli, F., Fajner, D., Nocentini, M. and Pasquali, G., "Novel Data about Solids Concentration Distribution in Vessels Stirred with Multiple Impellers" CHISA 87, Paper E5.5, Prague, 31 Aug-4 Sept, 1987

Magelli, F., Fajner, D., Nocentini, M. and Pasquali, G., "Solid Distribution in Vessels Stirred with Multiple Impellers" Chem Eng Sci, Vol 45, No 3, pp 615-625, 1990

Magelli, F., Fajner, D., Nocentini, M., Pasquali, G., Marisko, V. and Ditl, P., "Solids Concentration Distribution in Slurry Reactors Stirred with Multiple Axial Impellers" Chem Eng Process, Vol 29, pp 27-32, 1991

Mak, A., "Measurement of Solids Concentration and N_{js} in a 0.61 m Diameter Torispherical Base Stirred Vessel" FMP 1016, BHRA, March 1987

Mak, A., "Research Review : The Measurement of Power, Solids Suspension and Distribution in a 0.61 m Diameter Stirred Vessel" FMP 032, BHRA, April 1988(a)

Mak, A., "The Effect of Particle Size on Solids Suspension: A Literature Survey" FMP 1036, BHRA, August 1988(b)

Mak, A., Presentation to Fluid Mixing Processes (FMP) Steering Committee Meeting, 11-13th April 1989

Mak, A., Green, A. and Burnapp, R. T., "Flue Gas Desulphurisation Model Tests" Confidential Report for Babcock Contractors Limited, BHR Group Ltd, April 1990

Mak, A. and Ruszkowski, S. W., "Scaling-up of Solids Distribution in Stirred Vessels" IChemE

Sym Series No. 121, pp 379-395, 1990

Medek, J., "Power Characteristics of Agitators with Flat Inclined Blades" Int Chem Engg, Vol 20, No 4, pp 664-672, 1980

Mersmann, A., "Scale-up of Agitated Vessels for Suspension" 5th European Conf on Mixing, Wurzburg, W Germany, BHRA Additional Paper (10-12 June 1985)

Mersmann, A. and Laufhutte, H. D., "Scale-up of Agitated Vessels for Different Mixing Process" 5th European Conf on Mixing, Wurzburg, W German, BHRA Paper 28 (10-12 June 1985)

Molerus, O. and Latzel, W., "Suspension of Solid Particles in Agitated Vessel - I. Archimedes Numbers ≤ 40, II. Archimedes Numbers > 40, Reliable Prediction of Minimum Stirrer Angular Velocities" Chem Eng Sci, Vol 6, pp 1423-1437, 1987

Musil, L. and Vlk, J., "Suspending Solid Particles in an Agitated Conical-Bottom Tank" Chem Eng Sci, Vol 33, pp 21-25, 1978

Muskett, M, J. and Ruszkowski, S., "The measurement of Shaft Power and Blending Loads for a series of Impeller Types and Vessel Internals in a 0.61 m Diameter Stirred Vessel" FMP Report 007, January 1985, BHRA

Nagata, S., "Mixing - Principles and Applications" John Wiley & Sons, 1975

Narayanan, S., Bhatia, V. K., Guha, D. K. and Rao, M. N., "Suspension of Solids by Mechanical Agitation" Chem Eng Sci, Vol 24, pp 223-230, 1969

Nienow, A. W., "Suspension of Solids Particles in Turbine Agitated Baffled Vessels" Chem Eng Sci, Vol 33, pp 1453-1459, 1968

Nienow, A. W. and Miles, D., "The Effect of Impeller/Tank Configurations on Fluid-Particle Mass Transfer" Chem Eng Journal, Vol 15, pp 13-24, 1978

Niesmak, G., "Feststoffverteilung und Leistungsbedarf Gerührter Suspensionen" PhD Thesis, TU Braunschweig, 1982

Oroskar, A. R. and Turian, R. M., "The Critical Velocity in Pipeline Flow of Slurries" AIChE J, Vol 21, No 4, pp 550-558, 1980

Pavlushenko, I. S., Kostin, N. M. and Matveev, S. F., "About the Impeller Speed for Agitation of Suspensions" (in Russian) Zh Prikl Khim, Vol 30, pp 1160-1169, 1967

Penaz, F., Rod, V. and Rehakova, M., "Concentration Distribution of Suspension in a Mixed Vessel" Coll Czech Chem Commum, Vol 43, pp 848-861, 1978

Palmer, M. H., "Design Guide for Impeller Power Numbers" FMP 028, April 1987, BHRA

Raghav Rao, K. S. M. S., Rewatkar, V. B. and Joshi, J. B., "Critical Impeller Speed For Solid Suspension in Mechanically Agitated Contactors" AIChE J, Vol 34, No 8, pp 1332-1340, August 1988

Rieger, F. and Ditl, P., "Suspension of Solid Particles in Agitated Vessel" 4th European Conf on Mixing, Noordwijkerhout, The Netherlands, BHRA, pp 263-273, 27-29th April 1982

Rieger, F., Ditl, P. and Havelkova, O., "Suspension of Solid Particles - Concentration Profiles and Particle Layer on the Vessel Bottom" 6th European Conference on Mxing, Pavia, Italy, BHRA, pp 251-258, 24-26th May 1988

Ruszkowski, S., "Calibration of a Solids Concentration Probe and Measurement of Solids Distribution in a Stirred Vessel" FMP 004, BHRA, October 1985

Schlichting, H., "Boundary-Layer Theory" 7th Ed, McGraw-Hill, 1979

Schwartzberg, H. G and Treybal, R. E., "Fluid and Particle Motion in Turbulent Stirred Tanks" I & EC Fund., Vol 7, pp 1-12, Feb 1968

Shamlou, P. A. "Mechanism of Suspension of Coarse Particles in Liquids in Stirred Vessels" IChemE Sym Series No 121, pp 397-412, 1990

Shamlou, P. A., "Mechanisms of Particle Suspension in Liquids" Presentation, I Chem E Fluid Mixing Subject Group Meeting on Mechanics of Solids Suspension, University College London,

11th April 1991

Shamlou, P. A. and Koutsakos, E., "Solids Suspension and Distribution in Liquids under Turbulent Agitation" Chem Eng Sci, Vol 44, No 3, pp 529-542, 1989

Shamlou, P. A. and Zolfagharian, A., "Incipient Solid Motion in Liquids in Mechanically Agitated Vessels" I Chem E Symposium Series No. 108, pp 195-208, 1987

Squires, K. D. and Eaton, J. K., "Particle Response and Turbulence Modification in Isotropic Turbulence" Phys Fluids A, Vol 2, No 7, pp 1191-1203, July 1990

Subbarao, D. and Taneja, V. K., "Three Phase Suspensions in Agitated Vessels" 3rd European Conference on Mixing, York, England, BHRA Paper D3 (4-6th April 1979)

Susanto, J., "Multiphase Soild-liquid and Solid-liquid-gas Mixing in Stirred Tanks" MSc Thesis, New Jersey Institute of Technology, 1989

Staudinger, G., "Auslegung von Ruehrapparaten zum Suspendieren von Feststoffen" Verfahrenstechnik (Mainz), Vol 11, No 9, pp 508-516, 1977

Tatterson, G. B., Yuan, H-H. S. and Brodkey, R. S., "Stereoscopic Visualisation of the Flows for Pitched Blade Turbines" Chem Eng Sci, Vol 35, pp 1369-1375, 1980

Tay, M., Deutschlander, B and Tatterson, G., "Suspension Characteristics of Large Cylinders in Agitated Tanks" Chem Eng Commun, Vol 29, pp 89-99, 1984

Voit, H. and Mersmann, A., "General Statemant for the Minimum Stirrer Speed During Suspension" German Chem Eng, Vol 9, pp 101-106, 1986

Warmoeskerken, M. M. C. G., Speur, J. and Smith, J. M., "Gas-liquid Dispersion with Pitched Blade Turbines" Chem Eng Commun, Vol 25, pp 11-29, 1984

Weisman, J and Efferding, L. E., "Suspension of Slurries by Mechanical Mixers" AIChE J, Vol 6, No 3, pp 419-426, 1960

Wichterle, K. "Conditions for Suspension of Solids in Agitated Vessels" Chem Eng Sci, Vol 43, No 3, pp 467-471, 1988

Wiedmann, J. A., Steiff, A. and Weinspach, P. M., "Suspension Behaviour of Two and Three Phrase Stirred Reactors" German Chem Eng, Vol 8, pp 321-335, 1985

Zolfagharian, A., "Solid Suspension in Rotary-stirred and in Liquid-jet Stirred Vessels" PhD Thesis, University College London, June 1990

Zwietering, Th. N. "Suspending of Solid Particles in Liquid by Agitators" Chem Eng Sci, Vol 8, pp 244-253, 1958

Appendix A Solids Distribution Data for the 3 Geometrically Similar Impellers (Sec 4.3)

Vessel: 0.61 m (V=0.165 m^3), Downwards Pumping, C=T/4,

Solids: 30% Wt (14% Vol), 150-210 μm sand, ρ_S=2630 kg m^{-3}, ρ_{sv}=1228 kg m^{-3}, U_s=0.015 m s^{-1}

Probe Radial Position: T/6 from vessel wall

Buurman's Model for solids homogeneity: $$f(Fr^*) = \frac{\rho_L N^2 D^2}{g \Delta\rho d_p} \cdot \left(\frac{d_p}{D}\right)^{0.45} \geq 20$$

Table A.1 **Impeller: 45° PBT4(T/3), Po=1.73** (D=0.203 m)

Impeller Speed (N)	Power (W)	Volume Fraction of Solids at Different Depth (metres below fluid surface)					Relative Standard Deviation (RSD)	$f(Fr^*)$
		0.1	0.2	0.3	0.4	0.5		
200	27	0	0	0.260	0.247	0.252	0.99	6.7
250	53	0.067	0.187	0.180	0.179	0.180	0.39	10.5
300	92	0.149	0.160	0.147	0.152	0.152	0.10	15.1
350	145	0.150	0.153	0.138	0.145	0.145	0.06	20.6
400	217	0.148	0.150	0.133	0.142	0.141	0.05	26.9
450	309	0.150	0.146	0.131	0.141	0.140	0.05	34.1
500	424	0.150	0.145	0.132	0.139	0.139	0.05	42.1
550	564	0.153	0.147	0.134	0.142	0.140	0.06	50.9

Predicted N_{js} at 30% Wt = 285 rpm (P_{js} = 78 W)

Table A.2 **Impeller: 45° PBT4(T/2), Po=1.60 (D=0.298 m)**

Impeller Speed (N)	Power (W)	Volume Fraction of Solids at Different Depth (metres below fluid surface)					Relative Standard Deviation (RSD)	$f(Fr^*)$
		0.1	0.2	0.3	0.4	0.5		
60	5	0.001	0.037	0.039	0.016	0.494	1.52	1.1
90	16	0.002	0.087	0.192	0.171	0.155	0.57	2.5
120	37	0.007	0.194	0.204	0.174	0.171	0.58	4.4
150	72	0.134	0.167	0.164	0.147	0.144	0.13	6.9
180	125	0.143	0.157	0.147	0.134	0.135	0.07	9.9
210	198	0.144	0.153	0.138	0.131	0.132	0.07	13.5
240	296	0.145	0.151	0.132	0.126	0.130	0.08	17.6
270	421	0.147	0.151	0.128	0.128	0.128	0.09	22.2
300	577	0.148	0.153	0.129	0.131	0.132	0.08	27.5

Predicted N_{js} at 30% Wt = 224 rpm (P_{js} = 240 W)

Table A.3 **Impeller: 45° PBT4(T/1.7), Po=1.48** (D=0.368 m)

Impeller Speed (N)	Power (W)	Volume Fraction of Solids at Different Depth (metres below fluid surface)					Relative Standard Deviation (RSD)	$f(Fr^*)$
		0.1	0.2	0.3	0.4	0.5		
20	0.5	0	0	0.001	0.005	0.520	1.68	0.2
40	4	0	0.002	0.043	0.075	0.519	1.58	0.7
60	12	0.009	0.117	0.120	0.110	0.100	0.51	1.5
80	29	0.100	0.138	0.145	0.114	0.110	0.20	2.7
100	57	0.131	0.154	0.149	0.134	0.116	0.11	4.2
120	98	0.137	0.155	0.151	0.132	0.112	0.12	6.1
140	156	0.137	0.153	0.144	0.129	0.108	0.13	8.3
160	233	0.146	0.149	0.141	0.126	0.107	0.13	10.8
180	331	0.146	0.150	0.136	0.130	0.104	0.14	13.7
200	454	0.147	0.149	0.130	0.133	0.106	0.14	16.9

Predicted N_{js} at 30% Wt = 241 rpm (P_{js} = 795 W)

Appendix B Solids Distribution Data for Pitch Angle Experiments (Sec 4.4)

Vessel: 0.61 m (V=0.165 m^3), Downwards Pumping, C=T/4,

Solids: 30% Wt (14% Vol), 150-210 μm sand, ρ_S=2630 kg m^{-3}, ρ_{sv}=1228 kg m^{-3}, U_s=0.015 m s^{-1}

Probe Radial Position: T/6 from vessel wall

Buurman's Model for solids homogeneity: $$f(Fr^*) = \frac{\rho_L N^2 D^2}{g \Delta\rho d_p} \cdot \left(\frac{d_p}{D}\right)^{0.45} \geq 20$$

Table B.1 Impeller: 30° PBT4(T/3), Po=0.78 (D=0.202 m)

Impeller Speed (N)	Power (W)	Volume Fraction of Solids at Different Depth (metres below fluid surface)					Relative Standard Deviation (RSD)	$f(Fr^*)$
		0.1	0.2	0.3	0.4	0.5		
50	0.2	0	0	0	0.004	0.478	1.56	0.4
100	2	0	0	0.008	0.026	0.479	1.53	1.6
150	5	0	0	0.035	0.072	0.481	1.48	3.7
200	12	0	0	0.026	0.266	0.257	1.02	6.6
250	23	0	0.002	0.228	0.221	0.213	0.86	10.2
300	40	0.002	0.177	0.172	0.176	0.173	0.55	14.7
350	64	0.133	0.158	0.147	0.148	0.153	0.09	20.1
400	95	0.142	0.144	0.137	0.138	0.140	0.02	26.2
450	136	0.142	0.141	0.132	0.134	0.136	0.04	33.2
500	186	0.140	0.140	0.128	0.131	0.133	0.06	41.0
550	248	0.140	0.139	0.125	0.120	0.133	0.09	50.0

Predicted N_{js} at 30% Wt = 385 rpm (P_{js} = 83 W)

N.B. Distribution Data for 45° PBT4(T/3) are presented in Table A.1

Table B.2 **Impeller: 90° FBT4(T/3), Po=3.19 (D=0.203)**

Impeller Speed (N)	Power (W)	Volume Fraction of Solids at Different Depth (metres below fluid surface)					Relative Standard Deviation (RSD)	$f(Fr^*)$
		0.1	0.2	0.3	0.4	0.5		
50	0.8	0	0.003	0.005	0.005	0.475	1.54	0.4
100	6	0	0.003	0.059	0.067	0.479	1.45	1.7
150	21	0	0.004	0.024	0.260	0.266	1.02	3.8
200	50	0	0.004	0.219	0.215	0.218	0.85	6.7
250	98	0	0.170	0.184	0.180	0.170	0.56	10.5
300	169	0.094	0.156	0.161	0.158	0.155	0.21	15.1
350	268	0.130	0.145	0.145	0.143	0.143	0.05	20.6
400	400	0.130	0.138	0.140	0.136	0.135	0.04	26.9

Predicted N_{js} at 30% Wt = 264 rpm (P_{js} = 113 W)

Appendix C Solids Distribution Data for Dual Impeller Systems (Sec 4.5)

Vessel: 0.61 m (V=0.165 m^3), Downwards Pumping, C=T/4,

Solids: 30% Wt (14% Vol), 150-210 μm sand, ρ_s=2630 kg m^{-3}, ρ_{av}=1228 kg m^{-3}, U_t=0.015 m s^{-1}

Probe Radial Position: T/6 from vessel wall, diameter for both impellers are 0.203 m

Buurman's Model for solids homogeneity: $$f(Fr^*) = \frac{\rho_L N^2 D^2}{g \Delta\rho d_p} \cdot \left(\frac{d_p}{D}\right)^{0.45} \geq 20$$

Table C.1 Upper: 41° PBT4(T/3) at C=0.3T, Lower: 41° PBT4(T/3) at C=T/8, Po_c=2.32

Impeller Speed (N)	Power (W)	Volume Fraction of Solids at Different Depth (metres below fluid surface)					Relative Standard Deviation (RSD)	$f(Fr^*)$
		0.1	0.2	0.3	0.4	0.5		
30	0.1	0	0	0	0	0.471	1.55	0.2
60	1	0	0	0.004	0.004	0.473	1.55	0.6
90	3	0	0	0.011	0.090	0.469	1.46	1.4
120	8	0	0	0.063	0.206	0.384	1.18	2.4
150	15	0	0	0.099	0.269	0.269	0.97	3.8
180	27	0	0.101	0.217	0.202	0.206	0.67	5.5
210	42	0.018	0.179	0.176	0.167	0.172	0.50	7.4
240	63	0.128	0.157	0.151	0.146	0.152	0.10	9.7
270	90	0.139	0.151	0.140	0.137	0.147	0.05	12.3
300	123	0.143	0.146	0.135	0.134	0.145	0.04	15.1
330	163	0.144	0.145	0.132	0.133	0.134	0.05	18.3
360	212	0.146	0.144	0.131	0.131	0.135	0.06	21.8
390	270	0.147	0.142	0.128	0.131	0.141	0.06	25.6

Table C.2 Upper: 41° PBT4(T/3) at C=0.5T, Lower: 41° PBT4(T/3) at C=T/8, Po_c=2.30

Impeller Speed (N)	Power (W)	Volume Fraction of Solids at Different Depth (metres below fluid surface)					Relative Standard Deviation (RSD)	$f(Fr^*)$
		0.1	0.2	0.3	0.4	0.5		
30	0.1	0	0	0	0	0.480	1.57	0.2
60	1	0	0	0	0	0.471	1.55	0.6
90	3	0	0.006	0.007	0.003	0.487	1.58	1.4
120	8	0	0.023	0.060	0.165	0.342	1.02	2.4
150	15	0	0.035	0.186	0.192	0.212	0.72	3.8
180	26	0	0.135	0.199	0.191	0.196	0.61	5.5
210	42	0.081	0.174	0.161	0.159	0.161	0.27	7.4
240	62	0.141	0.152	0.141	0.140	0.145	0.05	9.7
270	89	0.144	0.145	0.135	0.137	0.138	0.03	12.3
300	122	0.144	0.142	0.132	0.133	0.137	0.04	15.1
330	162	0.144	0.142	0.130	0.133	0.134	0.05	18.3
360	210	0.144	0.142	0.129	0.132	0.138	0.05	21.8
390	267	0.146	0.141	0.129	0.1346	0.141	0.05	25.6

Predicted N_{js} at 30% Wt = 319 rpm (P_{js} = 146 W)

Table C.3 Upper: 41° PBT4(T/3) at C=0.7T, Lower: 41° PBT4(T/3) at C=T/8, Po_c=2.74

Impeller Speed (N)	Power (W)	Volume Fraction of Solids at Different Depth (metres below fluid surface)					Relative Standard Deviation (RSD)	$f(Fr^*)$
		0.1	0.2	0.3	0.4	0.5		
30	0.1	0	0	0	0	0.482	1.59	0.2
60	1	0	0	0	0	0.483	1.58	0.6
90	4	0	0	0	0	0.490	1.60	1.4
120	9	0.019	0.027	0.024	0.154	0.392	1.16	2.4
150	18	0.041	0.084	0.065	0.235	0.258	0.73	3.8
180	31	0.075	0.172	0.164	0.167	0.170	0.31	5.5
210	50	0.133	0.164	0.159	0.158	0.166	0.16	7.4
240	74	0.135	0.148	0.145	0.144	0.152	0.06	9.7
270	106	0.140	0.141	0.138	0.138	0.144	0.02	12.3
300	145	0.140	0.139	0.134	0.133	0.141	0.03	15.1
330	193	0.141	0.138	0.135	0.134	0.141	0.03	18.3
360	251	0.142	0.136	0.133	0.132	0.141	0.04	21.8
390	319	0.144	0.137	0.134	0.134	0.144	0.04	25.6

Predicted N_{js} at 30% Wt = 270 rpm (P_{js} = 106 W)

Table C.4 Upper: 41° PBT4(T/3) at C=0.3T, Lower: 90° FBT4(T/3) at C=T/8, Po_c=4.38

Impeller Speed (N)	Power (W)	Volume Fraction of Solids at Different Depth (metres below fluid surface)					Relative Standard Deviation (RSD)	$f(Fr^*)$
		0.1	0.2	0.3	0.4	0.5		
30	0.2	0	0	0	0	0.477	1.57	0.2
60	2	0	0	0	0	0.488	1.60	0.6
90	6	0	0	0.020	0.067	0.474	0.48	1.4
120	15	0	0	0.043	0.260	0.264	1.00	2.4
150	29	0	0	0.260	0.251	0.254	1.00	3.8
180	50	0	0.167	0.215	0.197	0.207	0.66	5.5
210	79	0.021	0.180	0.184	0.170	0.182	0.51	7.4
240	119	0.134	0.161	0.156	0.151	0.160	0.13	9.7
270	169	0.140	0.152	0.144	0.138	0.150	0.06	12.3
300	232	0.142	0.150	0.136	0.134	0.143	0.05	15.1
330	308	0.140	0.146	0.134	0.131	0.141	0.05	18.3
360	400	0.145	0.146	0.133	0.130	0.141	0.05	21.8
390	509	0.146	0.145	0.131	0.130	0.144	0.06	25.6

Predicted N_{js} at 30% Wt = 214 rpm (P_{js} = 84 W)

Table C.5 Upper: 41° PBT4(T/3) at C=0.5T, Lower: 90° FBT4(T/3) at C=T/8, Po_c=4.52

Impeller Speed (N)	Power (W)	Volume Fraction of Solids at Different Depth (metres below fluid surface)					Relative Standard Deviation (RSD)	$f(Fr^*)$
		0.1	0.2	0.3	0.4	0.5		
30	0.2	0	0	0	0	0.472	1.55	0.2
60	2	0	0	0	0	0.478	1.57	0.6
90	6	0	0	0	0	0.477	1.57	1.4
120	15	0	0.038	0.091	0.256	0.276	0.91	2.4
150	30	0	0.187	0.221	0.220	0.208	0.71	3.8
180	52	0	0.191	0.200	0.198	0.197	0.64	5.5
210	82	0.040	0.176	0.176	0.172	0.178	0.44	7.4
240	122	0.131	0.156	0.153	0.151	0.158	0.11	9.7
270	174	0.140	0.150	0.143	0.141	0.149	0.05	12.3
300	239	0.140	0.146	0.138	0.138	0.145	0.03	15.1
330	318	0.143	0.144	0.135	0.135	0.144	0.04	18.3
360	413	0.144	0.145	0.133	0.135	0.142	0.04	21.8
390	525	0.145	0.145	0.133	0.133	0.144	0.05	25.6

Predicted N_{js} at 30% Wt = 236 rpm (P_{js} = 116 W)

Table C.6 Upper: 41° PBT4(T/3) at C=0.7T, Lower: 90° FBT4(T/3) at C=T/8, Po_c=4.78

Impeller Speed (N)	Power (W)	Volume Fraction of Solids at Different Depth (metres below fluid surface)					Relative Standard Deviation (RSD)	$f(Fr^*)$
		0.1	0.2	0.3	0.4	0.5		
30	0.3	0	0	0	0	0.473	1.56	0.2
60	2	0	0	0	0	0.480	1.57	0.6
90	7	0	0	0	0	0.482	1.58	1.4
120	16	0.023	0.042	0.028	0.268	0.305	1.00	2.4
150	32	0.078	0.113	0.120	0.210	0.210	0.44	3.8
180	55	0.138	0.170	0.166	0.169	0.173	0.21	5.5
210	87	0.150	0.162	0.157	0.161	0.164	0.15	7.4
240	130	0.146	0.153	0.148	0.153	0.158	0.10	9.7
270	184	0.141	0.148	0.142	0.148	0.152	0.06	12.3
300	253	0.140	0.145	0.139	0.144	0.150	0.04	15.1
330	337	0.142	0.143	0.137	0.142	0.150	0.04	18.3
360	437	0.144	0.142	0.137	0.142	0.148	0.04	21.8
390	556	0.143	0.144	0.135	0.142	0.147	0.04	25.6

Predicted N_{js} at 30% Wt = 226 rpm (P_{js} =108 W)

Table C.7 Single 41° PBT4(T/3) at C=T/8, Po=1.69

Impeller Speed (N)	Power (W)	Volume Fraction of Solids at Different Depth (metres below fluid surface)					Relative Standard Deviation (RSD)	$f(Fr^*)$
		0.1	0.2	0.3	0.4	0.5		
30	0.1	0	0	0	0	0.483	1.58	0.2
60	0.7	0	0	0	0	0.474	1.57	0.6
90	2	0	0	0	0	0.482	1.58	1.4
120	6	0	0	0	0	0.475	1.56	2.4
150	11	0	0	0	0.301	0.288	1.17	3.8
180	19	0	0	0.089	0.268	0.272	0.98	5.5
210	31	0	0.042	0.229	0.206	0.213	0.77	7.4
240	46	0	0.185	0.194	0.177	0.188	0.60	9.7
270	66	0.104	0.167	0.167	0.157	0.168	0.22	12.3
300	90	0.135	0.152	0.150	0.144	0.155	0.08	15.1
330	120	0.139	0.148	0.142	0.145	0.152	0.06	18.3
360	156	0.139	0.145	0.138	0.143	0.151	0.04	21.8
390	198	0.138	0.144	0.136	0.139	0.147	0.03	25.6
420	247	0.139	0.143	0.134	0.138	0.145	0.03	29.7
450	304	0.140	0.141	0.133	0.139	0.145	0.03	34.1
480	369	0.141	0.139	0.132	0.139	0.146	0.04	38.8

Predicted N_{js} at 30% Wt = 272 rpm (P_{js} = 67 W)

Table C.8 Single 90° FBT4(T/3) at C=T/8, Po=3.62

Impeller Speed (N)	Power (W)	Volume Fraction of Solids at Different Depth (metres below fluid surface)					Relative Standard Deviation (RSD)	$f(Fr^*)$
		0.1	0.2	0.3	0.4	0.5		
30	0.2	0	0	0	0	0.477	1.57	0.2
60	2	0	0	0	0	0.479	1.57	0.6
90	5	0	0	0	0	0.474	1.56	1.4
120	12	0	0	0	0	0.473	1.56	2.4
150	24	0	0	0	0.300	0.295	1.18	3.8
180	41	0	0	0.254	0.247	0.250	0.98	5.5
210	65	0	0.149	0.218	0.210	0.217	0.68	7.4
240	97	0	0.181	0.192	0.182	0.192	0.60	9.7
270	138	0.115	0.169	0.170	0.162	0.173	0.23	12.3
300	190	0.140	0.157	0.155	0.147	0.160	0.11	15.1
330	253	0.139	0.149	0.147	0.139	0.152	0.06	18.3
360	328	0.139	0.144	0.139	0.136	0.148	0.04	21.8
390	417	0.138	0.144	0.137	0.135	0.146	0.04	25.6
420	521	0.144	0.151	0.135	0.140	0.147	0.05	29.7
450	640	0.144	0.149	0.133	0.141	0.149	0.05	34.1
480	777	0.145	0.147	0.136	0.142	0.149	0.05	38.8

Predicted N_{js} at 30% Wt = 244 rpm (P_{js} = 102 W)

Appendix D Just Suspension Results Measured in 4 Scales (T_{31}, T_{61}, T_{183} and T_{267})

Impeller: 45° PBT4(T/2,D/3.6), Downwards Pumping, C=T/4

Solids: 150-210 μm sand, ρ_S=2630 kg m^{-3}, U_s=0.015 m s^{-1}

Last suspension region: directly under the impeller in all cases

Visual N_{js} results were adjusted by using:

Adjusted N_{js} = Visual N_{js} / 1.07 (Section 3.9.3)

This is to allow comparison with UDF N_{js} made in T_{61}, T_{183} and T_{267}

's' value is the geometrical constant in Zwietering correlation

$$N_{js} = s\, \nu^{0.1} \left(\frac{g\, \Delta\rho}{\rho_L} \right)^{0.45} d_p^{0.2}\, X^{0.13}\, D^{-0.85}$$

Table D.1 Just Suspension Speed in T_{31} (D=0.153 m, V=0.0205 m^3)

% Wt	M_S (kg)	ρ_{av} (kg m^{-3})	% Vol	X	Visual N_{js} (rpm)	Adjusted N_{js} (rpm)	's' value
0.1	0.021	1001	0.04	0.1	198	185	5.3
0.3	0.062	1002	0.1	0.2	219	205	5.4
0.5	0.102	1003	0.2	0.5	242	226	5.3
1	0.206	1006	0.4	1.0	263	246	5.2
3	0.627	1026	1.2	3.1	298	279	5.1
5	1.058	1032	2.0	5.3	310	290	5.0
7	1.500	1045	2.8	7.5	321	300	4.9
10	2.185	1066	4.1	11.1	330	308	4.8
15	3.390	1103	6.3	17.7	339	317	4.7
20	4.680	1142	8.7	25.0	343	321	4.5

Table D.2 Just Suspension Speed in T_{61} (D=0.310 m, V=0.165 m^3, Po=1.52)

% Wt	M_S (kg)	ρ_{av} (kg m^{-3})	% Vol	X	Viusal N_{js} (rpm)	Adjusted N_{js} (rpm)	's' value	UDF N_{js} (rpm)	's' Value
5	8.51	1032	2.0	5.3	185	173	5.4	170	5.3
10	17.59	1066	4.1	11.1	201	188	5.4	-	-
15	27.29	1103	6.3	17.6	214	200	5.4	190	5.1
20	37.67	1142	8.7	25.0	228	213	5.5	-	-
25	48.81	1183	11.3	33.3	229	214	5.3	-	-
30	60.81	1228	14.0	42.9	241	225	5.4	-	-
40	87.76	1330	20.2	66.7	250	234	5.3	220	5.0

Table D.3 Just Suspension Speed in T_{183} (D=0.93 m, V=4.46 m^3, Po=1.75)

% Wt	M_S (kg)	ρ_{av} (kg m^{-3})	% Vol	X	UDF N_{js} (rpm)	's' value
1	44.8	1006	0.4	1.1	50	5.0
3	136.2	1026	1.2	3.9	59	4.9
5	229.9	1032	2.0	5.3	61	4.9
10	474.9	1066	4.1	11.1	72	5.2
15	736.7	1103	6.3	17.7	74	5.1
20	1017	1142	8.7	25.0	77	5.0
25	1318	1183	11.3	33.3	80	5.0
30	1642	1228	14.0	42.9	84	5.1

Table D.4 Just Suspension Speed in T_{267} (D=1.331 m, V=13.5 m^3, Po=1.75)

% Wt	M_S (kg)	ρ_{sv} (kg m^{-3})	% Vol	X	UDF N_{js} (rpm)	's' value
1	136	1006	0.4	1.0	44	5.9
2	273	1013	0.8	2.0	45	5.5
3	413	1026	1.2	3.9	49	5.5
5	697	1032	2.0	5.3	54	5.9
15	2233	1103	6.3	17.7	59	5.5
20	3082	1142	8.7	25.0	65	5.8
25	3994	1183	11.3	33.3	67	5.7
30	4975	1228	14.0	42.9	72	5.9

Appendix E Solids Distribution Data Measured in 3 Scales (T_{61}, T_{183} and T_{267})

Solids: 150-210 μm sand, ρ_S=2630 kg m^{-3}, U_t=0.015 m s^{-1}

Probe Radial Position: T/6 from vessel wall, unless otherwise stated

Buurman's Modified Froude No Model: $f\,(Fr^*) = \frac{\rho_L N^2 D^2}{g\,\Delta\rho\,d_p} \cdot (\frac{d_p}{D})^{0.45} \geq 20$

Table E.1 **Impeller: 45° PBT4(T/2,D/5.2), D=0.31 m, Vessel: T_{61} (V=0.165m^3), Solids: 15% Wt (6.3% V)**

Impeller Speed (N)	Volume Fraction of Solids at Different Depth (metres below fluid surface)					Relative Standard Deviation (RSD)	$f(Fr^*)$
	0.1	0.2	0.3	0.4	0.5		
30	0	0	0	0	0	1.12	0.3
60	0.002	0.002	0.003	0.003	0.004	1.07	1.2
90	0.021	0.039	0.034	0.035	0.039	0.54	2.6
120	0.030	0.064	0.075	0.066	0.067	0.28	4.7
150	0.054	0.067	0.068	0.059	0.060	0.10	7.3
180	0.061	0.067	0.064	0.057	0.059	0.07	10.5
210	0.064	0.067	0.060	0.056	0.058	0.08	14.3
240	0.065	0.068	0.057	0.055	0.057	0.10	18.7
270	0.067	0.067	0.056	0.055	0.056	0.11	23.6
300	0.066	0.067	0.055	0.055	0.058	0.11	29.2

Table E.2 **Impeller: 45° PBT4(T/2, D/5.2), D=0.31 m, Vessel: T_{61} (V=0.165 m^3), Solids: 20% Wt (8.7% V)**

Impeller Speed (N)	Volume Fraction of Solids at Different Depth (metres below fluid surface)					Relative Standard Deviation (RSD)	$f(Fr^*)$
	0.1	0.2	0.3	0.4	0.5		
30	0.003	0.003	0.003	0.003	0.004	1.10	0.2
60	0.009	0.016	0.015	0.016	0.012	0.95	1.2
90	0.008	0.055	0.079	0.069	0.061	0.53	2.6
120	0.007	0.101	0.122	0.107	0.108	0.54	4.7
150	0.069	0.097	0.097	0.090	0.093	0.14	7.3
180	0.084	0.093	0.090	0.084	0.084	0.05	10.5
210	0.090	0.095	0.086	0.081	0.085	0.06	14.3
240	0.091	0.095	0.083	0.080	0.083	0.07	18.7
270	0.093	0.095	0.081	0.081	0.083	0.08	23.6
300	0.093	0.097	0.080	0.081	0.083	0.09	29.2

Table E.3 **Impeller: 45° PBT4(T/2,D/5.2), D=1.333 m, Vessel: T_{267} (V=13.5 m^3), Solids: 15% Wt (6.3% V)**

Impeller Speed (N)	Volume Fraction of Solids at Different Depth (metres below fluid surface)					Relative Standard Deviation (RSD)	$f(Fr^*)$
	0.1	0.2	0.3	0.4	0.5		
10	0	0	0	0	0	1.12	0.3
20	0.007	0.011	0.007	0.013	0.011	0.95	1.2
30	0.004	0.047	0.047	0.050	0.049	0.52	2.8
40	0.003	0.073	0.071	0.072	0.074	0.50	5.0
50	0.054	0.070	0.064	0.065	0.069	0.10	7.8
60	0.061	0.067	0.060	0.061	0.061	0.05	11.2
70	0.059	0.066	0.058	0.057	0.062	0.07	15.2
80	0.060	0.063	0.057	0.056	0.060	0.08	19.9
90	0.064	0.063	0.058	0.056	0.063	0.07	25.2

Table E.4 **Impeller: 45° PBT4(T/2,D/5.2), D=1.333 m, Vessel: T_{267} (V=13.5 m^3), Solids: 20% Wt (8.7% V)**

Impeller Speed (N)	Volume Fraction of Solids at Different Depth (metres below fluid surface)					Relative Standard Deviation (RSD)	$f(Fr^*)$
	0.1	0.2	0.3	0.4	0.5		
10	0.002	0.004	0.003	0.003	0.003	1.08	0.3
20	0.003	0.008	0.031	0.027	0.015	0.91	1.2
30	0.003	0.100	0.117	0.118	0.190	0.81	2.8
40	0.003	0.105	0.111	0.118	0.107	0.56	5.0
50	0.074	0.099	0.100	0.101	0.090	0.15	7.8
60	0.082	0.093	0.089	0.091	0.085	0.05	11.2
70	0.087	0.090	0.089	0.087	0.081	0.04	15.2
80	0.087	0.089	0.086	0.085	0.079	0.05	19.9
90	0.089	0.092	0.087	0.085	0.077	0.07	25.2

Table E.5 **Impeller: 45° PBT4(T/2,D/3.6), D=0.31 m, T_{61} (V=0.165 m^3), 30% Wt (14% V), Po=1.52**

Impeller Speed (N)	Power (W)	Volume Fraction of Solids at Different Depth (metres below fluid surface)					Relative Standard Deviation (RSD)	$f(Fr^*)$
		0.1	0.2	0.3	0.4	0.5		
60	5	0	0.015	0.069	0.056	0.460	1.37	1.17
90	18	0	0.125	0.197	0.187	0.178	0.30	2.63
120	43	0.081	0.167	0.175	0.162	0.156	0.28	4.67
150	83	0.144	0.152	0.152	0.145	0.137	0.07	7.29
180	144	0.145	0.150	0.148	0.136	0.130	0.06	10.50
210	229	0.147	0.149	0.144	0.135	0.124	0.07	14.30
240	341	0.150	0.150	0.142	0.134	0.125	0.08	18.67
270	486	0.152	0.151	0.140	0.136	0.113	0.11	23.63
300	669	0.153	0.153	0.141	0.142	0.118	0.10	29.18

Table E.6 **Impeller: 45° PBT4(T/2,D/3.6), D=0.93 m, T_{183} (V=4.46 m^3), 30% Wt (14% V), Po=1.75**

Impeller Speed (N)	Power (W)	Volume Fraction of Solids at Different Depth (metres below fluid surface)					Relative Standard Deviation (RSD)	$f(Fr^*)$
		0.3	0.6	0.9	1.2	1.5		
20	55	0	0.002	0.013	0.027	0.535	1.69	0.71
30	187	0	0.009	0.069	0.053	0.537	1.63	1.60
40	443	0	0.123	0.165	0.159	0.144	0.52	2.85
50	865	0	0.160	0.186	0.171	0.164	0.55	4.45
60	1495	0.046	0.157	0.161	0.151	0.152	0.35	6.41
70	2374	0.123	0.150	0.150	0.135	0.136	0.08	8.72
80	3544	0.132	0.145	0.141	0.130	0.128	0.07	11.40
90	5046	0.134	0.140	0.133	0.122	0.126	0.09	14.42
100	6921	0.135	0.141	0.130	0.124	0.126	0.09	17.81

Table E.7 **Impeller: 45° PBT4(T/2,D/3.6), T_{183}, 30% Wt**
(Probe radial position: T/4 from vessel wall)

Impeller Speed (N)	Volume Fraction of Solids at Different Depth (metres below fluid surface)			Relative Standard Deviation (RSD)
	0.3	0.6	0.9	
30	0	0.002	0.061	1.07
40	0	0.072	0.165	0.80
45	-	-	0.187	-
50	0	0.165	0.182	0.75
55	-	0.166	0.174	-
60	0.082	0.161	0.162	0.33
65	0.115	0.159	0.157	0.18
70	0.139	0.152	0.146	0.07
75	0.138	0.145	0.141	0.03
80	0.136	0.144	0.136	0.04
85	0.140	0.142	0.134	0.03
90	0.139	0.141	0.134	0.03
95	0.138	0.139	0.131	0.05
100	0.140	0.138	0.129	0.06

Table E.8 **Impeller: 45° PBT4(T/2,D/3.6), T_{183}, 30% Wt**
(Probe radial position: T/10 from vessel wall)

Impeller Speed (N)	Volume Fraction of Solids at Different Depth (metres below fluid surface)					Relative Standard Deviation (RSD)
	0.3	0.6	0.9	1.2	1.5	
30	0	0.011	0.007	0.053	0.541	1.68
35	-	-	-	-	0.136	-
40	0	0.053	0.160	0.155	0.139	0.60
45	0	-	0.180	0.171	0.169	-
50	0	0.156	0.182	0.173	0.161	0.54
55	0	-	0.172	0.156	0.152	-
60	0.059	0.156	0.161	0.151	0.146	0.31
65	0.106	0.151	0.156	0.143	0.140	0.14
70	0.127	0.145	0.145	0.136	0.131	0.06
75	0.130	0.145	0.140	0.133	0.125	0.07
80	0.130	0.143	0.137	0.126	0.120	0.10
85	0.132	0.140	0.134	0.130	0.122	0.08
90	0.131	0.140	0.134	0.126	0.121	0.09
95	0.134	-	0.132	0.125	0.124	-
100	0.132	0.138	0.131	0.125	0.123	0.09

Table E.9 **Impeller: 45° PBT4(T/2,D/3.6), T_{183}, 30% Wt**
(Probe radial position: T/60 from vessel wall)

Impeller Speed (N)	Volume Fraction of Solids at Different Depth (metres below fluid surface)					Relative Standard Deviation (RSD)
	0.3	0.6	0.9	1.2	1.5	
30	0	0	-	0.106	0.546	-
40	0	0.092	0.181	0.142	0.183	0.57
45	0	-	0.186	-	-	-
50	0	0.156	0.188	0.165	0.178	0.56
55	-	0.158	0.179	-	-	-
60	0.051	0.160	0.169	0.142	0.154	0.35
65	-	0.150	0.160	-	-	-
70	0.120	0.146	0.153	0.127	0.134	0.10
75	0.128	0.142	0.146	-	-	-
80	0.134	0.143	0.145	0.118	0.127	0.10
85	0.131	0.139	-	-	-	-
90	0.133	0.135	0.137	0.116	0.123	0.11
95	0.134	0.139	0.135	0.113	-	-
100	0.136	0.136	0.132	0.111	0.120	0.13

Table E.10 **Impeller: 45° PBT4(T/2,D/3.6), D=1.331 m, T_{267} (V=13.5 m^3), 30% Wt (14% V), Po=1.75**

Impeller Speed (N)	Power (W)	Volume Fraction of Solids at Different Depth (metres below fluid surface)					Relative Standard Deviation (RSD)	$f(Fr^*)$
		0.45	0.9	1.35	1.8	2.25		
10	45	0.000	0.004	0.004	0.004	0.536	1.74	0.31
20	332	0.000	0.004	0.002	0.122	0.542	1.60	1.24
30	1122	0.000	0.058	0.199	0.196	0.188	0.67	2.79
40	2660	0.000	0.171	0.183	0.172	0.164	0.55	4.97
50	5195	0.127	0.159	0.158	0.151	0.139	0.11	7.76
60	8977	0.133	0.150	0.145	0.136	0.127	0.07	11.17
70	14255	0.139	0.148	0.139	0.130	0.122	0.08	15.21
80	21279	0.139	0.147	0.136	0.127	0.118	0.10	19.86
90	30297	0.144	0.146	0.136	0.133	0.118	0.09	25.14

Appendix F Just Suspension Results from Previous Study

Solids: 5% Wt 150-210 μm sand

All measurements were made in T_{61}, downward pumping

Table F.1 Just Suspension Speed For 45° PBT6(T/2)[1] and 90° PBT6(T/2)[2]

Impeller	Parameters	Clearance	
		N_{js} (rpm)	Po
45° PBT6(T/2,D/4.2)	C=T/4	176	1.77
90° FBT6(T/2,D/6)	C=T/4	134	3.40
	C=T/6	126	3.65
	C=T/8	120	3.79

Table F.2 Just Suspension Speed for 5 PBTs with Different Diameters (Mak 1989)

Impeller	Parameters	Clearance	
		C=T/4	C=T/8
45° PBT4(T/3.3,D/2.1)	N_{js} (rpm)	223	212
	Po	1.81	2.34
45° PBT4(T/2.5,D/2.8)	N_{js} (rpm)	183	133
	Po	1.68	2.15
45° PBT4(T/1.7,D/4.3)	N_{js} (rpm)	187	106
	Po	1.31	1.83
45° PBT4(T/1.4,D/5)	N_{js} (rpm)	131	109
	Po	1.48	1.53

[1] Mak 1988a [2] Unpublished data

Appendix G The One Dimensional Dispersion Model

Let's consider a fluid element of volume V, density ρ and moving with a velocity $\underline{v}$.

The mass of the fluid element:

$$M = \int_V \rho \, dV$$

From mass balance, the rate of change of mass, with respect to volume and density is:

$$\frac{\partial M}{\partial t} = \frac{\partial}{\partial t} \int_V \rho \, dV$$

$$= \int_V \frac{\partial \rho}{\partial t} \, dV + \int_A \rho \, (\underline{v} \, . \, d\underline{A})$$

where $\underline{A}$ is denoted to the surface area prescribed the fluid element and from the theorem of divergence:

$$= \int_V \frac{\partial \rho}{\partial t} \, dV + \int_V \nabla \, . \, (\rho \, \underline{v}) \, dV$$

$$\int_V (\frac{\partial \rho}{\partial t} + \nabla \, . \, \rho \, \underline{v}) \, dV$$

$$\frac{\partial \rho}{\partial t} + \nabla \, . \, \rho \, \underline{v} = r_i$$

r_i is the rate of mass formation and $\rho \, \underline{v}$ is the mass flux within the fluid element.

In order to account for the diffusion of solid particles, i.e. for the differential movement, dispersion coefficient, $D_{e,p}$ is used:

$$\text{Mass flux} = \underline{j}_i = -D_{e,p} \nabla C_i$$

∇C_i = concentration gradient

This is the flux relative to the centre of mass of the fluid at the point where the equation is applied. Therefore, the total net motion of a fluid element moving at velocity $\underline{v}$ is:

$$\underline{j}_i = \underline{v} C_i - D_{e,p} \nabla C_i$$

Hence, applying the continuity equation to the differential volume dV:

$$\text{since} \quad \frac{\partial \rho}{\partial t} + \nabla . \rho \underline{v} = r_i$$

$$\frac{\partial C_i}{\partial t} dV + \nabla . \rho \underline{v} \, dV = r_i \, dV$$

$$\frac{\partial C_i}{\partial t} + \nabla . (\underline{v} C_i - D_{e,p} \nabla C_i) = r_i$$

For constant dispersion coefficient:

$$\frac{\partial C_i}{\partial t} + \nabla . \underline{v} C_i - D_{e,p} \nabla^2 C_i = r_i$$

Where $\partial C_i/\partial t$: accumulation

$\nabla . \underline{v} C_i$: net flow due to convection

$D_{e,p} \nabla^2 C_i$: net flow due to diffusion

r_i: mass formation

Assuming both the solids and liquid phase is a continuum:

$$\text{ie } \partial C_i/\partial t = 0$$

There is no reaction or consumption of solid particles:

$$r_i = 0$$

Therefore $$\nabla \cdot \underline{v}\, C_i + D_{e,p}\, \nabla^2 C_i = 0$$

Assume a one dimensional steady state model and $\underline{v}$ is taking as the turbulent settling velocity of the solids:

$$\partial C_i/\partial x = \partial C_i/\partial y = 0$$
$$\text{and } \partial C_i/\partial z = \partial C_i/\partial h$$

$$\Rightarrow -D_{e,p} \frac{d^2 C_z}{dh^2} + U_t \frac{dC_z}{dh} = 0$$